

Biogeochemistry of carbon and nitrogen in the inland waters of India

A thesis submitted in partial fulfilment of the requirements
for the degree of

Doctor of Philosophy

in

Earth Sciences

by

Siddhartha Sarkar

(Roll No. 18330021)

Under the guidance of

Prof. Sanjeev Kumar

Geosciences Division

Physical Research Laboratory



Discipline of Earth Sciences
Indian Institute of Technology Gandhinagar

2023

Dedicated to
Maa, baba, didi, choton
and
my teachers

Declaration

I declare here that this thesis report represents my own ideas in my own words, and I have included others' ideas with appropriate citations from original sources. I also declare that I have followed all principles of academic honesty and integrity and have not misrepresented or fabricated or falsified any idea/fact/source/data in my submission. I understand that any violation of the above can cause disciplinary action by the Institute and can also evoke penal action from the sources which have thus not been properly cited or from whom permission has not been taken when needed.

Date:

Siddhartha Sarkar
(Roll No. 18330021)



Indian Institute of Technology Gandhinagar
Palaj, Gandhinagar, Gujarat – 382055
India

Certificate

This is to certify that the research work contained in the thesis entitled **“Biogeochemistry of bioavailable elements in the inland waters of India”** by **Mr Siddhartha Sarkar** (Roll No. 18330021) has been carried out under my supervision and this work has not been submitted elsewhere for a degree.

Date:

Prof Sanjeev Kumar
(Thesis Supervisor)
Geosciences Division
Physical Research Laboratory
Ahmedabad, India

Acknowledgements

In the summer of 2016, I (a young physics graduate) was back home from hostel, reminiscing old school days by playing NFS, Mafia, and Prince of Persia. Having spent most of my college days among like – minded crazy people busy in elections, card games, and travelling, I was as lost as one could be. As fate would have, under the ruling of an austere sister, I was forced to come up with a career plan. The freedom in academia, lesser hierarchy than other fields, funded expeditions and cruises, along with the glamour of a ‘Dr’ prefix was quite lucrative. Always captivated by movies like The Core, Twister, and The Day After Tomorrow along with BBC documentaries narrated by Sir David Attenborough, I was then determined to switch discipline and pursue a career in research in the field of Earth Sciences, hoping to land up in a lab in remote Arctic or Antarctica.

It has been a little over 5 years since my joining in PRL. Having spent lots of time on field and in lab, being happy and anxious, reading and writing, loosing almost all my hair and gaining several pounds, it is now time to end the sweet suffering and be done with my thesis. In this long pursuit, many a friends and foes were made who played their role and helped me grow into a better self and achieve this milestone. Here I take the opportunity to express my gratitude to them all with utmost humility and pleasure.

Although words would never suffice, I express my love and gratitude to maa and baba for their struggle and determination to provide us siblings descent education and for their undying faith in us. As baba always says, ‘জয়ের ধ্বজা নিয়ে এগিয়ে চলো’ we kept moving forward. I am highly grateful to my sister whose struggle started by guarding her toddler brothers, oiled and baking in the sun, from getting picked by monkeys. Ever since, we have caused her sleepless nights by our casual attitude towards health, relationships and career. I will forever be obliged for her constant efforts to keep us on track and the numerous pep talks in anxious moments. I will forever be indebted to my younger twin brother for playing the role of both sons, being responsible, and taking care of our parents during my long absence (which I will never be able to justify).

I extend my gratitude to my teachers from school and early academic years, for their guidance, motivation and words of wisdom that shaped the person I am now. I am especially grateful to Dr. Alok Kumar (my MSc dissertation supervisor) for his constant

encouragements to pursue research and for taking time outside coursework to guide me for the CSIR NET – JRF and GATE examinations. After several successful doctoral interviews when I was confused regarding which institute to join, I remember him saying that if research and a robust scientific training is the priority above all other aspects of a campus life, then PRL is the place for me.

Here at PRL, I was fortunate to have Prof Sanjeev Kumar as my doctoral supervisor. The relationship with one's supervisor is like Bertie Botts flavors of beans and it took us both a while to understand how the other functions. I am grateful for his patience and faith in me. After all, he had to deal with the enthusiast in me, with so many dreams and project ideas, ready to do it all. He gave me all the freedom that I demanded as a novice in academia and at the same time patiently waited for me to learn the virtues of the field of research. After endless debates and rebellious acts from my end, now when I look back, I see a Mufasa in him.

I am highly grateful to Prof R D Deshpande, Prof M G Yadav, Prof Ravi Bhushan, Prof J S Ray, Prof. Neeraj Rastogi, Prof. A D Shukla, Prof. L K Sahu, Dr A K Sudheer, Dr Amzad Hussain Laskar, Dr Arvind Singh, Dr Vineet Goswami, and Dr Harish Gadhavi for their encouragement and suggestions that improved my research. During the pandemic when we were suffering from delayed fieldwork and budget crisis, I remember the soothing words of Prof Deshpande (then Division Head), that he was there for us and that everything would be taken care of, which came true after all. From him, I learned that a smile and a warm greeting goes a long way and have a cascading effect on the day's journey of several individuals. His wisdom and outlook towards life have inspired me largely. I am highly grateful to Prof Rastogi (an ideal teacher) for his critical comments and the encouragement to push myself in research. I am grateful to Dr Arvind Singh for his constructive comments during division seminars and an outstanding gaming spirit during volleyball tournaments. The dinner stories at his place, about PRL alumni, especially of Lt Prof. R Ramesh and Lt Prof. D Lal will always motivate us.

I consider myself blessed to have an awesome group of people in GeoSIL, Dr Niharika Sharma, Sangeeta Verma, Dr Abdur Rahman, Dr. Mohammad Atif Khan, Dr Rayees Ahmed Shah, Ajayeta Rathi, Dr P Ragavan, Dr Saranya Puthalath and our most recent members Dr Sarwar Nizam and Janaarthan, for creating a happy working space and extending their continuing support. I am especially grateful to Dr Niharika Sharma for being a wonderful senior and guide, teaching me the nitty gritty of mass

spectrometry. The scientific discussions and debates with Dr Abdur Rahman and Dr P Ragavan will always be cherished. In the numerous field work that was accomplished, most of the time I found Dr Mohammad Atif Khan beside me, helping me selflessly with equal dedication and commitment. I will always cherish and be indebted to the hospitality and friendship of Dr Rayees Ahmed Shah and his family during my fieldwork in the Kashmir Valley.

I thank my GSDN colleagues, Dr P Kiran Kumar, Dr Anil Patel, Dr Harsh Oza, Dr Nisha Bharti, Dr Deepika Sahoo, Dr Amit Pandey, Dr Milan Kumar Mahal, Dr Parthasarathi Jena, Dr Himanshu Saxena, Sanjit Kumar Jena, Devaprasad, Monika Parmar (from AMOPH, but deserving this place in between the two), Deepak Kumar Rai, Nazir Ahmed, Swagatika Chakra, Chandrima Shaw, Shreya Mehta, Rahul Kumar Agarwal, Ranjan Kumar Mohanty, Dr. Naveen Pandey, Dr Suresh K, Virendra Kumar Padhya, Akash Ganguly, Pratheeksha Nayak, Mahesh Gaddam, Jitender Kumar, Rohit Meena, Bankim Bhai and Lakhan Bhai for making every occasion, may it be divisional seminars, volleyball, football, cricket and tug of war tournaments, acting sessions for the hindi pakhwada skits, or making Diwali decorations, memorable and full of excitement.

I thank all my friends in PRL, especially Dr. Parveen Sehrawat, Kimi, Mansi Gupta, Binal Patel, Dr Tanmoy Poddar, Akanksha Khandelwal, Debashish Pachhar, Bharathi, Gaurav Mitra, Gurucharan Mohanta, and others who stood by me during these years, helping me keep my sanity and make lots of lovely memories. I will always cherish the friendship and love of Supriya Pan, Shreya Mehta and Dr. Amit Pandey, along with our handsome Zorro and Hatchi who made lobby C and room 102, a second home.

During our various projects, we often ended up in crisis where we needed the help of our workshop to design samplers and chambers. I am deeply intended to Vaghela ji, Vipul uncle and other members of PRL workshop for their support. I thank Jaldhi Mehta and Pradeep Chauhan for helping me in all matters related to indents and purchase. Without their timely support, none of the field campaigns would have been as successful. I was always intimidated by their smiling faces and cheerful nature, stretching their limits to help research scholars even when burdened with loads of responsibilities. I would like to express my gratitude to Ganesh Bhai, along with Sunil, Dinesh and Suresh from PRL canteen for their love and care and that extra serving of anything delicious.

Finally, I would like to express my gratitude to the Department of Space, Government of India for funding the projects included in the thesis and the Physical Research Laboratory for the Junior (and Senior) Research Fellowship awarded to me for the last five years. I am grateful to the Director, PRL for his continuing support and encouragement towards my research activities and I extend my gratitude to the PRL academic committee for their critical comments and suggestions during the annual academic reviews.

Abstract

Inland waters are hotspots for carbon (C) and nitrogen (N) cycling and acts as active conduits of CH₄, CO₂, and N₂O to the atmosphere, with estimated emission rates of 95.18 Tg yr⁻¹, 2.1 Pg C yr⁻¹, and 10.6 – 19.8 G mol N yr⁻¹, respectively. However, inland waters have been included in the IPCC Assessment Reports only recently with large uncertainties in the estimates of fluxes and stocks of C and N in lakes and rivers. The production and consumption of greenhouse gases in aquatic systems are intrinsically regulated by several complex biogeochemical processes (like photosynthesis, mineralisation, nitrification, denitrification, methanogenesis, and methane oxidation) mediated by microorganisms. The rates and direction of biogeochemical processes is further governed by environmental factors like water temperature, pH, salinity, dissolved oxygen levels, flow velocity, and others. Climate gradient, land cover, land use, and the level of anthropogenic developments also have an impact on the in stream/lake process dynamics. With a changing climate and shifts in the hydrological regime of aquatic systems, it becomes challenging to understand the dynamics of C and N cycle, which further leads to increasing uncertainties in the global budgets. This thesis addresses crucial research questions regarding the biogeochemistry of C and N in inland waters (lakes and rivers) of India undergoing natural and anthropogenic changes.

Lakes across the globe are broadly classified as freshwater and saline, the latter contributing significantly to the global lake volume ($85 \times 10^3 \text{ km}^3$ to the total of $190 \times 10^3 \text{ km}^3$) and yet being highly unexplored in terms of biogeochemical processes. It has been observed that freshwater bodies are also getting saltier which has an adverse effect on their ecosystem functioning. The warming climate with added human perturbations of excess water consumption is causing inland lakes to shrink and loose surface area. These changes in lake morphometry and water quality are predicted to have a significant impact on lake ecosystem dynamics and biogeochemistry. This thesis attempts to address two important research questions regarding lake biogeochemistry: (i) the effect of lake volume reduction and (ii) the effect of salinization on the C and N biogeochemistry of both freshwater and saline lakes. To explore the effect of salinization on C and N biogeochemistry of freshwater lakes, seasonal sampling was conducted in a natural lake, that experienced volume reduction and salinity changes. It was observed that evaporative water loss could reach as high as 47 % of the lake volume

during a year. The reduction in lake volume in the freshwater lake was accompanied by increase in ionic concentrations and an increase in lake biomass. It is evident that salinization causes a shift from heterotrophy to autotrophy. The dynamics of dissolved greenhouse gases (CH_4 , CO_2 , and N_2O) was explored and it was observed that CH_4 production was highly dependent on the availability of substrate, whereas CO_2 concentrations dipped when primary productivity was high. N_2O was surprisingly lowest during periods of high lake biomass indicating a negative effect of productivity on N_2O production (competition for DIN/complete denitrification). In saline lake systems, it was observed that desiccation is accompanied by drastic increase in ionic concentration and electrical conductivity. Lake desiccation was further accompanied by increase in lake biomass and inorganic C concentrations. Stable isotopic composition of dissolved inorganic carbon (DIC), particulate organic carbon (POC), and particulate nitrogen (PN) revealed a coupling between primary productivity and inorganic C dynamics in saline lakes. In both saline and freshwater lakes, even at high nutrient conditions, the potential presence of dinitrogen (N_2) fixers was indicated by decreasing $\delta^{15}\text{N}_{\text{PN}}$ with increasing salinity and lake biomass. By exploring the biogeochemistry of salt pans and brine reservoir, it was observed that even in hypersaline environments, human modulations can establish distinct lake environments with different rates and directions of C and N cycling.

Rivers and streams act as both active and passive pipes for the transport and transformation of C and N along the land ocean continuum. The riverine export of C and N to the coastal region has implications in regulating the coastal biogeochemistry and constraining the global elemental budgets. Asian rivers accounts for $\sim 35\%$ of the global freshwater discharge and $\sim 70\%$ of total suspended matter (TSM) flux to the oceans. This thesis attempted to understand the sources and seasonality of total suspended matter and associated POC and PN in three large Asian rivers – Ganges, Mekong and Yellow. Using stable isotopic composition of C and N, it was deciphered that during high flow condition, allochthonous inputs dominated the organic matter pool and during low flow conditions, autochthonous inputs derived from enhanced primary productivity was dominant. During low flow conditions, low isotopic composition of PN indicated the possibility of N_2 fixation. The study also estimated the export fluxes of POC and PN to the coastal region. It was observed that fluxes and

yields of TSM and associated C and N decreased manifold over decades in the three river systems.

Riverine systems across the globe are facing the consequences of urbanization and engineering modifications of river channels by the construction of weirs, dams, riverfronts, and canals etc. This thesis also attempted to understand the effect of changes in flow regime and urbanisation on the riverine C and N biogeochemistry. It was observed that DIC, particulate matter (PM) and dissolved CH_4 , CO_2 , and N_2O increased manifold in the polluted reaches of river systems. Furthermore, increased residence time of water due to restricted flow enhanced primary production and was accompanied by elevated concentrations of dissolved CH_4 , CO_2 , and N_2O .

High altitude rivers and lakes are at the forefront of experiencing the effects of climate change and associated warming and changes in hydrological patterns. The thesis explored the transport and transformation of C and N in a high altitude river – lake continuum, focusing on the seasonality (i.e. as the system shifted from high flow ice melt season to low flow and productive periods). It was observed that DIC was high and particulate organic matter (POM) was low in pristine lower order streams with high flow velocity and primarily fed by melting snow. Furthermore, biomass increased as the river entered city limits as well as the lake system, which enhanced CH_4 production. CO_2 concentrations fell as the river – lake continuity shifted from net heterotrophy to autotrophy.

The last component of the thesis addressed the cycling of particulate black carbon (PBC) in aquatic systems. BC being assumed as refractory, has important implications in global climate by sequestering C in longer timescales. However, recent studies (although limited in number) have challenged the non-reactive nature of BC. The present study explored the sources, transport and transformation of PBC in the atmosphere – river – ocean continuum. The dynamics of PBC within the river continuum was highly complex with overlapping signatures of variable sources and possible transformations. However, significant increase in isotopic composition of PBC in the marine environment as compared to riverine and atmospheric BC pool indicated towards potential aging in the marine system.

Contents

Acknowledgements.....	1
Abstract.....	5
1. Introduction	21
1.1 Aquatic carbon cycle.....	23
1.2 Aquatic nitrogen cycle	25
1.3 Application of stable isotopes in C and N biogeochemistry	27
1.4 Carbon and nitrogen biogeochemistry in inland waters of India: Current understanding	28
1.5 Objectives of the thesis.....	29
1.6 Outline of the thesis.....	30
2. Methodology.....	33
2.1 Sampling campaigns	34
2.2 Sampling.....	37
2.3 Field measurements and laboratory analysis	37
2.3.1 Field parameters	37
2.3.2 Major ions.....	37
2.3.3 Dissolved inorganic nitrogen.....	39
2.3.4 Stable isotopes of oxygen in water	39
2.3.5 Dissolved inorganic carbon	39
2.3.6 Particulate organic matter and sediment organic matter	39
2.3.7 Dissolved gases.....	40
2.3.7.1 Gas Chromatography.....	40
2.3.7.2 Cavity Ring Down Spectroscopy	41
2.3.8 Particulate black carbon.....	42
2.4 Statistical analysis	42
3. Lake biogeochemistry.....	43
3.1 Lakes in transition: Effect of volume reduction and salinization on freshwater lakes.....	45
3.1.2 Study area	46
3.1.3 Sampling.....	46
3.1.4 Results	47
3.1.4.1 Physio-chemical parameters of the lake	47
3.1.4.2 Concentrations and isotopic compositions of DIC, POC, and PN	49
3.1.4.3 C and N contents in sediments, emergent macrophytes, and surface algae	51

3.1.4.4	Dissolved greenhouse gases in the lake	52
3.1.5	Discussion.....	52
3.1.5.1	Evaporation and salinization of lake water.....	52
3.2.5.2	Seasonality in dissolved inorganic carbon cycling	53
3.1.5.3	Lake biomass	54
3.2.5.4	Source of sedimentary organic matter	56
3.1.5.5	CH ₄ , CO ₂ , and N ₂ O dynamics in the lake	56
3.1.6	Conclusion.....	59
3.2	Biogeochemistry of a saline lake	60
3.2.1	Study area	61
3.2.2	Sampling.....	63
3.2.3	Results	63
3.2.3.1	Isotopic compositions of water.....	63
3.2.3.2	Hydrographic parameters, major ions, and nutrients	63
3.2.3.3	Dissolved inorganic carbon.....	66
3.2.3.4	Particulate organic matter contents and its isotopic compositions	67
3.2.3.5	Basic properties of sediments	68
3.2.4	Discussion.....	69
3.2.4.1	Hydrological characteristics of the lake.....	69
3.2.4.2	Lake nutrient dynamics and ion chemistry	69
3.2.4.3	Dissolved inorganic carbon cycling in the lake	70
3.2.4.4	Lake biomass and productivity	71
3.2.4.5	Organic matter contents in sediments	73
3.2.5	Conclusion.....	74
4.	River biogeochemistry	75
4.1	Total suspended matter dynamics in large rivers	77
4.1.1	Study area	77
4.1.2	Sampling.....	79
4.1.3	Results	79
4.1.3.1	Total suspended matter	79
4.1.3.2	Particulate organic carbon.....	81
4.1.6.3	Particulate nitrogen	81
4.1.6.4	Isotopic composition of total suspended matter.....	82
4.1.4	Discussion.....	83
4.1.4.1	Total suspended matter along the river continuum.....	83
4.1.7.2	Sources of riverine carbon and nitrogen	85
4.1.7.3	Seasonality in total suspended matter as inferred from elemental biogeochemistry	87
4.1.7.4	Yield and export fluxes of particulate organic carbon and nitrogen.....	90

4.1.8 Conclusion	93
4.2 Biogeochemistry of an engineered river system	94
4.2.1 Study area	95
4.2.2 Sampling.....	96
4.2.3 Results	97
4.2.3.1 Environmental parameters.....	97
4.2.3.2 Stable oxygen isotopic composition of river water	100
4.2.3.3 Dissolved inorganic carbon	100
4.2.3.4 Particulate organic matter.....	100
4.2.3.5 Dissolved CH ₄ , CO ₂ , and N ₂ O.....	103
4.2.4 Discussion.....	105
4.2.4.1 Temporal variation in dissolved inorganic carbon and particulate matter	105
4.2.4.2 Temporal variation in the dissolved CH ₄ , CO ₂ , and N ₂ O.....	109
4.2.4.3 Effect of engineered modifications on river biogeochemistry: Lined Canal, stagnant Riverfront, and the polluted Sabarmati Downstream	110
4.2.4.4 Fluxes of CH ₄ , CO ₂ , and N ₂ O.....	112
4.2.5 Conclusion	114
4.3 Biogeochemistry of high altitude river – lake continuum	115
4.3.1 Study area and sampling.....	116
4.3.3 Results	118
4.3.3.1 Basic environmental parameters.....	118
4.3.3.2 Dissolved inorganic carbon	120
4.3.3.3 Particulate organic carbon and its isotopic composition	121
4.3.3.4 Particulate nitrogen and its isotopic composition.....	123
4.3.3.5 Dissolved CH ₄ , CO ₂ , and N ₂ O.....	124
4.3.4 Discussion.....	126
4.3.4.1 Dissolved inorganic carbon biogeochemistry in the Jhelum River	126
4.3.4.2 Particulate matter dynamics along the river – lake continuum	127
4.3.4.3 Dissolved CH ₄ , CO ₂ , and N ₂ O.....	131
4.3.5 Conclusion	132
5. Particulate black carbon in aquatic systems	133
5.1 Transport and transformation of particulate black carbon in rivers	135
5.1.1 Sampling.....	135
5.1.2 Results and Discussion	137
5.1.2.1 Distribution of particulate black carbon in the river basins	137
5.1.2.2 Transformation of particulate black carbon in rivers	138
5.1.2.3 Transformation of PBC in engineered aquatic systems	140
5.1.2.4 Export fluxes and yields of particulate black carbon	142

5.1.3 Conclusions	142
5.2 Isotopic evidence for aging of particulate black carbon in the ocean	143
5.2.1 Sampling.....	143
5.2.2 Results	144
5.2.3 Discussion.....	146
5.2.3.1 Abundance and isotopic composition of PBC	146
5.2.3.2 Sources of PBC to the open ocean.....	146
5.2.3.3 Aging of PBC in ocean water	148
5.2.3.4 Significance of particulate black carbon in ocean C biogeochemistry	149
5.2.4 Conclusion	150
6. Summary and scope for future research	151
6.1 Summary	152
6.1.1 Lake biogeochemistry (freshwater and saline).....	152
6.1.2 River biogeochemistry.....	152
6.1.3 Particulate black carbon in aquatic systems	153
6.2 Scope for future research	154
References	155
List of Publications.....	183
Associated with thesis work.....	183
Publications through collaborative projects	183
Presentations at Conferences and Meetings	184

List of Tables

Table 2.1 Aquatic systems, sampling period, and measured parameters associated with individual thesis chapter (and sections).	36
Table 3.1 Basic sediment properties. SWC and SOM are sediment water content and sediment organic matter, respectively. $\delta^{13}\text{C}_{\text{SOM}}$ and $\delta^{15}\text{N}_{\text{TN}}$ are the stable carbon and nitrogen isotopic compositions of sediment organic matter and total nitrogen, respectively.	65
Table 4.1 Length, basin area, and annual discharge of the Ganges, Mekong, and the Yellow River systems.	90
Table 4.2 Concentrations, annual fluxes and yields of suspended particulate carbon and nitrogen in some Asian rivers. TSM, POC and PN values shown from the present study represents median concentrations of selected downstream locations [Ganges (Dry): G9 and G12; Ganges (Wet): G8, G9, G10 and G11; Mekong (Dry and Wet): M8 and M9; and Yellow (Wet): Y6].	92
Table 5.1 Summary of the least-square linear regression model equations in the Miller-Tans plots for PBC presented in Fig 5.7a with the parameters of the linear equation along with standard error in brackets for the slope, R^2 , and number of observations (n). An approximation of the $\delta^{13}\text{C}$ source values can be deduced from the slope of the Miller-Tans equation.....	148

List of Figures

Fig. 1.1 Simplified schematic of the aquatic carbon cycle.	24
Fig. 1.2 Simplified schematic of the aquatic nitrogen cycle.	26
Fig. 2.1 Map showing study areas. Shaded areas represent river basins and squares (red) are lakes sampled for the present study. Light grey denote the stations in the northern Indian Ocean and estuarine region from where already collected samples were analyzed for particulate black carbon.	35
Fig. 2.2 Picture of the (a) ion chromatography, (b) autoanalyzer, (c) gas bench –IRMS (MAT 253), (d) coulometer, (e) elemental analyzer, (f) IRMS (Delta V Plus), (g) gas chromatography, and (h) cavity ring down spectroscopy (Picarro) at the Physical Research Laboratory (PRL), India. These instruments are regularly used, including for this thesis, to generate data at PRL.	38
Fig. 3.1 Map of Nalsarovar showing sampling locations (white circles).	46
Fig. 3.2 Seasonal variability in lake water depth (shaded) and precipitation (bar charts). Sampling campaigns are denoted by dark red squares.	47
Fig. 3.3 Box-Whisker plots showing seasonal variation in (a) Temperature, (b) pH, (c) Conductivity and (d) $\delta^{18}\text{O}$ of lake water. Solid black line indicates the mean values.	48
Fig. 3.4 Seasonal variations in major cations and anions in the lake.	49
Fig. 3.5 Seasonal variation in (a) dissolved inorganic carbon (DIC), (b) $\delta^{13}\text{C}_{\text{DIC}}$, (c) particulate organic carbon (POC), (d) $\delta^{13}\text{C}_{\text{POC}}$, (e) particulate nitrogen (PN), and (f) $\delta^{15}\text{N}_{\text{PN}}$. Solid red lines indicate the mean values.	50
Fig. 3.6 Carbon and nitrogen isotopic composition of different organic matter pools in the lake. The symbols and lines indicate mean \pm stdev. The black square shows the source isotopic signature of organic matter deduced through graphical mixing model.	51
Fig. 3.7 Seasonal variation in concentrations and isotopic compositions of dissolved gases: (a) CH_4 , (b) $\delta^{13}\text{C}_{\text{CH}_4}$, (c) CO_2 , (d) $\delta^{13}\text{C}_{\text{CO}_2}$, and (e) N_2O . Solid red lines indicate the mean values.	53
Fig. 3.8 Relationship between DIC and $\delta^{13}\text{C}_{\text{DIC}}$ in (a) October, (b) February, and (c) August.	54
Fig. 3.9 Seasonal variation in the C/N ratio of particulate organic matter. Solid black lines indicate the mean values.	55
Fig. 3.10 PCA of measured parameters in Nalsarovar during different seasons.	57
Fig. 3.11 Miller Tans plots for (a) CO_2 and (b) CH_4 . Symbols with red outline indicate source isotopic signatures. The detailed statistics are provided in Table 3.1.	58
Fig. 3.12 (a) Study area and sampling locations (Sambhar salt lake, Rajasthan, India), (b) lake during winter, (c) lake during monsoon, (d) brine reservoir during winter, (e) brine reservoir during monsoon, (f) salt flats, and (g) salt pans. n represents the number of sampling locations during winter (W) and monsoon (M).	62

Fig. 3.13 Relationship between $\delta^{18}\text{O}$ and conductivity. Empty and filled symbols represent winter (W) and monsoon (M) samples, respectively. The $\delta^{18}\text{O}$ values are denoted in permil notation (‰) and conductivity is millisiemens per cm.....	64
Fig. 3.14 Relationship between NO_3^- and NH_4^+ during winter (W) and monsoon (M). Empty and filled symbols represent winter (W) and monsoon (M) samples, respectively.	66
Fig. 3.15 Relationship between dissolved inorganic carbon (DIC) and $\delta^{13}\text{C}_{\text{DIC}}$ during winter (W) and monsoon (M). Empty and filled symbols represent winter (W) and monsoon (M) samples, respectively.	67
Fig. 3.16 Seasonal variation in the (a) particulate organic carbon (POC), (b) particulate organic nitrogen (PON) and (c) C/N ratios in different sample classes. Winter and monsoon seasons are represented by light grey and dark grey shades respectively....	68
Fig. 3.17 Relationship between C and N isotopic composition of POM ($\delta^{13}\text{C}_{\text{POM}}$ and $\delta^{15}\text{N}_{\text{POM}}$) during winter (W) and monsoon (M). Empty and filled symbols represent winter (W) and monsoon (M) samples, respectively.	72
Fig. 4.1 Map showing sampling locations on the Ganges, Mekong, and Yellow River Basins (shaded).	78
Fig. 4.2 Variation of TSM, C/N, POC, $\delta^{13}\text{C}_{\text{POC}}$, PN and $\delta^{15}\text{N}_{\text{PN}}$ along the mainstem of Ganges (a, b, and c), Mekong (d, e, and f) and Yellow River (g, h, and i). Shaded area represents TSM, POC and PN in wet (blue) and dry (dark green) seasons respectively. Circles connected by solid lines represent C/N, $\delta^{13}\text{C}_{\text{POC}}$ and $\delta^{15}\text{N}_{\text{PN}}$ in wet (black circles) and dry (white circles) seasons. In Yellow river, dry seasons data is represented by scatter plot (dark green square and white circle).	80
Fig. 4.3 Correlation plots between measured parameters in the three river systems. The coefficient of correlation was derived from Spearman rank correlation (Circles) and Pearson's correlation (Squares). The coefficient of correlation (R) is shown in the figure ($p < 0.05$).....	84
Fig. 4.4 Graphical mixing model for tracking the sources of OC and N in TSM. Significant regressions obtained for OC in the (a) Ganges, (b) Mekong, and (c) Yellow River. Source organic matter isotopic signatures are shown by the slope of the regression. The regressions for wet seasons are bounded by a rectangular box. For the Yellow River, due to low sample size in the dry seasons, we used the data from Qu et al., 2020 for seasonal comparison. This graphical mixing model failed to distinguish the source signature of N except for (e) Mekong during the wet season (source $\delta^{15}\text{N}_{\text{PN}} = 9.1$ ‰).....	86
Fig. 4.5 Seasonal variation in (a) TSM, (b) C/N ratios, (c) % OC, (d) % N, (e) $\delta^{13}\text{C}_{\text{POC}}$ and (f) $\delta^{15}\text{N}_{\text{PN}}$. Red lines show mean values. Significant difference ($p < 0.001$) between the median TSM values were observed across seasons and river basins. The whole range of TSM were significantly different ($p < 0.05$) among Mekong (Dry) and Mekong (Wet). Similarly, median C/N were significantly different among different sample classes ($p < 0.001$). During each season, the whole range of C/N values were higher for the Mekong as compared to the Ganges ($p < 0.05$). Median values were significantly different in (c) with $p < 0.005$ and (d) $p < 0.05$. Median $\delta^{13}\text{C}_{\text{POC}}$ and $\delta^{15}\text{N}_{\text{PN}}$ were significantly different among each class ($p < 0.005$). The letters L, M and U represents sites from the lower, middle and upper reaches respectively.	89

Fig. 4.6 Study area and sampling locations in different sample classes (shown in the legend). The blue line represents the portion of the lined canal (Narmada Canal) flowing through the Sabarmati and Mahi River basins.....	95
Fig. 4.7 Field photographs of various sample classes defined for the present study... 96	
Fig. 4.8 (a) pH and (b) temperature in different sample classes. Blue and Grey represent high flow and low flow periods, respectively.....	97
Fig. 4.9 (a) Conductivity and (b) dissolved oxygen in different sample classes. Blue and Grey represent high flow and low flow periods, respectively.	98
Fig. 4.10 (a) Nitrate and (b) ammonium in different sample classes. Blue and Grey represent high flow and low flow periods, respectively.	99
Fig. 4.11 Dissolved inorganic carbon (DIC) (a) concentrations and (b) isotopic compositions in different sample classes. Blue and Grey represent high flow and low flow periods, respectively.	101
Fig. 4.12 Particulate organic carbon (POC) (a) concentrations and (b) isotopic composition in different sample classes. Blue and grey colour represent high flow and low flow periods, respectively.	102
Fig. 4.13 Particulate nitrogen (PN) (a) concentrations and (b) isotopic compositions in different sample classes. Blue and grey colour represents high flow and low flow periods respectively.	103
Fig. 4.14 Dissolved (a) CH ₄ , (b) CO ₂ , and (c)N ₂ O in different sample classes. Blue and grey colours represent high flow and low flow periods, respectively. For Sabarmati downstream, CH ₄ concentrations are shown by separate Y axis in red colour.....	104
Fig. 4.15 Relationships between DIC and $\delta^{13}\text{C}_{\text{DIC}}$ during (a) high flow and (b) low flow periods.....	106
Fig. 4.16 Correlation plots (Spearman Rank and *Pearsons) among measured parameters with significance level $p < 0.05$ during (a) high flow and (b) low flow periods.....	107
Fig. 4.17 C/N ratio in particulate matter in different sample classes. Blue and grey colour represents high flow and low flow periods respectively.	108
Fig. 4.18 Relationship between POC and $\delta^{13}\text{C}_{\text{POC}}$ during (a) high flow and (b) low flow periods.....	108
Fig. 4.19 Relationship between PN and $\delta^{15}\text{N}_{\text{PN}}$ during (a) high flow and (b) low flow periods. The PN concentration of Sabarmati Downstream is shown by a separate axis in red color.	109
Fig. 4.20 Spatial variability of emission fluxes of CH ₄ , CO ₂ , and N ₂ O during high flow (a, c, and d) and low flow (b, d, and f) periods.....	113
Fig. 4.21 Sampling locations in the Jhelum River basin in the Kashmir Valley.....	116
Fig. 4.22 Sampling locations in the Jhelum River basin in the Kashmir Valley.....	117
Fig. 4.23 (a) pH, (b) temperature, and (c) conductivity in the different stretches of the Jhelum River system and the Wular Lake during spring.....	119

Fig. 4.24 (a) Dissolved inorganic carbon concentrations (mM) and (b) stable isotopic composition of DIC in the different stretches of the Jhelum River system and Wular Lake.....	120
Fig. 4.25 (a) Concentration (μM) and (b) isotopic composition of particulate organic carbon along the mainstem and tributaries of the Jhelum and the Wular Lake.	122
Fig. 4.26 (a) Concentration (μM) and (b) isotopic composition of particulate nitrogen along the mainstem and tributaries of Jhelum and the Wular Lake.....	123
Fig. 4.27 (a) CH_4 , (b) CO_2 , and (c) N_2O concentrations along the mainstem and tributaries of Jhelum river and the Wular Lake.	125
Fig. 4.28 Relationships between DIC and $\delta^{13}\text{C}_{\text{DIC}}$ in (a) spring and (b) autumn.....	127
Fig. 4.29 Correlation plots (Spearman; $p < 0.05$) between measured parameters along the Jhelum mainstem and tributaries during (a) spring and (b) autumn.	128
Fig. 4.30 Correlation plots (Spearman; $p < 0.05$) between measured parameters in the Wular lake during (a) spring and (b) autumn.....	129
Fig. 4.31 C/N ratios of particulate matter in different sample classes.....	130
Fig. 4.32 Scatter plot showing relationship between particulate organic carbon and its isotopic composition during (a) spring and (b) autumn.....	130
Fig. 4.33 Scatter plot showing relationship between particulate nitrogen and its isotopic composition during (a) spring and (b) autumn.	131
Fig. 5.1 (a) Existing studies on particulate black carbon in riverine particulate matter, (b) the present study area representing the river basins, (c – g) locations of samples analyzed for particulate black carbon in the six river basins.	136
Fig. 5.2 Bulk particulate organic carbon (POC + PBC; Green boxes –left axis) and PBC (Black boxes – right axis) in Sabarmati, Mahi, and Narmada Canal during (a) Oct 2020 (high flow) and (c) Feb 2021 (low flow); Ambika, Girna, Banas and Berach during (b) Nov 2021 (post-monsoon) and (d) Aug 2022 (monsoon). Both sampling periods in Ambika, Girna, Banas and Berach represented high flow condition.....	137
Fig. 5.3 % PBC in the (a) Sabarmati, Mahi and Narmada Canal during Oct 2020 (High flow) and Feb 2021 (Low flow), and (b) Ambika, Girna, Banas and Berach rivers during Nov 2021 (Post monsoon) and Aug 2020 (Monsoon). $\delta^{13}\text{C}$ of bulk particulate organic carbon (POC + PBC) and PBC in Sabarmati, Mahi and Narmada Canal during (c) Oct 2020 and (d) Feb 2021; Ambika, Girna, Banas and Berach during (e) Nov 2021 and (f) Aug 2022. Both sampling periods in Ambika, Girna, Banas and Berach represented high flow condition.	139
Fig. 5.4 Spearman and Pearsons correlation (shown by †) between (a) distance from the river mouth and PBC, $\delta^{13}\text{C}_{\text{PBC}}$ and % PBC, and (b) PBC and $\delta^{13}\text{C}_{\text{PBC}}$ in different classes during sampling period. * shows correlations with $p < 0.05$. (c) Conceptual figure showing the process dynamics of PBC in each sample classes (SU = Sabarmati Upstream; SD = Sabarmati Downstream; RF = Riverfront; ST = Sabarmati Tributaries; NC = Narmada Canal; M = Mahi; LF = Low flow; HF = High flow).	141
Fig. 5.5 Map of existing studies on oceanic particulate black carbon. Circles numbered 1 – 7 represent the locations with PBC concentrations in μM (1: Fang et al. 2021; 2: Mari et al. 2017; 3: Flores-Cervantes et al. 2009; 4: Yang and Guo 2014; 5,6,7: Fang et al. 2016). The shaded box represents the present study region.	143

Fig. 5.6 Sampling locations showing the concentrations and isotopic compositions of particulate black carbon in the (a) northern Indian Ocean, (b) Mahanadi Estuary, and (c) Andaman Creeks. The average concentration and isotopic composition of PBC in the downstream reach of Sabarmati, along with Mahi and Ambika rivers are also shown by circles. The size of the circles denotes the concentration of PBC in μM and the labels denote the isotopic compositions in permil (‰). Sampling locations for atmospheric particulate matter are denoted by blue squares. 145

Fig. 5.7 (a) Miller Tans Plot for particulate black carbon (PBC). The slope of the regression represents the $\delta^{13}\text{C}_{\text{PBC}}$ of the source. The equations and statistics for each regression is shown in Table 5.1, (b) box – whisker plot showing the relative change is $\delta^{13}\text{C}_{\text{PBC}}$ between the calculated $\delta^{13}\text{C}_{\text{PBC}}$ of source (from Miller Tans Plot) and the observed values of $\delta^{13}\text{C}_{\text{PBC}}$ 147

Fig. 5.8 Scatter plot of PBC and $\delta^{13}\text{C}_{\text{PBC}}$ showing shift in concentration and isotopic composition from riverine to marine environment. For Sabarmati being an engineered river, samples from the downstream reach are considered. 149

List of Abbreviations

$\delta^{13}\text{C}$	Isotopic composition of carbon with respect to V-PDB
$\delta^{15}\text{N}$	Isotopic composition of nitrogen with respect to Air-N ₂
‰	Per mill (parts per thousand)
μM	Micromole per litre
μm	Micrometre
AS	Arabian Sea
AnS	Andaman Sea
BC	Black carbon
BoB	Bay of Bengal
C	Carbon
CH ₄	Methane
CO ₂	Carbon dioxide
CO ₃ ⁻	Carbonate
DBC	Dissolved black carbon
DIC	Dissolved inorganic carbon
DIN	Dissolved inorganic nitrogen
DNRA	Dissimilatory nitrate reduction to ammonium
DO	Dissolved oxygen
DOC	Dissolved organic carbon
DOM	Dissolved organic matter
DON	Dissolved organic nitrogen
EC	Electrical conductivity
ECD	Electron capture detector
FID	Flame ionization detector
GHGs	Greenhouse gases
HCO ₃ ⁻	Bicarbonate
IAEA	International Atomic Energy Agency
IPCC	Intergovernmental Panel on Climate Change
IRMS	Isotope-ratio mass spectrometry
N	Nitrogen
NH ₄ ⁺	Ammonium
nM	Nanomole per litre

N ₂ O	Nitrous Oxide
NO ₃ ⁻	Nitrate
NO ₂ ⁻	Nitrite
OM	Organic matter
PBC	Particulate black carbon
Pg	Petagram
PIC	Particulate inorganic carbon
POC	Particulate organic carbon
POM	Particulate organic matter
PN	Particulate nitrogen
PM	Particulate matter
ppb	Parts per billion
ppm	Parts per million
PRL	Physical Research Laboratory
SOM	Soil/sediment organic matter
T	Temperature
TCD	Thermal conductivity detector
Tg	Teragram
TSM	Total suspended matter
VPDB	Vienna PeeDee Belemnite

Chapter 1

Introduction

Carbon (C) and nitrogen (N) are essential elements that form the basis of all life forms on the Earth. The pathways of movement and cycling of these elements in the environment is termed as biogeochemical cycles. The cycling of different elements is interlinked by complex transformations mediated by microorganisms. The movement of these elements from one pool to another is controlled by several environmental factors and the bioavailability of these elements ultimately supports life. Although abundant in the Earth's atmosphere as N_2 gas (78 %), N largely acts as limiting nutrient for biological productivity due to limited availability of reactive N species (Dugdale and Wilkerson, 1992; Doering et al., 1995). Similarly, carbon dioxide (CO_2) in the atmosphere is vital for photosynthesis, which is the key source of energy for various food webs. C and N in the environment exist in various pools and each has its significance and environmental footprint. For instance, methane (CH_4), CO_2 , and nitrous oxide (N_2O) act as major greenhouse gases (GHGs) that are responsible for the warming of the atmosphere (Ciais et al., 2014). The residence time of these gases in the atmosphere is governed by the balance between sources and sinks across various reservoirs (terrestrial and aquatic). The inter – governmental panel on climate change (IPCC) has been synthesizing the reports from various working groups to constrain the budgets of GHGs (Solomon, 2007; Stocker, 2014; Masson – Delmotte et al., 2021). It is observed that the atmospheric CO_2 concentration has increased from ~ 278 part per million (ppm) in 1750 to 414.7 ± 0.1 ppm in 2021 (Gulev et al., 2021; Dlugokencky and Tans, 2022; Friedlingstein et al., 2022). Similarly, the atmospheric CH_4 concentrations reached 1857 parts per billion (ppb) in 2018, which is 2.6 times the estimated equilibrium value in 1750 (Ciais et al., 2014; Saunio et al., 2020). The atmospheric N_2O concentrations has increased from 275 ppb during preindustrial era to 329 ppb in 2015 (Forster et al., 2007; Davidson, 2009; Xu et al., 2017). The major sources of GHGs to the atmosphere are both natural [such as inland waters (rivers and lakes), wetlands, oceans, and soils] and anthropogenic like deforestation (and other land use changes), fossil fuel combustion, expansion of agricultural land and subsequent use of N fertilizers, and biomass burning (Galloway et al., 2004; Reay et al., 2012; Canadell et al., 2021).

Although it is well known that human activities are the primary cause for the drastic increase in atmospheric GHGs, including CO_2 , CH_4 , and N_2O , since the pre-industrial period (Ciais et al., 2014), natural systems are found to be much more

complex in terms of their role in mitigating or enhancing the climate crisis. Terrestrial systems along with the global ocean act as net sink of atmospheric CO₂ (~ 5.3 PgC yr⁻¹ and ~1.9 PgC yr⁻¹, respectively) (Masson – Delmotte et al., 2021). However, a major fraction (~ 2.5 PgC yr⁻¹) of the C sequestered by the land gets mobilised and ends up in the inland waters. Inland waters process most of this C resulting in an emission flux of 1.5 PgC yr⁻¹ and the remaining portion gets exported to the ocean (0.8 PgC yr⁻¹) or gets buried for longer timescales (0.2 PgC yr⁻¹) (Masson – Delmotte et al., 2021). The C burial potential of inland waters are disproportionately higher than the global oceans (C burial rate = 0.2 PgC yr⁻¹) considering the larger reservoir size of the later. Even after decades of research, there is still paucity of data for the stocks of different pools of C in the inland waters (otherwise relatively well constrained for terrestrial and oceanic systems). In case of N, the knowledge gap is even larger with no mention of burial rates and evasion fluxes from lakes in the IPCC Sixth Assessment Report (Masson – Delmotte et al., 2021). Recent studies have estimated the global N₂O emissions from inland waters to be ~ 10.6 – 19.8 G mol N yr⁻¹, with man-made reservoirs having the highest contribution (Maavara et al., 2018).

Inland waters comprise of diverse aquatic systems including both lotic (rivers and canals) and lentic (lakes and reservoirs) waterbodies. The total storage volume of global lakes is estimated to be ~ 181 × 10³ km³ of which 85 × 10³ km³ are saline in nature (Williams, 2002; Messenger et al., 2016). This reservoir capacity of global lakes is reducing at an alarming rate due to climate change and human perturbations (Yao et al., 2023). Similarly, the spatial extent and annual discharge of rivers and canals are highly dynamic and depends on recharge and level of human interventions. The huge spectrum of inland water bodies in terms of storage, catchment influence, physical and biogeochemical characteristics, and level of human induced changes makes it difficult and at the same time crucial to understand the nature of C and N biogeochemistry in these waterbodies. Below a brief description of aquatic C and N cycles is discussed, including an emerging domain of black carbon (BC) research in aquatic sciences.

1.1 Aquatic carbon cycle

Aquatic systems are hotspots for transformation of C among its various pools, which broadly include dissolved organic carbon (DOC), dissolved inorganic carbon (DIC), dissolved black carbon (DBC), particulate organic carbon (POC), particulate inorganic

carbon (PIC) and particulate black carbon (PBC). The sources of C in aquatic systems could be from outside the system [allochthonous (POC, DIC, DOC and soil organic carbon (SOC))] or produced *in situ* (autochthonous) (Fig 1.1). Once the C enters the aquatic system, it undergoes transformation depending on its residence time within the aquatic body and favourable environmental conditions. The rates of transformation are dependent on the microbial community composition, organic matter (OM) – mineral association, redox state, ambient oxygen levels and other factors (Richey et al., 2002; Keil and Mayer, 2014; Dittmar, 2015; Ward et al., 2017). However, the residence time of OM is less in inland water (2.5 ± 4.7 years) as compared to that in soils, oceans, and sediments (centennial to millennial; Catalan et al., 2016).

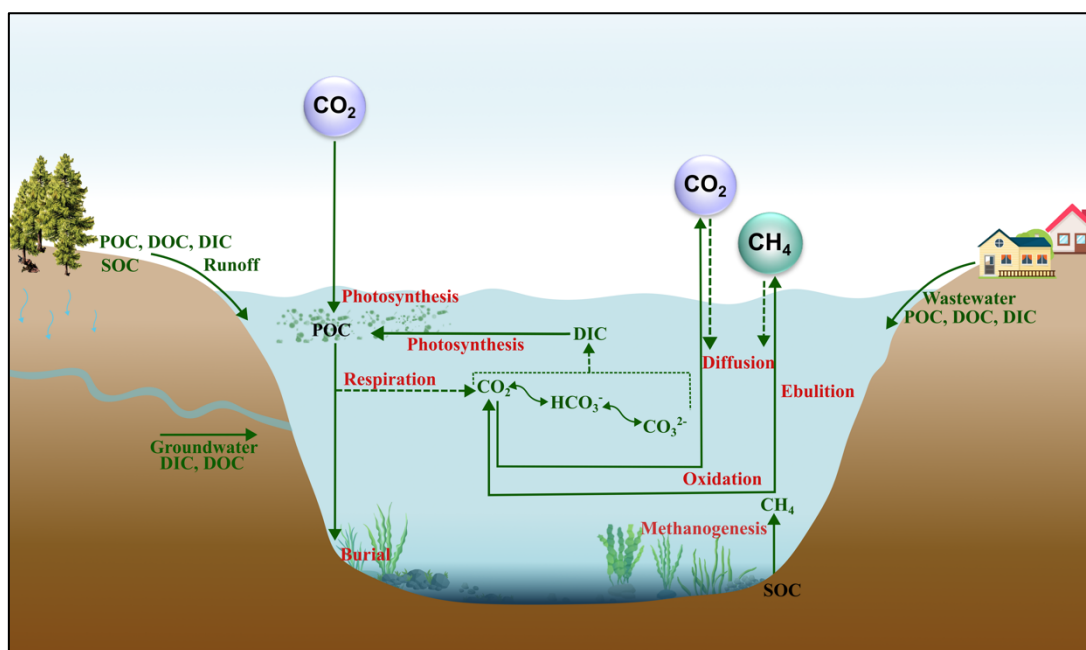


Fig. 1.1 Simplified schematic of the aquatic carbon cycle.

During photosynthesis, phytoplankton takes up C from DIC pool and produces organic molecules. Alternatively, surface blooms can directly sequester atmospheric CO_2 (Gu & Alexander, 1993; Zohary et al., 1994; Kiyashko et al., 1998). The primary productivity in aquatic systems is controlled by dissolved inorganic nitrogen [DIN: nitrate (NO_3^-), nitrite (NO_2^-) and ammonium (NH_4^+)] availability, light availability, water temperature, salinity, etc. Once C is fixed as particulate organic matter (POM), it stays in the system and eventually dies and starts to settle, during which mineralisation takes place and organic carbon (OC) is converted back to inorganic C by the release of CO_2 (Fig 1.1). The released CO_2 drives the carbonate chemistry and is coupled with the pH of the system. The remaining OM settles down to the sediments to either get further

mineralised or converted to CH₄ via the process of methanogenesis, or gets buried for longer timescales (Mendonca et al., 2017). The estimated rates of organic C burial in global lakes and reservoirs is $\sim 0.15 \text{ Pg C yr}^{-1}$ (Mendonca et al., 2017). The CH₄ produced in the sediments under sub – oxic/anoxic conditions gets removed from the water column by diffusion across the water – air interface and/or ebullition (as bubbles), the latter being an event process (Bastviken et al., 2004). The open water emission rates are affected by lake area, DOC, water depth, and the fraction of anoxic lake volume (Bastviken et al., 2004). The CH₄ in the water column during its transport and storage, can get oxidised to CO₂ and contribute to the inorganic C pool (Langenegger et al., 2022). Studies have observed coupling of CH₄ oxidation to oxic photosynthesis in anoxic waters (Milucka et al., 2015). The emission of CO₂ and CH₄ from the aquatic system is a significant loss mechanism of aquatic C.

Apart from the pools of C discussed above, BC which is a residue of incomplete combustion of OM is ubiquitous in nature. BC comprises of a whole spectrum from labile char to refractory soot (Goldberg, 1985; Coppola et al., 2022). The major sources of BC in the environment are wildfires, forest fires, biomass burning and fossil fuel combustion. After production, BC stays in the atmosphere for a shorter duration (Residence time of ~ 14 days) and most of it is sequestered in soils around the fire site (Coppola et al., 2022). Once mobilised, BC enters aquatic systems via surface runoff, rivers, and streams. Atmospheric deposition is also a major source of aquatic BC. Aquatic BC exists in two major pools (particulate and dissolved) which are defined according to measurement protocols (cut off size varies from 0.2 – 0.7 μm). Aquatic BC undergoes transformation via photodegradation and leaching, and sometimes photo flocculation to form bigger particles (Wagner et al., 2015, 2019; Coppola et al., 2022). A major portion of the aquatic BC pool eventually gets sequestered in the sediments to be stored for timescales ranging from centuries to millennia (Coppola et al., 2022).

1.2 Aquatic nitrogen cycle

The aquatic N cycle encompasses two vital aspects (i) input/output of reactive N and (ii) processes transforming the reactive N into its various forms (Fig 1.2). Nitrogen in aquatic system has multiple sources, mainly by direct atmospheric fixation by the diazotrophs which are a specialised group of prokaryotes, and allochthonous input via surface runoff and atmospheric deposition. Inorganic N is assimilated by primary

producers during photosynthesis to form OM (Leigh & Dodsworth, 2007; Fellbaum et al., 2012; Xu et al., 2012; Gilbert et al., 2016). Assimilation of NH_4^+ is usually preferred over NO_3^- at low DIN concentrations due to less energy requirements by phytoplankton (Wang & Macko, 2011; Schlesinger & Bernhardt, 2013; Gilbert et al., 2016; Xu et al., 2019). Similar to that in the C cycle, the OM later decompose to release NH_4^+ and/or get settled to the lake/river bottom. The process of mineralisation involves physical disintegration of particulate matter, solubilisation, and formation of dissolved organic nitrogen (DON) which then undergoes deamination to release NH_4^+ (Zhang et al., 2020). The released NH_4^+ gets oxidised to NO_3^- by chemoautotrophic microbes and at low dissolved oxygen (DO) levels, N_2O is produced during the process of nitrification (Stein, 2019). Recent studies have identified a group of proteobacteria which are involved in complete oxidation of NH_4^+ to NO_3^- by the processes of Comammox (Daims et al., 2015; Van Kessel et al., 2015). The reverse mechanism for the conversion of NO_3^- to NH_4^+ is termed as dissimilatory nitrate reduction to ammonium (DNRA) and is mediated by chemoautotrophs (Kamp et al., 2015; Kuypers et al., 2018). These microbes compete with denitrifiers for NO_3^- and OM (King and Nedwell, 1985). The major loss process of fixed N from aquatic system is denitrification, which converts NO_3^- to N_2 as the final product and N_2O as an intermediate product. Overall, anoxic conditions favour the process of denitrification (Zhang et al., 2020).

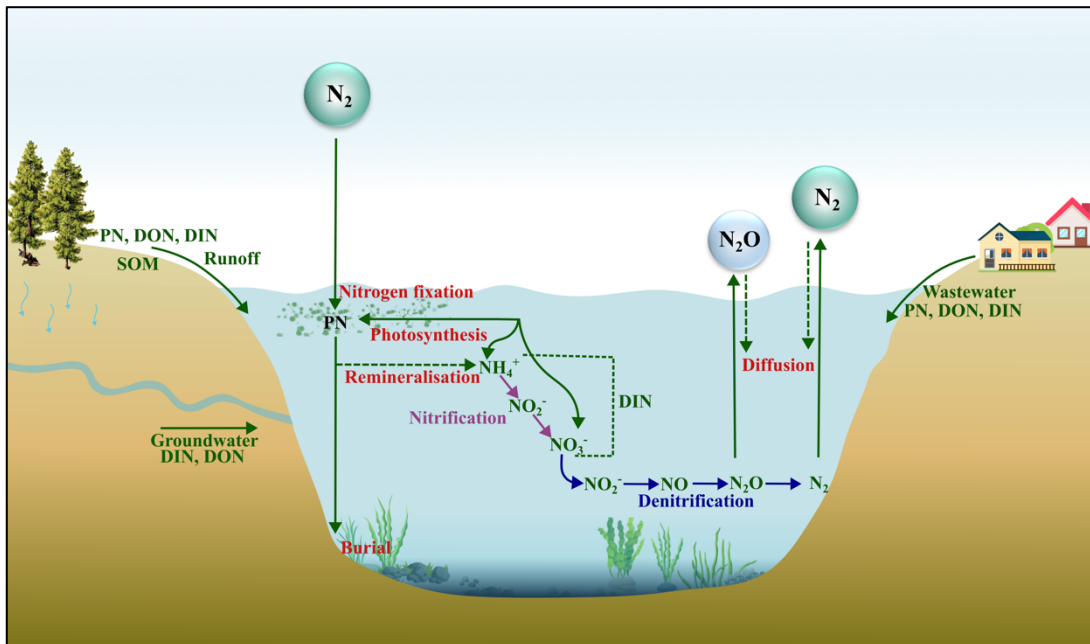


Fig. 1.2 Simplified schematic of the aquatic nitrogen cycle.

1.3 Application of stable isotopes in C and N biogeochemistry

To understand the nature of C and N cycling in aquatic systems, researchers have employed a wide variety of methods including basic analytical chemistry to quantify the pools of C and N, estimating the diversity and abundance of microbial communities, and applying physical models to estimate gas diffusivity. Stable isotopes of C and N, a primary tool employed in this thesis, have proven to be crucial to understand the biogeochemical processes in aquatic system. The isotopic composition of an element is denoted by the ‘ δ ’ notation expressed in per mil (‰),

$$\delta = \left(\frac{R_{sample}}{R_{standard}} - 1 \right) \times 1000$$

where R is the ratio of heavier to lighter isotope (Fry, 2006).

In the environment, the flow of elements from one pool to another experiences an associated fractionation in their stable isotopic composition. The average $\delta^{13}\text{C}$ of atmospheric CO_2 is ~ -8 ‰, which is getting even more depleted in ^{13}C due to large inputs of lighter C (^{12}C) from fossil fuel combustion. C_3 and C_4 plants take up atmospheric CO_2 during photosynthesis and there is an associated fractionation of ~ 20 ‰ and ~ 5 ‰, respectively. Therefore, C_3 and C_4 plants across the globe has a range of isotopic composition of ~ -32 to -22 ‰ and -14 to -9 ‰, respectively (Ehleringer et al., 1978, 1983). Similarly, aquatic algae taking up DIC has $\delta^{13}\text{C}$ in the range of -19 ‰ to -24 ‰. The C isotopic signatures of freshwater macrophytes and plankton range between -28 to -18 and -42 to -24 ‰, respectively (Kendall et al., 2001). The isotopic signatures of soil/sediment organic matter (SOM) reflect that of the dominant vegetation over the region (Bouttan, 1996).

The N isotopic signatures of SOM in most soils vary between $+2$ to $+5$ ‰, with cultivated soils showing lower values (Broadbent et al., 1980). $\delta^{15}\text{N}$ of atmospheric N is ~ 0 ‰, and during N_2 fixation by diazotrophs there is negligible fractionation resulting in ~ 0 ‰ isotopic composition of POM. During assimilation of DIN, the POM incorporates the isotopic signatures of NH_4^+ and NO_3^- . These values are widely used as end member values to calculate the fraction contribution to SOM from different C sources (autochthonous vs allochthonous) (Meybeck, 1982; Pocklington and Tan, 1987; Louchouart et al., 1997; 1999; Hopkinson et al., 1998). Apart from indicating the source of OM, the $\delta^{13}\text{C}_{\text{POM}}$ and $\delta^{15}\text{N}_{\text{POM}}$ reflect the seasonal dynamics of *in-situ*

biogeochemical processes like nutrient uptake and decomposition/respiration. For example, when there is a seasonal increase in $\delta^{13}\text{C}_{\text{POM}}$ and C/N ratios of POM, it could be an indicative of high growth period (Lehmann et al., 2004; Gu et al., 2011). For other pools of C, such as DIC, high $\delta^{13}\text{C}$ indicates high C uptake or enhanced CO_2 degassing, whereas low $\delta^{13}\text{C}$ indicates high OM degradation supplying isotopically depleted CO_2 . Through stable isotopic analysis, it is also possible to infer the prevalence of autochthonous POM and its dependency on bicarbonate (HCO_3^-) as a C source resulting in higher $\delta^{13}\text{C}$. In case of N, low $\delta^{15}\text{N}$ of POM indicates either the dominance of N_2 fixers or the influence of synthetic fertilizers, whereas high $\delta^{15}\text{N}$ of POM can be an indicative of human waste influence (Gu et al., 2009; Kopprio et al., 2014). The $\delta^{13}\text{C}$ of CO_2 and CH_4 indicates the various in lake/stream processes governing their production and consumption. The average $\delta^{13}\text{C}_{\text{CO}_2}$ and $\delta^{13}\text{C}_{\text{CH}_4}$ of dissolved CO_2 and CH_4 is $\sim -18\text{‰}$ and $\sim -60\text{‰}$, respectively (Begum et al., 2021). The depleted signatures are due to preferential release of lighter C from OM during degradation and methanogenesis. During CH_4 oxidation, the CO_2 pool gets isotopically depleted and the CH_4 pool gets enriched. Therefore, the use of stable isotopes in greenhouse gas studies becomes important to decipher the pathways of transformation.

1.4 Carbon and nitrogen biogeochemistry in inland waters of India: Current understanding

Given its vast geographical expanse and diversity, the inland waters of India have not been explored in detail, particularly with regards to cycling of C and N. Limited existing studies have largely focused on CH_4 , CO_2 , and N_2O dynamics in polluted waterbodies. Begum et al. (2021) explored the CH_4 , CO_2 , and N_2O dynamics in the Ganges, Mekong and Yellow river. They observed that polluted streams in the Ganges and Mekong had high levels of CO_2 and CH_4 . During low flow period, CO_2 , CH_4 , and N_2O were 1.6, 2, and 7 times higher than that in monsoon, respectively. Dissolved organic matter (DOM) and optical properties showed significant positive correlation with GHGs, implying effect of pollution on GHGs production. Similarly, Pickard et al. (2021) observed high emission of GHGs from two urban lakes, Jakkur and Bellandur in Bangalore, India. They observed that Bellandur Lake which was severely impacted by pollution had GHGs emission of $1,48,350 \pm 21,790 \text{ ton yr}^{-1} \text{ CO}_2$ equivalent. Another study observed the effects of pharmaceuticals and human induced water quality degradation on the supersaturation of CO_2 and CH_4 in the Cauvery River in southern India (Premke et al.,

2020). A recent work in the Kaveri River basin by Patel et al. (2023) observed that built up was the most crucial factor driving CH₄ emissions in an otherwise agriculture dominated watershed. The CH₄ fluxes were higher in urban river sites (294.15 ± 371.52 mmol m² d⁻¹) as compared to agricultural and forested sites (3.45 ± 9.72 mmol m² d⁻¹ and 1.26 ± 0.73 mmol m² d⁻¹, respectively). The most extensive work so far on estimating the GHGs emissions from inland waters of India was carried out by Selvam et al. (2014) in 45 waterbodies (lakes, rivers, reservoirs, wells and canals) in southern India. They measured both diffusive and ebullitive fluxes of CH₄ and CO₂. The estimated flux of CH₄ ranged from 0.01 – 52.1 mmol m⁻² d⁻¹ and CO₂ ranged from – 28.2 – 262.4 mmol m⁻² d⁻¹.

Other than CH₄ and CO₂, studies have also focused on the other pools of C. Reddy et al. (2019; 2021) quantified the export fluxes of DIC and POC from 70 mountainous rivers draining the western Ghats of India. They observed significant control of lithology, climate and sediment yields on the DIC export. POC was mostly derived from litter/riparian and autochthonous production. Chakrapani and Veizer (2005) and Das et al. (2005) studied the dynamics of DIC in Ganges and rivers draining the Deccan traps, respectively, using stable isotopic measurements. Furthermore, they explored the sources of DIC and weathering patterns in these rivers. Overall, there is scattered literature exploring the cycling of C and N in the inland waters of India with almost none exploring the coupling of various C and N pools. Moreover, these research works are very few in numbers compared to the diversity in types of aquatic systems found in India, ranging from freshwater to saline lakes, and monsoonal rivers to glacier fed rivers in the high altitude Himalayas. Furthermore, with rapid urbanisation there is an increasing number of urban water bodies (lakes and modified river channels) which needs to be studied to understand the nature of C and N cycling in these modified aquatic systems. Although the Indian subcontinent witnesses high emissions from industries and fossil fuel combustion, which are huge contributor to the atmospheric BC, little is known about their fate in the environment; specifically, when these BC particles end up in the aquatic systems. Only one study exists so far, exploring the movement of DBCs in the aquatic environments in southern India (Karthik et al., 2023).

1.5 Objectives of the thesis

In light of the above, the present thesis attempted to develop and improve the

understanding of C and N biogeochemistry in aquatic systems of India with specific focus on less explored systems (saline lakes and high altitude rivers) and emerging research questions related to inland waters (i.e., freshwater salinization, engineered modifications of river systems, and PBC cycling). As the various components of the aquatic C and N cycle are interrelated, they warrant interdisciplinary thinking and holistic approach to decipher the biogeochemical pathways of transformation. Therefore, the thesis focussed on the dynamics of POC, PN, DIC, dissolved CH₄, CO₂, and N₂O, and PBC in both lotic and lentic systems. Specifically, the thesis aimed to investigate the following:

- the role of reduction in lake volume and lake salinization on the biogeochemistry of freshwater lakes.
- the effect of lake desiccation on C and N biogeochemistry of saline lakes.
- the dynamics of total suspended matter and associated organic C and N in large river systems.
- the effect of engineering modifications of river channels on the in-stream C and N biogeochemistry and evasion of GHGs.
- the shift in C and N biogeochemistry along a river – lake continuum in high altitude climate setting.
- transport and transformation of PBC in the atmosphere – river – ocean continuum.

1.6 Outline of the thesis

Chapter 1

This chapter establishes the background of the study and the basic concepts related to the biogeochemical cycling of C and N in aquatic systems. The significance of inland waters in regulating the C and N budgets along with the current global and regional (India) understanding related to biogeochemistry of aquatic systems have also been discussed in brief. The emerging concept of cycling of PBC in the environment is also introduced along with the basics of stable isotopes, which has been employed as a tool in this thesis. The broad and specific objectives along with the outline of the thesis are also discussed in this chapter. Apart from the brief overview given in this chapter about the background to the research questions addressed in this thesis, individual chapters further elaborate the rationale for specific objectives as fulfilled in those chapters.

Chapter 2

This chapter briefly introduces the study areas selected to fulfil the objectives of the thesis and the details of the various sampling campaigns (details of the sampling sites for each study area are discussed in the individual chapters). The sample collection protocols and preservation techniques are discussed in brief. This chapter also discusses the various analytical techniques and methods used for the measurements of concentrations and isotopic compositions of different C and N pools.

Chapter 3

This chapter deals with the C and N biogeochemistry in lakes. The chapter is divided into two sections: the first section explores the effect of lake volume reduction and salinization on the biogeochemistry of a freshwater lake, and the second section further investigates the effect of desiccation on the biogeochemistry of a saline lake transitioning to a hypersaline lake.

Chapter 4

This chapter explores the C and N biogeochemistry in riverine systems. The chapter is divided into three sections. The first section explores the dynamics of suspended matter and associated organic C and N in large rivers with a major focus on the Ganges along with the Mekong and Yellow for comparison. The second section deals with the effect of engineered modifications of river systems on the in – stream biogeochemistry along with the dynamics of CH₄, CO₂, and N₂O. The last section explores the flow and transformation of C and N along with the dynamics of CH₄, CO₂ and N₂O in a high altitude river – lake continuum; specifically, tracking the shift in biogeochemical processes at the interface of a river – lake.

Chapter 5

This chapter explores the transport and transformation of PBC along the river continuum. Additionally, the fate of PBC in the marine environment is investigated using stable C isotopic signatures.

Chapter 6

This chapter summarizes the results obtained from the present study and discusses the scope for future research.

Chapter 2

Methodology

The fulfilment of the objectives outlined earlier required robust sampling and methodological strategy, which included sampling in inland waters of diverse characteristics. Depending on the objectives to be achieved in a particular system, the samples were collected to analyse different pools of C and N along with some environmental parameters. A brief overview of the sampling regions (campaigns) along with methodologies adopted in the thesis are described below.

2.1 Sampling campaigns

Samples for this thesis were collected from lakes (saline and freshwater) and rivers (modified and high altitude rivers). Sambhar Lake from the Indian state of Rajasthan was sampled to study hypersaline lake, whereas Nalsarovar located in the western Indian state of Gujarat was sampled for freshwater lake undergoing seasonal lake volume and salinity fluctuations (Fig. 2.1). Sabarmati River located in Gujarat was sampled to study a riverine system, which has undergone significant engineering modifications and Jhelum River located in the northernmost part of India (Kashmir Himalaya) was sampled to understand high altitude systems (Fig. 2.1). Samples collected from the Ganges, Yellow, and Mekong as a part of a collaborative project under Asia Pacific Network for Global Change was analyzed to decipher the suspended organic matter dynamics in the Ganges in comparison with Yellow and Mekong. Lastly, particulate matter samples collected from different oceanographic cruises in the Indian Ocean were analyzed to observe the fate of PBC in aquatic continuum (Fig. 2.1).

As the objectives of the thesis required sampling from diverse systems for different physical and biogeochemical parameters, chapter and theme-wise field campaigns conducted and parameters measured during this study are shown in Table 2.1. For continuity and clarity, details of the sampling locations in each sampled system are discussed in respective chapters.

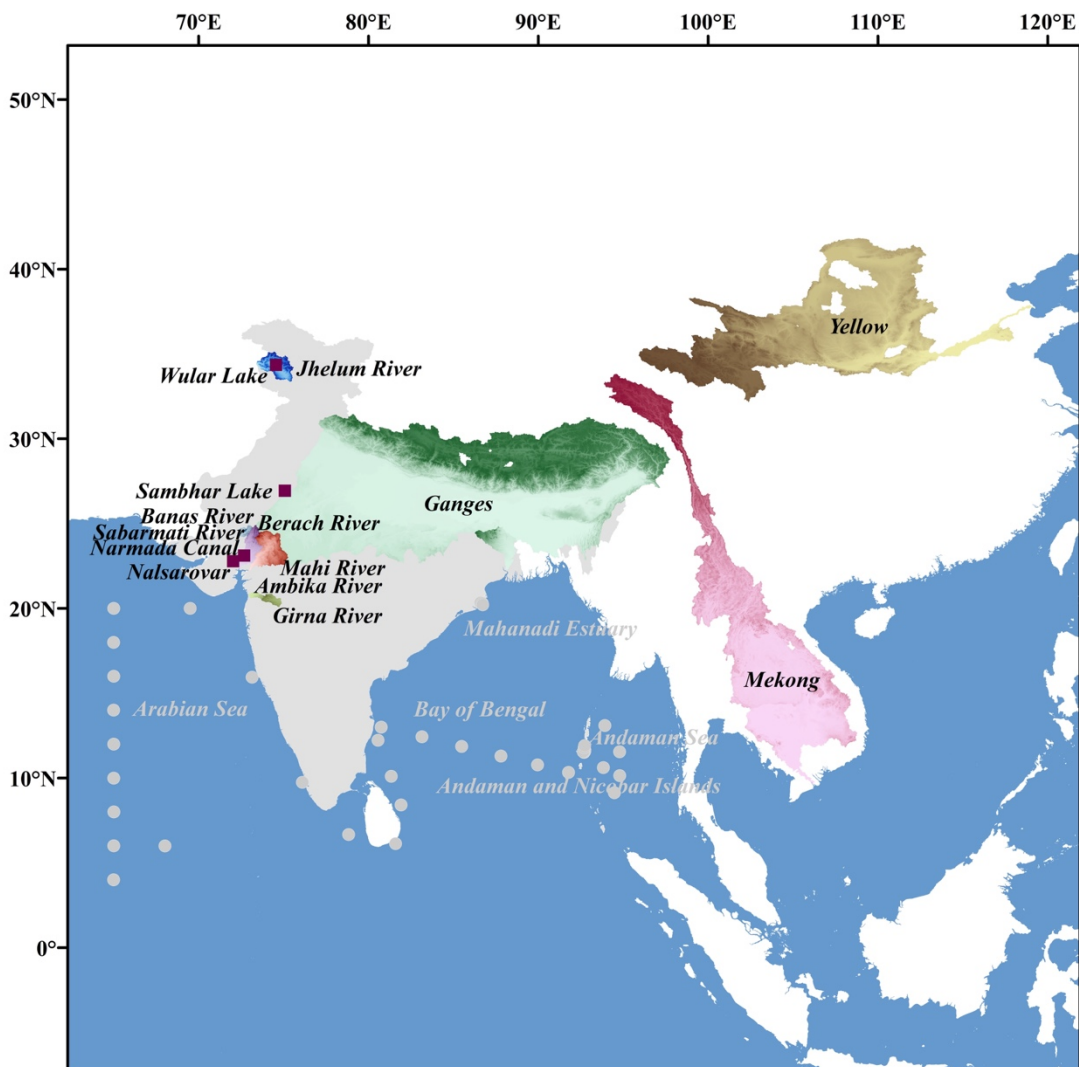


Fig. 2.1 Map showing study areas. Shaded areas represent river basins and squares (red) are lakes sampled for the present study. Light grey denote the stations in the northern Indian Ocean and estuarine region from where already collected samples were analyzed for particulate black carbon.

Table 2.1 Aquatic systems, sampling period, and measured parameters associated with individual thesis chapter (and sections).

Thesis Chapter	Aquatic Systems	Date of sampling	Parameters Measured
3.1	Lake – Nalsarovar	September 2020, February & August 2021	pH, T, EC, DO, major ions, NH_4^+ , $\delta^{18}\text{O}$, DIC, $\delta^{13}\text{C}_{\text{DIC}}$, POC, $\delta^{13}\text{C}_{\text{POC}}$, PN, $\delta^{15}\text{N}_{\text{PN}}$, SOM, $\delta^{13}\text{C}_{\text{SOM}}$, $\delta^{15}\text{N}_{\text{SOM}}$, CH_4 , $\delta^{13}\text{C}_{\text{CH}_4}$, CO_2 , $\delta^{13}\text{C}_{\text{CO}_2}$, and N_2O
3.2	Lake – Sambhar Lake	January 2019 and September 2019	pH, T, EC, major ions, NO_3^- and NH_4^+ , $\delta^{18}\text{O}$, DIC, $\delta^{13}\text{C}_{\text{DIC}}$, POC, $\delta^{13}\text{C}_{\text{POC}}$, PN and $\delta^{15}\text{N}_{\text{PN}}$
4.1	Rivers – Ganges, Mekong and Yellow	August 2016 – July 2019	TSM, POC, $\delta^{13}\text{C}_{\text{POC}}$, PN, and $\delta^{15}\text{N}_{\text{PN}}$
4.2	Rivers – Sabarmati and Mahi Reservoirs – Indrasi and Vatrak Canal – Narmada Canal	September 2020 and February 2021	pH, T, EC, DO, NO_3^- and NH_4^+ , $\delta^{18}\text{O}$, DIC, $\delta^{13}\text{C}_{\text{DIC}}$, POC, $\delta^{13}\text{C}_{\text{POC}}$, PN, $\delta^{15}\text{N}_{\text{PN}}$, CH_4 , CO_2 , and N_2O
4.3	River – Jhelum Lake – Wular	March 2021 and November 2021	pH, T, EC, DIC, $\delta^{13}\text{C}_{\text{DIC}}$, POC, $\delta^{13}\text{C}_{\text{POC}}$, PN, $\delta^{15}\text{N}_{\text{PN}}$, CH_4 , CO_2 , and N_2O
5.1	Rivers – Sabarmati and Mahi Canal – Narmada Canal Rivers – Banas, Berach, Ambika and Girna	September 2020 and February 2021	POC, $\delta^{13}\text{C}_{\text{POC}}$, PBC, $\delta^{13}\text{C}_{\text{PBC}}$
		November 2021 and August 2022	
5.2	Estuary – Mahanadi	October 2019	POC, $\delta^{13}\text{C}_{\text{POC}}$, PBC, $\delta^{13}\text{C}_{\text{PBC}}$
	Ocean – Arabian Sea	December 2019	
	Creeks – Andaman and Nicobar Islands	Nov – Dec 2020	
	Ocean – Bay of Bengal, Andaman Sea, Southern Arabian Sea	September – October 2021	

2.2 Sampling

Surface water samples were collected directly into sampling bottles in rivers/lakes and by Niskin bottles on oceanic cruises. Samples for major ions and stable isotopic (oxygen) measurement of water were collected in HDPE bottles and stored at room temperature. For DIC and dissolved gases, water samples were collected in serum glass bottles, closed air tight using butyl rubber septa and aluminium caps and poisoned with saturated HgCl_2 . For DIN, water samples were collected in HDPE bottles and kept frozen ($-20\text{ }^\circ\text{C}$) until analysis. Particulate matter was collected by filtering water onto pre combusted ($400\text{ }^\circ\text{C}$ for 4 hours) GF/F filters (Whatman $0.7\text{ }\mu\text{m}$). Filters were dried in an oven at $60\text{ }^\circ\text{C}$ to remove moisture and stored in petrislides until analysis. Surficial sediments and catchment soils were collected using a grab sampler and stored in HDPE zip lock bags at $-20\text{ }^\circ\text{C}$. The details of number of samples collected and specific modifications in methodology (if any) are discussed in each chapter.

2.3 Field measurements and laboratory analysis

2.3.1 Field parameters

Surface water temperature, pH, electrical conductivity (EC) and DO were measured *in situ* using handheld probes. DO in some of the field campaigns was measured using the Winkler Titration method following Grasshoff et al. (1983). Total suspended matter was estimated by calculating the difference in weight of the oven dried GF/F filters before and after sample filtration for particulate matter (Begum et al., 2021).

2.3.2 Major ions

Na^+ , K^+ , Ca^{2+} , Mg^{2+} , Cl^- , and SO_4^{2-} in water samples were measured using ion chromatography (Thermo Scientific, Germany; Fig 2.2a) following Mandal et al. (2021). Briefly, methane sulfonic acid (MSA) and a mixture of NaHCO_3 and NaCO_3 were used as eluents for cations and anions, respectively. CG16 and CS16 columns were used to separate cations, and AG23 and AS23 columns were used to separate anions. The ions were detected using a suppressed electrical conductivity detector (Thermo Scientific, Germany). The measurements of cations and anions were performed simultaneously. Standard solutions were prepared in laboratory for the calibration of cations and anions (using analytical grade NaNO_2 , $(\text{NH}_4)_2\text{SO}_4$, KNO_3 , $\text{CaCl}_2 \cdot 2\text{H}_2\text{O}$ and Mg metal for cations and multi elemental standard II (Merck) for anions, respectively).



Fig. 2.2 Picture of the (a) ion chromatography, (b) autoanalyzer, (c) gas bench –IRMS (MAT 253), (d) coulometer, (e) elemental analyzer, (f) IRMS (Delta V Plus), (g) gas chromatography, and (h) cavity ring down spectroscopy (Picarro) at the Physical Research Laboratory (PRL), India. These instruments are regularly used, including for this thesis, to generate data at PRL.

2.3.3 Dissolved inorganic nitrogen

NO_3^- and NH_4^+ in water samples were measured using San⁺⁺ continuous flow autoanalyzer (Skalar; Fig 2.2b) following Grasshoff et al. (1983). The autoanalyzer unit consists of an autosampler, peristaltic pumps, chemistry module and detectors. The analytical precision for both NH_4^+ and NO_3^- was $\pm 0.01 \text{ mg L}^{-1}$.

2.3.4 Stable isotopes of oxygen in water

The $\delta^{18}\text{O}$ of water was measured using IRMS (Delta V Plus, Thermo Scientific, Germany; Fig 2.2c) connected to the GasBench II following the standard gas equilibration method (Epstein & Mayeda, 1953). Briefly, water samples were kept in airtight exetainer vials, flushed with a mixture of He and CO_2 standard gas, and left for equilibration for 16 hours before analysis. The precision for repeat measurements of laboratory standards (NARM – Narmada water; $\delta^{18}\text{O} = -4.1\text{‰}$) was better than $\pm 0.1\text{‰}$. Long term precision of $< 0.1\text{‰}$ is achieved in the measurements of $\delta^{18}\text{O}$ of water at the Physical Research Laboratory, which is in agreement with the inter – laboratory calibration conducted by the International Atomic Energy Agency, Vienna.

2.3.5 Dissolved inorganic carbon

In the initial samples (Chapter 3.1), following standard method (Johnson et al., 1987). DIC concentrations were measured using a coulometer (UIC's model 5012; Fig 2.2d) with analytical precision $\pm 2\%$. Later, the DIC concentrations were also measured in GasBench II – IRMS using standard calibration curves (concentration – peak area) for known value of standard solutions prepared using Na_2CO_3 . The C isotopic composition of DIC ($\delta^{13}\text{C}_{\text{DIC}}$) was measured using an isotope ratio mass spectrometer (Delta V plus; Thermo Scientific, Germany) connected to a GasBench II (Thermo Scientific, Germany) following Bhavya et al. (2018). The precision for repeat measurements of standard with known isotopic composition (Na_2CO_3 ; $\delta^{13}\text{C} = -11.4\text{‰}$) was better than 0.1‰ .

2.3.6 Particulate organic matter and sediment organic matter

Filters for POC concentration and its stable isotopic composition ($\delta^{13}\text{C}_{\text{POC}}$) were fumigated in HCl vapours to remove any inorganic C and analysed using an elemental analyzer connected to IRMS (Flash 2000 and Delta V Plus, Thermo Scientific, Germany; Fig 2.2e and f). Filters for PN concentrations and isotopic composition ($\delta^{15}\text{N}_{\text{PN}}$) was not treated with HCl vapours. Sediments were treated with 1N HCl for 24

hours at 60 °C to remove inorganic carbon. The sediments were then rinsed thrice with deionized water followed by centrifugation. Sediments for N analysis were not treated with acid. IAEA standards of cellulose (IAEA-CH-3; $\delta^{13}\text{C} = -24.72\text{‰}$; C content = 44.4 %) and ammonium sulphate (IAEA-N-2; $\delta^{15}\text{N} = 20.3\text{‰}$; N content = 21.2 %) were used as laboratory standards for C and N contents and isotopic analysis. The analytical precision for C and N isotopic composition for repeat measurement of standards were better than 0.1 and 0.3‰, respectively. The precision for C and N contents were better than 10%.

2.3.7 Dissolved gases

Dissolved CH_4 , CO_2 , and N_2O were measured in water samples following the headspace equilibration method and using gas chromatography (McAuliffe, 1971; Elkins, 1980). Water samples were taken from airtight serum glass bottles using an airtight syringe (60 mL BD Plastipak) by creating a positive pressure within the sample bottles using helium gas (99.999 % purity). The amount of water sample taken (10 – 40 mL) would depend on the expected concentration of the gases. The sample in the syringe was equilibrated with a helium headspace by vigorously shaking for 5 minutes at laboratory temperature (Elkins, 1980). After equilibration, a 10 mL subsample of the helium headspace was taken and injected into the gas chromatography for analysis. For stable isotopic measurements of dissolved CH_4 and CO_2 , the same exercise was repeated using zero air (devoid of CH_4 and CO_2) as the gas used for equilibration.

2.3.7.1 Gas Chromatography

The gas chromatography technique is widely used for the separation of gases and analysis in small sample volumes. The gas chromatography used in this study (7890B, Agilent Technologies, USA; Fig 2.2g) is equipped with five packed columns and a methanizer – flame ionisation detector (FID) for the measurement of CH_4 and CO_2 and an electron capture detector (ECD) for the measurement of N_2O . In the Gas Chromatography, He was used as the carrier gas, N_2 as the makeup gas, and zero air and H_2 as fuel. Prior to sample analysis, the instrument was calibrated using four standard gas mixtures with varying concentrations of CH_4 (5000, 4993, 2003, and 506.8 ppb), CO_2 (995.2, 600, 411, and 98.3 ppm), and N_2O (1000, 495.7, 339.2, and 50.3 ppb) procured from Agilent Technologies, USA and DEUSTE Gas Solutions GmbH, Germany. The analytical precision for repeat measurements of standards were less than 3 %.

The dissolved concentrations in the actual samples were calculated following Wilson et al. (2018) as follows:

$$C_m = \frac{(\beta x P V_{wp} + \frac{xP}{RT} V_{hs})}{V_{wp}} \quad (i)$$

$$\ln\beta = A_1 + A_2 \left(\frac{100}{T}\right) + A_3 \ln\left(\frac{T}{100}\right) + A_4 \left(\frac{T}{100}\right)^2 + S \left[B_1 + B_2 \left(\frac{T}{100}\right) + B_3 \left(\frac{T}{100}\right)^2 \right] \quad (ii)$$

where, x = mole fraction (ppb) of gas measured in the headspace; V_{wp} = sample volume used for equilibration; V_{hs} = volume of helium used for equilibration; R = Gas constant (0.08205746 L atm K⁻¹ mol⁻¹); P = atmospheric pressure; T = equilibration temperature (K) in the laboratory; β = Bunsen solubility coefficient of the gases, which is a function of sample temperature (T) and salinity (S); A_1 , A_2 , A_3 , A_4 , B_1 , B_2 , B_3 , and B_4 are constants for different gases. β was calculated following Weiss and Price (1980) for N₂O; Wiesenburg and Guinasso (1979) for CH₄; and Weiss (1974) for CO₂. The flux for each gas across the water – air interface was calculated using the following equation:

$$\text{Flux} = k (C_m - C_e) \quad (iii)$$

$$k = 0.251 U_{10}^2 \left(\frac{Sc}{660}\right)^{-\frac{1}{2}} \quad (iv)$$

$$Sc = A + BT + CT^2 + DT^3 + ET^4 \quad (v)$$

where, C_m and C_e the measured and equilibrium concentration of gas; k = gas transfer velocity calculated following Wanninkhof (2014); U_{10} = wind speed acquired from MERRA – 2 reanalysis data (National Aeronautics and Space Administration (NASA)/Goddard Space Flight Center, <http://gmao.gsfc.nasa.gov/reanalysis/MERRA-2>, last accessed on 01/30/2023); Sc = Schmidt number calculated following Wanninkhof (2014).

2.3.7.2 Cavity Ring Down Spectroscopy

The equilibrated sample using zero air was analyzed by Cavity Ring Down Spectroscopy (G2201-I, Picarro, USA; Fig 2.2h) for C stable isotopic composition of CH₄ and CO₂. Prior to analysis, a one-point calibration was performed using a standard gas procured from National Oceanic and Atmospheric Division, Global Monitoring Division, USA ($\delta^{13}\text{C}_{\text{CH}_4} = -47.48 \text{ ‰}$ and $\delta^{13}\text{C}_{\text{CO}_2} = -8.788 \text{ ‰}$). The precision for

isotopic measurements from repeat measurements of standard gas was better than 1‰ and 0.3‰ for $\delta^{13}\text{C}_{\text{CH}_4}$ and $\delta^{13}\text{C}_{\text{CO}_2}$, respectively.

2.3.8 Particulate black carbon

Filters containing PM were fumigated with concentrated HCl for 48 hours to remove the inorganic C fraction and then dried at 40 °C. Subsamples for PBC analysis were treated following the CTO-375 method (Gustafsson et al. 2001) as this method is widely used for PBC quantification in aquatic systems (Mitra et al. 2002; Flores-Cervantes et al. 2009; Yang and Guo, 2014; Xu et al. 2016; Fang et al. 2016). Briefly, acid fumigated filters were heated at 375 °C for 24 hours in active airflow to remove the organic C fraction. The filters were then analyzed for C content (PBC) and its isotopic composition ($\delta^{13}\text{C}_{\text{PBC}}$) using an Elemental Analyzer (Flash 2000) interfaced with an IRMS (Delta V Plus, Thermo Scientific, Germany). Similar to POC, IAEA standard of cellulose (IAEA-CH-3; $\delta^{13}\text{C} = -24.72$ ‰; C content = 44.4 %) was used as laboratory standard for and isotopic analysis. The analytical precision for C contents and its isotopic composition were better than 10 % and 0.1 ‰, respectively.

2.4 Statistical analysis

Shapiro-Wilk test was applied to check the normality in the distribution of the data using SigmaPlot 14.0 (Systat, USA). To analyse significant difference in measured parameters across seasons and sample classes, a two-way analysis of variance (ANOVA) on ranks followed by pairwise multiple comparison (Holm-Sidak method) was performed. Alternatively, a one-way ANOVA on ranks using the Kruskal-Wallis's method followed by pairwise multiple comparison (Dunn's method) was performed to check significant differences between two datasets. Spearman rank correlation and Pearson's correlation among parameters were performed in R. Isotope mixing model was used to identify the source of POC and PN and CH₄ and CO₂. Briefly, the isotopic signature of the source was obtained from the slope of the regression between the C concentration of the pool of interest and the product of $\delta^{13}\text{C}$ and C concentrations (Miller and Tans, 2003). This method is based on the principle of conservation of mass and mixing of C sources with distinct isotopic signatures. This method was further extended for the source identification of N in TSM. Mixing models have been widely used in related studies around riverine DIC and GHGs (Campeau et al., 2017; O'Dwyer et al., 2020; Begum et al., 2021).

Chapter 3

Lake Biogeochemistry

Lakes have emerged as hotspots for C and N cycling and active conduits of CH₄, CO₂ and N₂O to the atmosphere (Bastviken et al., 2008). Catchment characteristics (viz. land use and vegetation cover) along with environmental parameters (viz. precipitation, temperature, and wind speed) affect the fluxes of C and N across the land/atmosphere-aquatic interface and concurrently govern the cycling of these elements within the aquatic system. Most of the research on aquatic C and N biogeochemistry have been focused on large freshwater lakes because of a high species richness and diversity in larger systems. However, recent research has observed that smaller lakes potentially harbor more species (richness and diversity) as compared to a larger lake of equivalent size (Richardson et al., 2022). Furthermore, the environmental controls on in-lake processes acts variably in shallow and deep-water lakes.

In this chapter C and N biogeochemistry in lentic systems which comprise of a shallow freshwater and a saline lake has been explored. Given the global crisis of freshwater salinisation (Kaushal et al., 2021) due to human activities as well as climate change, the first section of the chapter investigates the effect of salinisation on freshwater lake biogeochemistry. The second section focuses on the biogeochemistry of a lake that transitions from a saline to hypersaline lake. Saline lakes, by convention, are epi-continental or inland water bodies having salinity $> 3\text{ g L}^{-1}$ (Williams, 2002). They are an integral part of the biosphere and are widely distributed across the globe in regions where evaporation exceeds precipitation. Generally, saline lakes are assumed to be smaller in number and sparsely distributed across the globe. However, contrary to this general assumption about their size and distribution, saline lakes contribute significantly to the global lake volume, i.e., $85 \times 10^3 \text{ km}^3$ to the total of $190 \times 10^3 \text{ km}^3$ of global lakes (Williams, 2002). From the perennial Caspian Sea, Mono Lake, and the Dead Sea to the episodically recharged lakes, like Lake Eyre and Pyramid Lake, the saline lakes possess aesthetic, cultural, economic, ecological and scientific value. However, saline lakes remain an understudied component within the domain of lake research and warrants investigations especially in regard to elemental cycling.

3.1 Lakes in transition: Effect of volume reduction and salinization on freshwater lakes

Recent decades have witnessed increased effect of climate change and human perturbations on lake ecosystems (Schindler, 2009; Williamson et al., 2009; Jeppesen et al., 2014). Lake desiccation and salinization are two major threats to freshwater lakes and have the potential to severely alter the community structure, diversity and productivity of the system (Evans and Frick, 2001; Chapra et al., 2009; Corsi et al., 2010; Findlay and Kelly, 2011; Van and Swan, 2014; Herbert et al., 2015). Seasonal fluctuation in lake water level determines the abundance of the dominant plant types (submerged macrophytes, phytoplankton, or free-floating plants) (Scheffer, 1998; Scheffer and Carpenter, 2003; Scheffer and van Nes, 2007). The changing lake ecological status can alter the rates and directionality of various processes in the aquatic C and N cycle (Carpenter and Lodge, 1986; de Tezanos Pinto and O'Farrel, 2014; Hilt et al., 2017; Janssen et al., 2021). Specifically, freshwater salinization can seriously threaten ecosystem functioning, biodiversity and various ecosystem services (Herbert et al., 2015; Rounsevell et al., 2018; Zhao et al., 2021). Salinity is a key environmental factor in shaping the structure of freshwater ecosystems across the globe (Reid et al., 2019). Moreover, salinity controls species adaptation and speciation especially in aquatic organisms who use osmotic regulation to survive (Iglesias, 2020; Kaushal et al., 2021; Silver and Donini, 2021). The causes of freshwater salinization could be both natural (desiccation and weathering) and anthropogenic (use of road salts and water diversion) (Kaushal et al., 2005; Dugan et al., 2017; Corsi et al., 2020). The freshwater salinization syndrome encompasses the interrelationships between salinization and various biogeochemical processes in aquatic systems (Kaushal et al., 2021).

This chapter explores the seasonality in C and N biogeochemistry in a shallow lake and attempts to decipher the effect of environmental parameters on the same. To study the effect of lake volume change and salinization on the C and N pools, Nalsarovar Lake (situated in Gujarat, India) was chosen, which is a unique system as it transitions from a freshwater to saline system during a hydrological year. Furthermore, the lake water depth is the highest during post-monsoon season (September – November) and reduces during the following months to be the shallowest (< 1 m) during summer (March – May). Therefore, Nalsarovar Lake provides us with a natural laboratory to track the effect of lake volume reduction and salinization on various lake

processes. The specific objectives of the study were to: (i) track the coupling between salinity and lake volume and ultimately with the concentration of C and N pools, (ii) decipher the in-lake processes dominant at different salinity/ water level conditions, and (iii) observe the effect of salinization on the dissolved CH_4 , CO_2 , and N_2O dynamics.

3.1.2 Study area

Nalsarovar is a freshwater lake situated in the Thar Desert Biogeographic Province of the western India (Fig 3.1). Covering a maximum surface area of $\sim 120 \text{ km}^2$, the lake depth varies seasonally depending on the amount of recharge through precipitation and surface runoff during the monsoon, and by the subsequent seasonal water loss due to evaporation. The catchment of Nalsarovar is bounded by basaltic trap rocks, Juro-Cretaceous sandstone and igneous and metamorphic rocks in the west, northwest and extreme northeast, respectively (Prasad et al., 1997).

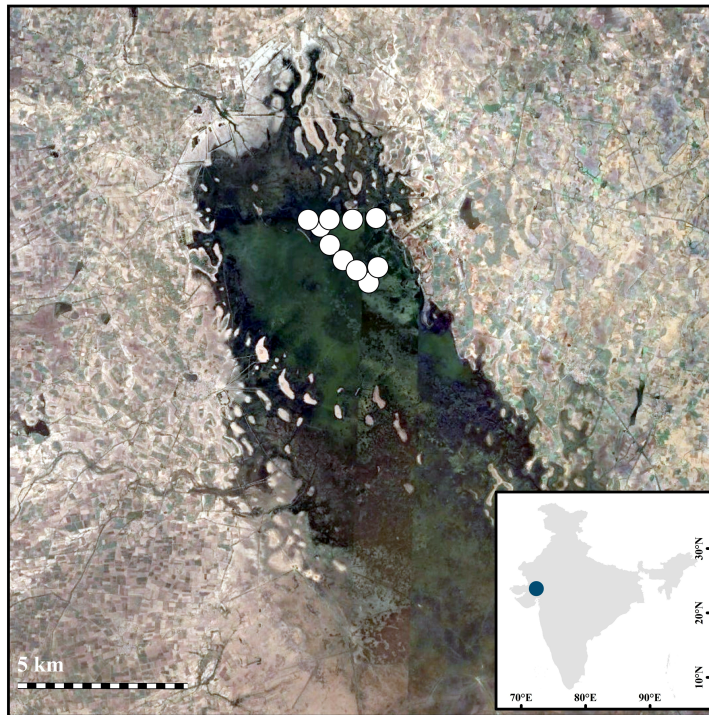


Fig. 3.1 Map of Nalsarovar showing sampling locations (white circles).

3.1.3 Sampling

To address the above objectives, sampling was conducted in the Nalsarovar Lake at 10 sites during three field campaigns (Fig 3.2). The first field was conducted during October 2020 when the lake was completely recharged and had the maximum water. This was followed by two other campaigns in February 2021 and August 2021, when

the lake level was steadily reducing. This sampling strategy was planned to track the shift in biogeochemical parameters across different hydrological regime. The protocol for lake water sampling for different parameters is discussed in chapter 2. Additionally, lake bottom sediment was collected during August 2021 ($n = 9$) using a grab sampler along with macrophytes ($n = 7$) and surface algae ($n = 5$) at random sites to constrain the end members of organic matter.

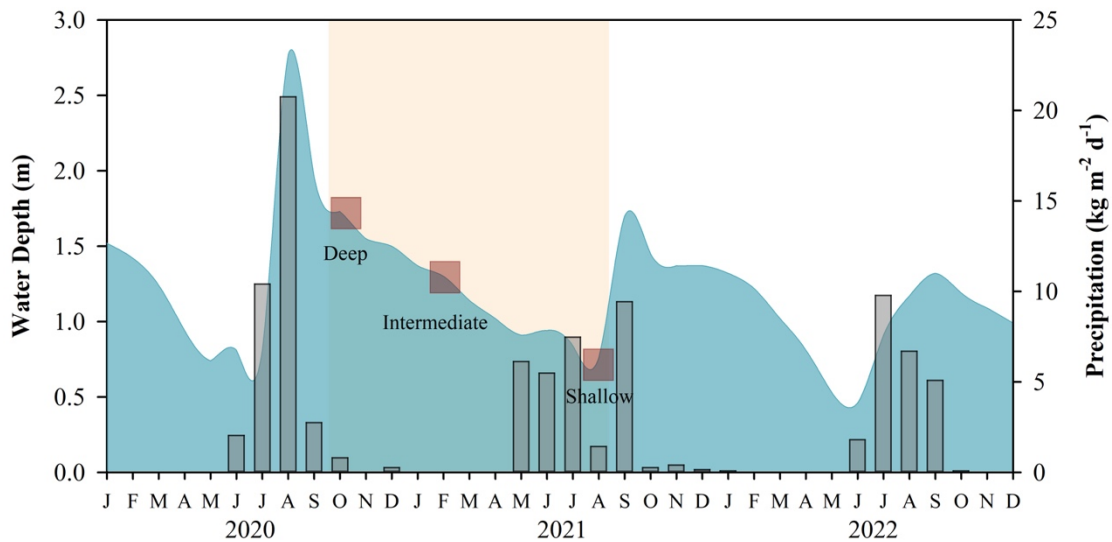


Fig. 3.2 Seasonal variability in lake water depth (shaded) and precipitation (bar charts). Sampling campaigns are denoted by dark red squares.

3.1.4 Results

3.1.4.1 Physio-chemical parameters of the lake

Nalsarovar experienced high seasonal variability in temperature, pH, and conductivity (Fig. 3.3). The highest water temperature (mean \pm stdev: 30.3 ± 1.2 °C) was observed during October, which decreased during February (24.2 ± 1.4 °C) to further increase by August (27.4 ± 0.2 °C) (Fig. 3.3a). pH ranged from 10.04 ± 0.21 , 8.67 ± 0.60 and 8.38 ± 0.42 during October, February and August, respectively (Fig. 3.3b). Lake conductivity increased manifold from 2.5 ± 0.3 during October to 5.9 ± 0.3 during February and reached as high as 10.0 ± 0.8 mS/cm during August (Fig. 3.3c). The lake was predominantly oxic across seasons with the lowest oxygen level (~ 5.09 mg/L) during October. The $\delta^{18}\text{O}$ of lake water increased from -1.0 ± 0.4 during October to 3.5 ± 0.2 during February and ultimately to 4.8 ± 0.2 during August (Fig 3.3d). Major cations (Na^+ , K^+ , Mg^{2+} and Ca^{2+}) increased steadily from October (Na^+ : 433.0 ± 58.8 mgL $^{-1}$, K^+ : 1.0 ± 0.2 mgL $^{-1}$, Mg^{2+} : 22.7 ± 3.9 mgL $^{-1}$, Ca^{2+} : 33.1 ± 6.9 mgL $^{-1}$) to

February (Na^+ : $961.5 \pm 85.7 \text{ mgL}^{-1}$, K^+ : $3.0 \pm 0.6 \text{ mgL}^{-1}$, Mg^{2+} : $62.3 \pm 4.5 \text{ mgL}^{-1}$, Ca^{2+} : $90.8 \pm 10.3 \text{ mgL}^{-1}$) and further till August (Na^+ : $1809.5 \pm 175.6 \text{ mgL}^{-1}$, K^+ : $12.2 \pm 1.9 \text{ mgL}^{-1}$, Mg^{2+} : $120.3 \pm 18.8 \text{ mgL}^{-1}$, Ca^{2+} : $122.5 \pm 31.8 \text{ mgL}^{-1}$) (Fig. 3.4). Similar increasing trend was observed for anions (October: $\text{Cl}^- = 549 \pm 94.9 \text{ mgL}^{-1}$ and $\text{SO}_4^{2-} = 259.7 \pm 34.5 \text{ mgL}^{-1}$; February: $\text{Cl}^- = 1468.0 \pm 99.5 \text{ mgL}^{-1}$ and $\text{SO}_4^{2-} = 574.2 \pm 22.1 \text{ mgL}^{-1}$; August: $\text{Cl}^- = 2956.0 \pm 287.5 \text{ mgL}^{-1}$ and $\text{SO}_4^{2-} = 971.0 \pm 221.8 \text{ mgL}^{-1}$) (Fig. 3.4) The NH_4^+ in the lake did not show significant change from October ($2.89 \pm 1.22 \text{ } \mu\text{M}$) to February ($2.30 \pm 1.26 \text{ } \mu\text{M}$), but significantly increased during August ($10.15 \pm 7.88 \text{ } \mu\text{M}$).

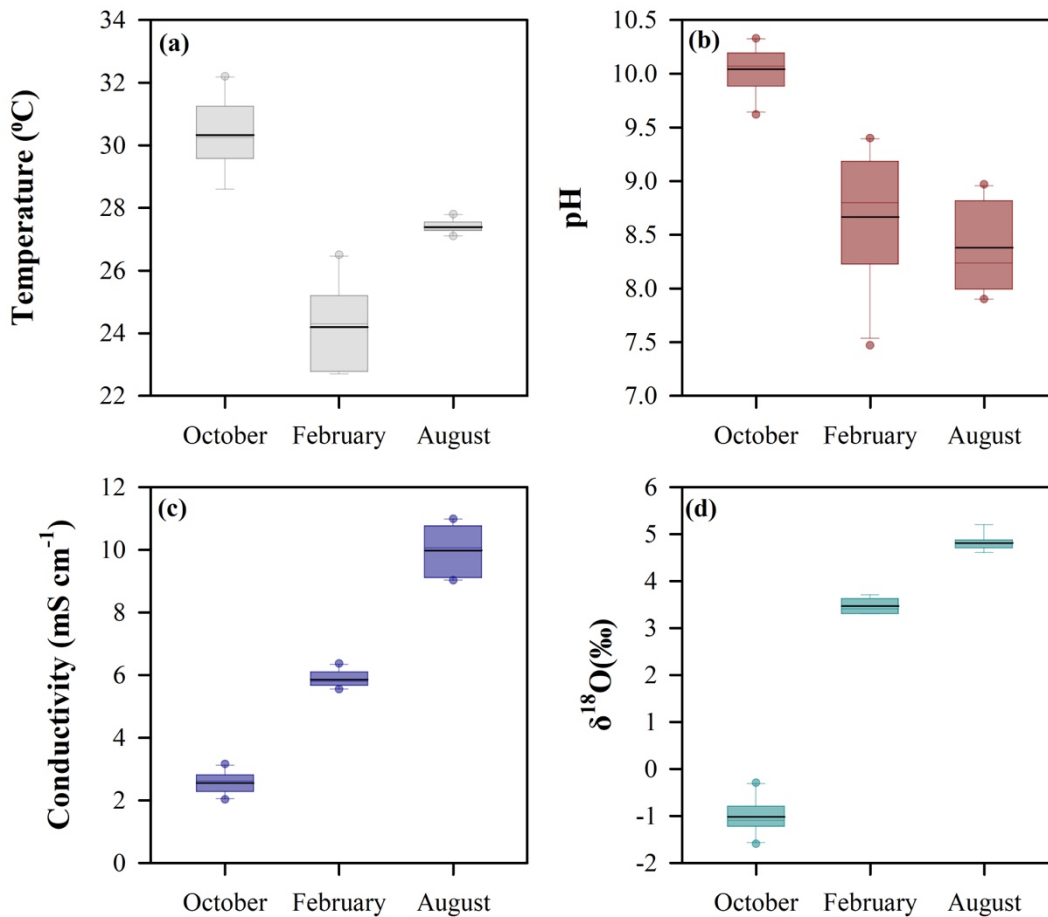


Fig. 3.3 Box-Whisker plots showing seasonal variation in (a) Temperature, (b) pH, (c) Conductivity and (d) $\delta^{18}\text{O}$ of lake water. Solid black line indicates the mean values.

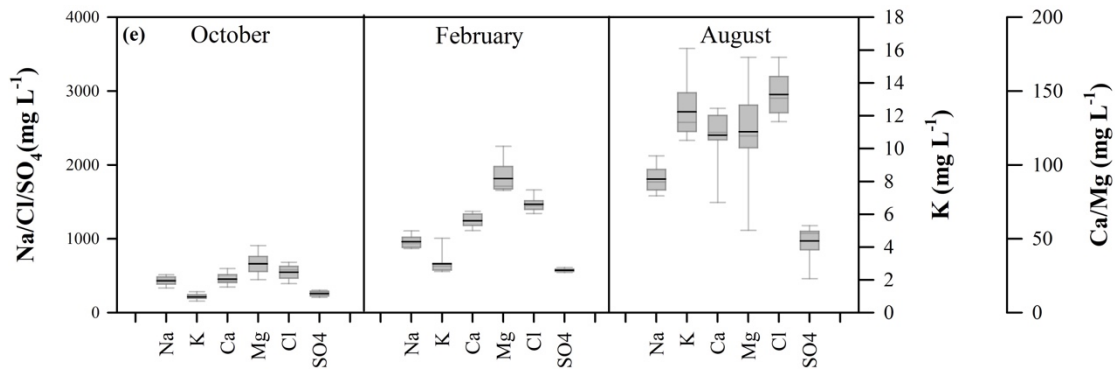


Fig. 3.4 Seasonal variations in major cations and anions in the lake.

3.1.4.2 Concentrations and isotopic compositions of DIC, POC, and PN

October witnessed a low and wide range of DIC concentrations (mean \pm SD $\sim 1.45 \pm 1.06$ mM) across the lake (Fig 3.5a). The DIC concentration increased steadily to 2.00 ± 0.91 mM during February and 3.07 ± 0.93 mM during August (Fig 3.5a). Such distinct seasonality was not reflected on the $\delta^{13}\text{C}_{\text{DIC}}$, with similar compositions during October ($\delta^{13}\text{C}_{\text{DIC}}$: -12.8 ± 1.0) and February ($\delta^{13}\text{C}_{\text{DIC}}$: -12.8 ± 1.2 ‰; Fig 3.5b). The isotopic composition was significantly higher during August ($\delta^{13}\text{C}_{\text{DIC}}$: -11.3 ± 0.8 ‰). Similar to the DIC, POC increased drastically from October (32.08 ± 5.89 μM) to February (62.13 ± 24.81 μM) and August (167.17 ± 131.94 μM), respectively (Fig 3.5c). However, the $\delta^{13}\text{C}_{\text{POC}}$ had similar signatures during October ($\delta^{13}\text{C}_{\text{POC}}$: -23.8 ± 0.6 ‰) and February ($\delta^{13}\text{C}_{\text{POC}}$: -23.5 ± 2.9 ‰), but decreased significantly during August ($\delta^{13}\text{C}_{\text{POC}}$: -25.7 ± 2.1 ‰) (Fig 3.5d). PN concentrations ranged from 2.43 to 4.19 μM during the October. The average concentration increased to 5.22 ± 2.28 μM during February and 37.38 ± 41.93 μM during August (Fig 3.5e). The $\delta^{15}\text{N}_{\text{PN}}$ steadily decreased from October ($\delta^{15}\text{N}_{\text{PN}}$: 4.6 ± 1.0 ‰) to February (2.5 ± 0.9 ‰) and August (1.3 ± 0.8 ‰; Fig 3.5f).

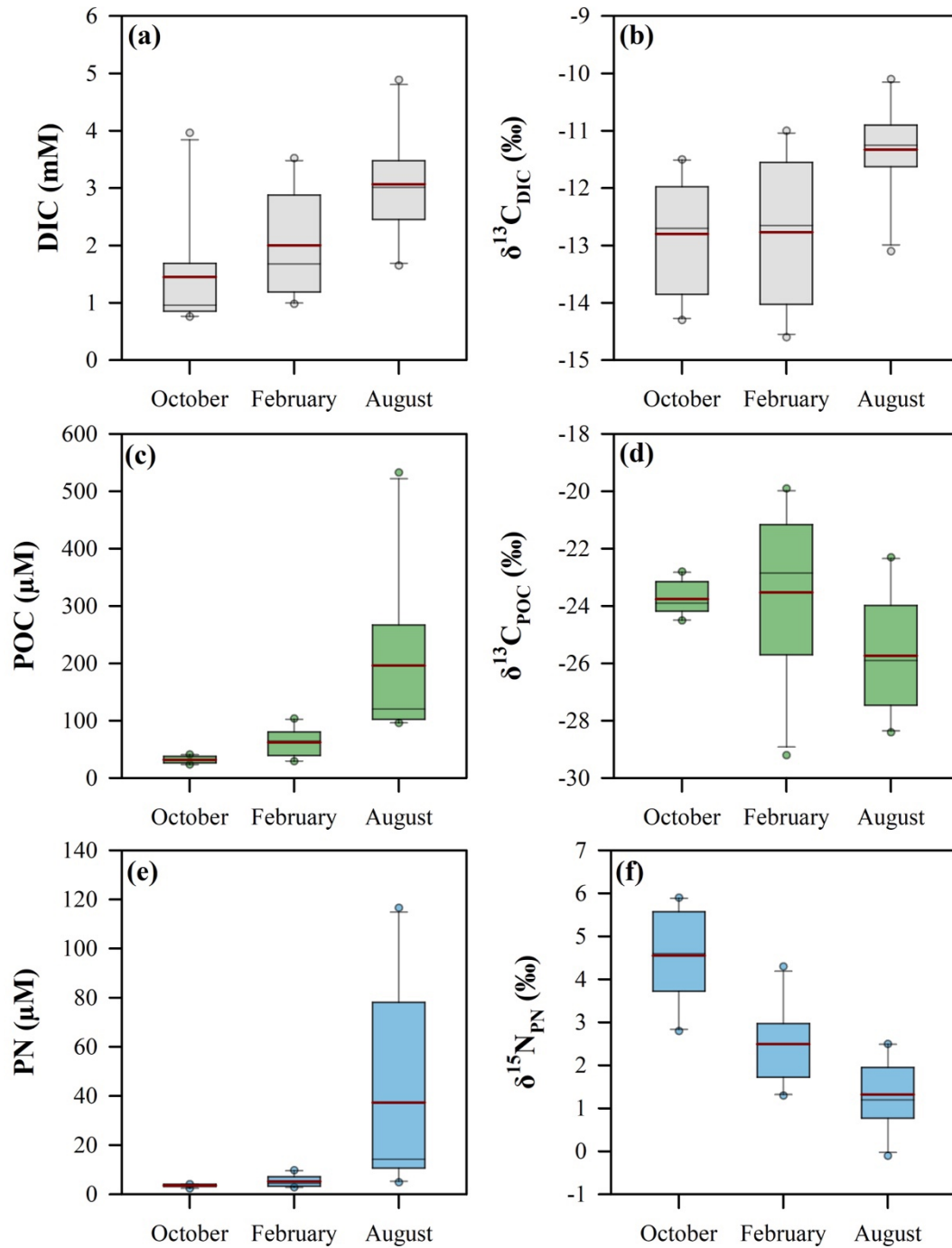


Fig. 3.5 Seasonal variation in (a) dissolved inorganic carbon (DIC), (b) $\delta^{13}\text{C}_{\text{DIC}}$, (c) particulate organic carbon (POC), (d) $\delta^{13}\text{C}_{\text{POC}}$, (e) particulate nitrogen (PN), and (f) $\delta^{15}\text{N}_{\text{PN}}$. Solid red lines indicate the mean values.

3.1.4.3 C and N contents in sediments, emergent macrophytes, and surface algae

The % OC in sediments varied from 0.56 to 2.87 with its isotopic composition ($\delta^{13}\text{C}_{\text{SOM}}$) in the range of -21.5 ± 1.4 ‰. The N content and $\delta^{15}\text{N}_{\text{SOM}}$ were in the range of 0.17 ± 0.10 ‰ and 4.3 ± 1.0 ‰, respectively. The emergent macrophytes showed high C and N contents at 46.89 ± 1.86 and 2.33 ± 0.65 ‰ respectively. The $\delta^{13}\text{C}$ of macrophytes ranged from -26.4 to -17.4 ‰ and its $\delta^{15}\text{N}$ varied from 0.9 to 8.4 ‰. Surface algal blooms showed 26.96 ± 3.39 and 1.50 ± 0.28 ‰ OC and ‰ N, respectively. The algae had highly enriched C ($\delta^{13}\text{C}$: -19.1 ± 1.2 ‰) and depleted N ($\delta^{15}\text{N}$: 0.3 ± 1.1 ‰) isotopic signatures (Fig 3.6).

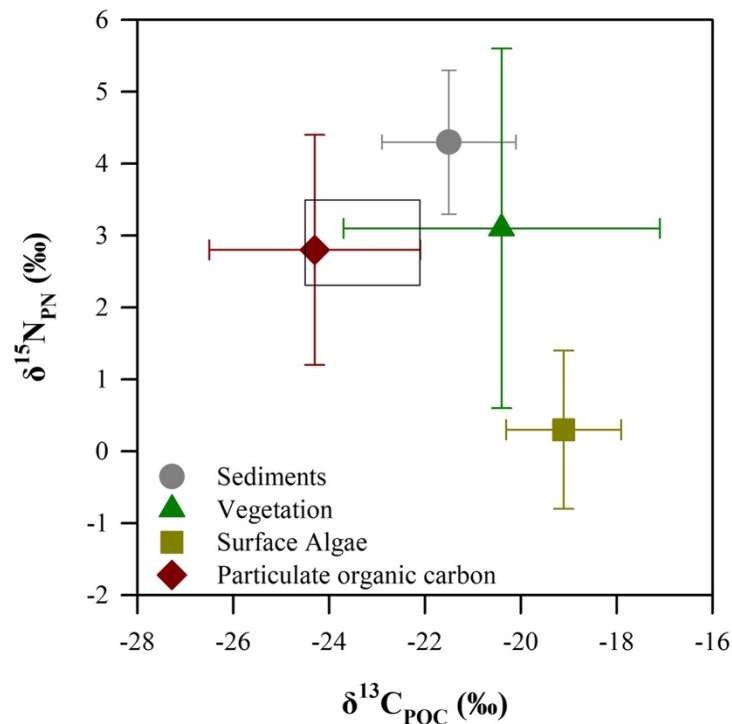


Fig. 3.6 Carbon and nitrogen isotopic composition of different organic matter pools in the lake. The symbols and lines indicate mean \pm stdev. The black square shows the source isotopic signature of organic matter deduced through graphical mixing model.

3.1.4.4 Dissolved greenhouse gases in the lake

CH₄ concentrations varied between 0.16 to 0.56 μM during October to increase during February (0.64 ± 0.38 μM) with an extremely high concentration of ~ 6.73 μM near a vegetated site (Fig. 3.7a). The lake CH₄ concentration further increased during August (7.88 ± 5.47 μM) with the vegetated site showing high CH₄ (~ 6.68 μM) again. The $\delta^{13}\text{C}_{\text{CH}_4}$ showed an increase during February (-46.8 ± 3.7 ‰) compared to October (-53.0 ± 4.4 ‰) and August (-55.4 ± 6.2 ‰) (Fig. 3.7b). The dissolved CO₂ concentrations in the lake witnessed a decline during February (0.16 ± 0.09 mM) compared to October (0.17 ± 0.05 mM) and August (0.32 ± 0.10 mM) (Fig. 3.7c). The $\delta^{13}\text{C}_{\text{CO}_2}$ during October (-10.6 ± 1.7 ‰) was close to that of atmospheric CO₂ (~ -8 ‰). During February, the $\delta^{13}\text{C}_{\text{CO}_2}$ decreased to -17.7 ± 1.2 ‰ and later increased to -15.6 ± 0.7 ‰ during August (Fig. 3.7d). Dissolved N₂O showed an exact opposite seasonality to that of the dissolved CO₂ with N₂O concentrations increasing from October (9.26 ± 0.89 nM) to February (11.85 ± 1.24 nM) and then falling drastically to 3.44 ± 2.11 nM during August (Fig. 3.7e).

3.1.5 Discussion

3.1.5.1 Evaporation and salinization of lake water

The increasing $\delta^{18}\text{O}$ of lake water from October to February and further to August reflects the temporal change in evaporative regime of the lake. Increase in $\delta^{18}\text{O}$ is attributed to the loss of lake water via evaporation leading to lighter isotopes preferentially getting removed during phase change from water to vapor (Fry, 2006). Rayleigh fractionation model was applied to estimate the change in lake volume due to loss via evaporation ($\delta^{18}\text{O}_{\text{February}} = (\delta^{18}\text{O}_{\text{October}} + 1000) \times f_{\text{ev}}^{(\alpha - 1)}$), where 0.9908 was taken as fractionation factor (α) at 25°C (Gat and Gonfiantini, 1981). The assumption behind using this model was that the lake gets recharged only by monsoonal precipitation and not by groundwater or surface water during the dry periods. Lakes situated in semi-arid climate usually feeds the groundwater during the dry period, thereby validating our assumption. Around ~ 39 % loss of lake water due to evaporation from October to February and ~ 47 % by August was estimated. This intense evaporation resulted in increased ionic concentration in the lake water (Fig. 3.4). Manifold increase in conductivity from October to February and further to August (Fig. 3.3c) is a direct result of decreasing lake volume due to evaporative loss.

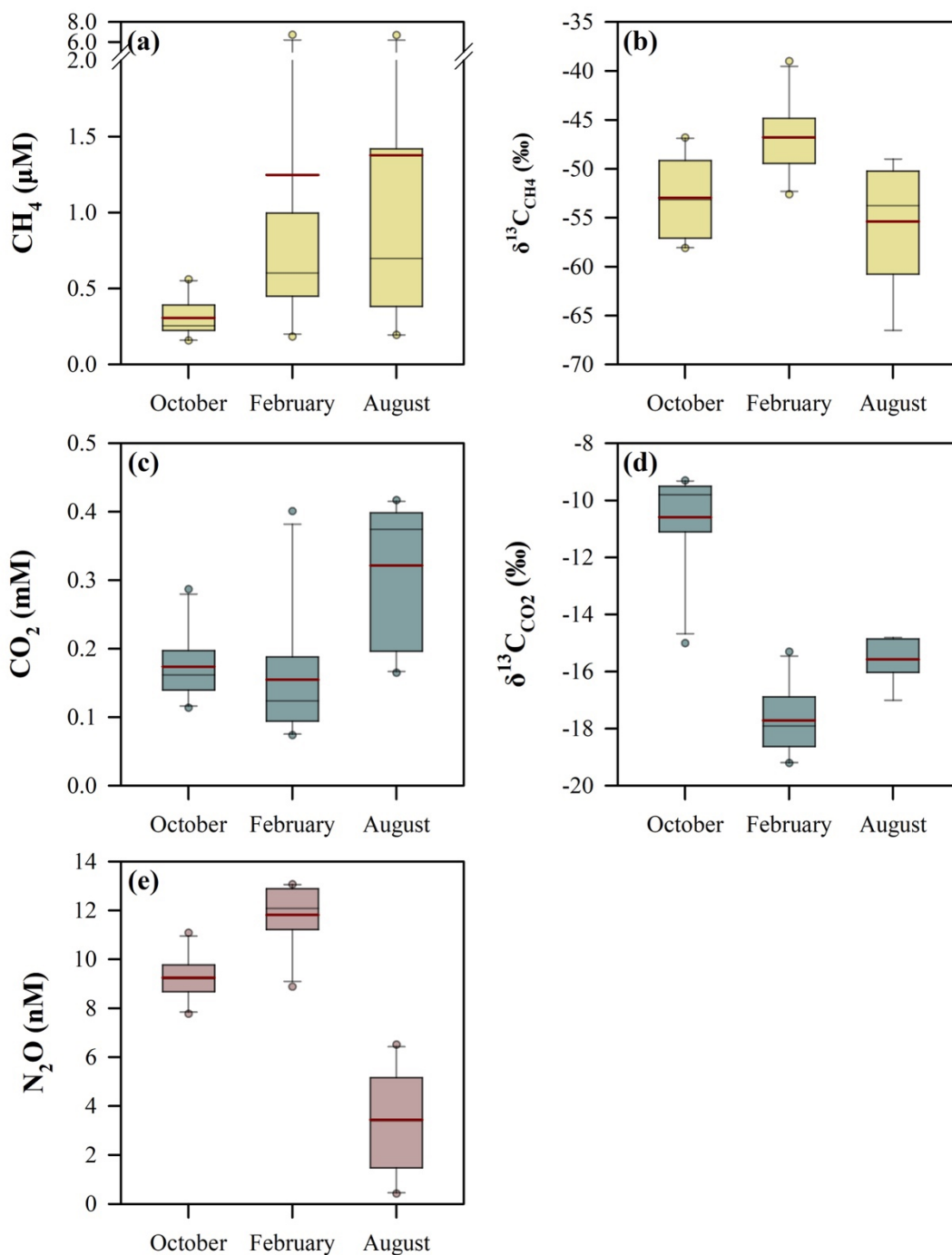


Fig. 3.7 Seasonal variation in concentrations and isotopic compositions of dissolved gases: (a) CH₄, (b) δ¹³C_{CH₄}, (c) CO₂, (d) δ¹³C_{CO₂}, and (e) N₂O. Solid red lines indicate the mean values.

3.2.5.2 Seasonality in dissolved inorganic carbon cycling

Dissolved inorganic carbon showed drastic increase in concentration as the lake volume decreased (Fig 3.4a). Carbon uptake during photosynthesis, carbonate precipitation/dissolution, OM degradation, and CO₂ degassing are the primary processes that govern the concentration and isotopic composition of lake DIC pool

(Alling et al., 2012; Sarkar et al., 2023a). Low DIC observed during October is attributed to dilution due to precipitation and surface runoff. The negative relationship between DIC and $\delta^{13}\text{C}_{\text{DIC}}$ ($p < 0.05$, Fig 3.8a) during October indicates inputs from two sources (decomposition of OM and/or atmospheric CO_2). Subsequently, DIC increased during February without any significant change in $\delta^{13}\text{C}_{\text{DIC}}$. Weak relationship between the concentration and isotopic composition of DIC during February (Fig 3.8b) limits us from inferring dominant processes controlling the increase in concentration. However, shrinking of lake volume without drastic shift in lake processes seems to be the possible causal factor for increasing DIC with similar isotopic composition.

The positive relationship between DIC and $\delta^{13}\text{C}_{\text{DIC}}$ during August could be attributed to calcium carbonate precipitation (Aling et al., 2012). However, that process is dominant at low salinities which was not the case during August. Therefore, the plausible explanation again lies in the fact that there is an increase in lake DIC due to reducing lake volume and the increase in $\delta^{13}\text{C}_{\text{DIC}}$ could be due to enhanced DIC uptake during primary production. Also, the evasion of CO_2 (Fig 3.7c) from the lake might have led to an increase in the isotopic composition of the residual DIC pool. The loss of lighter DIC fraction coupled with an increase in overall concentration due to reduction in lake volume might be responsible for the strong positive relationship observed between DIC and $\delta^{13}\text{C}_{\text{DIC}}$ at high salinity (Fig 3.8c).

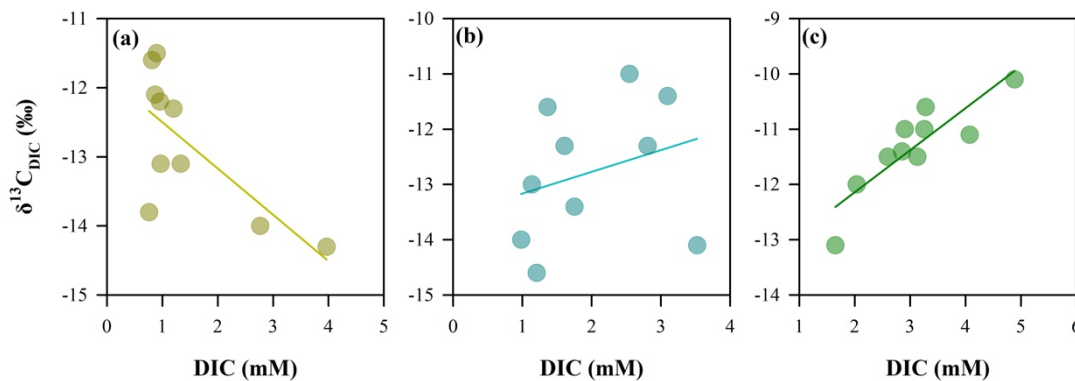


Fig. 3.8 Relationship between DIC and $\delta^{13}\text{C}_{\text{DIC}}$ in (a) October, (b) February, and (c) August.

3.1.5.3 Lake biomass

Particulate organic matter is an indicator of lake biomass and its *in-situ* production is governed by the availability of nutrients and favorable environmental conditions (water

temperature, turbulence, and light availability). Nalsarovar witnessed sharp increase in POC and PN concentrations from October to August (Fig 3.5 c & e). This is accompanied by reduction in lake volume and increase in ionic concentrations. An increase in C/N ratio of POM from October to February was also observed, which declined in August (Fig 3.9). Post February, as the POM concentration increased, simultaneous decline in $\delta^{15}\text{N}_{\text{PN}}$ and $\delta^{13}\text{C}_{\text{POC}}$ was also observed. This increase in concentration of POM with decline in isotopic compositions of C and N points towards cumulative effect of reduction in lake volume leading to accumulation of organic matter and change in species and nutrient source.

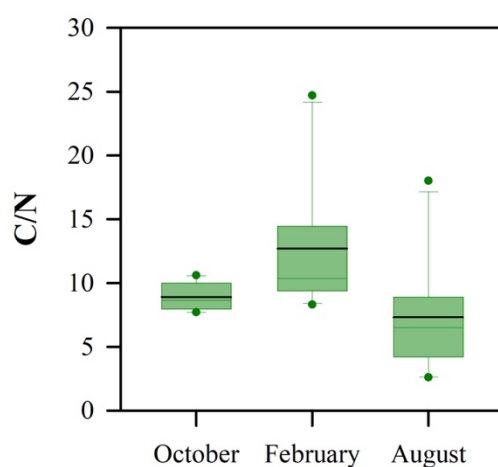


Fig. 3.9 Seasonal variation in the C/N ratio of particulate organic matter. Solid black lines indicate the mean values.

The lowering of $\delta^{15}\text{N}_{\text{PN}}$ from October to August indicates a shift in N source for in-lake production in the lake from DIN to atmospheric N_2 . As the lake volume decreases, degassing of NH_3 from the system is expected, causing increase in the isotopic composition of the remaining DIN pool (Isaji et al., 2019c). If the in-lake production was sustained through this isotopically enriched DIN pool as a N source during low lake volume condition (August), higher than observed isotopic composition of POM was expected. However, the observed $\delta^{15}\text{N}_{\text{PN}}$ was ~ 1.5 ‰. This could also result from the supply of detrital organic matter from the catchment due to relatively low $\delta^{15}\text{N}$ of detrital organic matter (Kumar et al., 2004). But there was no supply of such organic matter during August due to absence of precipitation that time. Therefore, it is speculated that the lake is possibly favorable for N_2 fixation, which is reflected in low $\delta^{15}\text{N}_{\text{PN}}$. N_2 fixation is a process by which diazotrophs fix atmospheric N_2 with negligible isotopic fractionation and therefore the OM tends to show isotopic signatures

close to ~ 0 ‰. This conjecture needs to be validated through quantification of N_2 fixation rate measurements in the Nalsarovar. High $\delta^{15}N_{PN}$ during October, on the other hand, indicated uptake of DIN with relatively higher isotopic signatures and/or inputs from the terrestrial sources. The extremely high POM concentrations during August as compared to February further indicated the signature of surface blooms, which were visible during field sampling.

3.2.5.4 Source of sedimentary organic matter

Organic matter in lake sediments is primarily derived from sinking particulate which might have been produced *in situ* or received through surface runoff. The $\delta^{13}C_{SOM}$ provides a fair idea about the dominant source of OM along with the transformations taking place in the water column. Applying graphical mixing model (Miller and Tans, 2003), the source isotopic signature of SOM was estimated to be around -23.3 ± 1.2 ‰ for C and 2.9 ± 0.6 ‰ for N (Fig 3.6). These values indicate that lake particulate matter is the primary source of C and N to the sediments with little contribution from emergent macrophytes. Furthermore, the increase in isotopic composition of both C and N in sediments as compared to the source signatures indicates remineralization of OM in the water column and post sedimentation.

3.1.5.5 CH₄, CO₂, and N₂O dynamics in the lake

CH₄ concentrations in the lake increased steadily as the lake volume reduced and the lake biomass increased. This increase in CH₄ might be primarily governed by the increase in the supply of OM which acts as a substrate for CH₄ production as evident from the strong positive correlation between CH₄ and POC (Fig. 3.10). The $\delta^{13}C_{CH_4}$ increased from October to February and later decreased during August. The $\delta^{13}C_{CH_4}$ was strongly correlated to C/N ratio and $\delta^{13}C_{POC}$, particularly during February, which was a productive period as reflected by the high C/N ratio of POM (Fig 3.10). The increase in isotopic composition of CH₄ from October to February may be attributed to slight increase in the isotopic composition of the substrate (i.e., lake particulate matter). As such, the median increase in $\delta^{13}C_{POC}$ was ~ 1 ‰, whereas the median increase in $\delta^{13}C_{CH_4}$ was ~ 6.3 ‰. CO₂ concentrations in the lake reduced slightly during February which might be attributed to uptake during primary production. However, the CO₂ dynamics in the lake was complex and seemed to be controlled by several processes leading to mixed isotopic signatures. For instance, uptake during primary productivity

would result in a decrease in concentration and increase in $\delta^{13}\text{C}_{\text{CO}_2}$. Similarly, decomposition of OM would increase the CO_2 concentrations with depleted $\delta^{13}\text{C}_{\text{CO}_2}$. During February, a slight decrease in CO_2 along with a significant reduction in $\delta^{13}\text{C}_{\text{CO}_2}$ was observed. The fall in $\delta^{13}\text{C}_{\text{CO}_2}$ accompanied by concurrent increase in $\delta^{13}\text{C}_{\text{CH}_4}$ indicates possible oxidation of CH_4 to CO_2 during this period. Conversely, high $\delta^{13}\text{C}_{\text{CO}_2}$ ($-10.6 \pm 1.7 \text{‰}$) during October indicates CO_2 in equilibration with the atmosphere and the depletion during later months suggests a coupling between primary production and respiration.

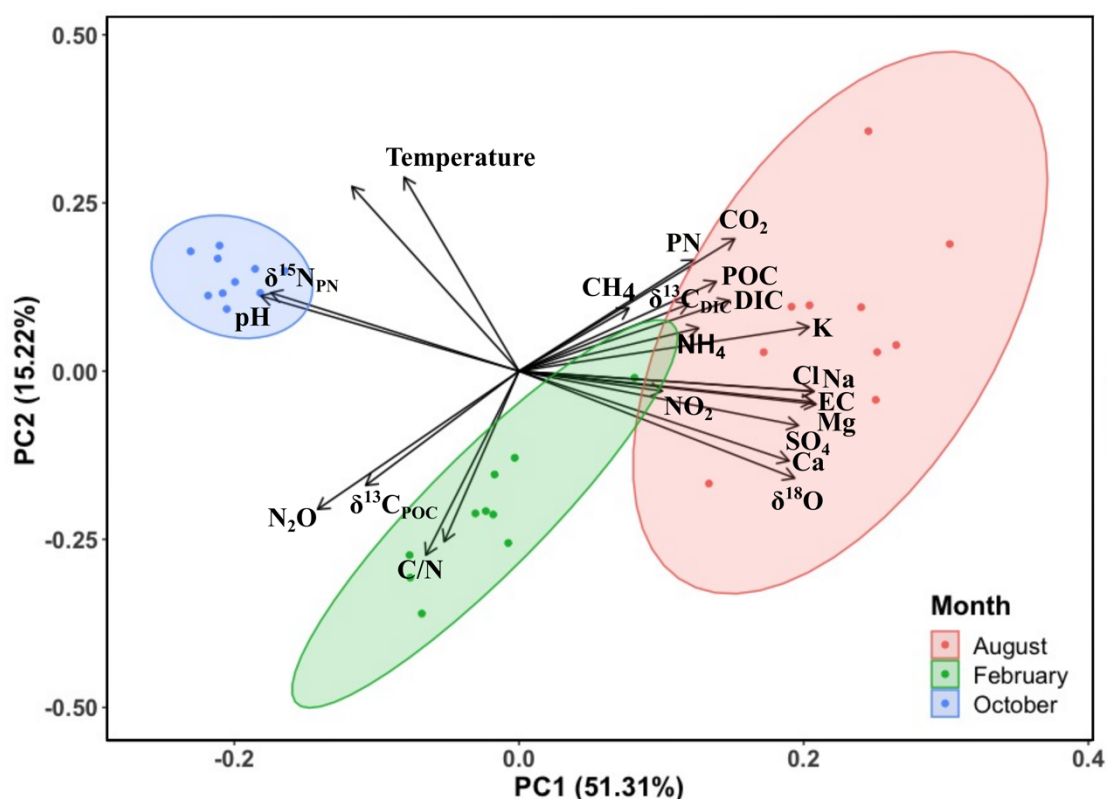


Fig. 3.10 PCA of measured parameters in Nalsarovar during different seasons.

The use of graphical mixing model (Miller and Tans, 2003) in this study helped to calculate the source isotopic signatures of CH_4 and CO_2 (Fig 3.11; Table 3.1). The $\delta^{13}\text{C}_{\text{CO}_2\text{-SOURCE}}$ during October was $\sim -7.7 \pm 1.7 \text{‰}$ which later decreased to $-19.4 \pm 0.7 \text{‰}$ during February and increased to $-14.9 \pm 0.7 \text{‰}$ during August (Table 3.1). This supports the earlier argument on the shift of the lake from a well-mixed system in equilibration with the atmosphere during October to enhanced respiration and/or CH_4 oxidation during February. The $\delta^{13}\text{C}_{\text{CH}_4\text{-SOURCE}}$ followed a similar trend as CO_2 with enriched source during October $\sim -47.6 \pm 2.8 \text{‰}$ and depleted during February (-53.0

± 0.5 ‰) and August (-51.9 ± 1.0 ‰). Increase in N_2O from October to February and sharp decrease during August was observed. During February, the low water temperature might have decreased the activity of N_2O reductase in denitrification, favoring N_2O accumulation in lake (Veraart et al., 2011; Kortelainen et al., 2020). Furthermore, the sharp decline during August might be because of high POM in surface waters, indicative of algal blooms (with low $\delta^{15}\text{N}$ signatures), which upon settling might have caused anoxia in the sediments, reducing the efficiency of the coupled nitrification- denitrification process (Zhu et al., 2020; Liang et al., 2022; Song et al., 2022). The N_2O concentrations in lake showed a balance between production and consumption of N_2O , through the coupled nitrification and denitrification processes (Wenk et al., 2016; Quick et al., 2019). However, quantification of these processes might reveal a better picture. Studies have found a significant inverse relationship between N_2O concentrations and surface DO (and Chlorophyll a level) (Webb et al., 2019). It has also been argued that even at high DIN concentration (as the case with Nalsarovar during August), there can be undersaturation of N_2O in the lake due to competition among denitrifiers and primary producers for DIN. N_2O systematics (and undersaturation) has not been explored in detail in aquatic systems compared to CO_2 and CH_4 , especially for shallow lakes where the absence of stratification induced denitrification complicates the possible N_2O consumption pathways.

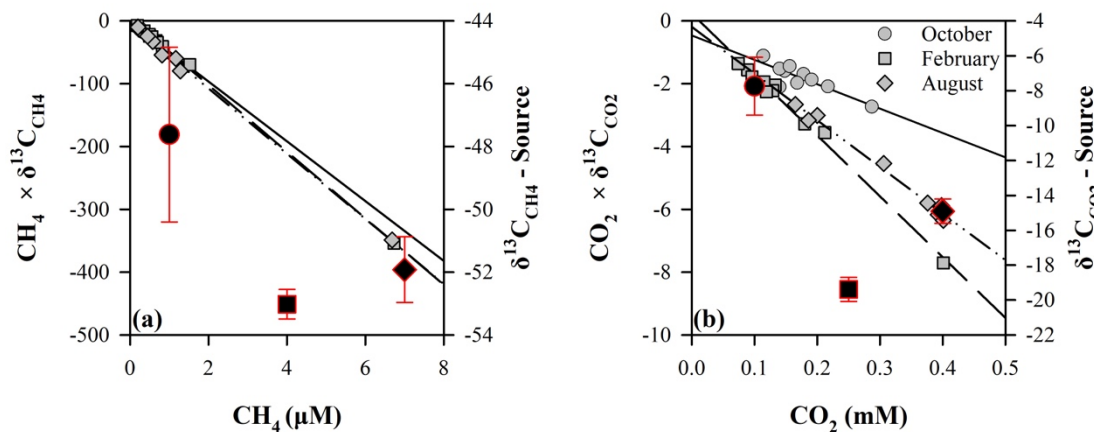


Fig. 3.11 Miller Tans plots for (a) CO_2 and (b) CH_4 . Symbols with red outline indicate source isotopic signatures. The detailed statistics are provided in Table 3.1.

Table 3.1 Summary of the least-square linear regression model equations in the Miller-Tans plots for CO₂ and CH₄ presented in Fig 3.11 with the parameters of the linear equation along with standard error in brackets for the slope, R², and number of observations (n). An approximation of the δ¹³C source values can be found in the slope of the Miller-Tans equation.

Month	Equation	R ²	n
Miller – Tans Plot: δ¹³C_{CO2} – CO₂			
October	δ ¹³ C _{CO2} × CO ₂ = -7.74 (±1.66) × CO ₂ -0.47 (±0.30)	0.73	10
February	δ ¹³ C _{CO2} × CO ₂ = -19.39 (±0.69) × CO ₂ +0.23 (±0.12)	0.99	10
August	δ ¹³ C _{CO2} × CO ₂ = -14.90 (±0.70) × CO ₂ -0.18 (±0.22)	0.99	8
Miller – Tans Plot: δ¹³C_{CH4} – CH₄			
October	δ ¹³ C _{CH4} × CH ₄ = -47.62 (±2.78) × CH ₄ -1.43 (±0.92)	0.97	10
February	δ ¹³ C _{CH4} × CH ₄ = -53.02 (±0.47) × CH ₄ +3.82 (±1.05)	0.99	10
August	δ ¹³ C _{CH4} × CH ₄ = -51.92 (±1.05) × CH ₄ -3.71 (±2.60)	0.99	8

3.1.6 Conclusion

The present study explores the effect of lake volume reduction and increasing salinity on the C and N biogeochemistry of shallow lakes. Evidently, reduction in lake volume was the primary cause of increasing ionic concentration which affected the lake productivity and other microbially mediated processes. At higher salinity, increase in lake biomass indicated a shift from heterotrophy to autotrophy. Furthermore, even at high nutrient condition, evidence for the presence of N₂ fixers were observed through decreasing δ¹⁵N_{PN} with increasing salinity and lake biomass. Dissolved CH₄, CO₂, and N₂O were controlled by complex interactions of several environmental parameters. CH₄ showed a clear dependence on availability of substrate, whereas CO₂ concentrations dipped during winter when biomass and C/N were relatively high, potentially showing role of uptake by biota. N₂O was surprisingly lowest during period of high lake biomass indicating a negative effect of productivity on N₂O production (competition for DIN/complete denitrification).

3.2 Biogeochemistry of a saline lake

The biogeochemistry of saline lakes differs from freshwater ecosystems largely in terms of their high productivity (Hammer, 1981; Melack, 1981; Blomqvist et al., 2004; Shadrin et al., 2015) and associated high rates of OM burial and calcium carbonate precipitation (Last, 1993; Jellison et al., 1996; Mirzoyeva et al., 2015). Bedrock geology and weathering in the catchment usually drive the acidic or alkaline nature of such lakes (Deocampo & Renaut, 2016). In general, nutrients and major ions tend to accumulate within the basin in the terminal or desiccation stage, giving rise to high salinity and productivity (Jones & Deocampo, 2003). Unlike $\text{HCO}_3^-/\text{CO}_3^{2-}$ in freshwater lakes, Na^+ and Cl^- are the dominant ions in saline lakes (Eugster & Hardie, 1978). The biota present in saline lakes is uniquely adapted to high salinity, and some even survive desiccation (Williams, 2002). The halophilic (salt-tolerant) organisms have the ability to optimise their metabolism by migrating across layers of oxidised and reduced environments by using diurnal fluctuations in pH and Eh (Shadrin et al., 2015). Saline lakes also harbour species like archaeobacteria (Oren, 1999), ancient stromatolites (Walter et al., 1980), and micro-niches to support a wide range of co-existing organisms (Oren, 1999). These also serve as breeding grounds and foraging sites for a large population of colonial and migratory water birds (Conway et al., 2005; Timms, 2007; Sangha, 2008; Andrei et al., 2009).

Saline lakes play a vital role in global C dynamics through efficient nutrient cycling and productivity to actively regulate the atmospheric concentrations of CO_2 and CH_4 (Horsefield et al., 1994; Blomqvist et al., 2004; Duarte et al., 2008; Camacho et al., 2017). Carbonate systems with chemically enhanced CO_2 exchange rates are much more prevalent in saline lakes (Duarte et al., 2008). Efficient nutrient recycling inside the microbial mats of saline salt pans has also been reported (Isaji et al., 2019a). In view of changing climate with large shifts in precipitation pattern and rise in mean temperatures, lakes in arid and semi-arid regions of the world are shrinking and desiccating (Williams, 1996; Jellison et al., 2008; Messenger et al., 2016; Gross, 2017). These desiccating inland waters have recently gained much attention in terms of being a source of CH_4 and CO_2 to the atmosphere (Marce et al., 2019; Keller et al., 2020; Paranaíba et al., 2022). Humans have appeared as a major threat to these ecosystems by causing surface runoff diversions for agricultural purposes, salinization, and mining (Nissenbaum, 1993; Williams, 1993; 1996; Zheng, 2001; Wurtsbaugh et al., 2017).

Although limnologists have extensively explored the elemental biogeochemistry in lakes across the globe, methodological investigations using stable isotopes are scarce in the field of saline lakes research and completely lacks from the regions like the Indian subcontinent.

In this study, using elemental and stable isotope approaches, the effect of changing salinity and lake volume on concentrations of C and N pools and the associated biogeochemical processes of a saline lake transitioning into a hyper saline have been explored. During the study, it was hypothesised that: (i) lake desiccation would elevate the ionic concentrations, specifically DIC and DIN pools; (ii) POM concentrations in lake would increase with lake turning into hypersaline; and (iii) human alterations of the natural environment of saline lakes by engineered modifications (building brine reservoirs and salt pans) would increase/decrease the residence time of water in each system. These interventions would create distinct lake environments showing unique biogeochemical signatures.

3.2.1 Study area

The sampling for the present work was conducted during winter (January) and monsoon (September) seasons of 2019 at the Sambhar Salt Lake (henceforth Sambhar) located in the state of Rajasthan in north-west India (Fig 3.12). Sambhar, formed as a result of neo-tectonism and aeolian segmentation of paleo-channels and streams, is a terminal lake in an endorheic river basin (Amal, 1990; Deshmukh & Rai, 1991; Roy, 1999). The lithology of the region consists of a Precambrian basement (schists, phyllites, and quartzites) overlain by quaternary deposits of clay and silt (Aggarwal, 1951). There are only two active channels, namely Roopangarh and Mendha, which drains into the lake for few wet days during the monsoon (Yadav et al., 2007). The catchment area of the lake is $\sim 7560 \text{ km}^2$ and the lake surface area varies seasonally between latitudes $26^{\circ}52' - 27^{\circ}02' \text{ N}$ and longitude $74^{\circ}53' - 75^{\circ}13' \text{ E}$. The width of the lake varies between 3.2 – 11.2 km, with a maximum length of $\sim 22.5 \text{ km}$ and surface area of $\sim 225 \text{ km}^2$ (Sinha & Raymahashay, 2004). The lake remains dry for most part of the year to reach a maximum reported depth of ~ 3 meters during post-monsoon (Sinha & Raymahashay, 2004). The lake falls in the rain shadow region of the Aravalli range and receives a mean annual precipitation of 100 – 500 mm (Sinha & Raymahashay, 2004). In the recent decades, Sambhar has been subjected to huge anthropogenic stress due to the construction of a brine reservoir, construction of new rail route near the eastern

wing of the basin, and establishment of numerous salt pans spread across the perimeter of the lake.

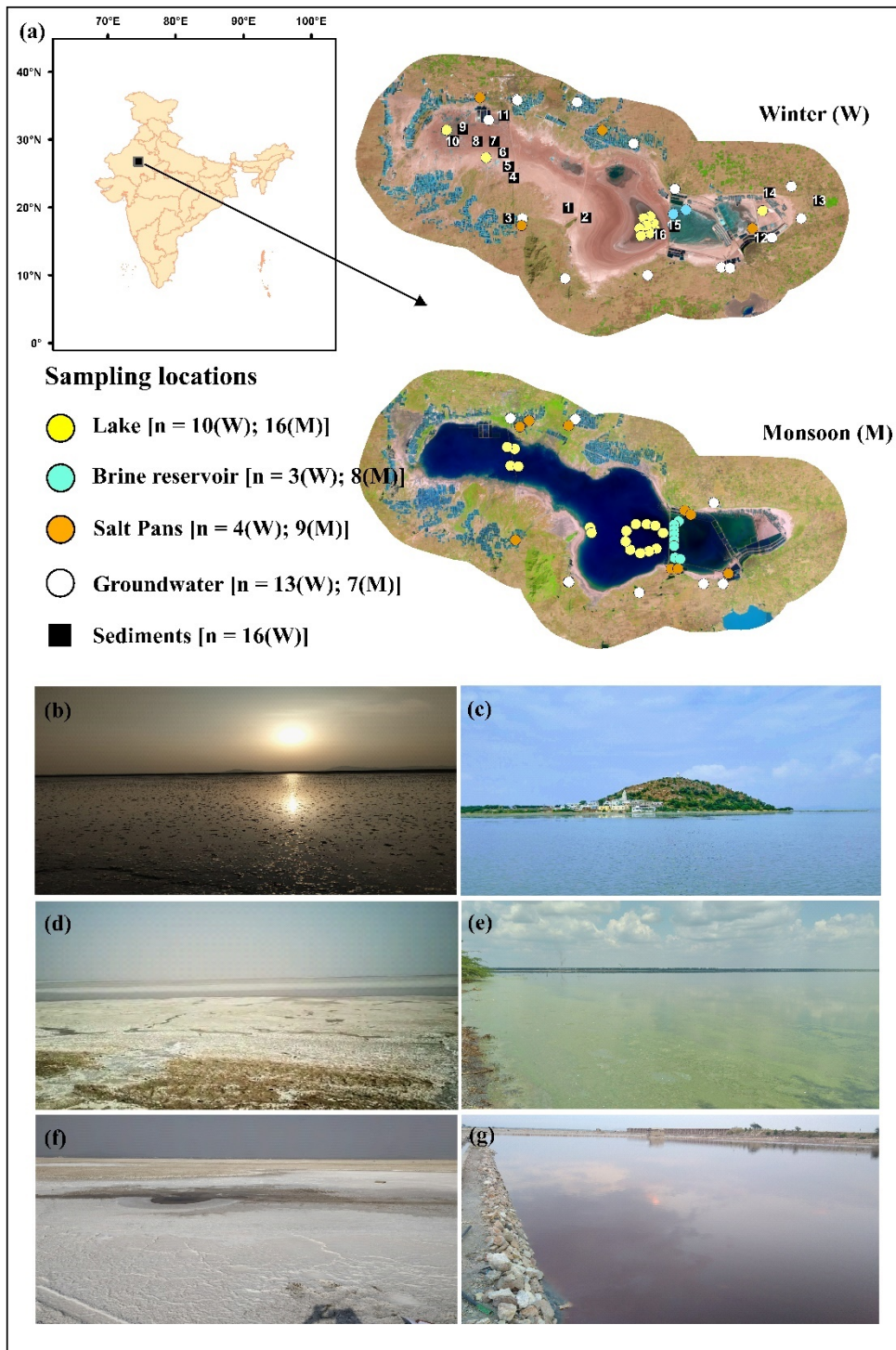


Fig. 3.12 (a) Study area and sampling locations (Sambhar salt lake, Rajasthan, India), (b) lake during winter, (c) lake during monsoon, (d) brine reservoir during winter, (e) brine reservoir during monsoon, (f) salt flats, and (g) salt pans. n represents the number of sampling locations during winter (W) and monsoon (M).

3.2.2 Sampling

Four distinct aquatic environments representing different physiochemical conditions across seasons were sampled within the study area. These environments include (a) lake region, (b) brine reservoir, separated from the natural lake by an embankment, (c) salt pans, spread across the perimeter of the basin, and (d) groundwater, where samples were collected from the tube wells (reaching deeper aquifers) and dug wells (open wells recharged by shallow groundwater) situated in clustered settlements around the lake (Fig 3.12). Due to logistic reasons, accessibility, and significant reduction in lake surface area, number of samples collected during winter and monsoon were not same. Even within season, particularly during winter, samples for some parameters were lost either during transportation or analysis. The protocols for water sampling are briefly discussed in chapter 2. In addition to collection of water samples, samples from the top 15 cm of the exposed lake sediments were collected using a corer (after removing the salt crusts/litter) at sixteen locations in different parts of the basin during winter (Fig 3.12).

3.2.3 Results

3.2.3.1 Isotopic compositions of water

The general $\delta^{18}\text{O}$ signatures of the samples were low during monsoon compared to the winter season (Fig 3.13). Except for the groundwater [$\delta^{18}\text{O}$ (mean \pm stdev): -4.2 ± 0.9 ‰ to -3.3 ± 2.2 ‰], $\delta^{18}\text{O}$ value of the samples collected from different aquatic environments in the Sambhar region showed seasonal variation from monsoon to winter. Lake surface water showed the highest enrichment (~ 20.4 ‰) during winter, followed by brine reservoir (~ 12.6 ‰). The salt pans witnessed nearly 5.7 ‰ increase from monsoon to winter.

3.2.3.2 Hydrographic parameters, major ions, and nutrients

The lake and the brine reservoir witnessed a seasonal shift from a relatively low pH system (lake ~ 8.0 ; brine ~ 8.3) during monsoon to a highly alkaline environment (lake ~ 8.8 ; brine ~ 9.2) during winter. In contrast, the mean pH of the salt pans and groundwater was high during monsoon (pH 8.6 & 8.1) and decreased in winter (pH 8.1 & 7.6). Conductivity increased manifold in the lake (28 times) and the brine reservoir (11 times) from monsoon (lake: 13.58 ± 1.32 mS cm^{-1} ; brine: 45.08 ± 1.26 mS cm^{-1}) to winter (lake: 373.52 ± 120.09 mS cm^{-1} ; brine: 480.26 ± 82.25 mS cm^{-1}).

Conductivity was primarily regulated by Na^+ and Cl^- dominant ions in the basin with low but detectable K^+ and Mg^{2+} during monsoon. SO_4^{2-} concentrations increased significantly during late winter in all the sampling classes.

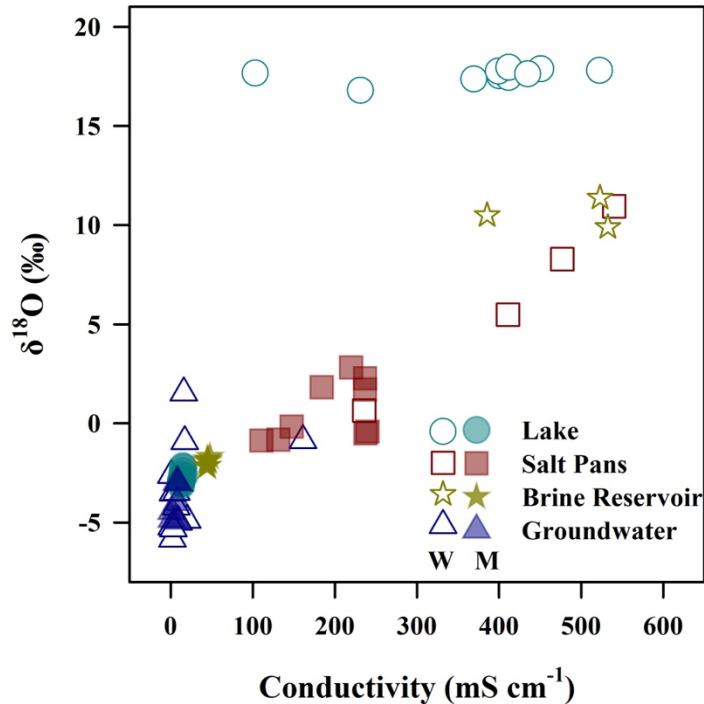


Fig. 3.13 Relationship between $\delta^{18}\text{O}$ and conductivity. Empty and filled symbols represent winter (W) and monsoon (M) samples, respectively. The $\delta^{18}\text{O}$ values are denoted in permil notation (‰) and conductivity is millisiemens per cm.

In general, NH_4^+ was the dominant inorganic form of N over NO_3^- in the region. The NH_4^+ in lake experienced maximum reduction during monsoon to $4.1 \pm 2.9 \mu\text{mol N L}^{-1}$ in contrast to the minor change in concentrations for brine reservoir to $270.0 \pm 44.1 \mu\text{mol N L}^{-1}$. NH_4^+ in the groundwater and salt pans around the lake showed a wide range without much seasonality. Low NO_3^- concentrations were observed for lake and brine samples during both the seasons (Fig 3.14). Salt pans showed a wide range in NO_3^- concentrations during both winter ($51.3 \pm 69.1 \mu\text{mol N L}^{-1}$) and monsoon ($8.4 \pm 10.7 \mu\text{mol N L}^{-1}$) seasons (Fig 3.14). NO_3^- concentrations were the highest in groundwater, showing relatively lower values during monsoon ($78.2 \pm 49.7 \mu\text{mol N L}^{-1}$) compared to the winter ($131 \pm 90 \mu\text{mol N L}^{-1}$). Lake $\text{NH}_4^+ / \text{NO}_3^-$ was very high (~ 20) in winter and decreased drastically (~ 1.7) during monsoon. However, the ratio did not change much for the brine reservoir (~ 37.8 to ~ 36.7).

Table 3.1 Basic sediment properties. SWC and SOM are sediment water content and sediment organic matter, respectively. $\delta^{13}\text{C}_{\text{SOM}}$ and $\delta^{15}\text{N}_{\text{TN}}$ are the stable carbon and nitrogen isotopic compositions of sediment organic matter and total nitrogen, respectively.

Sample ID	pH	Conductivity ($\mu\text{S}/\text{cm}$)	SWC ($\text{gH}_2\text{O}/\text{g}$ dry sediment)	%C	$\delta^{13}\text{C}_{\text{SOM}}$	%N	$\delta^{15}\text{N}_{\text{TN}}$	C/N	$\text{NH}_4\text{-N}$ ($\mu\text{mol}/\text{L}$)	$\text{NO}_3\text{-N}$ ($\mu\text{mol}/\text{L}$)
S1	10.26	23.21	0.260	0.43	- 19.2	0.04	7.0	8.68	18.46	0.47
S2	10.24	14.78	0.151	0.24	- 21.1	0.03	5.2	6.78	26.46	0.06
S3	8.31	0.15	0.003	0.09	- 20.8	0.01	8.8	6.01	NA	16.26
S4	10.29	12.10	0.108	0.18	- 20.7	0.03	8.3	5.71	13.88	0.06
S5	9.14	23.56	0.197	0.28	- 20.2	0.02	8.0	10.50	NA	2.75
S6	10.15	12.54	0.165	0.32	- 20.2	0.04	7.3	6.47	13.56	0.40
S7	10.20	12.54	0.073	0.48	- 20.1	0.05	9.0	7.68	5.62	NA
S8	9.90	13.96	0.271	0.53	- 20.2	0.06	8.7	7.91	NA	NA
S9	9.88	17.88	0.289	0.54	- 19.7	0.06	7.6	7.24	2.10	NA
S10	9.48	10.62	0.212	0.46	- 19.7	0.06	8.9	6.46	1.81	2.59
S11	10.26	6.89	0.181	0.37	- 20.1	0.04	7.2	8.46	1.07	NA
S12	10.40	9.41	0.281	0.05	- 23.8	0.01	17.0	5.87	NA	NA
S13	8.32	0.18	0.009	0.20	- 20.0	0.02	9.6	7.26	NA	NA
S14	10.48	2.20	0.281	0.32	- 20.4	0.03	10.6	9.59	0.63	0.63
S15	10.20	13.00	0.127	1.76	- 23.3	0.14	8.6	10.69	NA	NA
S16	9.19	14.56	0.207	1.58	- 22.0	0.21	6.5	6.43	2.08	0.65

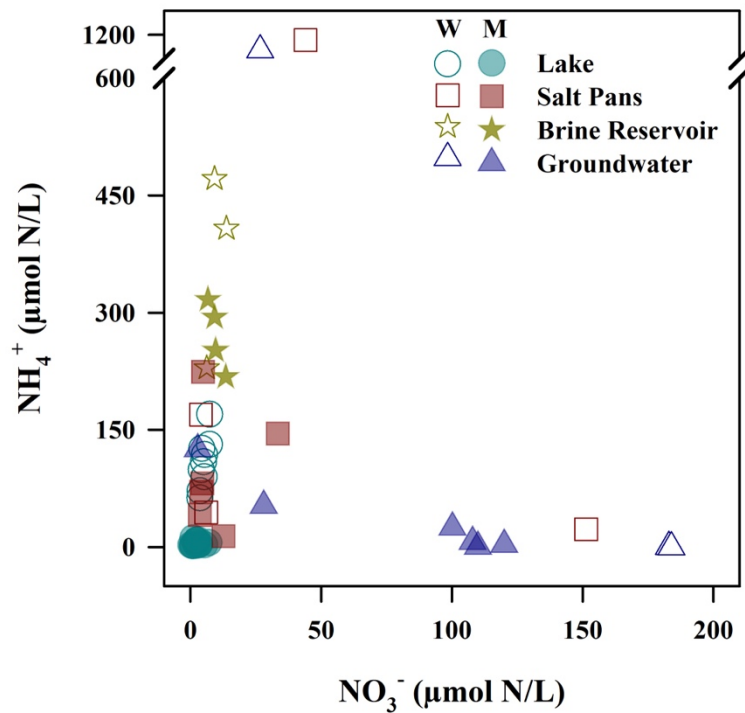


Fig. 3.14 Relationship between NO_3^- and NH_4^+ during winter (W) and monsoon (M). Empty and filled symbols represent winter (W) and monsoon (M) samples, respectively.

3.2.3.3 Dissolved inorganic carbon

The DIC concentration in lake and brine reservoir increased manifold from monsoon to winter followed by an increase in $\delta^{13}\text{C}_{\text{DIC}}$ (Fig 3.15). In brine reservoir, DIC increased from 15.6 ± 1.5 to 234.1 ± 12.0 mM, accompanied by an increase in $\delta^{13}\text{C}_{\text{DIC}}$ by around 1.6 ± 1.5 ‰. The lake witnessed a similar increase in DIC from 3.6 ± 0.6 to 68.5 ± 4.7 mM. The change in $\delta^{13}\text{C}_{\text{DIC}}$ was higher in lake (~ 5.0 ‰) as compared to that in brine reservoir (~ 1.6 ‰). Groundwater did not show much seasonality in DIC concentrations or its isotopic signature and had wide distribution (9.8 ± 4.4 mM and -9.7 ± 3.1 ‰ in monsoon; 14.6 ± 9.3 and -8.0 ± 2.4 ‰ in winter). However, the groundwater was most depleted in $\delta^{13}\text{C}_{\text{DIC}}$ compared to other reservoirs (Fig 3.15). Salt pans, similar to groundwater, had negligible seasonal variations in their isotopic composition. An outlier was observed in salt pan during monsoon, having $\delta^{13}\text{C}_{\text{DIC}}$ value of 2.8 ‰. However, during monsoon, the DIC concentrations in salt pans (53.3 ± 22.5 mM) remained higher than in the lake and brine reservoir.

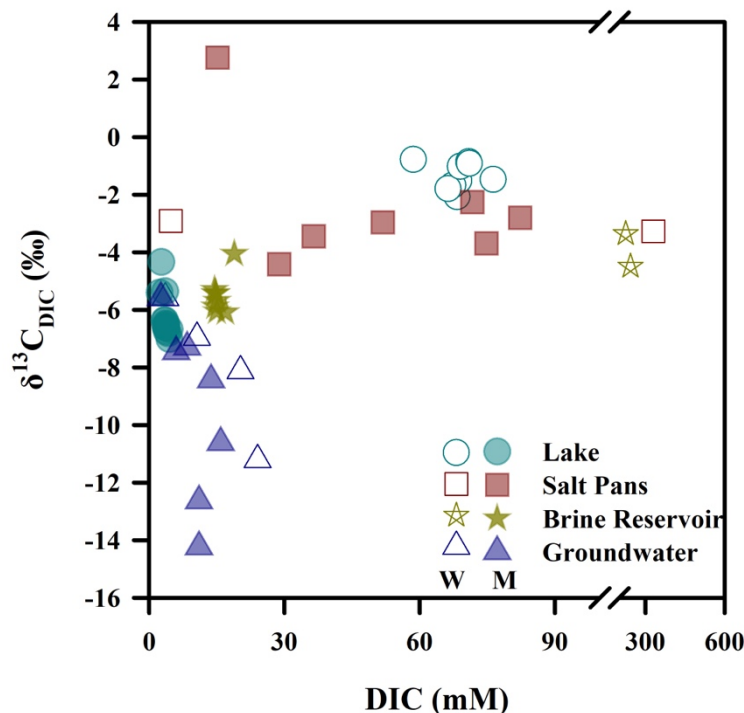


Fig. 3.15 Relationship between dissolved inorganic carbon (DIC) and $\delta^{13}\text{C}_{\text{DIC}}$ during winter (W) and monsoon (M). Empty and filled symbols represent winter (W) and monsoon (M) samples, respectively.

3.2.3.4 Particulate organic matter contents and its isotopic compositions

POM (POC and PON) concentrations were the highest for brine samples followed by salt pans and lake water during both seasons (Fig 3.16). The range of POC and PON concentrations in brine was high and narrow during the winter season (POC: 57.8 to 164.2 mM, PON: 4.3 to 14.9 mM), which further widened during monsoon (POC: 3.0 to 171.9 mM, PON: 0.3 to 46.1 mM) with values mostly skewed towards the lower end (Fig 3.16). The POC concentrations in salt pan increased, whereas PON concentration decreased in the monsoon compared to the winter season. The lake water showed very low POC (0.3 to 0.6 mM) during the monsoon, which increased up to 22.9 mM in the winter season (Fig 3.16). Similar to POC, the PON concentration of the lake was also higher in winter compared to the monsoon season. The C:N ratio of the samples was less than 20 and was higher during winter than the monsoon season for all the aquatic environments (Fig 3.16).

The $\delta^{13}\text{C}_{\text{POM}}$ showed clear seasonal shifts in the lake and brine reservoir (Fig 3.17). For lake, $\delta^{13}\text{C}_{\text{POM}}$ (‰) increased from -28.9 ± 1.8 in monsoon to -23.6 ± 0.7 in winter. It was opposite for brine reservoir where $\delta^{13}\text{C}_{\text{POM}}$ (‰) decreased from monsoon

(-20.6 ± 1.5) to winter (-24.8 ± 0.2). The salt pans showed a wide range of $\delta^{13}\text{C}_{\text{POM}}$ signatures without significant seasonal variations (-22.9 ± 3.7 in monsoon and -21.2 ± 2.2 in winter). $\delta^{15}\text{N}_{\text{POM}}$ showed peculiar variations within and across seasons with high heterogeneity. In both the seasons, $\delta^{15}\text{N}_{\text{POM}}$ of lake and brine reservoir were low (< 8) as compared to the higher $\delta^{15}\text{N}_{\text{POM}}$ in salt pans (> 14 ‰). However, a few pans showed low $\delta^{15}\text{N}_{\text{POM}}$ (< 6 ‰) values during monsoon as well. A decrease in the mean $\delta^{15}\text{N}_{\text{POM}}$ from monsoon to winter for both lake ($4.6 \pm 1.9 \rightarrow 2.3 \pm 1.0$) and brine reservoir ($4.0 \pm 2.8 \rightarrow 0.6 \pm 0.7$) was also observed.

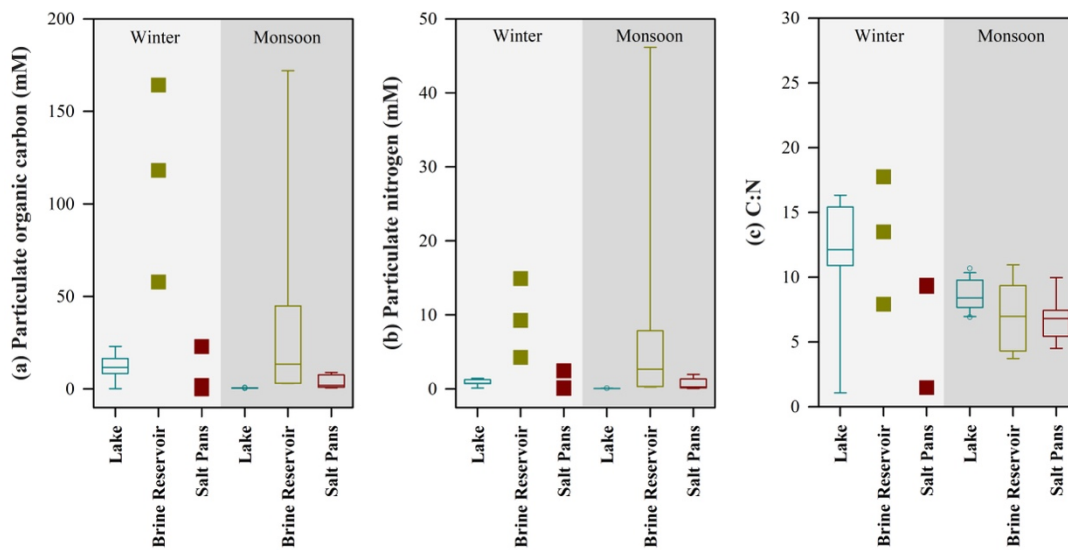


Fig. 3.16 Seasonal variation in the (a) particulate organic carbon (POC), (b) particulate organic nitrogen (PON) and (c) C/N ratios in different sample classes. Winter and monsoon seasons are represented by light grey and dark grey shades respectively.

3.2.3.5 Basic properties of sediments

The pH of the sediments was alkaline throughout and ranged from 8.3 to 10.7 (Table 3.2). Conductivity and soil water content showed large variation within the lake sediments, particularly due to very low values at S3 and S13, which were the farthest sites from the periphery of the lake (Table 3.2). The SOC and TN of the sediments were low (Table 3.2) and similar to that observed in semi-arid soils (Sharma and Kumar, 2022). Among all the samples, sediments collected from near the lake and the brine reservoir (S15 & S16) showed the highest TOC and TN contents (Table 3.2). Despite this, there was no significant variation in $\delta^{13}\text{C}_{\text{TOC}}$ and $\delta^{15}\text{N}_{\text{TN}}$ of the samples collected from different sectors (Table 3.2). The C:N ratio in sediments remained nearly constant and did not show much variation in the lake (Table 3.3). NH_4^+ concentrations were high

at the periphery of the central region (S1, S2) and on the western side (S4 and S6) of the lake. NO_3^- was low at most locations and showed highest value at S3 (Table 3.2).

3.2.4 Discussion

3.2.4.1 Hydrological characteristics of the lake

$\delta^{18}\text{O}$ of water samples collected from different classes showed significant seasonal variations (Fig 3.13). The $\delta^{18}\text{O}$ of samples were low during monsoon because of inputs from isotopically depleted rainwater (Yadav, 1997). The water oxygen became more highly enriched during winter because of intense evaporation. Estimate of the evaporative loss in each aquatic environment using the Rayleigh fractionation equation was performed ($\delta^{18}\text{O}_{\text{Winter}} = (\delta^{18}\text{O}_{\text{Monsoon}} + 1000) \times f_{\text{Ev}}^{(\alpha-1)} - 1000$). Lake was assumed as a terminal setting where the only input of water is from rain, and the loss happens via evaporation and seepage. From the Na^+/Cl^- ratios of the lake water and its pH, it can be concluded that the major source of water is precipitation and surface runoff, not groundwater, which is consistent with an earlier study (Yadav, 2007). This assumption was supported by field observations of surrounding dug wells which remained recharged even during winter when the lake started to desiccate. Therefore, it appears that groundwater input to the lake was negligible. For the fractionation factor (α) at 25°C, a value of 0.9908 was used (Gat and Gonfiantini, 1981). Using the Rayleigh equations, it was calculated that the lake lost ~ 89 % while brine lost ~ 74 % of its surface water from monsoon to winter. The difference in evaporative loss between the lake and reservoir can be attributed to the larger surface area/volume of the lake. This estimation was not possible for salt pans because they were spread all across the perimeter, utilising groundwater at different frequencies and mixing them with different grades of brine, thereby making it difficult to constrain the source of water. It seems that the $\delta^{18}\text{O}$ of salt pans are modified by the fraction of each source and the residence time of the water in the pans, thereby resulting in older pans showing highly enriched $\delta^{18}\text{O}$ signatures.

3.2.4.2 Lake nutrient dynamics and ion chemistry

NH_4^+ and NO_3^- concentrations in the different sectors of sambhar lake (Fig 3.14) showed drastic seasonal variations with low NH_4^+ concentrations during the monsoon seasons, probably due to dilution effect, later reaching very high concentration by winter. This increase in nutrient concentration could be attributed to the shrinking lake

size during the dry period. The increase in the concentration of NH_4^+ agreed with our hypothesis of increasing ion concentration with lake desiccation that occurs in winter. However, the NO_3^- concentrations did not increase at the same magnitude as NH_4^+ , indicating other controls over the NO_3^- dynamics. Sambhar lake witnesses large flocks of migratory birds during the winter season, which might cause subsequent guantrophication as a result of overcrowding of birds (mostly flamingos) in a reduced lake surface area (Batanero et al., 2017). Their guano might be a dominant source of NH_4^+ to the lake during this period (Manny et al., 1994; Post et al., 1998; Kitchell et al., 1999; Hahn et al., 2007,2008; Huang & Isobe, 2012; Dessborn et al., 2016). The role of water birds in regulating the nutrient dynamics of such arid lakes during breeding and wintering periods by importing nutrients from foraging areas and also many a time causing bioturbation of sediments, releasing nutrients to the surface waters is well documented (Glassom & Branch, 1997; Bodelier et al., 2006; Rodríguez-Pérez & Green, 2006). High NH_4^+ concentrations were observed in the brine reservoir even during monsoon, probably due to the presence of large volumes of pre-existing slurry, which reduced the dilution effect of monsoon precipitation. During winter, the very high NH_4^+ concentration in the brine could have been supported by efficient recycling of OM supported by high surface organic biomass. Furthermore, presence of thick microbial mats on the surface of the brine reservoir (as observed during sampling) might have prevented the escape of NH_3 from the brine during the low gas solubility phase in increased salinity conditions (Isaji et al., 2019b). This was not the case in lake water, where the shallow depth and the absence of surface microbial mats would have easily supported gaseous exchange. Interestingly, the $\text{NO}_3^-/\text{NH}_4^+$ ratios decreased in all the sampling classes from monsoon to winter, suggesting significant inhibition of nitrification in high salinity and pH conditions (Isaji et al., 2019b) as hypothesized initially.

3.2.4.3 Dissolved inorganic carbon cycling in the lake

Sambhar Lake witnessed high seasonal variation in the DIC concentration and $\delta^{13}\text{C}_{\text{DIC}}$ (Fig 3.15). During monsoon, heavy rainfall and runoff resulted in a large change in the lake volume with low DIC concentration. The relatively lower pH of surface waters during monsoon reflected the increased role of dissolved CO_2 in the DIC pool, which was also seen in decreased $\delta^{13}\text{C}_{\text{DIC}}$ (Bade et al., 2004). Surface runoff after a long summer from the watershed dominated by plants has been reported to have low $\delta^{13}\text{C}_{\text{DIC}}$

(Gu et al., 2006). Towards winter, in agreement with the hypothesis, the DIC concentration increased manifold, primarily due to shrinking lake volume (Fig. 3.15). Also, the shallow water depth during this period was easily affected by local wind motions resulting in suspension of loose sediments, which might also contribute to an increased DIC (Song et al., 2013). The increase in DIC concentration in both the lake and the brine reservoir during winter was accompanied by increase in $\delta^{13}\text{C}_{\text{DIC}}$. This isotopic enrichment was higher in the lake water as compared to the brine reservoir, and therefore could be attributed to higher rates of CO_2 evasion from the lake water during this period leading to increased $\delta^{13}\text{C}_{\text{DIC}}$ in the remaining pool. This explanation is further supported by the higher evasion rates of gases in low solubility conditions at higher salinities. Preliminary data of dissolved CO_2 (not included in this study) indicates the lake acting as a source of CO_2 to the atmosphere during the winter.

3.2.4.4 Lake biomass and productivity

In Sambhar Lake, productivity increased from monsoon to winter which can be observed indirectly from the elevated OM concentration (both POC and PON; Fig 3.16) and relatively higher C:N ratio during winter (Fig 3.16). Although we envisaged an effect of lake desiccation on the POM dynamics, the observed increase in POM concentrations from monsoon to winter were very high. Simultaneous increase in $\delta^{13}\text{C}_{\text{POM}}$ (Fig 3.17) of the lake during winter also appeared to be a result of increased productivity and uptake of enriched DIC as discussed earlier (Hollander & McKenzie, 1991; Zohary et al., 1994; Gu et al., 2006, 2011). It is known that in HCO_3^- dominated system, when the growth rate is high, planktons consuming HCO_3^- as a C source show elevated $\delta^{13}\text{C}_{\text{POM}}$ (Mook et al., 1974). The presence of cyanobacterial blooms during winter might have also contributed to the high $\delta^{13}\text{C}_{\text{POC}}$ due to the direct uptake of atmospheric CO_2 at the water surface-atmosphere interface by the surface blooms (Gu & Alexander, 1993; Zohary et al., 1994; Kiyashko et al., 1998). This behaviour of the surface blooms along with the diffusive CO_2 fluxes could ultimately decide the net CO_2 budget of the lake.

In contrast, at a few sites in the brine reservoir, the C:N was higher during monsoon, possibly due to allochthonous source of particulate matter from the banks of the reservoir dominated by terrestrial plants (Sterner & Elser, 2002; Naftz et al., 2008b), which were absent near the lake. The brine reservoir experienced lowering in $\delta^{13}\text{C}_{\text{POC}}$ during winter compared to monsoon with opposite trend in $\delta^{13}\text{C}_{\text{DIC}}$. From the C:N ratio,

it is evident that the higher $\delta^{13}\text{C}_{\text{POM}}$ in the brine during monsoon reflected the isotopic signature of the allochthonous inputs of POM (Grey et al., 2001). The salt pans were spread all across the periphery of the lake with mixed environmental settings. Furthermore, the use of groundwater controlled the isotopic composition of DIC and therefore of POM in the salt pans.

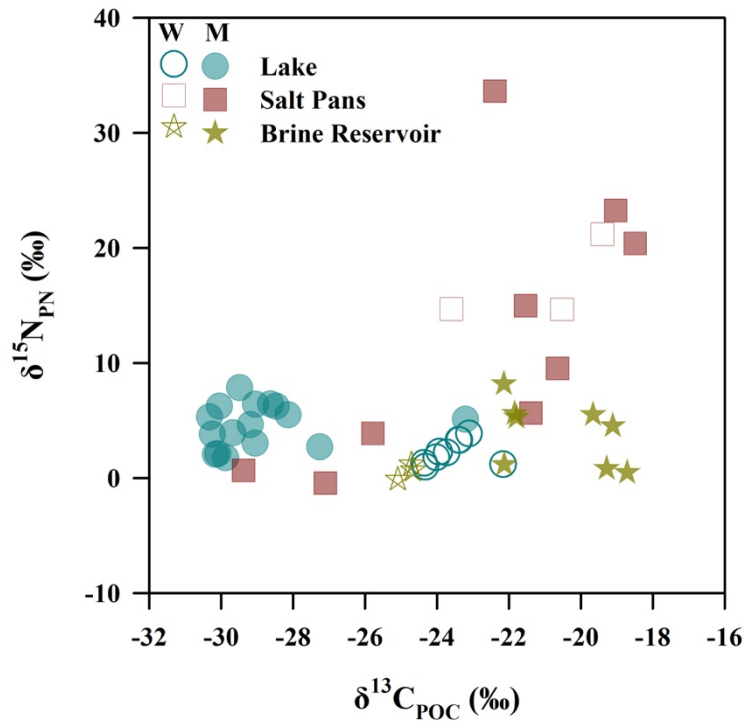


Fig. 3.17 Relationship between C and N isotopic composition of POM ($\delta^{13}\text{C}_{\text{POM}}$ and $\delta^{15}\text{N}_{\text{POM}}$) during winter (W) and monsoon (M). Empty and filled symbols represent winter (W) and monsoon (M) samples, respectively.

The $\delta^{15}\text{N}_{\text{POM}}$ of the lake varied from ~ 0 to 7.9 ‰. During late winter, when productivity was high, the low $\delta^{15}\text{N}_{\text{POM}}$ might be associated with N_2 fixation as N_2 fixers use N_2 (0 ‰) as their sole N source and show negligible fractionation during fixation (Hoering and Ford, 1960; Delwiche and Steyn, 1970; Estep and Vigg, 1985; Gu and Alexander, 1996). Although activity of N_2 fixers is known to be less in lakes with high DIN and therefore $\delta^{15}\text{N}_{\text{POM}}$ is usually high, Sambhar appears to indicate a different story. However, quantification of N_2 fixation rates would be needed to confirm the same. It has been reported that $\delta^{15}\text{N}_{\text{POM}}$ increases from oligotrophic to eutrophic lakes and decreases in hypereutrophic lakes (Gu et al., 2006). This decrease in $\delta^{15}\text{N}_{\text{POM}}$ is usually attributed to the presence of N_2 fixing cyanobacteria (Gu and Alexander, 1993; Havens et al., 1998; Chapman & Schelske, 1997; Vuorio et al., 2006; Gondwe et al., 2008).

Also, with high cyanobacterial blooms, the decomposition of biomass releases isotopically light DIN (Gu et al., 2006). Uptake of this DIN as a N source might also contribute to low $\delta^{15}\text{N}_{\text{POM}}$ observed in the Sambhar. During monsoon, the surface runoff from the watershed might have brought isotopically enriched DIN resulting in higher $\delta^{15}\text{N}_{\text{POM}}$. Nitrification and denitrification in the soils of the watershed affected by the use of nitrogenous fertilizers lead to an enrichment in their isotopic signature (Paerl and Fogel, 1994). Nitrification during low salinity and pH conditions of the monsoon can result in isotopically enriched NH_4^+ and, therefore, high $\delta^{15}\text{N}_{\text{POM}}$ (Syvaranta et al., 2006). Also, in relatively low DIN condition during monsoon, less isotope fractionation while uptake of nutrients might have also contributed to the observed higher $\delta^{15}\text{N}_{\text{POM}}$ (Jones et al., 2004). In the salt pans, high rates of evaporation cause dissociation of NH_4^+ to $\text{NH}_3(\text{g})$, which degasses out, leaving an isotopically enriched NH_4^+ pool (Isaji et al., 2019c). Uptake of this NH_4^+ might be a causal factor for extremely high $\delta^{15}\text{N}_{\text{POM}}$ in the salt pan.

Overall, significant differences in seasonal patterns in C and N cycling in the three studied environments (Lake, brine reservoir, and salt pans) were observed, which further supported our hypothesis of considerable effect of human interventions on lake biogeochemistry.

3.2.4.5 Organic matter contents in sediments

Isotopic analysis of SOM provides an idea about the sources of OM and its transformation in the water column and post sedimentation (Meyers, 2003). Sambhar desiccates seasonally, leaving behind large expanse of salt flats. Attempt was made to understand the post deposition dynamics and fate of the SOM resulting from the high productivity of surface waters. The $\delta^{13}\text{C}_{\text{SOM}}$ and C/N ratios (Table 3.2) suggested largely autochthonous source of OM with negligible terrestrial inputs (Meyers, 1994). Low organic C content ($< 2 \text{ mg kg}^{-1}$) in sediments of the lake pointed towards the possibility of high degradation of OM. Low organic C burial efficiency has been observed in lakes with dominant autochthonous sources of OM (Sobek et al., 2011) as these OM are highly prone to mineralisation. The degradation of these autochthonous OM, unlike allochthonous inputs, is unaffected by oxygen availability (Kristensen et al., 1995; Hulthe et al., 1998; Bastviken et al., 2004b; Sobek et al., 2009). Therefore, it appears that Sambhar Lake witnesses high rates of productivity followed by degradation. The $\delta^{13}\text{C}_{\text{SOM}}$ during winter showed $\sim 3 \text{ ‰}$ and 9 ‰ increase with respect

to $\delta^{13}\text{C}_{\text{POM}}$ of late winter and monsoon, respectively. This increase in C isotopic composition from surface to sedimentary OM also indicated high rates of OM degradation. The difference of $\sim 2.5\text{‰}$ to $\sim 4.5\text{‰}$ between $\delta^{15}\text{N}_{\text{TN}}$ and $\delta^{15}\text{N}_{\text{POM}}$ also suggested high mineralization of POM to NH_4^+ within the water column and post deposition resulting in isotopic enrichment of residual OM (Robinson, 2001). To support the findings of this study, knowledge of the rates of biogeochemical processes active in the lake on seasonal scale would be ideal.

3.2.5 Conclusion

This study focussed on cycling of C and N in hypersaline lake, brine reservoir, and salt pans to understand the temporal flow and associated biogeochemical processes of these elements in sub-tropical extreme environments. The studied settings were distinct from each other with respect to physical and chemical characteristics and the extent of anthropogenic influence. The lake experienced desiccation from monsoon to winter, leading to change in water chemistry. The brine, which harboured extensive microbial mats, retained water during the studied period. The OM in the lake was of autochthonous origin, whereas the same in brine was influenced by the allochthonous supply from the nearby vegetation. The shift in lake morphometry across seasons was accompanied by drastic change in elemental biogeochemistry of the system. Significant build-up in NH_4^+ concentration in lake water from monsoon to winter, posed huge potential to produce toxic blooms, which could act as a substrate for methanogenesis, suggesting potential role of saline lakes as a source of atmospheric CH_4 . Observed low $\delta^{15}\text{N}_{\text{POM}}$ suggested N_2 fixation in the lake and brine, which was contrary to the general understanding of lack of N_2 fixers in nutrient rich environment and needs quantification to prove as such. DIC in the lake and brine showed significant increase in concentration from monsoon to winter, followed by an isotopic enrichment, indicating the potential role of lake desiccation in modulating C cycling of hypersaline environment.

Chapter 4

River Biogeochemistry

Rivers act as active conduits for the transport of C and N from the terrestrial to the marine system. Research on riverine biogeochemical cycling of C and N is gaining momentum with the inclusion of inland waters in the IPCC budgets and the identification of flowing waters as hotspots for greenhouse gas emissions (Masson – Delmotte et al., 2021). The processes involved in the riverine C and N cycling varies across space and time due to shifts in environmental variables (temperature and precipitation) and changes in catchment characteristics (lithology, land use, and land cover). These factors govern the allochthonous loading of nutrients along with particulate and dissolved forms of C and N to the streams. It is estimated that inland waters receive $\sim 1.7 \text{ Pg C yr}^{-1}$ from catchment soils, which then undergoes processing and burial to release $\sim 0.7 \text{ Pg C yr}^{-1}$ back to the atmosphere as CH_4 and CO_2 and sequester $\sim 0.2 \text{ Pg C yr}^{-1}$ in the sediments. The rivers and streams are assumed to transport the remaining $\sim 0.8 \text{ Pg C yr}^{-1}$ and $0.046 \text{ Pg N yr}^{-1}$ to the oceans in the form of particulate and dissolved forms (Hope et al., 1994; MacKenzie et al., 2002; McKee, 2003; Suchet et al., 2003; Cole et al., 2007; Ciais et al., 2014; Biddanda, 2017). This flux of C, if not constrained, could disturb the climate budgets and offset our climate predictions to a large extent. N is closely connected to C in the global biogeochemical cycle and often acts as a limiting nutrient, thereby making its flow vital along the land ocean continuum. With increasing human perturbations to the biosphere and a changing climate, the movement and fluxes of C and N along the river continuum has been largely altered over the past decades. Therefore, it is prudent to explore different kinds of flowing water systems vis-à-vis biogeochemical cycling.

The first section of this chapter explores the transport and transformation of TSM and associated OC and N along the Ganges during high flow and low flow conditions. For comparison with other large Asian rivers, the Mekong and Yellow River were also included in this study. In recent decades, rivers across the globe are facing shift in their hydrological regime due to natural as well as human induced changes. The nature of biogeochemical processes in river channels experiencing these hydrological changes needs to be investigated in detail. The second section of this chapter explores the C and N biogeochemistry of an engineered river system situated in a tropical and subtropical climate setting. In the context of diversity of riverine systems across climate gradients and watershed characteristics, the last section of this chapter deals with the biogeochemistry of a high-altitude river – lake systems focusing on the seasonality (spring vs autumn) and process dynamics at the river – lake transition.

4.1 Total suspended matter dynamics in large rivers

Among the world's rivers, those originating from the Tibetan Plateau carry ~ 70 % of the global suspended sediments to the oceans (Milliman and Meade, 1983; Ran et al., 2013). Tropical monsoonal rivers such as the Ganges and Mekong, originating from the Himalayan highland, have high sediment yields as well (Lu et al., 2010). The suspended matter load in rivers represents an aggregation of minerals and OM, which acts as a substrate for several microbially mediated processes that often releases CO₂, CH₄, and N₂O as by-products. Understanding the sources and fate of OM is therefore vital to constrain the loss processes of C and N from these systems. Furthermore, with increasing urbanisation and human induced changes in the flow regimes of world rivers, it is essential to revisit the export fluxes of TSM and associated C and N from the rivers. In this study, principally, an attempt has been made to understand the dynamics of C and N in TSM of the Ganges, which has been compared with two other major Asian rivers (Mekong and Yellow). The specific aims of the study were to understand (i) seasonal and spatial variations in C and N in TSM along the river continuum across the altitudinal gradient, (ii) the effect of seasonality on their concentrations and isotopic compositions along with underlying processes, and (iii) the export fluxes of C and N from these rivers and potential long-term changes compared to previous studies.

4.1.1 Study area

The Ganges, Mekong, and Yellow River originate from the Himalayan mountains and the Tibetan plateau (Fig 4.1). The source of the Ganges is the Gangotri Glacier in the Garhwal Himalaya. With headwaters at the elevation of 3800 m (Gaumukh), the mainstem of the Ganges forms later at Devprayag with the confluence of the Alaknanda and Bhagirathi Rivers (Singh, 2007). Thereafter, the river descends down into the plains and traverses a journey of ~2700 Kilometer (km), with a catchment of 1,260,000 km² (Parua, 2010). Once the river enters the Gangetic plains, it passes through major cities like Kanpur, Prayagraj, Varanasi, and Patna. A major tributary of the Ganges (i.e., the Yamuna) passes through Delhi and joins the mainstem near Prayagraj. The river supports large human population along its banks, providing water for irrigation and drinking purposes. Two bifurcated distributaries of Ganges, Hooghly and Padma, flow through India and Bangladesh, respectively. The Padma River confluence with two major rivers in Bangladesh, i.e., Brahmaputra and Meghna, before discharging into the

Bay of Bengal (Parua, 2010).

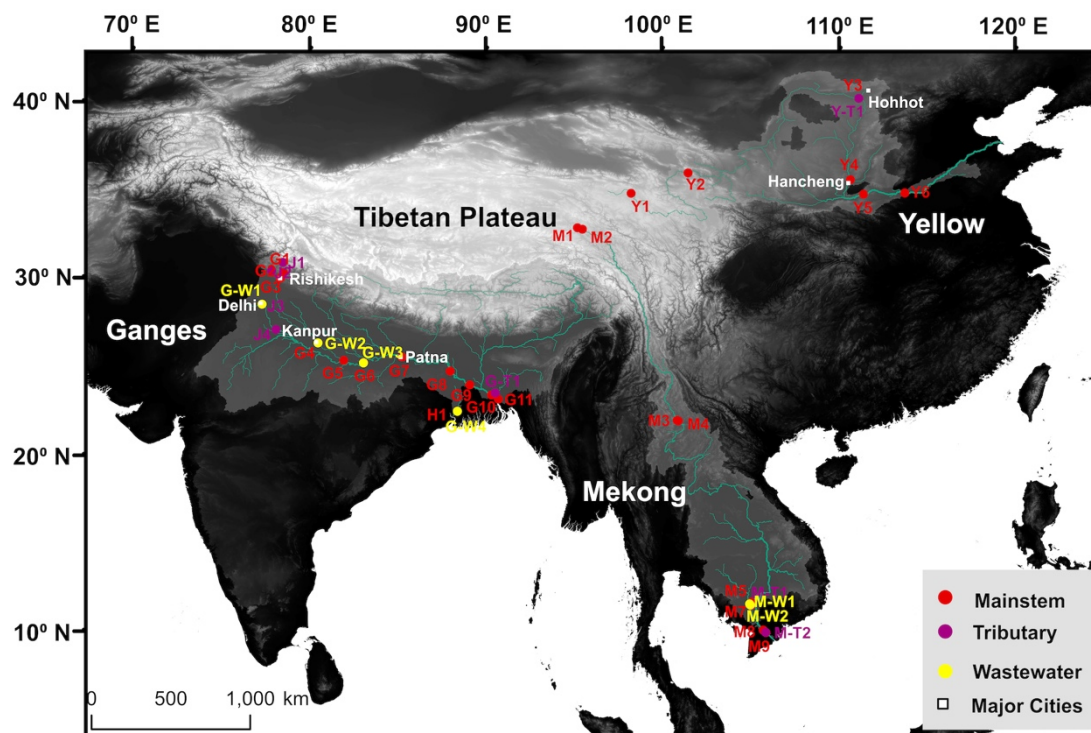


Fig. 4.1 Map showing sampling locations on the Ganges, Mekong, and Yellow River Basins (shaded).

Rising at an altitude of 5000 – 6000 m at the source in the Tibetan Plateau, the Yellow River covers around 5464 km, draining a catchment of 753,000 km² to finally discharge into the Bohai Sea near Shandong Province, China (Xu and Ma, 2009; Peng et al., 2010; Miao et al., 2011; Ran et al., 2013). The upper reaches of the Yellow River are predominantly an arid setting with complex geological structures, mainly comprising of old metamorphosed rocks, carbonates and modern fluvio-lacustrine sediments (Wang et al., 2012; Ran et al., 2013). In the middle reaches, the river drains the loess plateau, with abundant Quaternary loess deposits (Zhang et al., 1995; Chen et al., 2005; Wu et al., 2005). Finally, the lower reaches reflect a flat alluvial plain. The lower reaches have extensive man-made levees along its banks giving the perched riverbed an elevation of 3-4 m higher than the surrounding floodplains (BCRS, 2000; Peng et al., 2010).

The Mekong River originates at an elevation of 4968 m in the Tibetan Plateau and flows southwards through several countries (China, Myanmar, Thailand, Lao PDR, Cambodia, and Vietnam) to drain into the South China Sea. The channel length of the river is around 4800 km and the drainage basin area is 795,000 km². The Ganges,

Mekong, and Yellow River support around 400, 70, and 107 million people in its basins (Parua, 2010; Gao and Wang, 2017; Park et al., 2018; MRC, 2019).

4.1.2 Sampling

The sampling for the present study was carried out as a part of a larger joint project between Republic of Korea, India, China, Cambodia, Bangladesh, USA, Vietnam and Singapore (funded through Asia-Pacific Network for Global Change Research) aimed at assessing the dynamics of GHGs in these anthropogenically modified Asian river systems (Begum et al., 2021). Sampling campaigns were carried out by the collaborators along the mainstem reaches of the Ganges, Mekong, and Yellow River along with few tributaries and wastewater drains between August 2016 and July 2019 (Begum et al., 2021). The mainstems were divided in upper, middle and lower reaches. Wastewater samples were collected at outlets of natural streams or constructed drains used for discharging urban sewage (Supplement Table 1, Begum et al., 2021). Sampling was conducted during the wet (July – September; Ganges: $n = 21$, Mekong: $n = 11$ and Yellow: $n = 7$) and the dry (Jan – May; Ganges: $n = 9$, Mekong: $n = 9$ and Yellow: $n = 2$) seasons to capture the high and low flow conditions (Fig 4.1). Briefly, water samples were collected at 10-20 cm below the surface using polycarbonate bottles or a portable water sampler (Masterflex E/S, Cole-Parmer, USA; Begum et al., 2021). TSM was quantified at the Ewha Womans University, Republic of Korea (Begum et al., 2021). C and N concentrations and isotopic compositions were measured at the Physical Research Laboratory, India.

4.1.3 Results

4.1.3.1 Total suspended matter

Total suspended matter (TSM) concentration was high during the monsoon season in the mainstem of all the three river systems (Ganges: (mean \pm stdev) 263.5 ± 232.9 mg L⁻¹; Mekong: 136.3 ± 106.4 mgL⁻¹; Yellow: 707.4 ± 944.2 mg L⁻¹; Fig 4.2a, d & g). In the Ganges basin, high TSM was observed in the Yamuna (a major tributary of Ganges) near Dakpatthar Barrage (1940.6 mg L⁻¹), Delhi (254.4 mg L⁻¹) and at several sites in the Ganges mainstem along major cities (393 mg L⁻¹ near Rishikesh; 341.3 mg L⁻¹ near Kanpur; 416.9 mg L⁻¹ near Patna; 828.2 mg L⁻¹ at Hardinge Bridge near Kushtia, and 416.6 mg L⁻¹ at the confluence of Ganges and Brahmaputra near Mawa). TSM in the Mekong mainstem was the highest in the upstream reaches (128.5 ± 64.1 mg L⁻¹),

followed by the middle reaches ($82.4 \pm 26.3 \text{ mg L}^{-1}$) and tributaries ($54.7 \pm 2.7 \text{ mg L}^{-1}$) (Fig 4.2d). In the Yellow River, very high TSM were observed at two downstream sites near the outlet of loess plateau (1941.6 mg L^{-1}) and upstream of Sanmenxia Dam, Hancheng ($1909.2 \pm 64.1 \text{ mg L}^{-1}$) (Fig 4.2g). During the dry season, TSM was low in the Ganges ($53.9 \pm 34.9 \text{ mg L}^{-1}$) and Mekong ($20.7 \pm 6.0 \text{ mg L}^{-1}$), whereas high TSM load was observed at the sites along the middle reaches of the Yellow River (1656.4 mg L^{-1}) (Fig 4.2a, d & g). Wastewater TSM concentrations were around $116.2 \pm 36.4 \text{ mg L}^{-1}$ in the Ganges and $111.7 \pm 54.7 \text{ mg L}^{-1}$ in the Mekong.

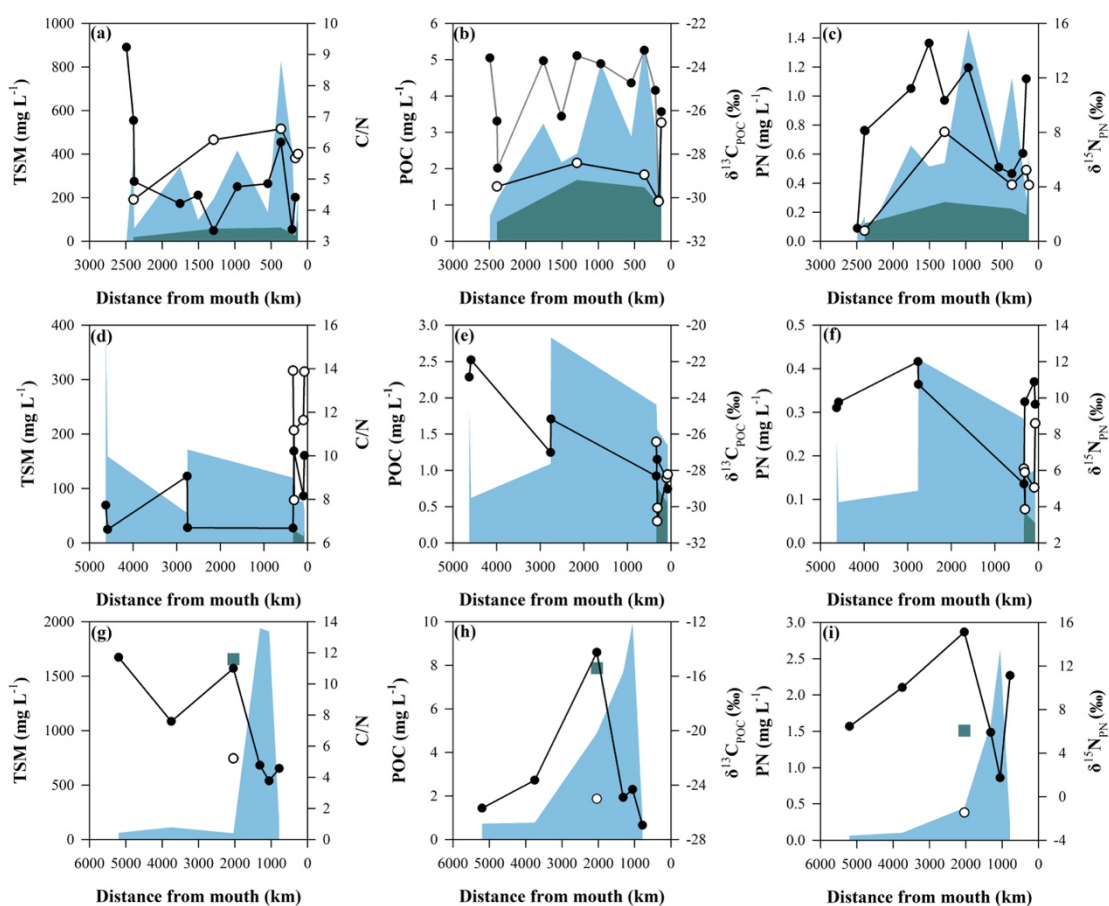


Fig. 4.2 Variation of TSM, C/N, POC, $\delta^{13}\text{C}_{\text{POC}}$, PN and $\delta^{15}\text{N}_{\text{PN}}$ along the mainstem of Ganges (a, b, and c), Mekong (d, e, and f) and Yellow River (g, h, and i). Shaded area represents TSM, POC and PN in wet (blue) and dry (dark green) seasons respectively. Circles connected by solid lines represent C/N, $\delta^{13}\text{C}_{\text{POC}}$ and $^{15}\text{N}_{\text{PN}}$ in wet (black circles) and dry (white circles) seasons. In Yellow river, dry seasons data is represented by scatter plot (dark green square and white circle).

4.1.3.2 Particulate organic carbon

During monsoon, POC (organic C of TSM) concentrations varied significantly along the mainstem of the Ganges (average $\sim 2.58 \pm 1.50 \text{ mg L}^{-1}$) with low values near the headwaters ($1.01 \pm 0.27 \text{ mg L}^{-1}$), which increased towards the middle ($3.12 \pm 1.07 \text{ mg L}^{-1}$) and downstream reaches ($3.09 \pm 1.85 \text{ mg L}^{-1}$) (Fig 4.2b). The highest POC concentration ($\sim 39.47 \text{ mg L}^{-1}$) was observed in the wastewater draining into the Ganges. The Yamuna also followed a similar trend with increasing POC from the headwaters (0.52 mg L^{-1}) to urban location near Delhi (8.39 mg L^{-1}). In general, the mean POC in the Ganges mainstem declined from monsoon to dry season (Fig 4.2b); however, the station on the Yamuna near Delhi showed an increase in the POC ($\sim 16.89 \text{ mg L}^{-1}$). Compared to the Ganges, the average concentration of POC in the Mekong was relatively low during monsoon ($1.57 \pm 0.65 \text{ mg L}^{-1}$), with 1.84 mg L^{-1} in the upstream reach, later falling to 0.62 mg L^{-1} and steadily increasing to 2.83 mg L^{-1} in the middle reach (Fig 4.2e). Downstream reaches of the Mekong River had POC $\sim 1.55 \pm 0.26 \text{ mg L}^{-1}$ with even lesser concentration ($1.21 \pm 0.17 \text{ mg L}^{-1}$) at the lower reaches where two tributaries join. During the dry season, Mekong had very low POC (downstream: $0.69 \pm 0.12 \text{ mg L}^{-1}$, tributaries: $0.79 \pm 0.24 \text{ mg L}^{-1}$) (Fig 4.2e). Similar to that in the Ganges, the highest POC in the Mekong River basin was observed at the wastewater discharge site ($\sim 4.71 \text{ mg L}^{-1}$ in monsoon and $21.28 \pm 21.87 \text{ mg L}^{-1}$ during the dry season). The Yellow River had a wide range of POC along its mainstem ($4.15 \pm 3.99 \text{ mg L}^{-1}$) with lower concentration in the upstream reach ($0.75 \pm 0.03 \text{ mg L}^{-1}$) to increase in the middle ($5.85 \pm 3.86 \text{ mg L}^{-1}$) (Fig 4.2h).

4.1.6.3 Particulate nitrogen

During monsoon, PN (total N component of TSM) in the Ganges mainstem varied between 0.08 to 1.46 mg L^{-1} (mean: 0.60 ± 0.40) (Fig 4.2c). Similar to POC, the upstream reach had low PN ($0.12 \pm 0.06 \text{ mg L}^{-1}$) as compared to the middle ($0.76 \pm 0.40 \text{ mg L}^{-1}$) and downstream reach ($0.64 \pm 0.36 \text{ mg L}^{-1}$). The highest PN was observed in the wastewaters ($2.75 \pm 3.20 \text{ mg L}^{-1}$) followed by that in the Yamuna ($1.24 \pm 0.86 \text{ mg L}^{-1}$). PN was low during the dry season ($0.25 \pm 0.13 \text{ mg L}^{-1}$) except for the site in Yamuna near Delhi ($\sim 2.60 \text{ mg L}^{-1}$) (Fig 4.2c). PN in the Mekong during monsoon had a low range ($0.20 \pm 0.11 \text{ mg L}^{-1}$) with the upstream site having PN at 0.24 mg L^{-1} . PN showed a wide range in the middle ($0.21 \pm 0.18 \text{ mg L}^{-1}$) and downstream reaches (0.19

$\pm 0.07 \text{ mg L}^{-1}$) with low values for tributaries ($0.13 \pm 0.02 \text{ mg L}^{-1}$) (Fig 4.2f). PN decreased during the dry season with average concentration $\sim 0.06 \pm 0.03 \text{ mg L}^{-1}$ in the downstream reaches and $\sim 0.09 \pm 0.04 \text{ mg L}^{-1}$ in the tributaries (Fig 4.2f). In the Yellow River, PN showed a wide range ($0.84 \pm 1.05 \text{ mg L}^{-1}$) with low concentrations in the upstream region ($0.08 \pm 0.03 \text{ mg L}^{-1}$) and higher concentrations with wider range (1.22 ± 1.12) mg L^{-1} in the middle reaches (Fig 4.2i). The PN was high in the Yellow River during the dry period with concentration $\sim 1.51 \text{ mg L}^{-1}$. In all the river basins, the highest PN concentrations were observed in the wastewaters (Ganges: $2.75 \pm 3.20 \text{ mg L}^{-1}$ in monsoon and 2.40 mg L^{-1} in dry period; Mekong: 1.00 mg L^{-1} in monsoon and $2.01 \pm 1.58 \text{ mg L}^{-1}$ in dry period).

In the Ganges and the Mekong, C/N (POC/PN) ratio in TSM were lower during the wet period. In the Ganges, the C/N ratio near the headwaters were $\sim 8.1 \pm 1.7$, and dropped near the middle (4.3 ± 0.6) and lower reaches (4.7 ± 1.2) (Fig 4.2a). In the Mekong the C/N ratio remained similar along the mainstem during the wet period (8.1 ± 1.5) (Fig 4.2d). Similar to the Ganges, the Yellow River witnessed a fall in C/N ratio during the wet period from the upper (9.7 ± 2.9) to the middle (6.5 ± 3.9) and lower (4.5) reaches (Fig 4.2g). During the dry period, C/N ratios were relatively higher in the Ganges mainstem (5.7 ± 0.9) and downstream reaches of the Mekong (11.7 ± 2.4) (Fig 4.2a & d).

4.1.6.4 Isotopic composition of total suspended matter

$\delta^{13}\text{C}_{\text{POC}}$ didn't show much variation along the whole continuum of the Ganges River (monsoon: $-25.4 \pm 2.2\text{‰}$; dry: $-28.7 \pm 1.4\text{‰}$) (Fig 4.2b). However, during monsoon, the $\delta^{15}\text{N}_{\text{PN}}$ was high in the middle reaches ($11.4 \pm 2.4\text{‰}$) as compared to the other sections (mainstem mean: $8.6 \pm 4.0\text{‰}$; upstream: $4.0 \pm 4.6\text{‰}$; downstream: $7.19 \pm 3.21\text{‰}$; Fig 4.2c). The Yamuna had the lowest $\delta^{15}\text{N}_{\text{PN}}$ with average value $\sim 2.0 \pm 1.4\text{‰}$. In the Ganges, the average $\delta^{15}\text{N}_{\text{POC}}$ decreased during the dry season to $4.5 \pm 2.6\text{‰}$. The Mekong River showed similar range as the Ganges for $\delta^{13}\text{C}_{\text{POC}}$ (Monsoon: $-26.3 \pm 2.7\text{‰}$; Dry: $-28.8 \pm 1.7\text{‰}$) and $\delta^{15}\text{N}_{\text{POC}}$ (Monsoon: $9.7 \pm 2.0\text{‰}$; Dry: $5.9 \pm 1.7\text{‰}$) (Fig 4.2e & f). The $\delta^{13}\text{C}_{\text{POC}}$ was highest in the Yellow River (Monsoon: $-23.3 \pm 4.6\text{‰}$; Dry: -25.0‰) (Fig 4.2h). $\delta^{15}\text{N}_{\text{POC}}$ was high in the Yellow River during monsoon ($8.4 \pm 4.7\text{‰}$) and surprisingly showed negative value during the dry period (-1.5‰) (Fig 4.2i).

Overall, we also observed consistently higher $\delta^{13}\text{C}_{\text{POC}}$ during monsoon in the three rivers. The wastewater isotopic signatures for $\delta^{13}\text{C}_{\text{POC}}$ and $\delta^{15}\text{N}_{\text{PN}}$ in the Ganges were $-25.8 \pm 0.4\text{‰}$ and $3.5 \pm 3.8\text{‰}$, respectively. The same for the Mekong were $-25.8 \pm 0.7\text{‰}$ and $2.5 \pm 1.6\text{‰}$, respectively.

4.1.4 Discussion

4.1.4.1 Total suspended matter along the river continuum

Overall, TSM varied over a broad range along the continuum of the studied rivers with relatively higher concentrations near major urban areas. In the Ganges, for example, high TSM were observed near major urban clusters like Rishikesh, Kanpur and Patna. This is generally attributed to different levels of anthropogenic activities, including agricultural practices, which play a significant role in mobilizing the surface soils and subsequent loading into the river (Asselman et al., 2003; Walling and Fang, 2003; Hunter and Walton, 2008). Furthermore, higher TSM near major cities could be a result of wastewater inputs. The Mekong River had lower TSM concentrations compared to the Ganges with decreasing concentrations from upstream to downstream. Along the continuum, abruptly low TSM was observed downstream of Jinghong Dam, Yunnan, which could be attributed to enhanced sedimentation upstream of the dam. During the dry periods, only the downstream sites were sampled and they showed low TSM concentrations, typical of clear waters. All sites in the Yellow River except for those within the loess plateau region during the wet periods, and Hohhot during the dry months, had TSM below 500 mg L^{-1} . The high TSM load near the middle reaches of Yellow River was potentially due to the high soil erosion in the loess plateau region. Intensive rainfall in the middle reaches (the loess plateau) has been attributed as the causal factor for high discharge and TSM as compared to upstream and downstream sites (Ran et al., 2013). Earlier studies have also recognized the loess plateau to supply 90% of the sediments in the Yellow River (Zhang et al., 1990; Milliman and Syvitski, 1992; Chen et al., 2005; Yu et al., 2013; Wang et al., 2010, 2016, 2017).

The increase in TSM in the middle reaches of the Yellow River basin was accompanied by an abrupt increase in $\delta^{13}\text{C}_{\text{POC}}$ and $\delta^{15}\text{N}_{\text{PN}}$. A similar increase in $\delta^{15}\text{N}_{\text{PN}}$ was observed in the Ganges with decrease in altitude (Fig 4.3a).

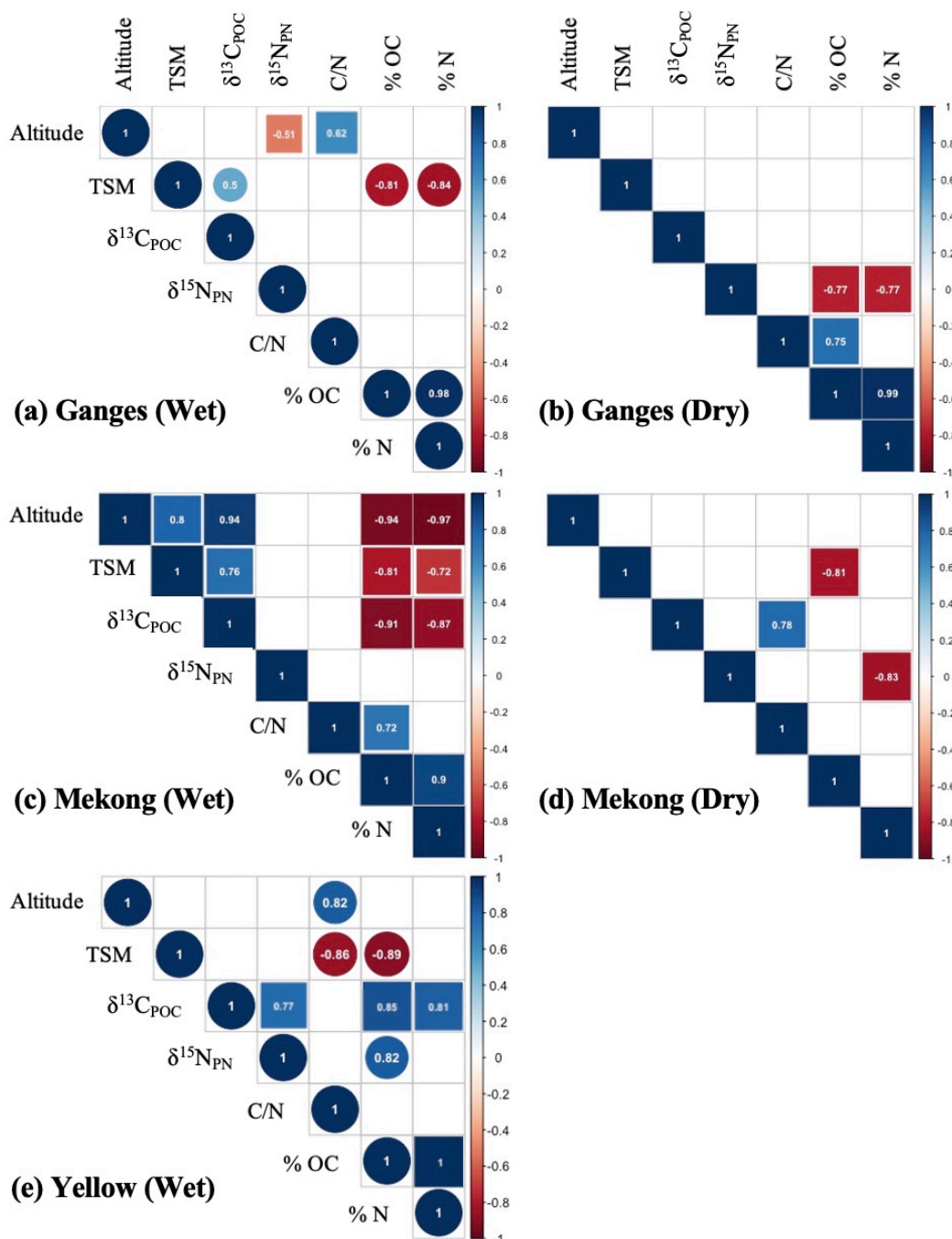


Fig. 4.3 Correlation plots between measured parameters in the three river systems. The coefficient of correlation was derived from Spearman rank correlation (Circles) and Pearson's correlation (Squares). The coefficient of correlation (R) is shown in the figure ($p < 0.05$).

This increase in isotopic signatures of TSM can either be a result of inputs of OM with enriched isotopic signatures or in-stream processes altering the isotopic composition of TSM. It was also observed that the altitude exercised a significant control on C/N ratios of TSM in the river basins (Fig 4.3a & e) which was quite obvious in the Ganges but not conclusive in the Mekong and Yellow, particularly due to lower sample size. During

the wet season, with decrease in altitude, the C/N ratios started to fall ($r = 0.35$, $p < 0.05$; Pearson), reflecting the dominance of allochthonous OM inputs in the upstream reaches mainly consisting of plant litter having high C/N. In contrast, the C/N ratios were negatively correlated with altitude during the dry periods ($r = -0.85$, $p < 0.05$; Spearman), which suggested OM inputs of high C/N ratios into the rivers as the river order increased.

Apart from the above-mentioned control of terrain on TSM across the three rivers, the Mekong River also displayed significant positive relationship between altitude and TSM loading (Fig 4.3c). With decreasing altitude, the TSM concentrations in the Mekong fell consistently accompanied by an increase in its organic C and N contents. This relationship between TSM and its organic contents to altitude provides an insight into the effect of damming and changes in flow regime of the river on its TSM dynamics. The upstream reaches of the Mekong showed the signatures of intense weathering and erosion with high TSM load and low organic content, whereas the lower reaches displayed decrease in TSM loading and increase in organic content, characteristic of productive waters.

4.1.7.2 Sources of riverine carbon and nitrogen

The TSM in rivers is a derivative of *in situ* primary producers, plant litter, and soil (Ittekkot, 1988; Hillebrand et al., 2018). Different environmental and hydrological factors (precipitation, runoff, catchment land cover, discharge, etc.) control the relative dominance of each source. For instance, rivers with high discharge generally have high turbidity due of excessive sediment loading, which prevents light penetration, thereby decreasing primary production. Such rivers have a dominant allochthonous sources of OM. On the other hand, low discharge rivers with relatively low TSM loads are favorable for *in situ* productivity (Leithold et al., 2006; Ran et al., 2013).

In the present study, isotope mixing model did not clearly distinguish among the prospective OM sources such as C3 plants, C4 plants, SOM, and *in situ* phytoplankton. However, the source of OM was significantly enriched in ^{13}C during the wet seasons compared to the dry season (by 1.4 ‰ in the Ganges and 10.9 ‰ in Mekong) (Fig 4.4).

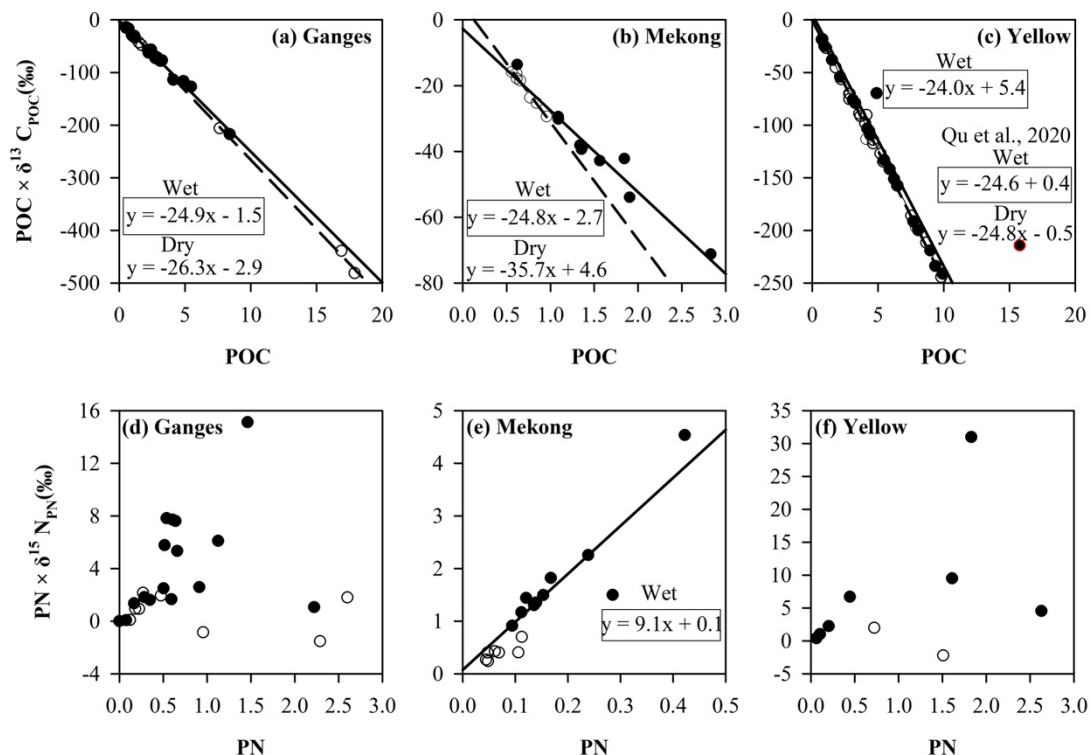


Fig. 4.4 Graphical mixing model for tracking the sources of OC and N in TSM. Significant regressions obtained for OC in the (a) Ganges, (b) Mekong, and (c) Yellow River. Source organic matter isotopic signatures are shown by the slope of the regression. The regressions for wet seasons are bounded by a rectangular box. For the Yellow River, due to low sample size in the dry seasons, we used the data from Qu et al., 2020 for seasonal comparison. This graphical mixing model failed to distinguish the source signature of N except for (e) Mekong during the wet season (source $\delta^{15}N_{PN} = 9.1$ ‰).

Except for Mekong during the wet seasons (source $\delta^{15}N_{PN} = 9.1$ ‰), the mixing models did not clearly identify the N sources as a strong linear regression was not achieved (Fig 4.4). The lack of correlation could be attributed to point source N pollution along the river continuum, prevalent in urbanized river systems (Zhang et al., 2015). The relationship between TSM concentrations and its organic C and N contents provide insight into vegetation versus soil contributions. If organic C and N contents increase with TSM, it suggests contribution from *in situ* phytoplankton or terrestrial litter (C3 and C4). Significant negative relationships between TSM and organic C and N contents in the Ganges and Mekong were observed (Fig 4.3a & c), whereas with only organic C during the wet season was observed in the Yellow River (Fig 4.3e). Such relationships indicated inputs from soil OM with low C and N contents to TSM (Meybeck and Raghu, 1995; Ludwig et al., 1996). This observation was further supported by positive correlations between TSM and $\delta^{13}C_{POC}$ in the Ganges and Mekong during the wet

period (Fig 4.3a & c), as SOM is generally associated with high $\delta^{13}\text{C}$. Similarly, a decrease in C/N ratio with increase in TSM in the Yellow River during the wet period indicated SOM as the dominant source of OM, which is consistent with high sediment load derived from the loess plateau. Previous studies have also reported the middle reaches of the Yellow River to be rich in highly decomposed loess deposits which have high $\delta^{13}\text{C}$ signatures (Zhang et al., 1990, 1992; Chen et al., 2005). During the dry season, N contents showed significant negative relationship with $\delta^{15}\text{N}_{\text{PN}}$ (Fig 4.3b & d) indicating association of increase in productivity with enhanced N fixation by phytoplankton.

4.1.7.3 Seasonality in total suspended matter as inferred from elemental biogeochemistry

The Asian rivers are subjected to high seasonality in their hydrological regime, which in turn governs the *in situ* elemental biogeochemistry. The TSM is usually a function of the discharge and also reflects the level of anthropogenic disturbances within the watershed (Li et al., 2008; Chang et al., 2021). Higher TSM concentrations were observed during the wet season than in the dry period in all the three rivers (Fig 4.5a), which is in agreement with studies elsewhere (Dunne and Ongweny, 1976; Kitheka et al., 2005; Tamooch et al., 2012). The low C/N that accompanied the high TSM during the wet season indicated terrestrial inputs of SOM having low C/N (Fig 4.5b). The TSM and C/N ratio obey an inverse relationship in an environmental setting prone to aeolian and fluvial erosion (Weiguo, 2002; Boix-Fayos et al., 2015). Generally, the surficial soil of the catchment holding the remains of parent plant material with high C/N is likely to be removed first leaving behind SOM with relatively low C/N. With successive erosion events, the rivers draining such terrain would receive this OM resulting in higher TSM with low C/N (Weiguo, 2002). Contrary to the general observations of low C/N during low flow conditions, representing fine algal materials and phytoplankton (C/N: 4.6 to 7.5, Bordowskiy 1965; Muller 1977; Meybeck 1982; Balakrishna and Probst, 2005; Ellis et al., 2012), we observed relatively higher C/N ratio during the dry season. This might be due to high growth period, wherein competition for nutrients likely resulted in higher C uptake relative to N by phytoplankton resulting in higher C/N of TSM. As such productivity increases during the low flow conditions under reduced turbidity which is favorable for algal growth (Beusen et al., 2005). Possible increase in productivity during the dry period is also

reflected on higher organic C and N contents in TSM (Fig 4.5c & d). In contrast, organic C in TSM decreased during the high flow condition (Fig 4.5c), reflecting the C content of SOM (Giresse and Maley, 1998; Coyne et al., 2004). Although decomposition of OM during high flow conditions might also result in lower OC in TSM and associated increase in $\delta^{13}\text{C}_{\text{POC}}$, the negative relationship observed between TSM and % OC and % N (Fig 4.3a, c, & e) indicates addition of TSM with low OM content. Similar negative relationship between OM and TSM have been reported in the Yellow River basin during high flow periods (Beusen et al., 2005; Ellis et al., 2012).

Generally, C/N ratios, when used solely, do not convincingly distinguish the sources and relative contributions (autochthonous versus allochthonous) of OM to riverine systems (C/N for phytoplankton: 4.6 to 7.5, aquatic plants: 4 to 12, degraded SOM: low C/N; Bordowskiy, 1965; Meybeck, 1983; Naiman 1983; Muller, 1977) as these systems have large catchments and several biogeochemical processes simultaneously regulate the elemental ratios (Meyers, 1997; Milliman et al., 1984). However, in conjunction with stable isotopes, they can be a robust tool to study aquatic elemental biogeochemistry. In this study, relatively lower $\delta^{13}\text{C}_{\text{POC}}$ (Fig 4.5e) in all the river basins during the dry season was observed, which possibly indicated increased *in situ* primary production, which has a general range between -40 to -22 ‰ (Kendall et al., 2001). As described earlier, low flow conditions with clear and less turbid water are favourable for primary productivity and algal growth. Phytoplankton in such an environmental setting, i.e., well oxygenated and non-eutrophic, can have isotopically depleted organic C signatures (Leng et al., 2006). Yu et al (2019) employed dual isotopic ($\delta^{13}\text{C}$ and $\Delta^{14}\text{C}$) source apportionment and observed similar signatures of enhanced primary production in the Yellow River due to less turbidity and suitable water temperature during spring and summer. Furthermore, higher $\delta^{13}\text{C}_{\text{POC}}$ during the wet season showed signatures of terrestrial inputs, with higher C4 contribution, in the Yellow River. Unlike earlier observations of a lack of seasonality in the isotopic composition of POM in the Mekong River (Ellis et al., 2012), our results showed significant increase in the C and N isotopic signatures during the wet seasons. Similar to C, relatively higher $\delta^{15}\text{N}_{\text{PN}}$ during the wet season is indicative of SOM and the low $\delta^{15}\text{N}_{\text{PN}}$ during the dry season is indicative of *in situ* production with the low (~ 0 ‰) signatures representing N_2 fixation during high growth phase (Fig 4.5f).

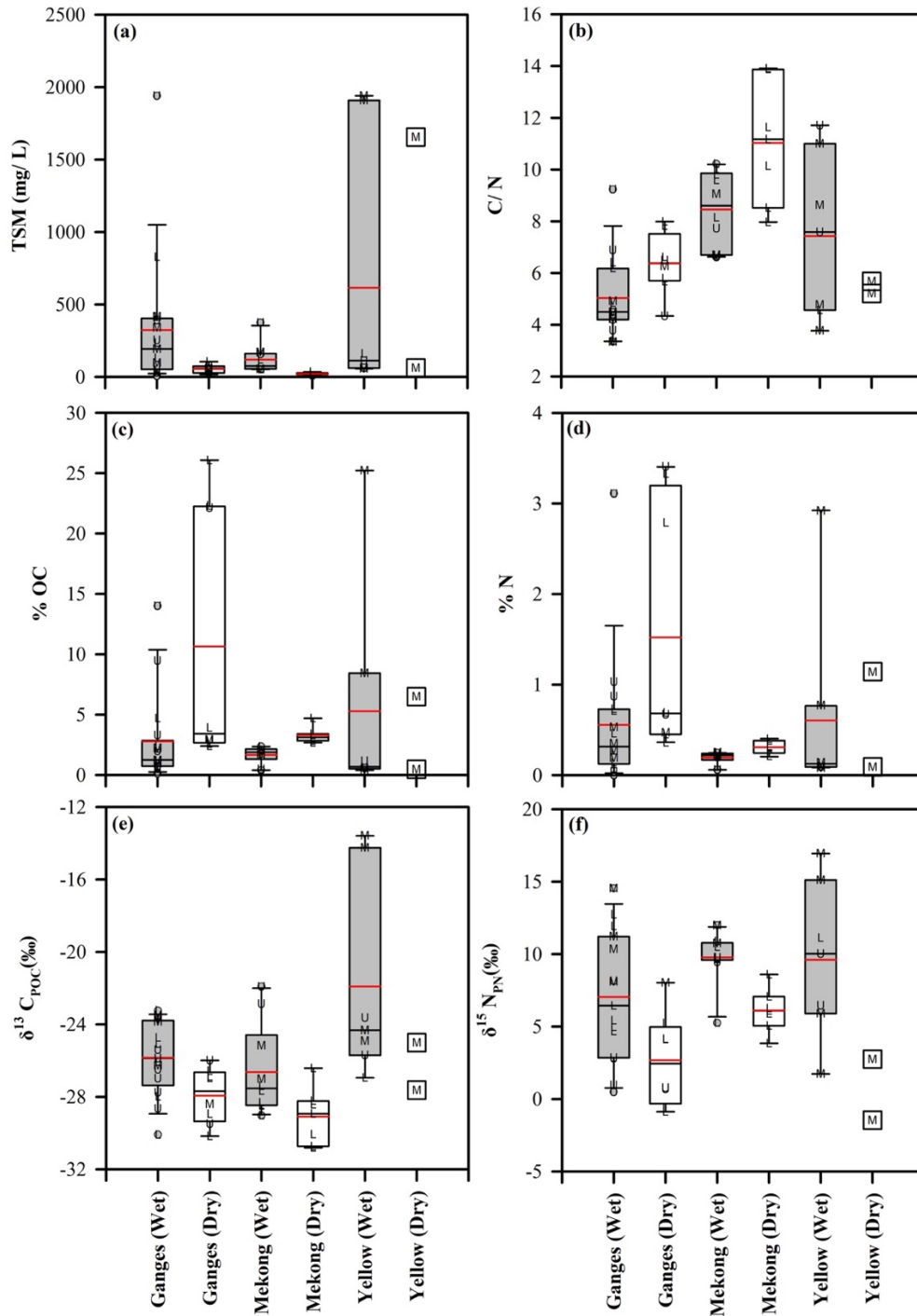


Fig. 4.5 Seasonal variation in (a) TSM, (b) C/N ratios, (c) % OC, (d) % N, (e) $\delta^{13}C_{POC}$ and (f) $\delta^{15}N_{PN}$. Red lines show mean values. Significant difference ($p < 0.001$) between the median TSM values were observed across seasons and river basins. The whole range of TSM were significantly different ($p < 0.05$) among Mekong (Dry) and Mekong (Wet). Similarly, median C/N were significantly different among different sample classes ($p < 0.001$). During each season, the whole range of C/N values were higher for the Mekong as compared to the Ganges ($p < 0.05$). Median values were significantly different in (c) with $p < 0.005$ and (d) $p < 0.05$. Median $\delta^{13}C_{POC}$ and $\delta^{15}N_{PN}$ were significantly different among each class ($p < 0.005$). The letters L, M and U represents sites from the lower, middle and upper reaches respectively.

4.1.7.4 Yield and export fluxes of particulate organic carbon and nitrogen

The fluxes and yields of OM were calculated based on the following equations:

$$F_{\text{TSM}} = Q \times \text{TSM} \quad (1)$$

$$F_{\text{POC (or PN)}} = F_{\text{TSM}} \times [\% \text{ OC (or \% N)}_{\text{TSM}}] \quad (2)$$

$$F_{\text{POC (or PN)}} = Q \times (\text{POC or PN}) \quad (3)$$

$$Y_{\text{POC or PN}} = F_{\text{POC or PN}} / A \quad (4)$$

here, TSM is the median TSM concentration at the lower sampling sites (i.e., outlet), Q is the annual discharge, F_{TSM} is the annual flux of TSM, F_{POC} is the annual flux of organic C, F_{PN} is the annual flux of N, A is the catchment surface area and Y_{POC} is the annual yield of POC from the catchment. The discharge data were taken from the existing literature (Table 4.1) and the values used for flux calculation are shown in Table 4.2.

Table 4.1 Length, basin area, and annual discharge of the Ganges, Mekong, and the Yellow River systems.

River	Length (km)	Basin area ($\times 10^3 \text{ km}^2$)	Discharge ($\text{km}^3 \text{ yr}^{-1}$)	References
Ganges	2700	1260	1270*	Parua (2010); Milliman & Farnsworth (2011)
Mekong	4800	880	550	MRC (2019) Milliman & Farnsworth (2011)
Yellow	5500	753	15	Milliman & Farnsworth (2011)

Assuming a catchment area of $980 \times 10^3 \text{ km}^2$, annual sediment load and yield for the Ganges have been reported to be $\sim 1060 \times 10^9 \text{ kg y}^{-1}$ and $1340 \times 10^3 \text{ kg km}^{-2} \text{ y}^{-1}$, respectively (Milliman and Farnsworth, 2011). Similarly, for the Yellow and the Mekong Rivers, the sediment load has been estimated at $1100 \times 10^9 \text{ kg y}^{-1}$ and $150 \times 10^9 \text{ kg y}^{-1}$, whereas their yields are $1500 \times 10^3 \text{ kg km}^{-2} \text{ y}^{-1}$ and $190 \times 10^3 \text{ kg km}^{-2} \text{ y}^{-1}$, respectively (Milliman and Farnsworth, 2011). Estimates of C and N fluxes from the Ganges River system is scarce and only one study reported organic C flux to be $6 \times 10^9 \text{ kg y}^{-1}$ (Aucour et al., 2006). For the Ganges, our calculation estimated the annual TSM export flux at $202 \times 10^9 \text{ kg y}^{-1}$, which indicated significant decrease in the suspended load and its C content (at present $F_{\text{POC}} = 2.4 \times 10^9 \text{ kg y}^{-1}$) over the years. TSM flux from

the Yellow River has been known to reduce drastically over the decades. Milliman and Farnsworth (2011) reported ~ 10 times reduction of TSM export from the Yellow River in recent decades, from 1100 Mt y^{-1} (Qian and Dai, 1980) to $< 100 \text{ Mt y}^{-1}$ (Wang et al., 2006), attributing the major cause of this decline to be excessive water consumption and droughts. For the Yellow River, the early export flux of organic C was estimated to be $6.1 \times 10^9 \text{ kg y}^{-1}$ in 1987 (Zhang et al., 1992). Later, a reduction by a factor of 15 by the year 2009 was observed (Wang et al., 2012). The estimates calculated based on the wet season data from the present study showed further reduction by a factor of 10 since Wang et al. (2012). Paucity of dry season observation from the Yellow River during the present study restricted us from providing a well constrained annual flux estimate. This high reduction in POC flux in the Yellow River within a decade is not surprising, considering the steady fall in river discharge and associated sediment load over the last 60 years (Wang et al., 2015). Apart from the construction of dams and landscape engineering, large scale vegetation restoration projects and associated reduction in soil erosion rates have been identified as the causal factors for the decline in sediment load in the Yellow River (Wang et al., 2015). In the last decade, a large fall in the export fluxes were observed in the Mekong River basin as well. Ellis et al. (2012) reported an annual flux of $76.3 \times 10^9 \text{ kg y}^{-1}$ and $1.67 \times 10^9 \text{ kg y}^{-1}$ for TSM and organic C, respectively, during the year 2006. Our results indicated ~ 6 times decrease in organic C flux for the Mekong River.

Transport of N in rivers are generally assumed to be dominantly in the form of dissolved inorganic ions. However, Ittekkot and Zhang (1989) highlighted the global significance of the movement of particulate N within river corridors. They estimated a net global riverine flux of $\sim 33 \times 10^9 \text{ kg N y}^{-1}$ in the form of PN among which $\sim 80\%$ was supposedly delivered by large river systems like the Ganges, Mekong, and Yellow River. Following the work by Ittekkot and Zhang (1989), studies on PN fluxes and yields are still limited from the Asian rivers systems. Our flux calculations showed the Ganges with the highest PN flux followed by the Mekong and the Yellow Rivers (Table 4.2). Similar to organic C, significant reduction in PN flux was also observed for three studied river basins (Table 4. 2).

Chapter 4 River Biogeochemistry

Table 4.2 Concentrations, annual fluxes and yields of suspended particulate carbon and nitrogen in some Asian rivers. TSM, POC and PN values shown from the present study represents median concentrations of selected downstream locations [Ganges (Dry): G9 and G12; Ganges (Wet): G8, G9, G10 and G11; Mekong (Dry and Wet): M8 and M9; and Yellow (Wet): Y6].

River	TSM (mg L ⁻¹)	POC (mg L ⁻¹)	PN (mg L ⁻¹)	F _{POC} (×10 ⁸ kg y ⁻¹)	Y _{POC} (×10 ² kg km ⁻² y ⁻¹)	F _{PN} (×10 ⁶ kg y ⁻¹)	Y _{PN} (kg km ⁻² y ⁻¹)	References
Ganges (Dry)	44	0.528	0.007	24	19	34	27	This study
Ganges (Wet)	274.3	3.292	0.046					
Mekong (Dry)	17.5	0.209	0.003	2.8	3.5	3.9	4.9	This study
Mekong (Wet)	67.5	0.810	0.011					
Yellow (Dry) (At Tongguan)	1656.4	19.900	0.278	0.44	0.59	0.62	0.83	This study
Yellow (Wet)	161.2	1.934	0.027					
Yellow Lijin	3589	13.279	2.512	4.1	5.45*	69	91.63*	Ran et al., 2013
Yellow Lijin	2522	11.679	5.411	3.89	5.17*	134	177.96*	Wang et al., 2012
Mekong	80.8	2.010	0.188	16.7	18.98*	150	170.46*	Ellis et al., 2012
Rivers draining the Western Ghats (India)	83	2.860	NA	7.9	70.3	NA	NA	Reddy et al., 2021

(*recalculated from the fluxes from the respective studies and the basin area from Table 4.1)

4.1.8 Conclusion

The present study attempted to compare the flow of C and N in its particulate form (POC and PN) between dry and wet periods among three large Asian river systems. Given the global implication in constraining their fluxes and isotopic signatures, this study deciphered the effect of seasonality on the POC and PN fluxes and the associated biogeochemical processes that might have a significant control over their process dynamics. In the three studied river systems, altitude seemed to have a strong control over the C/N ratios and C isotopic signatures of TSM. Furthermore, in the Yellow River basin, the loess plateau was the major driver of suspended matter dynamics. Application of a mixing model revealed an enriched C isotopic signature of the source OM in the Ganges and Mekong during the wet seasons which was attributed to allochthonous inputs (SOM and C4 vegetation). Using the same model for N source identification, the $\delta^{15}\text{N}_{\text{PN (Source)}}$ for the Mekong River was also constrained. Primary production dominated in all the three river systems during the dry seasons with evidences of N_2 fixation as well. The high C/N ratios that accompanied the high growth phase during this study disagreed with the general understanding of low C/N during low flow conditions, indicating that competition for nutrients can shoot up the C/N ratios of POM beyond the known range of values. The fluxes and yields of C and N estimated in this study showed drastic reduction over the decades in these river basins and also provided a modest number that could be used in models for global budgeting.

4.2 Biogeochemistry of an engineered river system

Riverine systems across the globe have experienced large scale modifications in their channel leading to shifts in the flow regime. The current status of free flowing rivers is disheartening with only ~ 37 % of rivers longer than 1000 km retaining their free flowing status for the entire length and only 23 % of the all the rivers are draining into the global oceans uninterrupted (Grill et al., 2019). The characteristics of a free flowing river is its ability to facilitate the movement of water along with organisms, sediments, OM, nutrients, and energy. The natural flow of river channels has been altered by human interventions through multiple ways by directly placing structures like dams and levees along longitudinal and/or lateral flow paths or indirectly altering the hydrological, thermal, and sediment regimes (Nilsson and Berggren, 2000; Olden, 2016). Engineered modifications of river channels have been linked to detrimental effects on terrestrial and freshwater species (Nilsson and Berggren, 2000; Vorosmarty et al., 2010; Benchimol and Peres, 2015; Lees et al., 2016).

Urban rivers experience severe anthropogenic stress as they receive huge quantities of treated and untreated sewage. The wastewater has elevated concentrations of DIC, DOM, and suspended particulate matter, which plays a crucial role in shaping the downstream C and N biogeochemistry. High biological oxygen demand of wastewater rapidly creates an anoxic environment in the water column, affecting the niches for microbes and therefore changing the magnitude and direction of microbially mediated processes like methanogenesis, nitrification, and denitrification (Begum et al., 2021). Begum et al. (2021) explored the greenhouse gas dynamics in three large Asian rivers and identified localised impacts of pollution in the production of GHGs. Similarly, Yang et al. (2018) observed increased DIC concentration in river reach impacted by wastewater discharge and noted the input of isotopically lighter DIC through sewage. This study explores the effect of engineered modification on riverine C and N biogeochemistry. The hypotheses of the study were: (i) the reduction of flow velocity (i.e. water stagnancy) would enhance primary productivity resulting in high biomass and subsequent increase in concentration of dissolved GHGs and (ii) wastewater input would contribute to GHGs concentrations via direct input as well as its enhanced production due to anoxic environment and substrate availability.

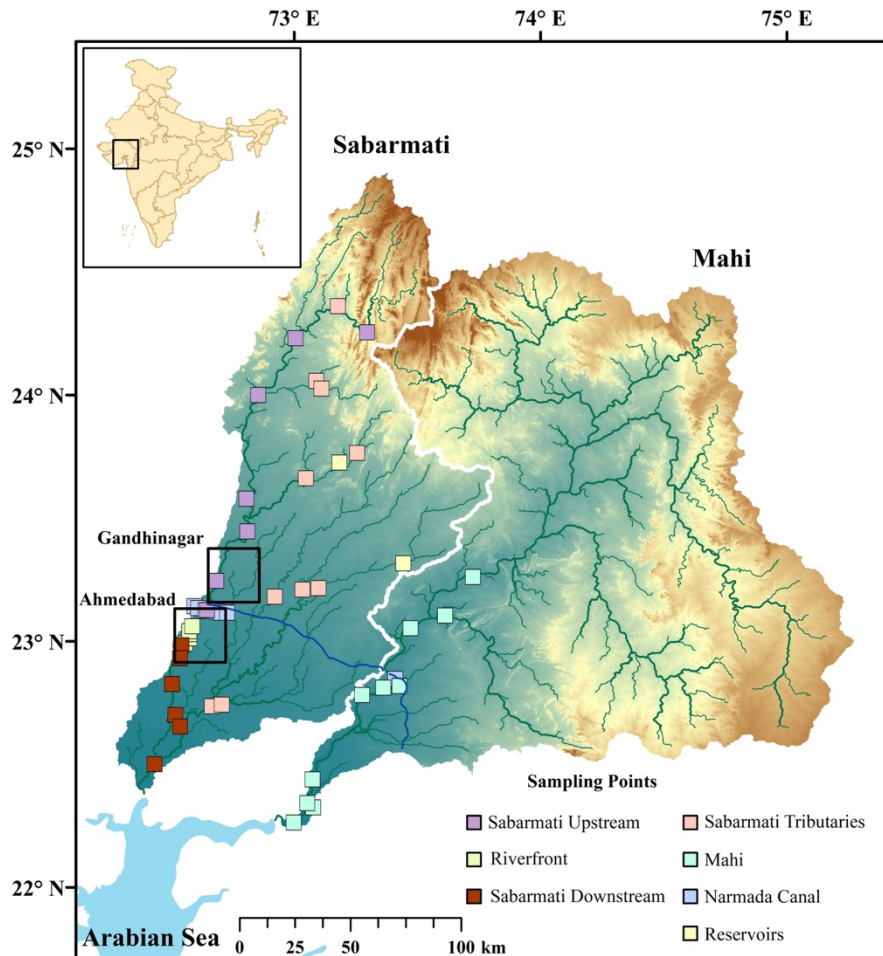


Fig. 4.6 Study area and sampling locations in different sample classes (shown in the legend). The blue line represents the portion of the lined canal (Narmada Canal) flowing through the Sabarmati and Mahi River basins.

4.2.1 Study area

The Sabarmati River has its headwaters in the Aravalli hills and flows ~ 371 kms draining a catchment of 21,674 km² to ultimately drain into the Arabian Sea (Central Water Commission, 2009). Two megacities namely Gandhinagar and Ahmedabad (population > 6 million) are established along the banks of the river and the latter is responsible for the discharge of large amounts of wastewater and industrial effluents into the river (Mohanty et al., 2021). The Mahi River rises near the Mahi Kanta hills (Vindhya range) in the western part of Madhya Pradesh. It is bound by the Aravalli hills and the Vindhyas, in the north and south respectively. The Mahi river traverses a length of 583 km before draining into the Arabian Sea. Compared to the Sabarmati, the Mahi benefits from lesser anthropogenic stress on the river health. The overall climate of the region is largely semi – arid.

4.2.2 Sampling

To address the above hypotheses, sampling was conducted in the Sabarmati and Mahi river (Fig. 4.6). Samples were collected during two field campaigns covering a high flow (HF; October, 2020) and low flow (LF; February, 2021) periods along the mainstem and selected tributaries (Fig 4.6). The Sabarmati Basin was divided into different classes based on the level of engineered modifications, such as (a) Sabarmati upstream (Relatively pristine; n = 7 (HF) and 5 (LF)), (b) Riverfront (Stagnant flow; n = 5 (HF and LF)), (c) Sabarmati downstream (Highly polluted; n = 6 (HF) and 5 (LF)), and (d) Tributaries (n = 11 (HF) and 7 (LF)) (Fig. 4.6 and Fig. 4.7). For comparison, Mahi River (free flowing river and in the same hydroclimate setting; n = 9 (HF) and 8 (LF)) was selected as control due to lower anthropogenic stress. Samples were also collected from the Narmada Canal (lined; n = 10 (HF and LF)) which feeds the riverfront (Fig 4.7). Additionally, two reservoirs were sampled (Vatrak (n = 1 (HF and LF)) and Indrasi (n = 1 (HF))) in the Sabarmati basin.

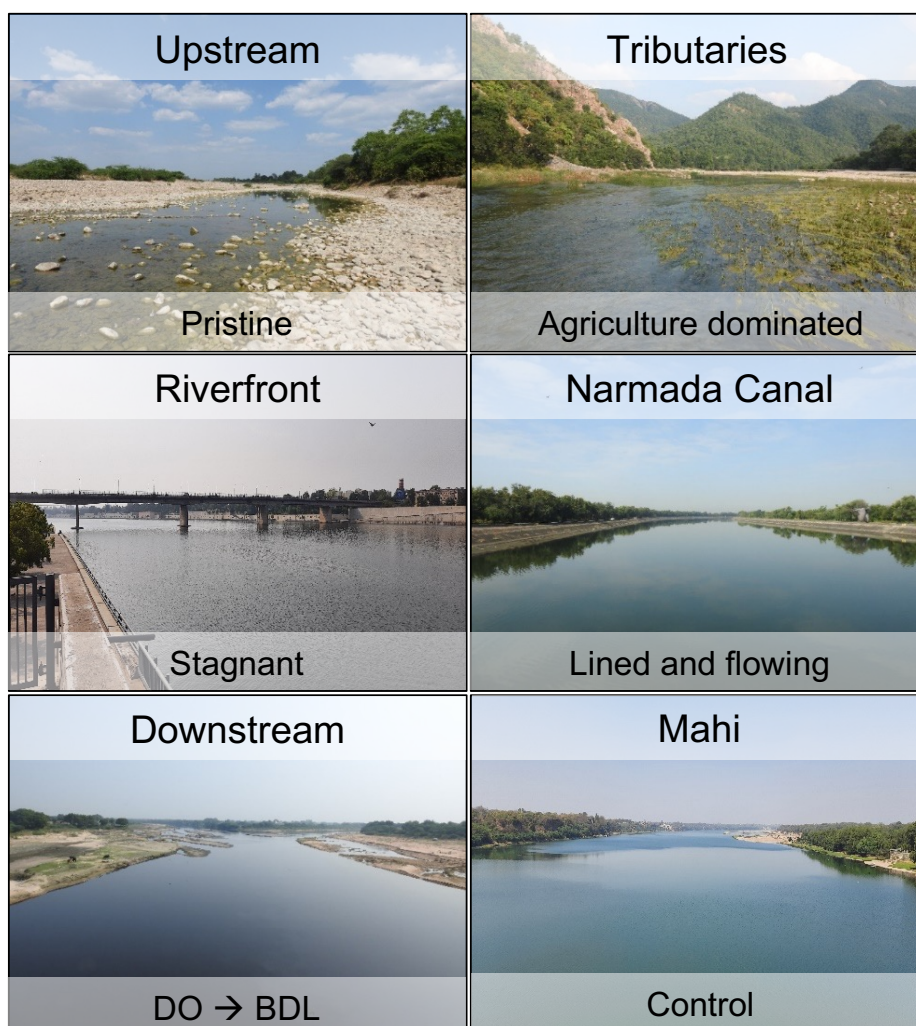


Fig. 4.7 Field photographs of various sample classes defined for the present study.

4.2.3 Results

4.2.3.1 Environmental parameters

The water quality parameters showed seasonality as well as spatial variability across different sample classes. pH was relatively higher during the high flow periods compared to low flow in the Sabarmati upstream (HF (mean \pm stdev) = 8.72 ± 0.32 ; LF = 8.37 ± 0.52), Sabarmati downstream (HF = 7.82 ± 0.17 ; LF = 7.77 ± 0.35), Sabarmati tributaries (HF = 8.36 ± 0.50 ; LF = 8.37 ± 0.19), Mahi (HF = 8.62 ± 0.18 ; LF = 8.50 ± 0.19), and Narmada Canal (HF = 8.44 ± 0.15 ; LF = 8.32 ± 0.11). In the Riverfront, pH increased during the low flow (HF = 7.98 ± 0.19 ; LF = 8.89 ± 0.33) (Fig 4.8a).

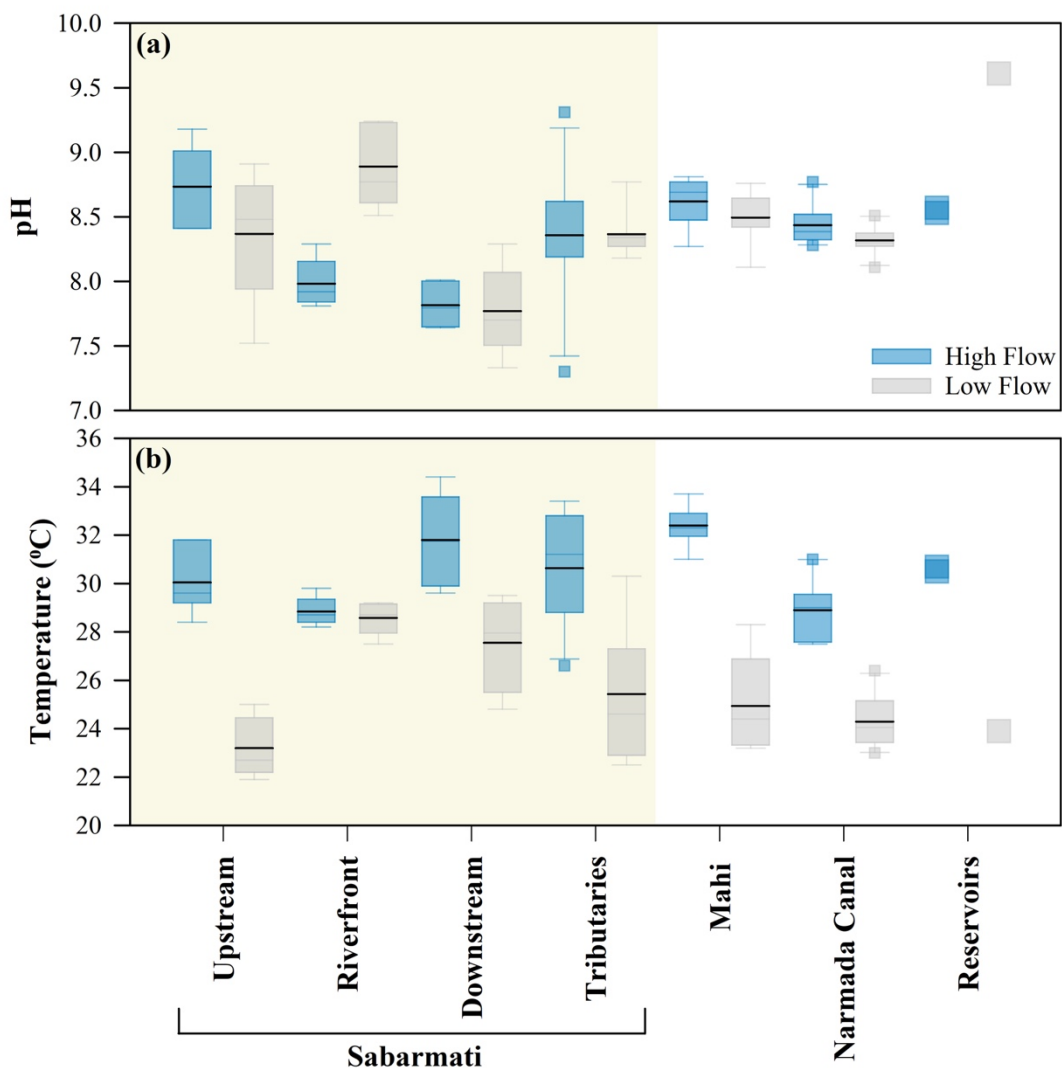


Fig. 4.8 (a) pH and (b) temperature in different sample classes. Blue and Grey represent high flow and low flow periods, respectively.

Water temperature was higher during the high flow compared to low flow in Sabarmati upstream (HF = 30.0 ± 1.3 °C; LF = 23.2 ± 1.2 °C), Sabarmati downstream (HF = 31.8

± 1.9 °C; LF = 27.6 ± 2.0 °C), Sabarmati tributaries (HF = 30.6 ± 2.2 °C; LF = 25.4 ± 2.7 °C), Mahi (HF = 32.4 ± 0.8 °C; LF = 24.9 ± 1.9 °C), and Narmada Canal (HF = 28.9 ± 1.3 °C; LF = 24.3 ± 1.1 °C). However, no significant change in water temperature in the riverfront was observed (HF = 28.8 ± 0.6 °C; LF = 28.6 ± 0.7 °C) (Fig 4.8b). EC has similar range in all sample classes ($0.23 - 0.85$ mS cm⁻¹) except for Sabarmati downstream (HF = 1.69 ± 0.68 mS cm⁻¹; LF = 2.13 ± 0.57 mS cm⁻¹) and Sabarmati tributaries (HF = 0.82 ± 0.57 mS cm⁻¹; LF = 1.76 ± 2.74 mS cm⁻¹) (Fig 4.9a).

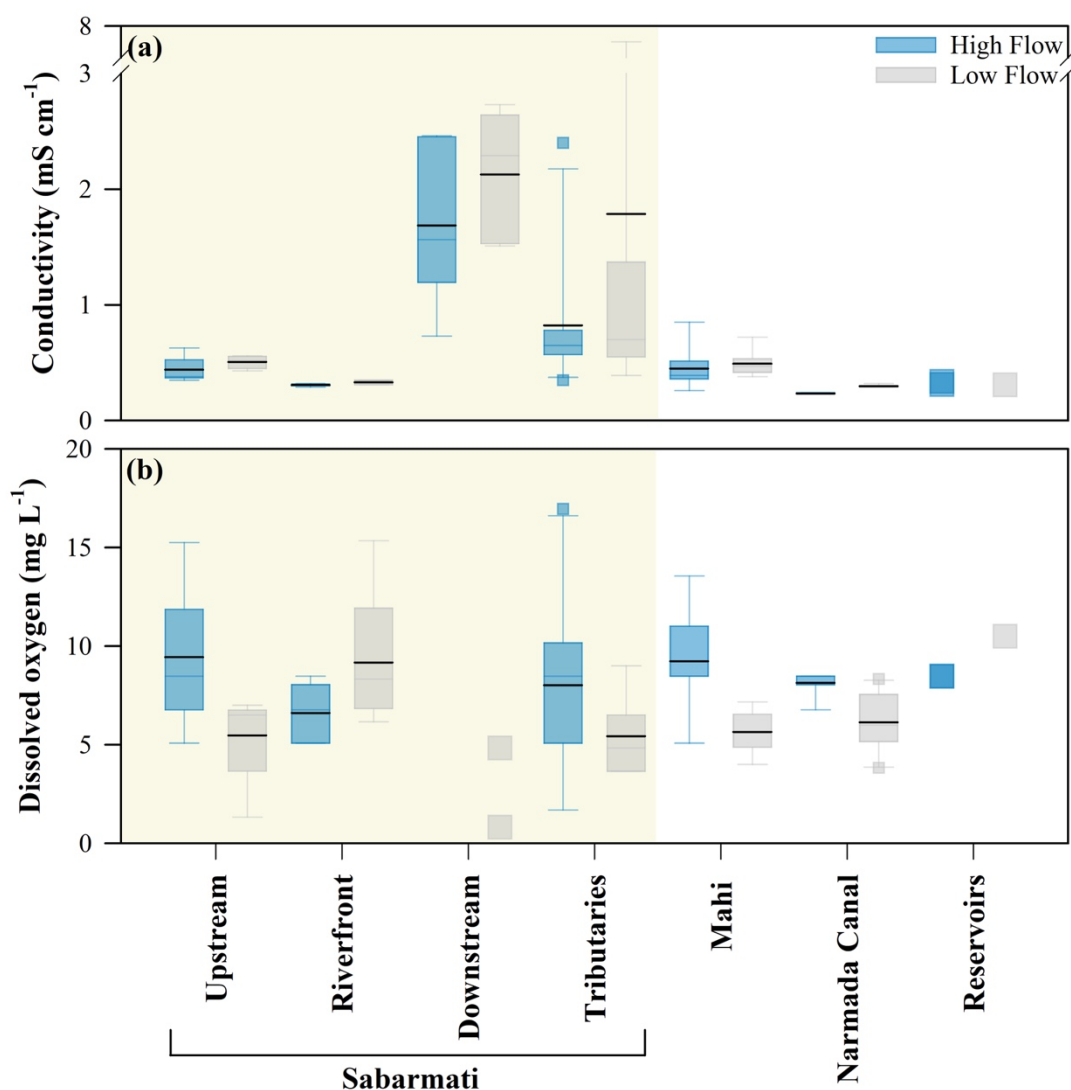


Fig. 4.9 (a) Conductivity and (b) dissolved oxygen in different sample classes. Blue and Grey represent high flow and low flow periods, respectively.

DO was higher during high flow in Sabarmati upstream (HF = 9.45 ± 3.37 mg L⁻¹; LF = 5.47 ± 2.34 mg L⁻¹), Sabarmati tributaries (HF = 8.02 ± 4.86 mg L⁻¹; LF = 5.44 ± 1.94 mg L⁻¹), Mahi (HF = 9.23 ± 2.41 mg L⁻¹; LF = 5.65 ± 1.03 mg L⁻¹), and Narmada Canal (HF = 8.14 ± 0.71 mg L⁻¹; LF = 6.14 ± 1.46 mg L⁻¹). In the riverfront, DO

increased during the low flow period (HF = $6.61 \pm 1.52 \text{ mg L}^{-1}$; LF = $9.18 \pm 3.57 \text{ mg L}^{-1}$). DO was below detection limit (BDL) in the Sabarmati downstream during high flow (all sites) and extremely low during low flow (3 sites = BDL; 2 sites = $2.84 \pm 2.83 \text{ mg L}^{-1}$) (Fig 4.9b). On the basin scale, NO_3^- was generally higher than NH_4^+ : Sabarmati upstream [HF ($\text{NO}_3^- = 24.98 \pm 20.28 \text{ }\mu\text{M}$; $\text{NH}_4^+ = 5.63 \pm 2.89 \text{ }\mu\text{M}$) and LF ($\text{NO}_3^- = 1.21 \pm 1.04 \text{ }\mu\text{M}$; $\text{NH}_4^+ = 1.85 \pm 0.59 \text{ }\mu\text{M}$)], riverfront [HF ($\text{NO}_3^- = 33.29 \pm 7.21 \text{ }\mu\text{M}$; $\text{NH}_4^+ = 28.81 \pm 7.39 \text{ }\mu\text{M}$) and LF ($\text{NO}_3^- = 23.54 \pm 4.79 \text{ }\mu\text{M}$; $\text{NH}_4^+ = 15.81 \pm 6.66 \text{ }\mu\text{M}$)], Sabarmati tributaries [HF ($\text{NO}_3^- = 94.56 \pm 46.78 \text{ }\mu\text{M}$; $\text{NH}_4^+ = 23.67 \pm 44.35 \text{ }\mu\text{M}$) and LF ($\text{NO}_3^- = 17.80 \pm 21.58 \text{ }\mu\text{M}$; $\text{NH}_4^+ = 29.31 \pm 62.90 \text{ }\mu\text{M}$)], and Mahi [HF ($\text{NO}_3^- = 40.01 \pm 18.33 \text{ }\mu\text{M}$; $\text{NH}_4^+ = 8.07 \pm 13.33 \text{ }\mu\text{M}$) and LF ($\text{NO}_3^- = 18.83 \pm 19.30 \text{ }\mu\text{M}$; $\text{NH}_4^+ = 4.41 \pm 1.60 \text{ }\mu\text{M}$)].

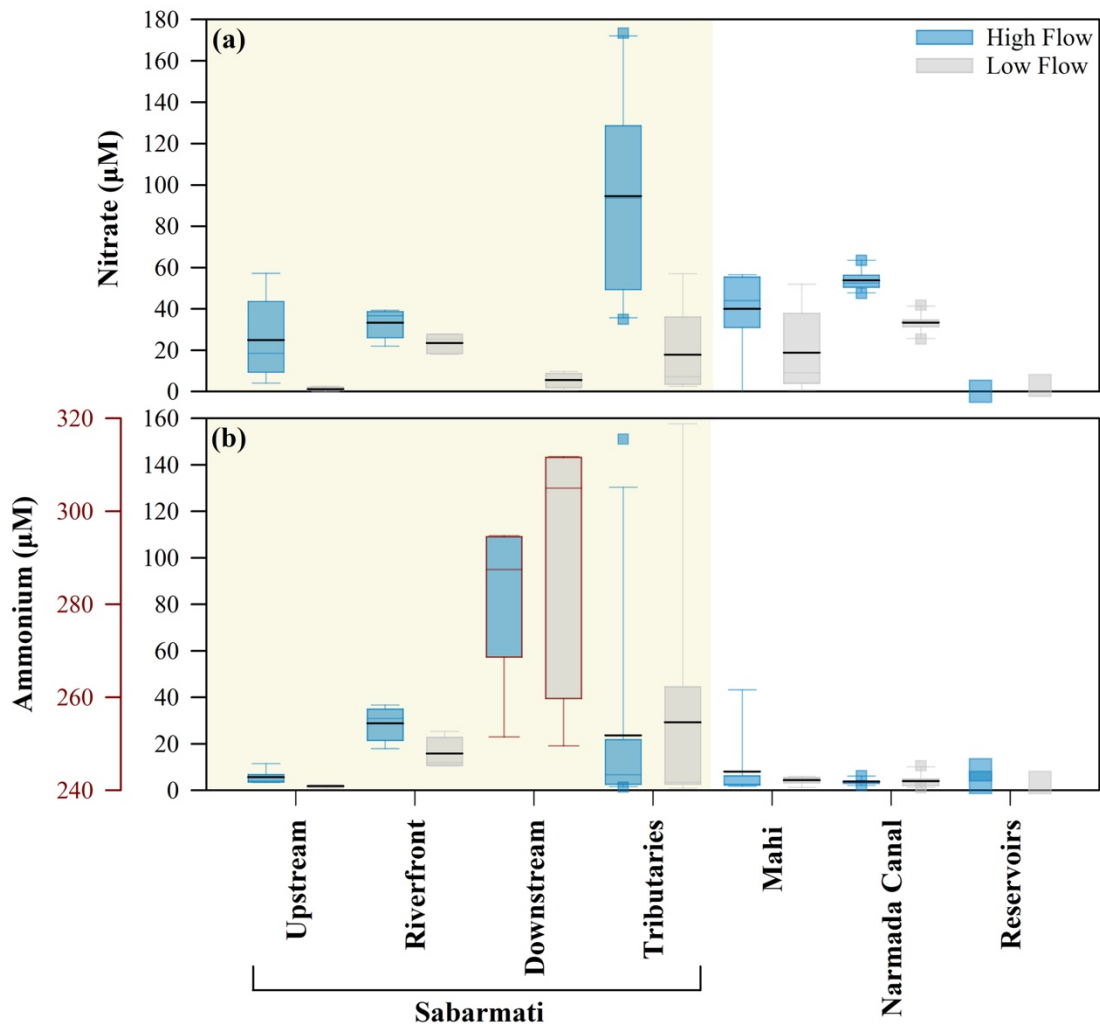


Fig. 4.10 (a) Nitrate and (b) ammonium in different sample classes. Blue and Grey represent high flow and low flow periods, respectively.

Interestingly, Sabarmati downstream showed very high DIN concentrations with higher NH_4^+ than NO_3^- [HF ($\text{NO}_3^- = \text{BDL}$; $\text{NH}_4^+ = 282.80 \pm 17.94 \mu\text{M}$) and LF ($\text{NO}_3^- = 5.55 \pm 3.76 \mu\text{M}$; $\text{NH}_4^+ = 289.55 \pm 28.25 \mu\text{M}$)] (Fig 4.10).

4.2.3.2 Stable oxygen isotopic composition of river water

$\delta^{18}\text{O}$ showed steady increase from high flow to low flow in Sabarmati upstream (HF = $-3.4 \pm 0.3 \text{‰}$; LF = $-2.1 \pm 0.7 \text{‰}$), riverfront (HF = $-5.3 \pm 0.3 \text{‰}$; LF = $-5.1 \pm 0.1 \text{‰}$), Sabarmati downstream (HF = $-4.6 \pm 0.3 \text{‰}$; LF = $-3.4 \pm 0.3 \text{‰}$), Sabarmati tributaries (HF = $-3.3 \pm 1.5 \text{‰}$; LF = $-1.2 \pm 3.2 \text{‰}$), Mahi (HF = $-3.5 \pm 1.7 \text{‰}$; LF = $-2.4 \pm 1.2 \text{‰}$), Narmada Canal (HF = $-5.7 \pm 0.6 \text{‰}$; LF = $-5.1 \pm 0.4 \text{‰}$), and reservoirs (HF = $-3.5 \pm 0.5 \text{‰}$; LF = -0.6‰).

4.2.3.3 Dissolved inorganic carbon

Dissolved inorganic carbon increased along the continuum of Sabarmati during both high and low flow periods (Fig 4.11a). There was no significant change in concentration across flow regime in Sabarmati upstream (HF = $3.03 \pm 1.04 \text{ mM}$; LF = $2.29 \pm 0.69 \text{ mM}$), riverfront (HF = $3.62 \pm 1.99 \text{ mM}$; LF = $2.40 \pm 0.39 \text{ mM}$), Sabarmati downstream (HF = $10.36 \pm 5.35 \text{ mM}$; LF = $9.11 \pm 4.41 \text{ mM}$), Sabarmati tributaries (HF = $4.24 \pm 1.74 \text{ mM}$; LF = $4.87 \pm 3.02 \text{ mM}$), Mahi (HF = $3.40 \pm 1.56 \text{ mM}$; LF = $3.39 \pm 0.69 \text{ mM}$), Narmada Canal (HF = $2.46 \pm 1.39 \text{ mM}$; LF = $2.13 \pm 0.61 \text{ mM}$), and reservoirs (HF = $1.86 \pm 0.46 \text{ mM}$; LF = 1.18 mM). Stable isotopic composition of DIC showed variation with higher mean values during high flow period in Sabarmati upstream (HF = $-5.6 \pm 1.6 \text{‰}$; LF = $-6.8 \pm 1.7 \text{‰}$) and reservoirs (HF = $-3.1 \pm 0.8 \text{‰}$; LF = -7.4‰) (Fig 4.11b). The $\delta^{13}\text{C}_{\text{DIC}}$ increased during low flow in riverfront (HF = $-8.3 \pm 0.6 \text{‰}$; LF = $-7.0 \pm 1.0 \text{‰}$), Sabarmati downstream (HF = $-11.3 \pm 0.5 \text{‰}$; LF = $-10.2 \pm 1.0 \text{‰}$), Sabarmati tributaries (HF = $-8.3 \pm 1.3 \text{‰}$; LF = $-7.7 \pm 1.0 \text{‰}$), Mahi (HF = $-7.5 \pm 1.1 \text{‰}$; LF = $-7.3 \pm 0.9 \text{‰}$), and Narmada Canal (HF = $-9.9 \pm 0.4 \text{‰}$; LF = $-9.4 \pm 0.2 \text{‰}$) (Fig. 4.11b).

4.2.3.4 Particulate organic matter

Average particulate organic carbon concentrations were below $500 \mu\text{M}$ for all sample classes during both high and low flow periods except for Sabarmati downstream (HF = $808 \pm 355 \mu\text{M}$; LF = $1674 \pm 1085 \mu\text{M}$) (Fig 4.12a). Low average POC was observed in the Narmada Canal during both periods (HF = $56.63 \pm 7.99 \mu\text{M}$; LF = $77.80 \pm 21.61 \mu\text{M}$) and Sabarmati upstream during low flow ($55.35 \pm 36.61 \mu\text{M}$) (Fig 4.12a).

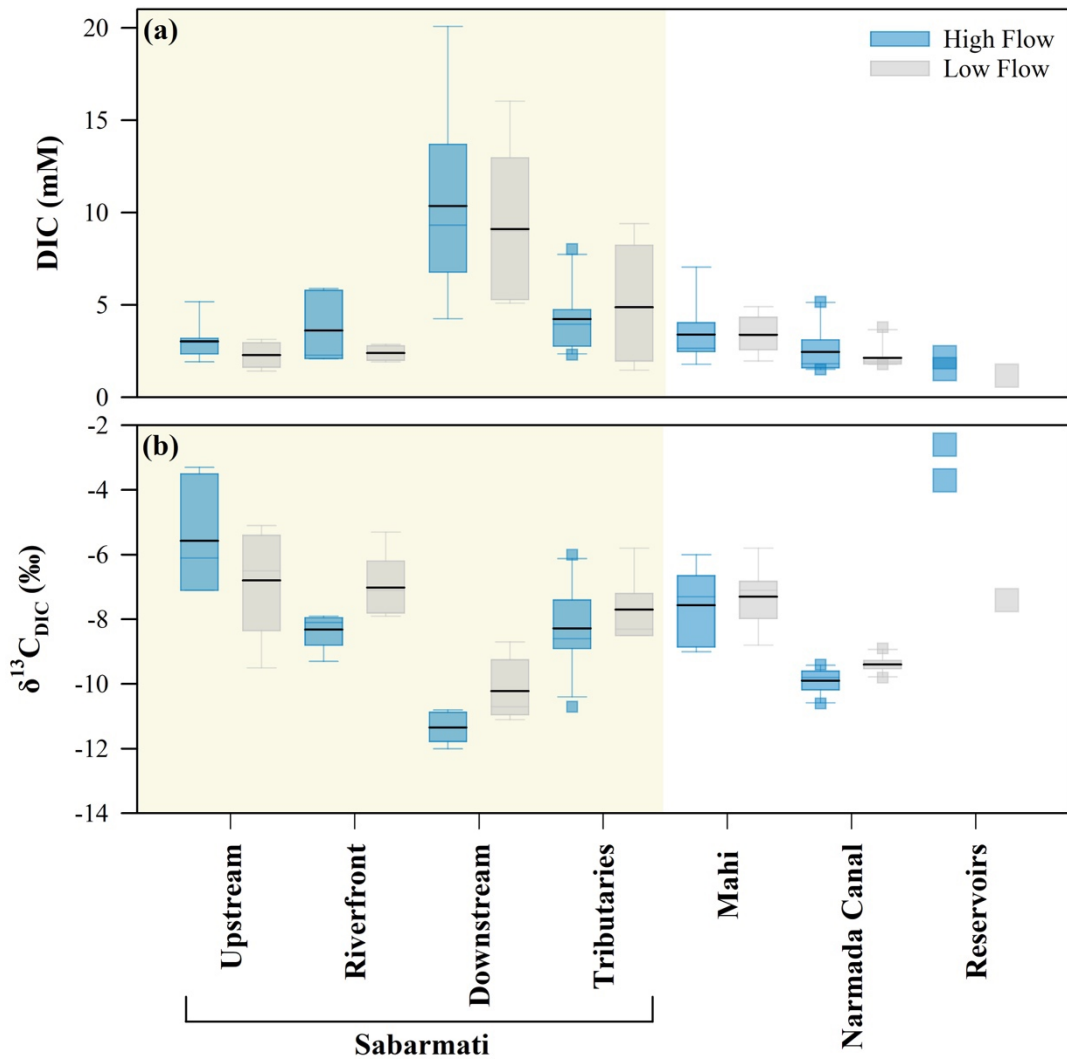


Fig. 4.11 Dissolved inorganic carbon (DIC) (a) concentrations and (b) isotopic compositions in different sample classes. Blue and Grey represent high flow and low flow periods, respectively.

Similar to POC, average PN concentrations were below $120 \mu\text{M}$ except for Sabarmati downstream (HF = $138 \pm 61 \mu\text{M}$; LF = $218 \pm 133 \mu\text{M}$) (Fig 4.13a). The lowest PN concentrations were observed in Sabarmati upstream (HF = $16.74 \pm 11.02 \mu\text{M}$; LF = $6.76 \pm 4.84 \mu\text{M}$) and Narmada Canal (HF = $8.38 \pm 2.12 \mu\text{M}$; LF = $10.62 \pm 3.33 \mu\text{M}$) (Fig 4.13a). Stable isotopic composition of POC increased during low flow period in Sabarmati upstream (HF = $-29.2 \pm 2.1 \text{‰}$; LF = $-25.2 \pm 2.9 \text{‰}$), Sabarmati tributaries (HF = $-28.1 \pm 2.7 \text{‰}$; LF = $-27.0 \pm 2.1 \text{‰}$), Mahi (HF = $-32.0 \pm 2.6 \text{‰}$; LF = $-26.7 \pm 3.3 \text{‰}$), Narmada Canal (HF = $-31.9 \pm 1.2 \text{‰}$; LF = $-28.6 \pm 2.5 \text{‰}$), and reservoirs (HF = $-29.6 \pm 0.3 \text{‰}$; LF = -23.3‰) (Fig 4.12b).

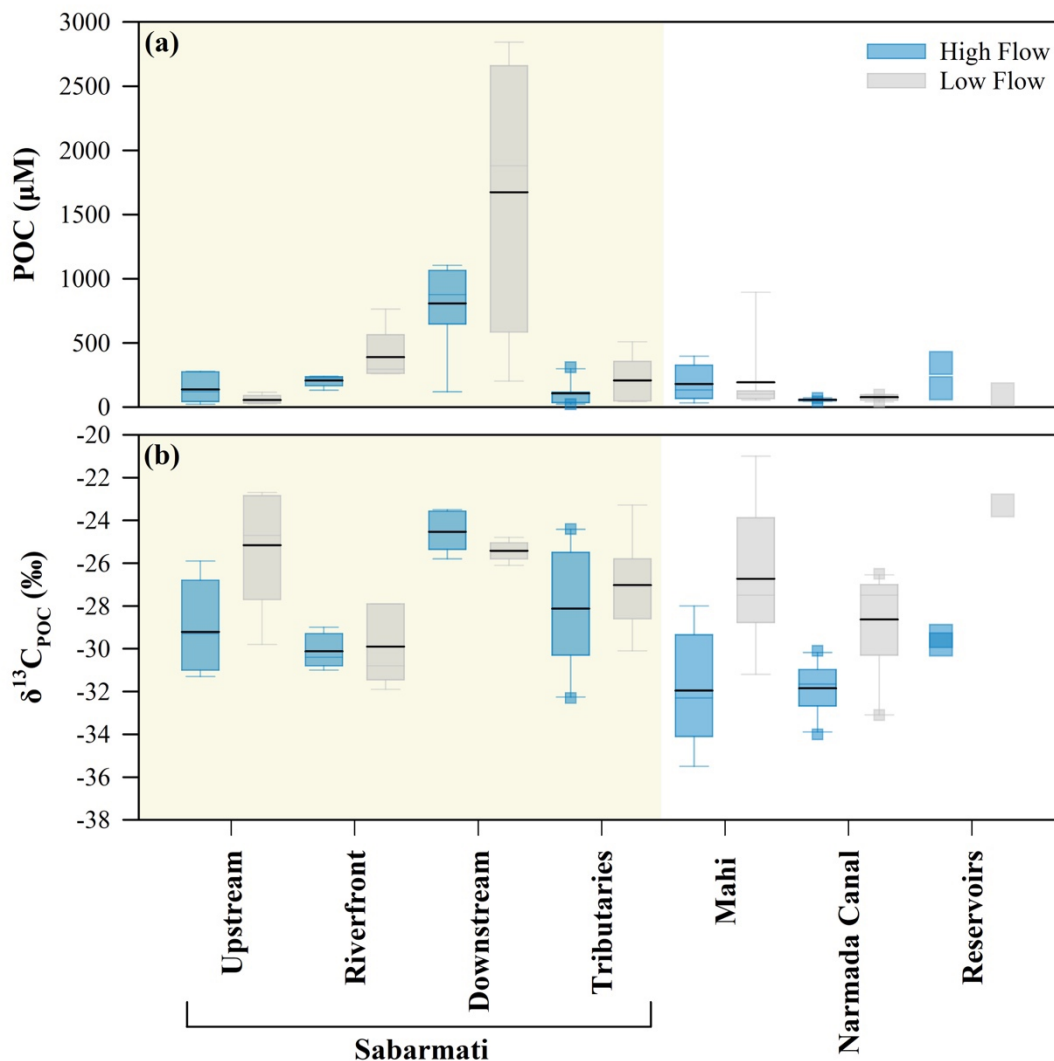


Fig. 4.12 Particulate organic carbon (POC) (a) concentrations and (b) isotopic composition in different sample classes. Blue and grey colour represent high flow and low flow periods, respectively.

The riverfront (HF = -30.1 ± 0.8 ‰; LF = -29.9 ± 1.9 ‰) and Sabarmati downstream (HF = -24.5 ± 0.9 ‰; LF = -25.4 ± 0.5 ‰) did not show temporal change in $\delta^{13}\text{C}_{\text{POC}}$ (Fig 4.12b). The $\delta^{15}\text{N}_{\text{PN}}$ showed clear increase from high to low flow periods in the riverfront (HF = 0.2 ± 0.9 ‰; LF = 4.7 ± 2.5 ‰), Mahi (HF = 5.0 ± 2.2 ‰; LF = 9.2 ± 1.9 ‰), Narmada Canal (HF = 4.2 ± 1.0 ‰; LF = 8.1 ± 1.5 ‰), and reservoirs (HF = 1.5 ± 3.5 ‰; LF = 9.4 ‰) (Fig 4.13b). Not much temporal change was observed in Sabarmati upstream (HF = 7.8 ± 2.4 ‰; LF = 7.1 ± 3.0 ‰), Sabarmati downstream (HF = 0.9 ± 3.3 ‰; LF = 0.6 ± 1.8 ‰), and Sabarmati tributaries (HF = 6.6 ± 12.1 ‰; LF = 3.4 ± 4.5 ‰) (Fig 4.13b).

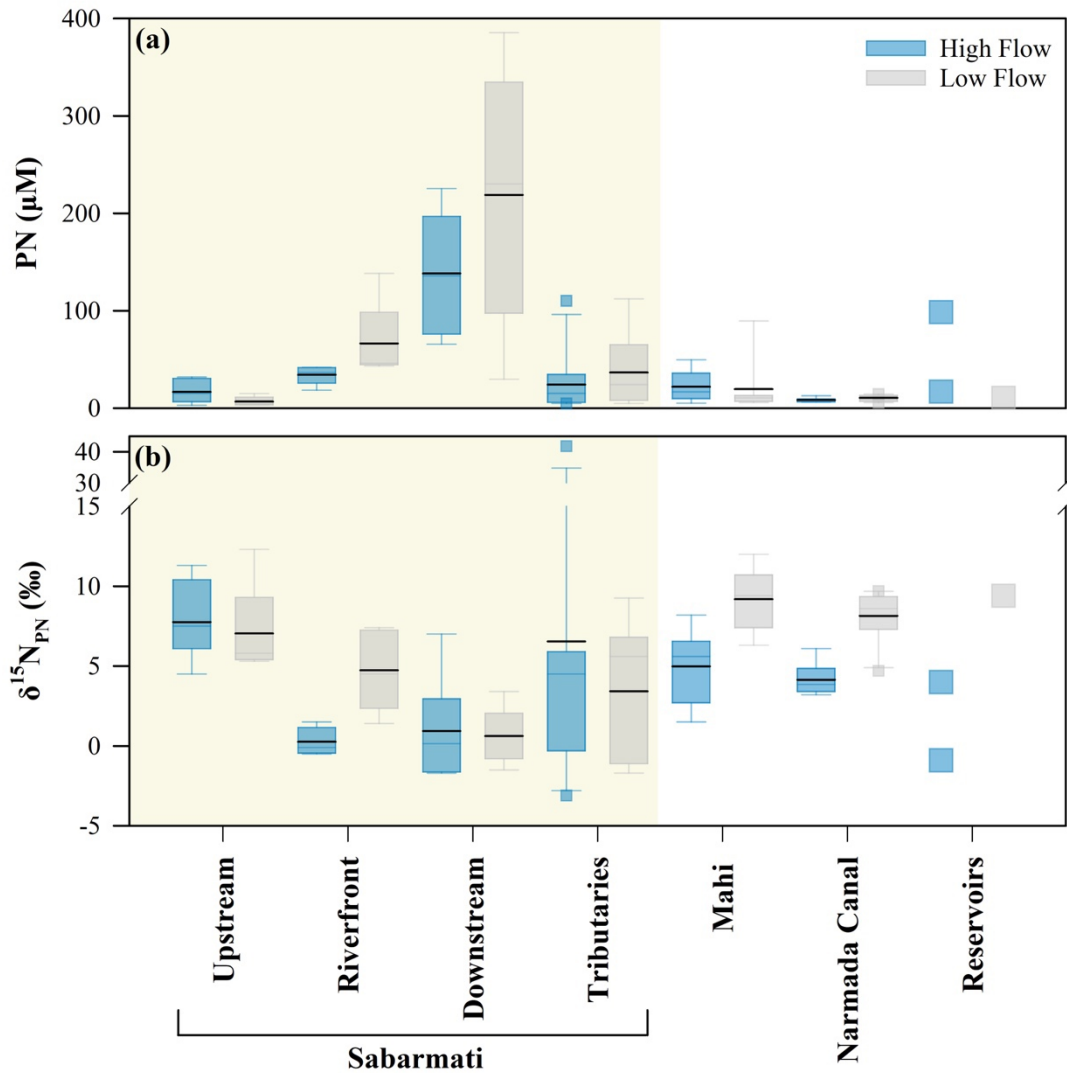


Fig. 4.13 Particulate nitrogen (PN) (a) concentrations and (b) isotopic compositions in different sample classes. Blue and grey colour represents high flow and low flow periods respectively.

4.2.3.5 Dissolved CH₄, CO₂, and N₂O

Dissolved CH₄ in the sampled classes lacked clear seasonality except for Narmada Canal with higher concentration during high flow (518 ± 211 nM) compared to low flow (93 ± 35 nM) (Fig 4.14a). Low CH₄ concentrations was also observed in the Sabarmati upstream (HF = 277 ± 127 nM; LF = 311 ± 196 nM). Extremely high CH₄ was observed in the Sabarmati downstream during both periods (HF = 35.94 ± 15.24 µM; LF = 71.92 ± 58.08 µM). Dissolved CO₂, however, showed temporal variations with generally higher concentrations during the high flow period. Dissolved CO₂ was higher in Sabarmati downstream (HF = 3857 ± 1568 µM; LF = 2885 ± 798 µM) compared to Sabarmati upstream (HF = 1411 ± 130 µM; LF = 1246 ± 432 µM), riverfront (HF = 1499 ± 95 µM; LF = 1081 ± 64 µM), Sabarmati tributaries (HF = 1731

$\pm 1023 \mu\text{M}$; LF = $1589 \pm 991 \mu\text{M}$), Mahi (HF = $1564 \pm 167 \mu\text{M}$; LF = $1127 \pm 413 \mu\text{M}$), Narmada Canal (HF = $1326 \pm 40 \mu\text{M}$; LF = $648 \pm 100 \mu\text{M}$), and reservoirs (HF = $1222 \pm 134 \mu\text{M}$; LF = $293 \mu\text{M}$) (Fig 4.14b). Similar to CO_2 , higher N_2O concentrations during high flow periods were observed.

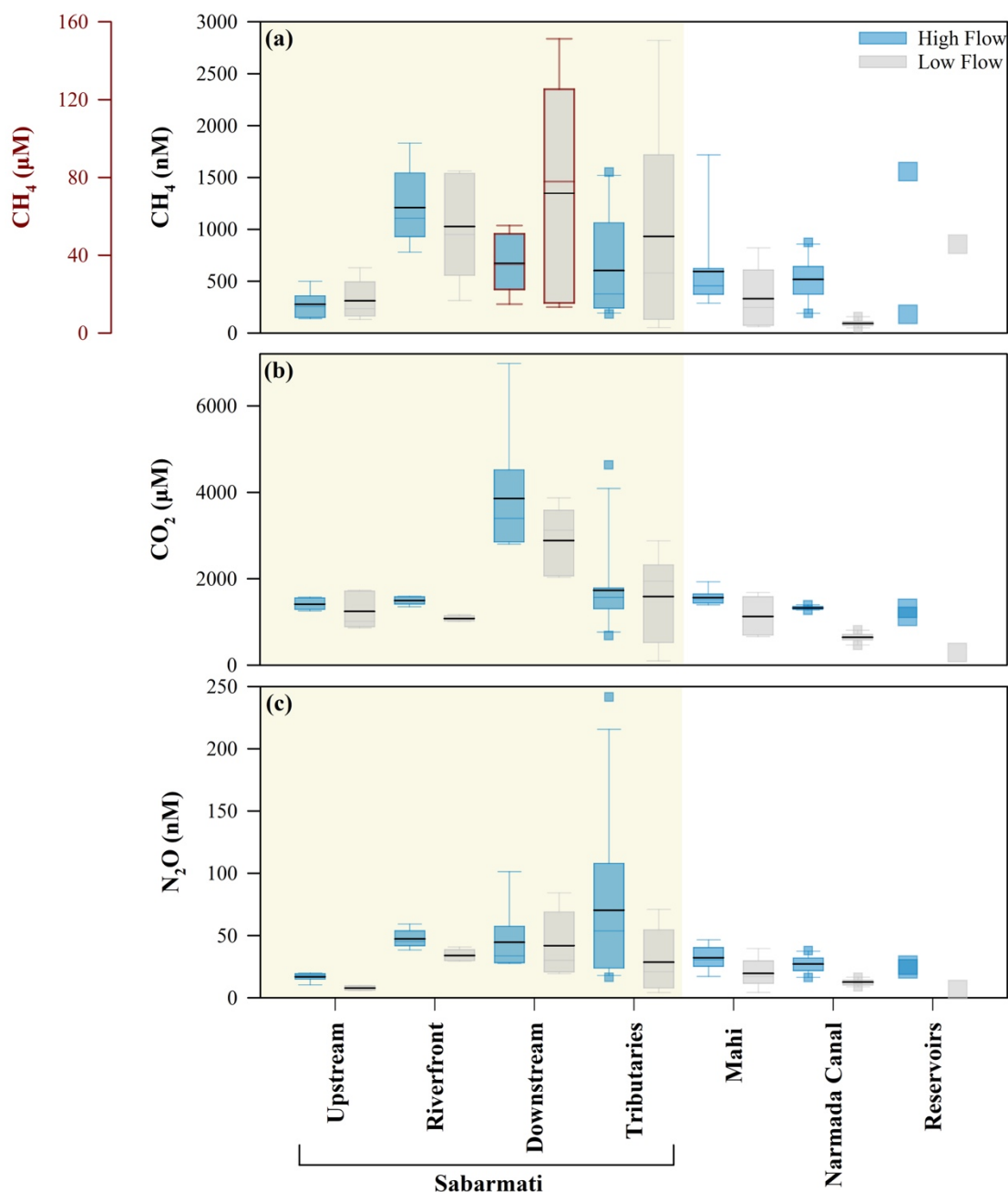


Fig. 4.14 Dissolved (a) CH_4 , (b) CO_2 , and (c) N_2O in different sample classes. Blue and grey colours represent high flow and low flow periods, respectively. For Sabarmati downstream, CH_4 concentrations are shown by separate Y axis in red colour.

Higher N_2O in Sabarmati tributaries (HF = $70.4 \pm 65.1 \text{ nM}$; LF = $28.5 \pm 25.6 \text{ nM}$) was observed compared to Sabarmati upstream (HF = $16.9 \pm 3.3 \text{ nM}$; LF = $7.8 \pm 1.8 \text{ nM}$), riverfront ($47.2 \pm 7.6 \text{ nM}$; LF = $34.0 \pm 4.6 \text{ nM}$), Sabarmati downstream (HF = $44.5 \pm$

28.5 nM; LF = 41.9 ± 27.2 nM), Mahi (HF = 32.1 ± 9.6 nM; LF = 19.5 ± 11.5 nM), Narmada Canal (HF = 27.0 ± 6.9 nM; LF = 12.5 ± 2.6 nM), and reservoirs (HF = 24.7 ± 2.1 nM; LF = 6.5 nM) (Fig 4.14c).

4.2.4 Discussion

4.2.4.1 Temporal variation in dissolved inorganic carbon and particulate matter

The Sabarmati and Mahi River basins receive heavy rainfall during the Indian Summer Monsoon (July - September) which is reflected in high discharge during the post monsoon season. During the sampling, it was observed that the river networks were connected only during high flow periods. During the low flow condition, the channel got fragmented and at several location isolated patches were observed. It is evident from the sharp increase in $\delta^{18}\text{O}$ of surface waters from high to low flow period that evaporative water loss is dominant during the low flow. Therefore, it would be appropriate to consider these stagnant water bodies more like lentic systems and expect dominant biogeochemical processes to behave accordingly. Increase in EC during low flow period is also an indicator of the effect of evaporative water loss and subsequent accumulation of dissolved ions (Fig 4.9, 4.10 and 4.11a). The DIC concentration did not increase significantly across flow regime, however there was a shift in its isotopic composition (Fig 4.11a). The $\delta^{13}\text{C}_{\text{DIC}}$ was higher in Sabarmati upstream during high flow condition and the same was with the reservoirs in the upstream catchments (Fig 4.11b). Higher $\delta^{13}\text{C}_{\text{DIC}}$ during high flow periods indicate addition of DIC from the catchment via surface runoff. Weathering of carbonate terrains would elevate the isotopic composition of the riverine DIC and is usually observed in lower order streams with more catchment influence (Campeau et al., 2017). The other reaches of Sabarmati and Mahi along with the Narmada Canal showed increase in $\delta^{13}\text{C}_{\text{DIC}}$ during low flow condition. This increase clearly indicates a shift towards a more productive system where uptake of DIC (preferentially the lighter C) by primary producers results in the increase in isotopic composition of the DIC pool. A strong -ve relationship was observed between DIC and $\delta^{13}\text{C}_{\text{DIC}}$ during both high flow (Fig 4.15a & 4.16a) and low flow (Fig 4.15b & 4.16b) periods. This relationship was derived to track the variability in DIC across both Sabarmati and Mahi River basins along with the Narmada Canal. Decrease in $\delta^{13}\text{C}_{\text{DIC}}$ with increasing DIC indicated addition of isotopically depleted DIC into the system which could be a result of degradation of OM and subsequent

release of CO₂. The effect of CO₂ is further observed in the significant ($p < 0.05$) –ve relationship between DIC and pH (Fig 4.16a & b).

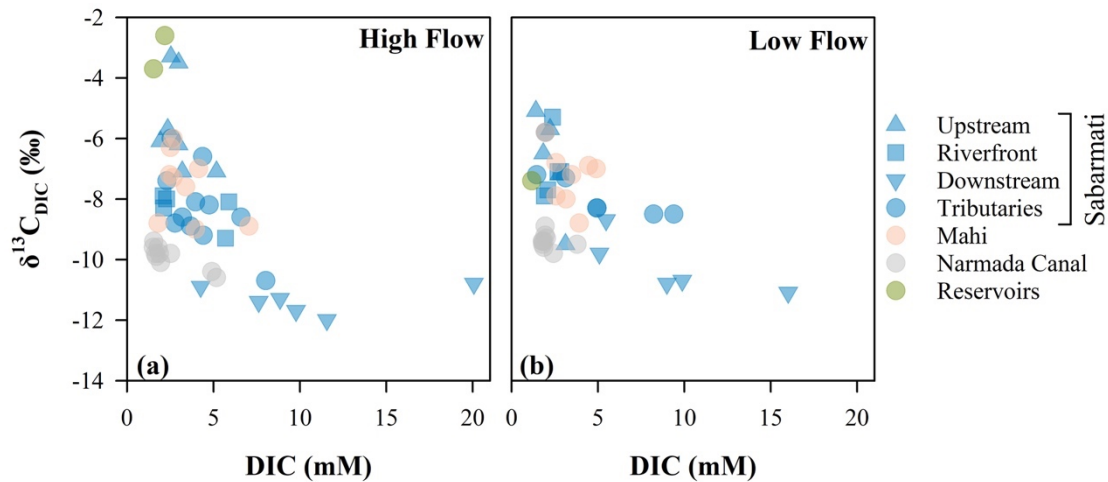


Fig. 4.15 Relationships between DIC and $\delta^{13}\text{C}_{\text{DIC}}$ during (a) high flow and (b) low flow periods.

The particulate matter concentration in the river channels increased during low flow periods except for Sabarmati Upstream where high POM was observed during high flow (Fig 4.12a & 4.13a). The increase in concentrations of POC and PN is attributed to increased primary productivity during low flow condition. Clear waters and less turbidity are favourable for primary production (Beusen et al., 2005). This is also reflected in higher C/N ratio observed in the Narmada Canal and Mahi during low flow conditions (Fig 4.17), but in other sample classes the C/N ratio remained statistically similar. The average $\delta^{13}\text{C}_{\text{POC}}$ showed variability with relative increase during low flow conditions in the Sabarmati upstream, tributaries, Narmada Canal, Mahi and reservoirs. This increase indicated uptake of isotopically enriched (¹³C) DIC during the low flow period. Significant +ve relationship ($p < 0.05$; Fig 4.16b) was observed between water temperature and POC concentrations during low flow, suggesting higher temperature favored productivity. Furthermore, POC and $\delta^{13}\text{C}_{\text{POC}}$ showed a +ve relationship during high flow period supporting the above argument of a coupling between the DIC and POC pools (Fig 4.16a and Fig 4.18a). PN showed similar trends in concentrations as POC with no significant temporal variation. A significant –ve relationship ($p < 0.05$, Spearman) observed between PN and $\delta^{15}\text{N}_{\text{PN}}$ during both high and low flow indicated potential N₂ fixation or uptake of DIN of low $\delta^{15}\text{N}$ coming from catchment runoff (Fig. 4.16 and 4.19).

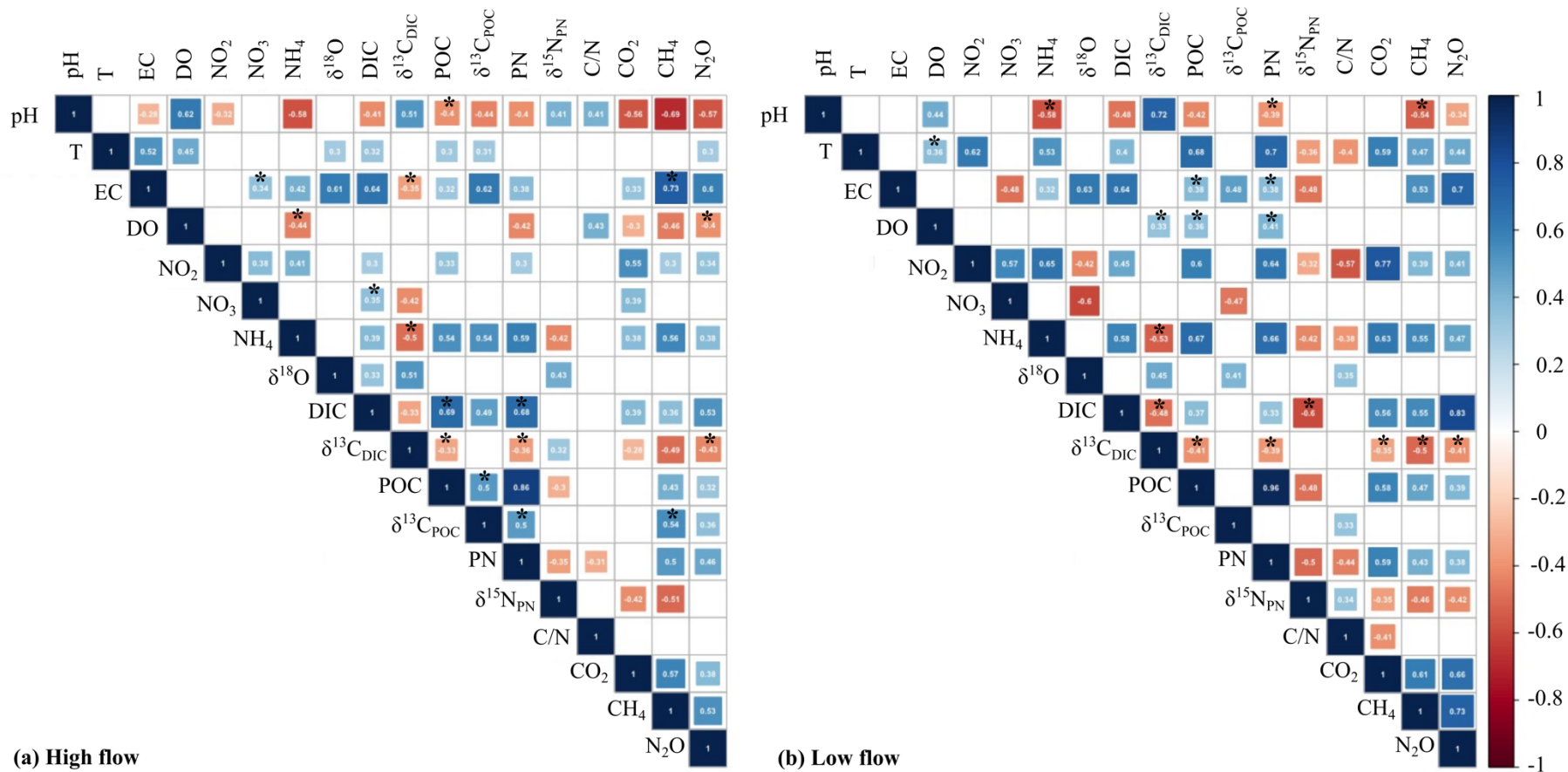


Fig. 4.16 Correlation plots (Spearman Rank and *Pearsons) among measured parameters with significance level $p < 0.05$ during (a) high flow and (b) low flow periods.

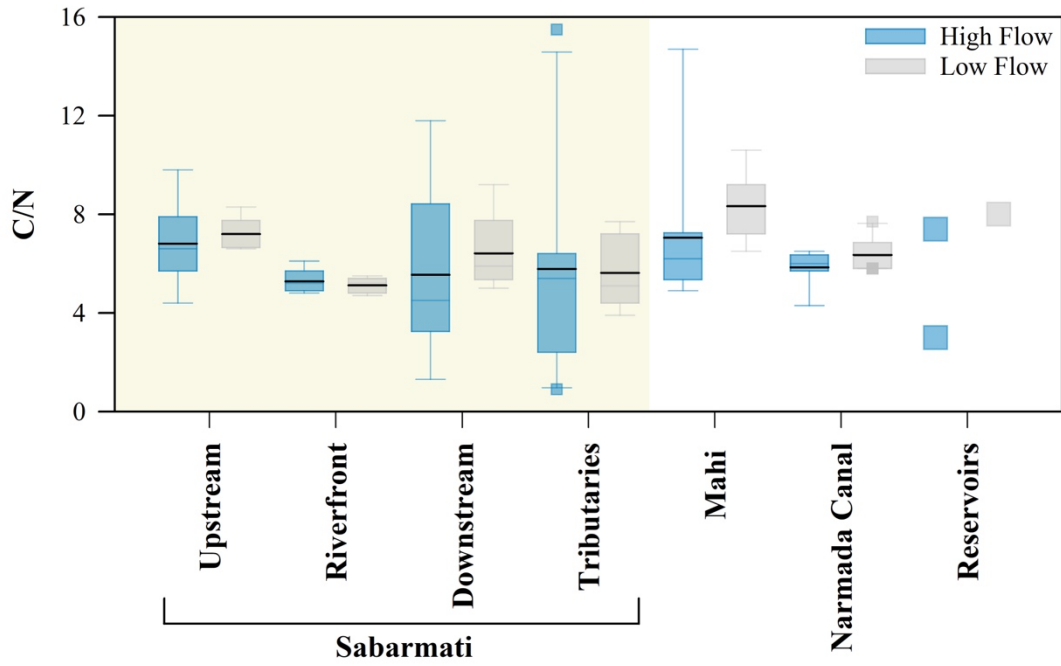


Fig. 4.17 C/N ratio in particulate matter in different sample classes. Blue and grey colour represents high flow and low flow periods respectively.

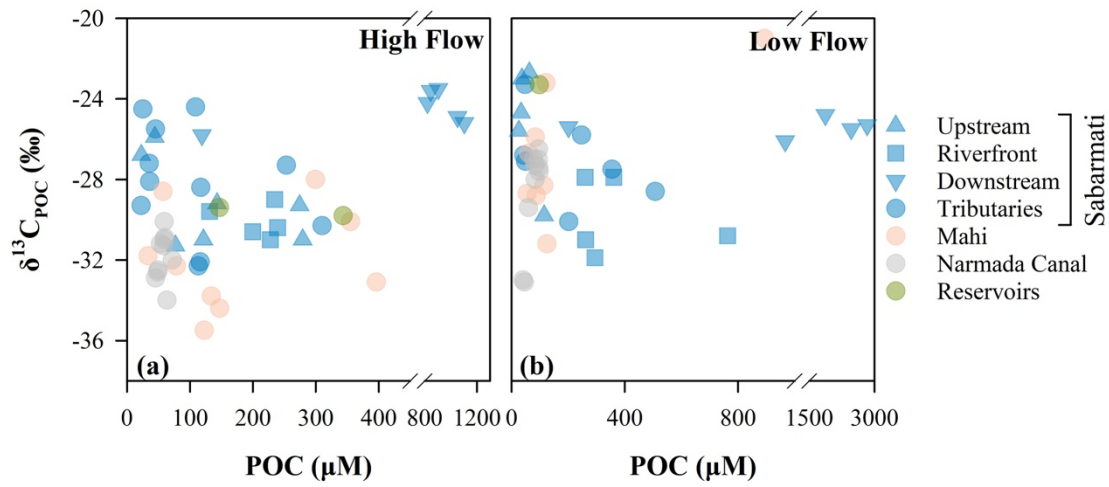


Fig. 4.18 Relationship between POC and $\delta^{13}C_{POC}$ during (a) high flow and (b) low flow periods.

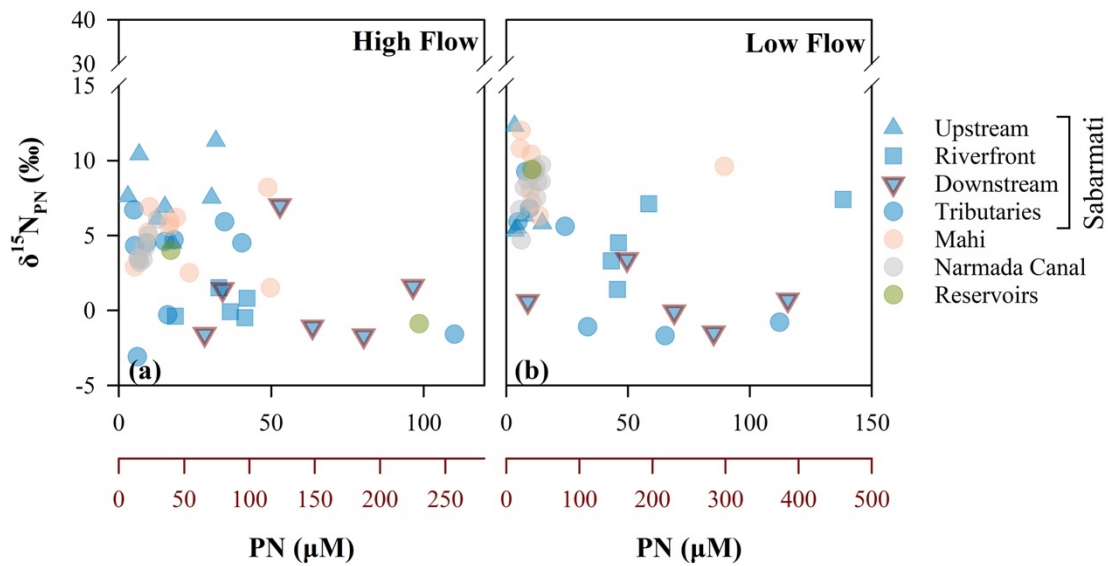


Fig. 4.19 Relationship between PN and $\delta^{15}\text{N}_{\text{PN}}$ during (a) high flow and (b) low flow periods. The PN concentration of Sabarmati Downstream is shown by a separate axis in red color.

4.2.4.2 Temporal variation in the dissolved CH_4 , CO_2 , and N_2O

Temporal variation in dissolved GHGs are controlled by several factors including supply of OM to act as substrate for decomposition, supply of inorganic forms of N to participate in the nitrification and denitrification pathways, oxic-anoxic conditions, temperature, primary productivity and respiration (Bastviken et al., 2011; Begum et al., 2021). These components vary widely across river basins depending on catchment type, dominant land use (agriculture, plantations, etc.), and river flow velocity. In this study, except the Narmada Canal, no temporal variability in dissolved CH_4 concentrations (Fig 4.14a) were observed due to sufficient supply of OM during both high and low flow periods for methanogenesis. Reduction in CH_4 concentrations in the Narmada Canal during low flow could be due to the cut off of allochthonous inputs of organic matter at the inlet from the Narmada River. CO_2 and N_2O showed temporal variability with relatively higher concentration during high flow period. As the Sabarmati and Mahi river basins are agriculture dominated watersheds, they witness extensive use of fertilisers and manures. Surface runoff during monsoon washes and drains large quantities of N compounds to the river and this in turn facilitates the N_2O production through nitrification and nitrifier denitrification, leading to higher N_2O during high flow periods. This is further supported by the significant +ve correlation between DIN and N_2O concentrations ($p < 0.05$, Fig 4.16). Similarly, CO_2 is driven by

the coupling of primary production and respiration, the latter being the causal factor for CO₂ supersaturation in aquatic systems (Cole et al., 2007). It is observed that the balance between the production and respiration is highly sensitive to environmental variables like nutrient availability, DO, DOC concentrations etc., and a system can rapidly switch from a heterotrophic source of CO₂ to an autotrophic sink (Wang et al., 2017). During the low flow periods, clear water and low flow conditions favours primary production resulting in consumption of CO₂. On the contrary, during high flow periods, turbid waters limit primary production and CO₂ consumption, and the allochthonous OM received through surface runoff acts as substrate for mineralisation and CO₂ production. Furthermore, inputs of DIC via surface runoff also enhances the CO₂ concentration in the system. Overall observed significant –ve relationship between dissolved CO₂ and the $\delta^{13}\text{C}_{\text{DIC}}$ ($p < 0.05$; Fig 4.16) indicates that CO₂ brings in lighter C isotopes to the DIC pool, indicative of mineralisation of OM. It is also observed that increase in water temperature enhances the production of CH₄ and CO₂ during low flow ($p < 0.05$, Fig 4.16a) and N₂O during both high and low flow periods ($p < 0.05$, Fig 4.16). This indicates enhanced microbial activity at higher temperatures.

4.2.4.3 Effect of engineered modifications on river biogeochemistry: Lined Canal, stagnant Riverfront, and the polluted Sabarmati Downstream

The spatial variation of the various pools of C and N from headwater to downstream reach of Sabarmati provides an idea of the effect of modifications of river channel on the C and N biogeochemistry in urban setting. The Narmada Canal, which is a lined canal shows the effect of lining and lack of direct catchment influence on biogeochemistry. The biomass of the riverfront was higher than that in the Narmada Canal during both high and low flow periods (Fig 4.12a & 4.13a). The water in the Riverfront is received from the Narmada Canal, and the higher biomass reflects higher productivity at stagnant conditions. Furthermore, the increased productivity is accompanied by a decrease in $\delta^{15}\text{N}_{\text{PN}}$ (Fig 4.13b), which indicates enhanced N₂ fixation with increasing productivity, particularly in the absence of any allochthonous inputs. Particulate matter concentrations were very high in the polluted downstream reach of the Sabarmati with high $\delta^{13}\text{C}_{\text{POC}}$ and low $\delta^{15}\text{N}_{\text{PN}}$ (Fig 4.12 and 4.13). The elevated particulate matter in the downstream reach is caused by inflow of treated and untreated wastewater with high suspended load. In case of DIC, no significant change in concentrations was observed between the Narmada Canal and the riverfront. However,

the $\delta^{13}\text{C}_{\text{DIC}}$ in the riverfront was higher during both high and low flow periods, indicating preferential uptake of lighter DIC during primary production. The Sabarmati downstream witnesses manifold increase in the DIC concentrations compared to Sabarmati upstream (Fig 4.11a). Wastewater inputs have been identified as a significant contributor to riverine DIC of low stable isotopic composition (Hu et al., 2018; Yang et al., 2018). Similar trends in DIC of Sabarmati downstream were observed, where $\delta^{13}\text{C}_{\text{DIC}}$ was extremely low compared to the other sample classes. The low $\delta^{13}\text{C}_{\text{DIC}}$ in the polluted downstream reach was attributed to high CO_2 release from degradation of OM along with high CO_2 inputs via wastewater discharge. It has been noted elsewhere that urban rivers receive GHG's fluxes from treated and untreated sewage (Li et al., 2020; Begum et al., 2021). Caniani et al. (2019) observed a CO_2 concentration of ~ 30 mM in the final effluent from wastewater treatment plants. Manifold higher CO_2 in the Sabarmati downstream compared to the other reaches of the river was observed during this study as well (Fig 4.14b). The high EC of the Sabarmati downstream indicated its ability for rapid decomposition of OM for microbial production (Quick et al., 2019).

It has been observed that anthropogenic perturbations enhance the fluxes of GHG's from global rivers (Garnier et al., 2013; Alshboul et al., 2016; Deemer et al., 2016; He et al., 2017; Yoon et al., 2017; Jin et al., 2018; Li et al., 2020). However, the synergistic effect of impoundments and wastewater discharge on the riverine CH_4 , CO_2 , and N_2O emissions needs to be explored in great depth. Research have found enhanced emission of GHGs in eutrophic and impounded river channels due to supply of OM, nutrients, and presence of diverse microbial communities (Wang et al., 2017; Begum et al., 2021). In this study, apart from CO_2 , CH_4 and N_2O also showed high spatial variability along the level of anthropogenic developments. For instance, CH_4 and N_2O significantly increased in the riverfront compared to the Narmada Canal (Fig 4.14a and c). This is attributed to the productive waters and the availability of OM as substrate for methanogenesis and higher OM in the sediments is expected to provide favorable low oxygen environment for denitrification. Construction of a dam or weir reduces the flow velocity of the water, traps sediments on its bed and develop a favorable anoxic environment for methanogenesis (Maeck et al., 2013; Stanley et al., 2016).

Furthermore, Sabarmati downstream witnessed extremely high CH_4 concentrations which could be a result of several factors (input via wastewater discharge, methanogenesis in anoxic waters, sedimentary methanogenesis, and reduced

CH₄ oxidation). Wastewater inputs have been known to have 0.9 – 1699.9 nM of N₂O and 0.06 – 455.8 μM of CH₄ (Begum et al., 2021). It has been documented that processes enhancing GHGs production prefer low DO environment (Cotovicz et al. 2016; Quick et al. 2019). High inputs of biological oxygen demand and nutrients enhances the production of CO₂ and other GHGs via mechanisms like photo and biodegradation of OM in the water column and metabolic processes at the anoxic bottom sediments (Yoon et al., 2017; Begum et al., 2021; Kim et al., 2019). Additionally, wastewater discharge is high in OM but depleted in DO. This enhances the production of CH₄ via anaerobic respiration (Sobek et al. 2005; Humborge et al. 2010; Alshboul et al., 2016; Li et al., 2020). The DO concentration below detection limit, as observed in the Sabarmati downstream, might have further prevented the oxidation of the CH₄ in the water column, causing supersaturation (Li et al., 2020). Additionally, there is competition between NH₄⁺ and CH₄ oxidising bacteria for DO, resulting in co-accumulation of the two species in the sediments and water column (Han et al., 2018). The accumulation of CH₄ and NH₄⁺ in the Sabarmati downstream indicated towards this competition (Fig 4.16).

4.2.4.4 Fluxes of CH₄, CO₂, and N₂O

CH₄ fluxes showed temporal variation with the highest emissions from the polluted reaches of Sabarmati downstream (HF = 7659 ± 2990 μM m⁻²d⁻¹; LF = 18424 ± 14847 μM m⁻²d⁻¹) compared to Sabarmati upstream (HF = 56 ± 25 μM m⁻²d⁻¹; LF = 68 ± 45 μM m⁻²d⁻¹), riverfront (HF = 238 ± 75 μM m⁻²d⁻¹; LF = 268 ± 140 μM m⁻²d⁻¹), Sabarmati tributaries (HF = 126 ± 104 μM m⁻²d⁻¹; LF = 220 ± 233 μM m⁻²d⁻¹), Narmada Canal (HF = 100 ± 39 μM m⁻²d⁻¹; LF = 20 ± 8 μM m⁻²d⁻¹), Mahi (HF = 131 ± 98 μM m⁻²d⁻¹; LF = 75 ± 65 μM m⁻²d⁻¹), and reservoirs (HF = 181 ± 203 μM m⁻²d⁻¹; LF = 191 μM m⁻²d⁻¹) (Fig 4.20). Except for downstream, CO₂ fluxes did not show significant temporal and spatial variation. As expected, the flux was the highest in the Sabarmati downstream (HF = 861 ± 366 mM m⁻²d⁻¹; LF = 749 ± 237 mM m⁻²d⁻¹) compared to Sabarmati upstream (HF = 295 ± 33 mM m⁻²d⁻¹; LF = 275 ± 97 mM m⁻²d⁻¹), riverfront (HF = 284 ± 22 mM m⁻²d⁻¹; LF = 301 ± 14 mM m⁻²d⁻¹), Sabarmati tributaries (HF = 372 ± 240 mM m⁻²d⁻¹; LF = 392 ± 269 mM m⁻²d⁻¹), Narmada Canal (HF = 267 ± 17 mM m⁻²d⁻¹; LF = 142 ± 24 mM m⁻²d⁻¹), Mahi (HF = 353 ± 43 mM m⁻²d⁻¹; LF = 267 ± 110 mM m⁻²d⁻¹), and reservoirs (HF = 260 ± 30 mM m⁻²d⁻¹; LF = 64 mM m⁻²d⁻¹).

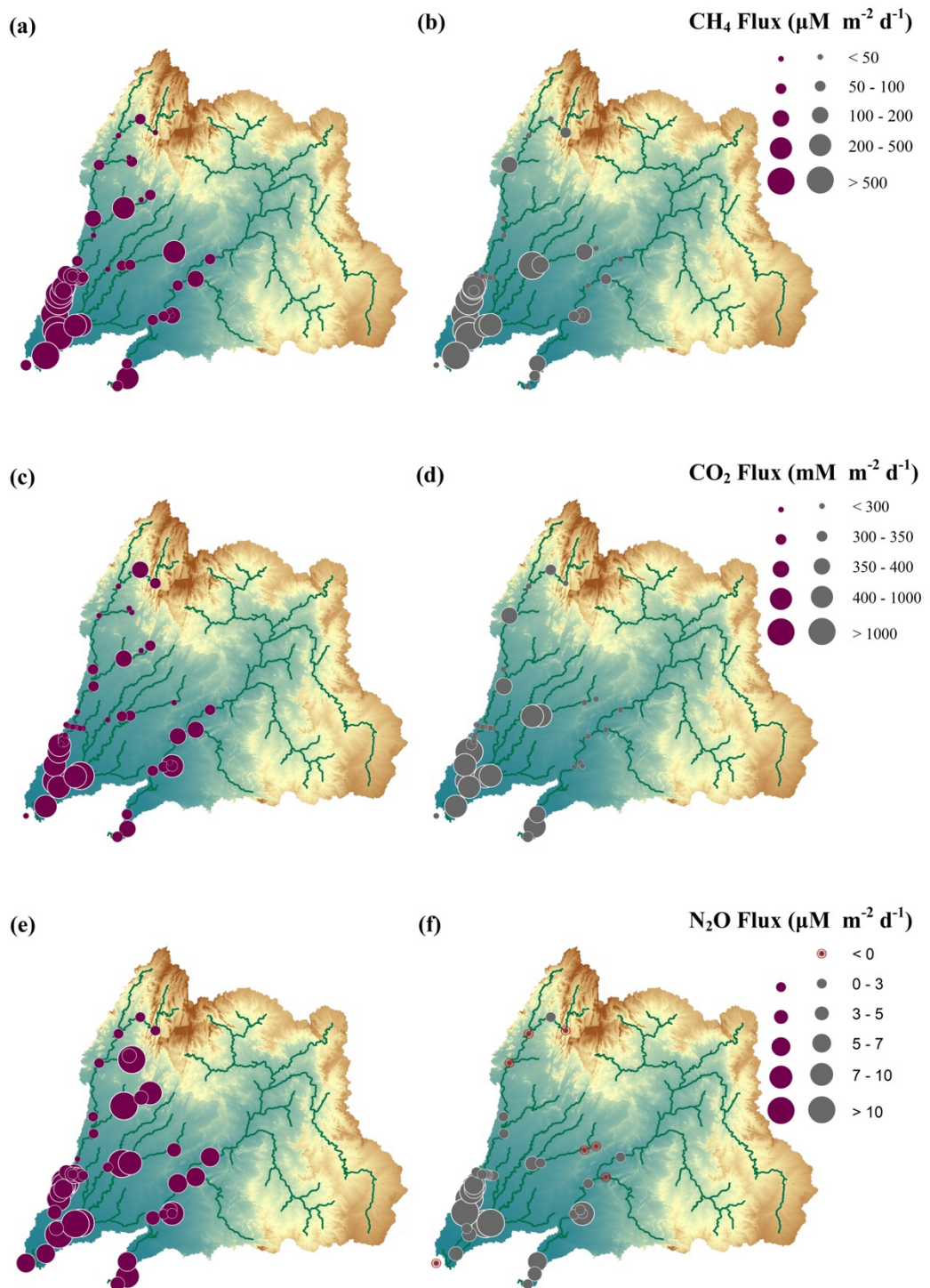


Fig. 4.20 Spatial variability of emission fluxes of CH₄, CO₂, and N₂O during high flow (a, c, and d) and low flow (b, d, and f) periods.

The Sabarmati and Mahi river basins witnessed high temporal variability in the N₂O emission fluxes. All the sampled classes acted as a net source during high flow periods but several sites behaved as a sink for N₂O during the low flow periods (Fig 4.20 e and f). Unlike CH₄ and CO₂, N₂O showed the highest fluxes along the Sabarmati tributaries during high flow (HF = $13.1 \pm 12.6 \mu\text{M m}^{-2}\text{d}^{-1}$; LF = $5.2 \pm 6.9 \mu\text{M m}^{-2}\text{d}^{-1}$) compared to Sabarmati upstream (HF = $2.1 \pm 0.7 \mu\text{M m}^{-2}\text{d}^{-1}$; LF = $-0.1 \pm 0.4 \mu\text{M m}^{-2}\text{d}^{-1}$), riverfront (HF = $7.9 \pm 1.5 \mu\text{M m}^{-2}\text{d}^{-1}$; LF = $6.9 \pm 1.2 \mu\text{M m}^{-2}\text{d}^{-1}$), Sabarmati downstream (HF = $8.4 \pm 6.9 \mu\text{M m}^{-2}\text{d}^{-1}$; LF = $8.2 \pm 7.8 \mu\text{M m}^{-2}\text{d}^{-1}$), Narmada Canal (HF = $3.9 \pm 1.3 \mu\text{M m}^{-2}\text{d}^{-1}$; LF = $0.9 \pm 0.6 \mu\text{M m}^{-2}\text{d}^{-1}$), Mahi (HF = $5.7 \pm 2.2 \mu\text{M m}^{-2}\text{d}^{-1}$; LF = $2.6 \pm 2.6 \mu\text{M m}^{-2}\text{d}^{-1}$), and reservoirs (HF = $3.7 \pm 0.5 \mu\text{M m}^{-2}\text{d}^{-1}$; LF = $-0.4 \mu\text{M m}^{-2}\text{d}^{-1}$). The sites witnessing -ve fluxes of N₂O were mainly from Sabarmati upstream and Sabarmati tributaries during low flow. It is documented that N₂O production is mainly governed by nutrient supply and DO levels (Wang et al., 2015; He et al., 2017; Mwanake et al., 2019). Furthermore, Schade et al. (2016) observed enhanced competition for resources between denitrifiers and methanogens in the headwater streams as compared to nutrient rich urban rivers.

4.2.5 Conclusion

The present study explores the C and N biogeochemistry of an engineered river system (Sabarmati River) along with a parallel free flowing Mahi River. Along the river continuum, it was observed that anthropogenic developments significantly enhanced the C and N loading into the river channels. DIC, POM, and dissolved GHGs increased manifold in the polluted downstream reach of the Sabarmati. The study also explores the effect of channel modification resulting in increased residence time of water in certain river sections. There was significant change in C and N dynamics as the water from flowing Narmada Canal was pumped into the riverfront where it was stagnant. POM increased with stagnancy indicating enhanced primary productivity followed by elevated concentrations of GHGs. The study highlights the direct effects of riverfront construction and wastewater discharge on the various in-stream processes. Urban rivers warrant extensive research to avoid underestimation of GHGs fluxes in the global scenario.

4.3 Biogeochemistry of high altitude river – lake continuum

The river – lake continuum as an integrated aquatic system has only recently been recognised and studied by aquatic scientists who were earlier divided as stream ecologists and limnologists (Jones, 2010). Rivers and lakes are hotspots for nutrient cycling, however the manner in which the C and N flows and are processed varies. Rivers are more like passive pipes at high flow and active pipes at low flow conditions, incorporated justly in the pulse-shunt concept (Raymond et al., 2016). Lakes, on the other hand, are active units for elemental processing and also act as sites for long term burial of C and N (Cole et al., 2007; Bastviken et al., 2011). In the river – lake continuum, lakes are known to be active sink for N and C (Harrison et al., 2009; Xu et al., 2018). Researchers have highlighted the need to study both lotic and lentic systems as an integrated aquatic component playing the role of conduit and reactor of terrestrial C and N. This must also incorporate the retention time within streams and lakes to quantify the biogeochemical filtering of elements (Cole et al., 2007; Tranvik et al., 2009; Bouwman et al., 2013).

High altitude lakes and rivers are facing the direct effects of a changing climate with shifts in the hydrological regime and associated fluxes of C and N from the catchment. Recent studies from the streams and lakes in the Tibetan Plateau found supersaturation of CO₂, CH₄, and N₂O which were strongly correlated to in lake/stream parameters like DOC, DIN, water temperature, and water depth (Qu et al., 2017; Yan et al., 2018). However, studies with high spatial and seasonal resolution are highly warranted from these regions at the forefront of global change. The present study explores the flow of C and N along the mainstem and tributaries of the Jhelum River and attempts to understand the shift in biogeochemical processes as the river drains into the Wular Lake. Specifically, the study focuses on the reasons for (i) spatial and seasonal variation in the concentrations of POC, PN, DIC and dissolved CH₄, CO₂ and N₂O, and (ii) changes in the concentration of the above mentioned pools at the interface of the Jhelum River and the Wular Lake.

4.3.1 Study area and sampling

The Jhelum River is a major tributary of the Indus River System and traverses through the Kashmir valley in the northern Indian territory of the Jammu and Kashmir. The river originates near Verinag in Anantnag and flows northwest all the way to Kichhama in Baramullah district. The river passes through the heart of the Srinagar City and meets the Wular Lake to emerge again. The basin area of the Jhelum is $\sim 33,670 \text{ km}^2$ and the length of the river is $\sim 129 \text{ km}$ (Mir & Jeelani, 2015). The altitude of the valley ranges from 1100 to > 5400 meters amsl (above mean sea level). The major tributaries of Jhelum are Sandrin, Bringi, Arapath, Lidder, Arapal, Sind, and Pohru joining the mainstem in the right bank and Rimbiara, Vishav, Doodganga, Sukhnag, Romshi and Ningal joining the mainstem in the left bank. The Jhelum basin is characterized by high structural hills in the upper basin along with numerous Karewas (small mounds), colluvial fans, and alluvium filled river valley (Mir et al. 2016).

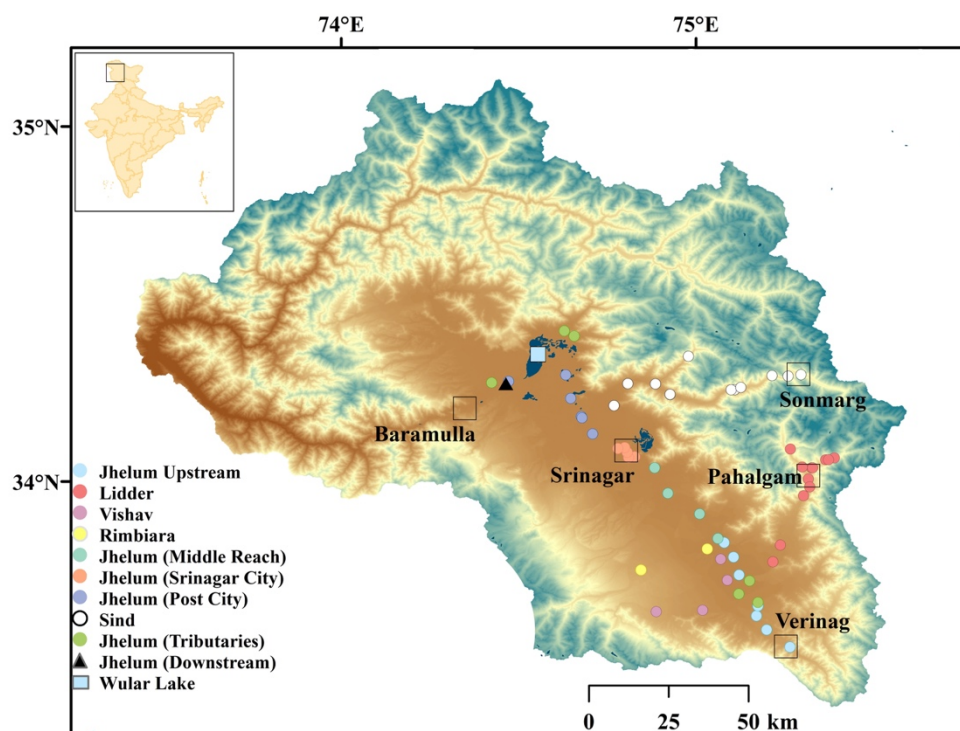


Fig. 4.21 Sampling locations in the Jhelum River basin in the Kashmir Valley.

The Wular Lake is the largest freshwater lake of Asia and is situated within the flow path of the Jhelum river (Fig 4.21 and 4.22). The lake is situated $\sim 34 \text{ km}$ northwest of the Srinagar city and at an altitude of 1530 m amsl (Sheikh et al., 2013). Rivers (Erin and Madhumati) draining the Pir Panjal Mountains in the north of the Wular, drains into the lake. The major seasons in the Kashmir valley is divided into spring (March –

May), summer (June – August), autumn (September – November) and winter (December – March) (Mehmood et al., 2017). Among these, January is the coldest and July is the warmest. March – May (spring) receives the maximum precipitation in the form of rainfall (Rather et al., 2016).



Fig. 4.22 Sampling locations in the Jhelum River basin in the Kashmir Valley.

Sampling for this study was conducted in the Jhelum River, its major and minor tributaries, and the Wular Lake (Fig 4.21 and 4.22) during March 2021 and November 2021 to capture the post melt (spring) and post-summer (autumn) seasons. Unfortunately, there was some technical glitch in the field during autumn and the basic parameters (temperature, pH, EC) measured could not be retrieved. Therefore, for the calculation of GHGs concentrations during autumn, the reach average data for salinity from spring was used. This strategy was adopted as it has been noticed in the previous

studies that the electrical conductivity during autumn and spring remains within the range of $0.2 - 0.4 \text{ mS cm}^{-1}$ (Rather et al., 2016). Additionally, sensitivity analysis of GHGs concentrations for a salinity range of 0.1 to 0.45 g/L (maximum and minimum in the region during autumn and spring) was performed and the observed variation was $< 0.3 \%$ for CO_2 and N_2O , and $< 0.04 \%$ for CH_4 .

4.3.3 Results

4.3.3.1 Basic environmental parameters

During spring, the pH of the different sample classes varied between 8.33 ± 0.30 , with Jhelum upstream, Lidder and Sind showing relatively higher mean pH (Fig 4.23a). The water temperature was lowest in Sind ($5.3 \pm 2.7 \text{ }^\circ\text{C}$) compared to other major tributaries ($9.5 \pm 3.9 \text{ }^\circ\text{C}$), the mainstem ($11.7 \pm 2.8 \text{ }^\circ\text{C}$), and Wular Lake ($13.4 \pm 2.5 \text{ }^\circ\text{C}$) (Fig 4.23b). The electrical conductivity was in the range of $230 \pm 92 \text{ } \mu\text{S cm}^{-1}$ with relatively lower mean values in the Lidder and Vishav (Fig 4.23c).

Due to absence of basic water quality parameters for the autumn season, available literature was referred to establish a background. Rather et al. (2016) conducted seasonal sampling along the mainstem of the Jhelum River and tracked the seasonality in basic parameters like pH, temperature, conductivity, and DIN among several others. Water temperature was high in summer (mean $\sim 18 \text{ }^\circ\text{C}$) and low in winter (mean $\sim 7 \text{ }^\circ\text{C}$) with spring and autumn showing similar range ($11 - 14 \text{ }^\circ\text{C}$) (Rather et al., 2016). Similar to temperature, dissolved oxygen also showed similar range during spring and autumn ($\sim 7 - 10 \text{ mg L}^{-1}$) (Rather et al., 2016). Nitrate was the dominant form of DIN with higher ammonical nitrogen during autumn as compared to spring and the reverse seasonality for nitrate nitrogen (Rather et al., 2016).

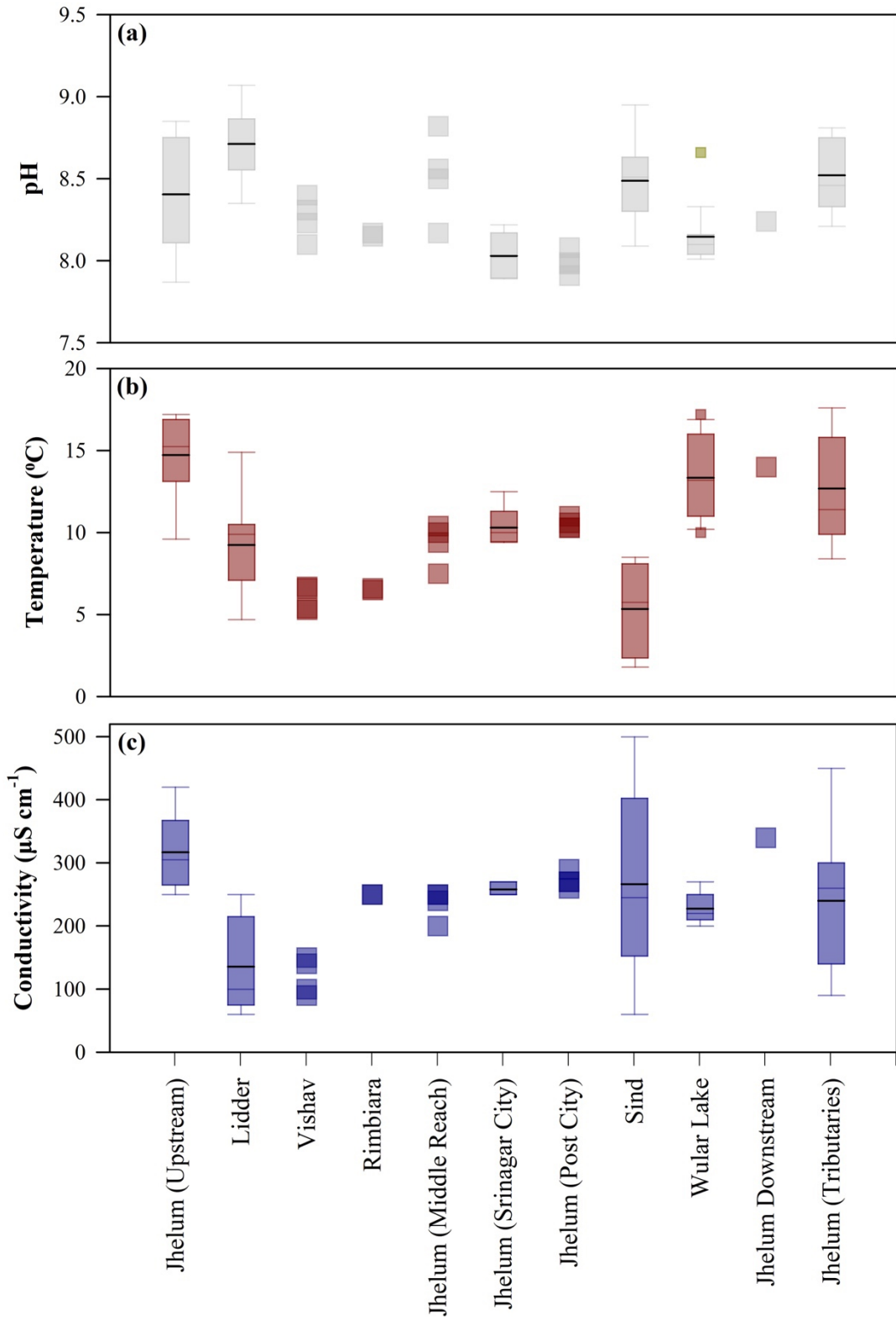


Fig. 4.23 (a) pH, (b) temperature, and (c) conductivity in the different stretches of the Jhelum River system and the Wular Lake during spring.

4.3.3.2 Dissolved inorganic carbon

Except for the Wular, in general, average DIC concentrations were relatively higher during spring compared to autumn (Fig 4.24a). The Jhelum upstream showed relatively higher DIC (spring = 2.13 ± 0.73 mM; autumn = 1.38 ± 0.58 mM) compared to the middle reaches (spring = 1.16 ± 0.20 mM; autumn = 0.59 ± 0.18 mM), reach within city limits (spring = 1.23 ± 0.08 mM; autumn = 1.00 ± 0.06 mM), post city (spring = 1.39 ± 0.08 mM; autumn = 1.01 ± 0.08 mM), and the downstream site (spring = 1.95 mM; autumn = 0.87 mM).

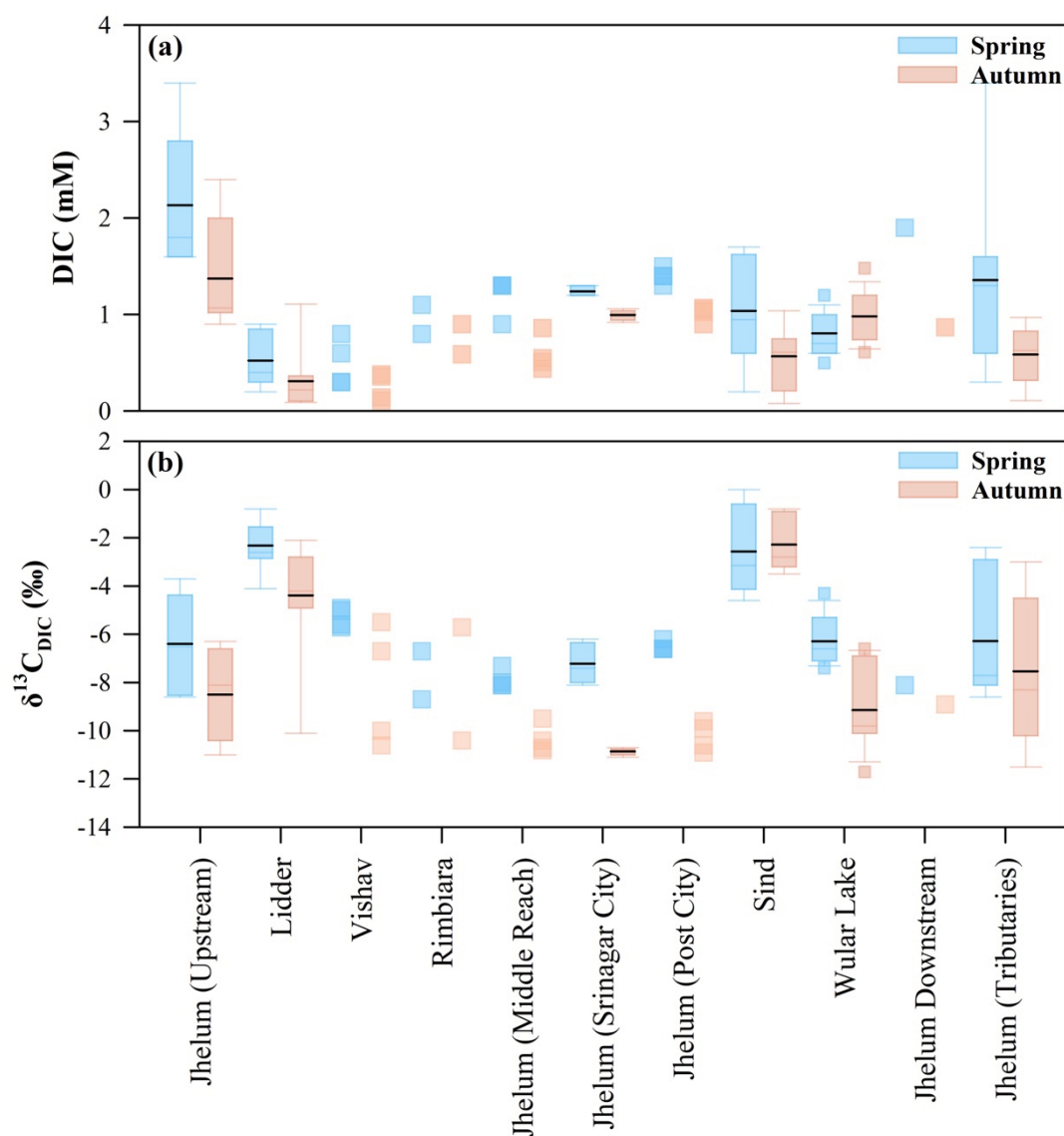


Fig. 4.24 (a) Dissolved inorganic carbon concentrations (mM) and (b) stable isotopic composition of DIC in the different stretches of the Jhelum River system and Wular Lake.

Among the tributaries of the Jhelum, Lidder (spring = 0.53 ± 0.29 mM; autumn = 0.31 ± 0.32 mM) and Vishav (spring = 0.49 ± 0.22 mM; autumn = 0.25 ± 0.14 mM) showed lower DIC concentrations compared to Sind (spring = 1.05 ± 0.54 mM; autumn = 0.56 ± 0.33 mM) and other minor tributaries (spring = 1.35 ± 1.01 mM; autumn = 0.59 ± 0.31 mM). The Wular lake behaved differently from the lentic systems with relatively lower DIC during spring (0.79 ± 0.20 mM) compared to autumn (0.98 ± 0.24 mM) (Fig 4.24a).

The $\delta^{13}\text{C}_{\text{DIC}}$ showed distinct seasonality in all sample classes (except Sind) with higher values during spring compared to autumn (Fig 4.24b). Furthermore, Lidder (spring = -2.3 ± 1.0 ‰; autumn = -4.4 ± 2.4 ‰) and Sind (spring = -2.6 ± 1.8 ‰; autumn = -2.3 ± 1.1 ‰) showed higher $\delta^{13}\text{C}_{\text{DIC}}$ compared to Jhelum upstream (spring = -6.4 ± 2.0 ‰; autumn = -8.5 ± 1.8 ‰), Vishav (spring = -5.3 ± 0.4 ‰; autumn = -8.2 ± 2.5 ‰), Rimbiara (spring = -7.7 ± 1.4 ‰; autumn = -8.0 ± 3.3 ‰), Jhelum middle reaches (spring = -7.9 ± 0.4 ‰; autumn = -10.4 ± 0.6 ‰), Jhelum within city limits (spring = -7.2 ± 0.8 ‰; autumn = -10.9 ± 0.1 ‰), Jhelum post city (spring = -6.5 ± 0.2 ‰; autumn = -10.2 ± 0.6 ‰), Jhelum tributaries (spring = -6.3 ± 2.6 ‰; autumn = -7.5 ± 3.2 ‰), and Jhelum downstream (spring = -8.1 ‰; autumn = -8.9 ‰). Similar to the streams, the Wular Lake also showed significant decrease in $\delta^{13}\text{C}_{\text{DIC}}$ from spring (-6.3 ± 1.0 ‰) to autumn (-9.1 ± 1.7 ‰).

4.3.3.3 Particulate organic carbon and its isotopic composition

The POC pool showed spatial variability among the tributaries and mainstem of the Jhelum River with higher concentration in the latter (Fig 4.25a). During the spring, there were erratic rain events which reflected in very high POC in the Vishav (spring = 397.44 ± 284.72 μM ; autumn = 41.75 ± 24.43 μM) and Rimbiara (spring = 560.74 ± 277.46 μM ; autumn = 57.42 ± 19.27 μM) rivers, which was also visible in the high suspended load. The POC concentration was high in the Jhelum upstream (spring = 99.57 ± 75.32 μM ; autumn = 113.64 ± 132.80 μM), Jhelum middle reaches (spring = 127.94 ± 89.07 μM ; autumn = 168.24 ± 75.78 μM), Jhelum within city limits (spring = 249.44 ± 93.38 μM ; autumn = 80.64 ± 7.45 μM), Jhelum post city (spring = 196.63 ± 22.11 μM ; autumn = 90.04 ± 55.75 μM), and Jhelum downstream (spring = 236.89 μM ; autumn = 49.74 μM). Lidder (spring = 27.83 ± 13.88 μM ; autumn = 35.66 ± 42.60 μM) and Sind (spring = 35.77 ± 16.57 μM ; autumn = 29.86 ± 14.05 μM) showed low concentration of POC during both spring and autumn compared to minor tributaries (spring = 79.07 ± 52.33 μM ; autumn = 53.04 ± 22.45 μM). The Wular had relatively

higher average POC concentration during spring ($133.68 \pm 94.82 \mu\text{M}$) as compared to autumn ($104.60 \pm 39.92 \mu\text{M}$).

The $\delta^{13}\text{C}_{\text{POC}}$ did not show significant seasonal or spatial variation across the Jhelum River and its tributaries ($-24.6 \pm 0.9 \text{‰}$; Fig 4.24b). However, $\delta^{13}\text{C}_{\text{POC}}$ was relatively low in the Wular (spring = $-26.1 \pm 1.7 \text{‰}$; autumn = $-25.7 \pm 1.2 \text{‰}$) compared to rivers, which also affected the Jhelum downstream site (spring = -25.2‰ ; autumn = -26.3‰).

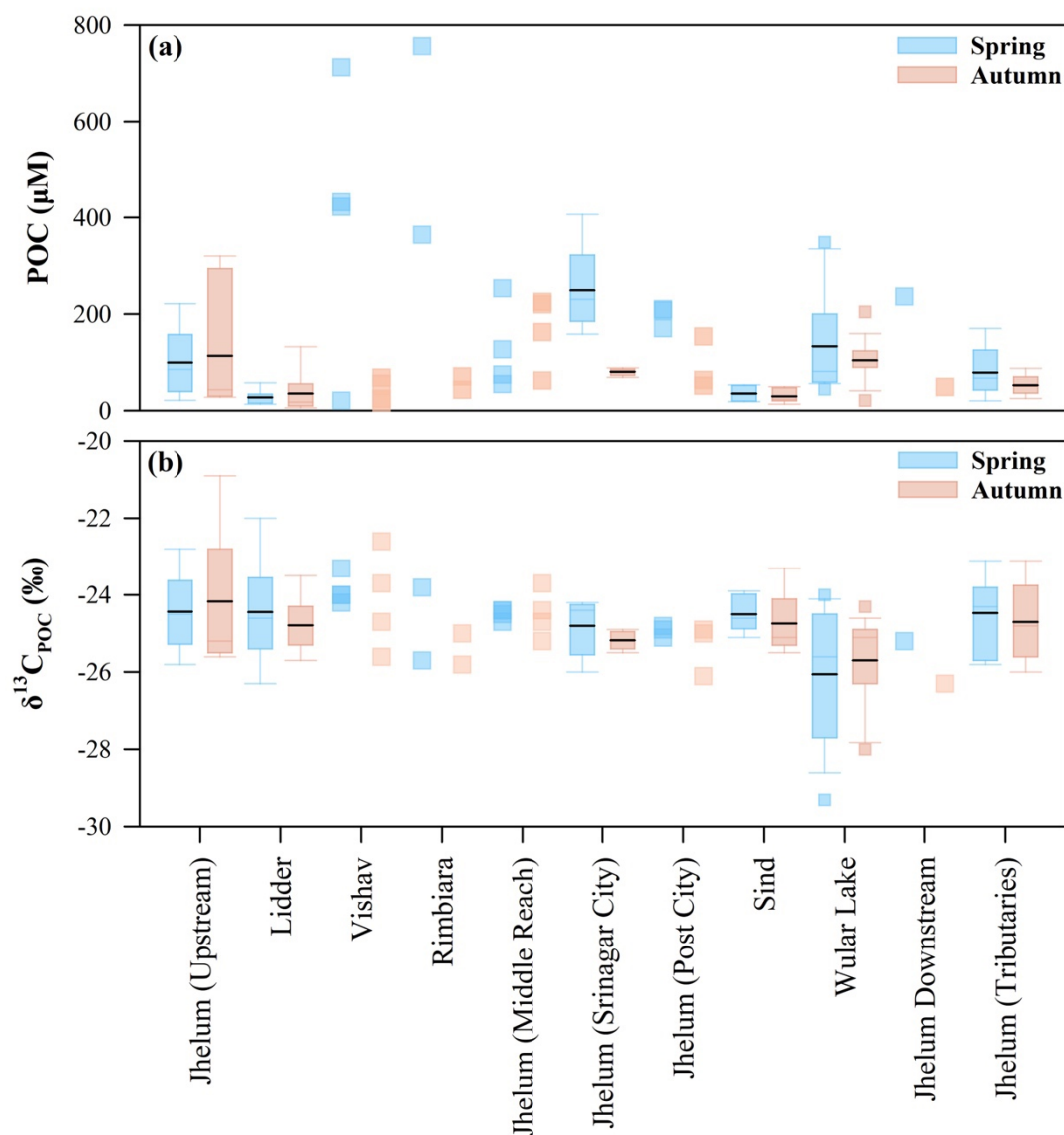


Fig. 4.25 (a) Concentration (μM) and (b) isotopic composition of particulate organic carbon along the mainstem and tributaries of the Jhelum and the Wular Lake.

4.3.3.4 Particulate nitrogen and its isotopic composition

Similar to POC, PN showed higher concentrations in the Vishav (spring = 41.58 ± 27.80 μM ; autumn = 4.29 ± 2.42 μM), Rimbiara (spring = 49.56 ± 24.35 μM ; autumn = 5.22 ± 2.58 μM), and the Jhelum within city limits (spring = 32.23 ± 20.63 μM ; autumn = 10.01 ± 0.93 μM) (Fig 4.26a). Sind (spring = 2.89 ± 1.32 μM ; autumn = 2.60 ± 1.17 μM) and Lidder (spring = 3.27 ± 1.77 μM ; autumn = 3.71 ± 4.70 μM) showed the lowest PN concentrations. In the Wular Lake, PN was higher in spring (13.57 ± 8.05 μM) compared to autumn (6.54 ± 2.04 μM).

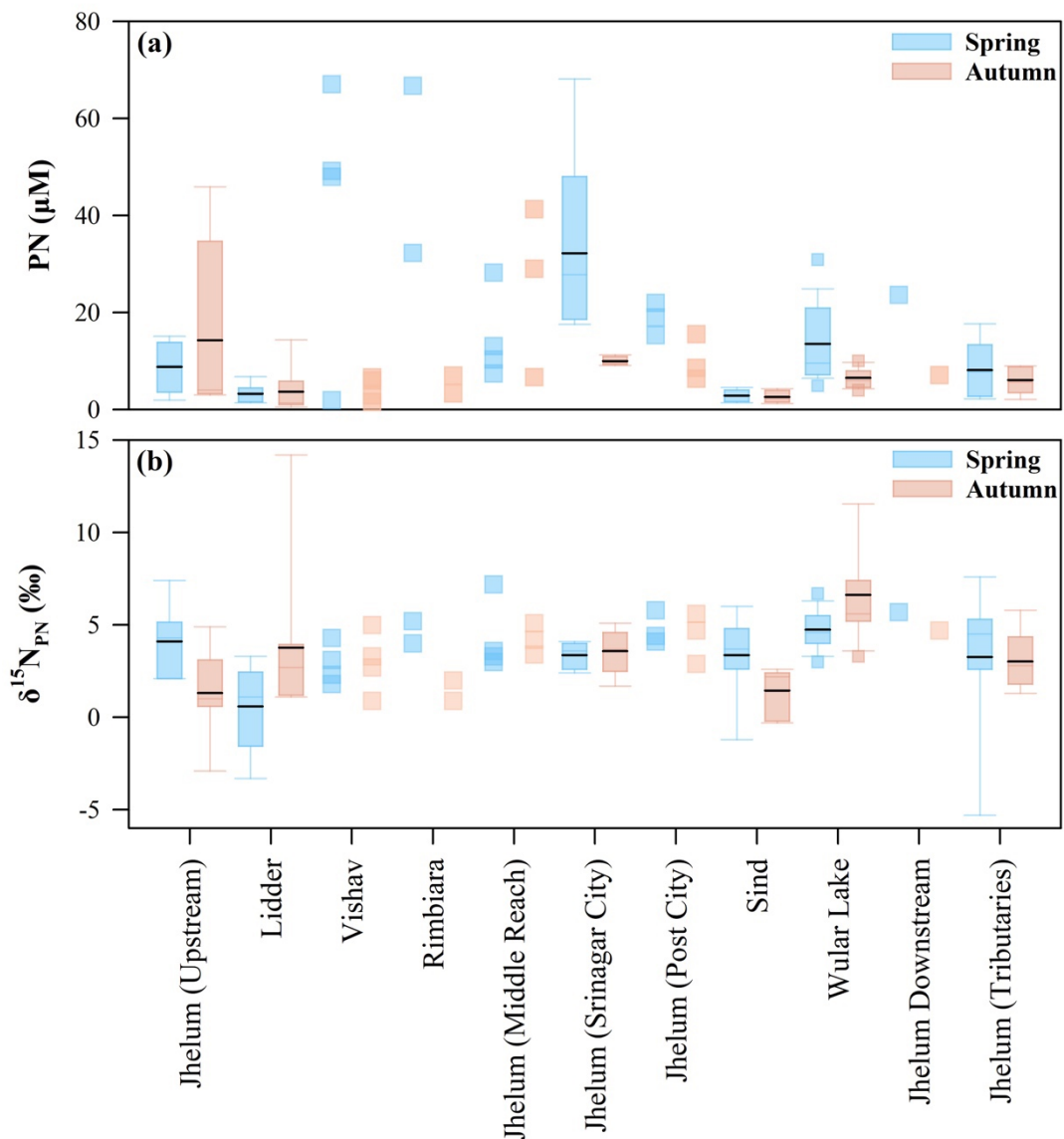


Fig. 4.26 (a) Concentration (μM) and (b) isotopic composition of particulate nitrogen along the mainstem and tributaries of Jhelum and the Wular Lake.

The $\delta^{15}\text{N}_{\text{PN}}$ did not show any consistent seasonality across different reaches of the Jhelum. The lowest values were observed in the Lidder during the spring ($0.6 \pm 2.4 \text{ ‰}$; Fig 4.26b). Overall the $\delta^{15}\text{N}_{\text{PN}}$ ranged between $2.5 \pm 1.3 \text{ ‰}$ along the Jhelum mainstem and its various tributaries. In the Wular Lake, $\delta^{15}\text{N}_{\text{PN}}$ was lower in spring ($4.7 \pm 1.0 \text{ ‰}$) compared to autumn ($6.6 \pm 2.9 \text{ ‰}$).

4.3.3.5 Dissolved CH_4 , CO_2 , and N_2O

CH_4 concentrations varied spatially as well as seasonally along the Jhelum – Wular continuum, with lower concentrations during the spring (Fig 4.27a). Extremely low concentrations were observed in the Lidder (spring = $13.61 \pm 2.44 \text{ nM}$; autumn = $12.79 \pm 8.92 \text{ nM}$), Vishav (spring = $56.04 \pm 37.22 \text{ nM}$; autumn = $169.47 \pm 176.86 \text{ nM}$), Rimbiara (spring = $100.44 \pm 118.64 \text{ nM}$; autumn = $234.35 \pm 304.07 \text{ nM}$) and Sind (spring = $22.34 \pm 20.13 \text{ nM}$; autumn = $37.58 \pm 31.53 \text{ nM}$) with several locations having CH_4 below the detection limit. CH_4 concentrations were high in the Jhelum upstream (spring = $205.63 \pm 286.01 \text{ nM}$; autumn = $492.09 \pm 642.66 \text{ nM}$) and increased further in the middle reaches (spring = $431.82 \pm 173.98 \text{ nM}$; autumn = $754.21 \pm 291.03 \text{ nM}$) and Jhelum within city limits (spring = $492.64 \pm 203.04 \text{ nM}$; autumn = $1357.57 \pm 270.71 \text{ nM}$). CH_4 concentrations in the Jhelum decreased post city limits during autumn (spring = $551.11 \pm 72.30 \text{ nM}$; autumn = $945.28 \pm 213.13 \text{ nM}$) probably due to inflow of water from Sind. In the Wular Lake, average CH_4 was relatively higher in the autumn ($509.48 \pm 207.86 \text{ nM}$) compared to spring ($376.61 \pm 150.59 \text{ nM}$) as compared to autumn. The Jhelum downstream (spring = 320.66 nM ; autumn = 589.44 nM) had similar CH_4 concentrations as the Wular Lake. CO_2 concentrations showed significant decrease from spring to autumn at all sampling locations (Fig 4.27b). In the Jhelum upstream, CO_2 was high during spring ($1106.32 \pm 352.74 \text{ } \mu\text{M}$) compared to autumn ($604.54 \pm 82.77 \text{ } \mu\text{M}$). The CO_2 concentrations remained high in the mainstem of Jhelum in the middle reaches (spring = $1242.56 \pm 112.22 \text{ } \mu\text{M}$; autumn = $439.60 \pm 66.76 \text{ } \mu\text{M}$), even though CO_2 in Lidder (spring = $440.07 \pm 130.03 \text{ } \mu\text{M}$; autumn = $264.48 \pm 206.55 \text{ } \mu\text{M}$), Vishav (spring = $631.03 \pm 265.07 \text{ } \mu\text{M}$; autumn = $202.66 \pm 133.21 \text{ } \mu\text{M}$) and Rimbiara (spring = $915.82 \pm 368.14 \text{ } \mu\text{M}$; autumn = $494.04 \pm 205.30 \text{ } \mu\text{M}$) were relatively lower. The CO_2 concentrations at Jhelum within city limits (spring = $1147.11 \pm 152.94 \text{ } \mu\text{M}$; autumn = $511.14 \pm 29.62 \text{ } \mu\text{M}$) and post city (spring = $1282.87 \pm 77.45 \text{ } \mu\text{M}$; autumn = $473.30 \pm 46.81 \text{ } \mu\text{M}$) were in the similar range. The Wular Lake witnessed large seasonal

variation in CO₂ concentration (spring = 1335.01 ± 141.19 μM; autumn = 435.98 ± 122.09 μM).

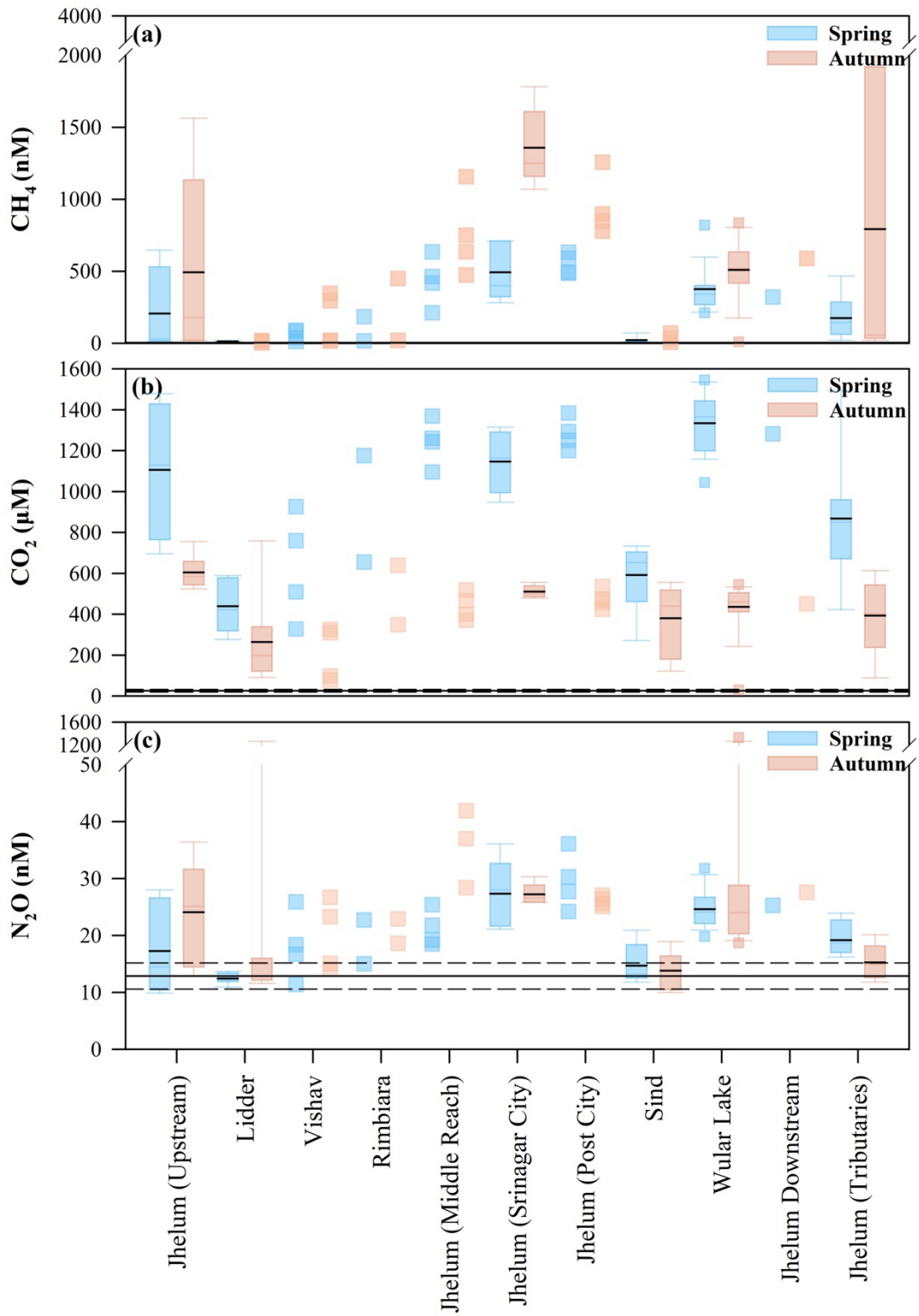


Fig. 4.27 (a) CH₄, (b) CO₂, and (c) N₂O concentrations along the mainstem and tributaries of Jhelum river and the Wular Lake.

The N_2O did not show significant seasonal variation across the studied reaches (Fig 4.27c). However, it was observed that there is a spatial variability in N_2O concentrations with higher values along the mainstem of the Jhelum River compared to the tributaries. Two locations had very high N_2O concentrations during autumn in Lidder (346.30 nM) and the Wular lake (1334.58 nM) respectively. Excluding these high values, N_2O concentrations along the Jhelum mainstem was $\sim 25.79 \pm 8.55$ nM, tributaries $\sim 15.70 \pm 4.14$ nM, and Wular lake $\sim 25.26 \pm 7.22$ nM.

4.3.4 Discussion

4.3.4.1 Dissolved inorganic carbon biogeochemistry in the Jhelum River

Dissolved inorganic carbon in the Jhelum River showed distinct seasonal variation with higher DIC during spring as compared to autumn (Fig 4.24a). This increase in DIC during spring is attributed to influx of weathered C and contribution from soil CO_2 during the melt season. Higher DIC in the upstream reaches of the Jhelum mainstem along with some tributaries indicates enhanced carbonate weathering by lower order streams. Lidder and Sind, which are two major tributaries of the Jhelum and are fed by melting snow, show low DIC concentrations but high $\delta^{13}C_{DIC}$. High $\delta^{13}C_{DIC}$ is a signature of carbonate weathering which might be prevalent in the Lidder and Sind catchments. The DIC concentrations in the middle reaches of Jhelum mainstem along with the stretch within city limits and post city show low $\delta^{13}C_{DIC}$ which is indicative of contribution from remineralisation of OM which is a possibility in higher order streams due to both increased productivity (and availability of OM as substrate) and allochthonous inputs of DIC through wastewater and storm water drains. DIC decreased from spring to autumn along the continuum of the Jhelum river. This decrease in DIC concentration along with subsequent reduction in $\delta^{13}C_{DIC}$ indicates initial uptake of DIC in the system during the productive summer followed by mineralisation during autumn. A significant –ve correlation between DIC and $\delta^{13}C_{DIC}$ ($p < 0.05$; Fig 4.28, 4.29, and 4.30) was observed, which supports the above inference. In the Wular Lake, an increase in DIC concentration from spring to autumn with a decrease in $\delta^{13}C_{DIC}$ indicated mineralisation of OM as the dominant source of DIC (Alling et al., 2012). Overall, the DIC dynamics in the Jhelum – Wular continuum was governed by allochthonous inputs of higher $\delta^{13}C_{DIC}$ during spring and the coupling of primary productivity and decomposition during autumn.

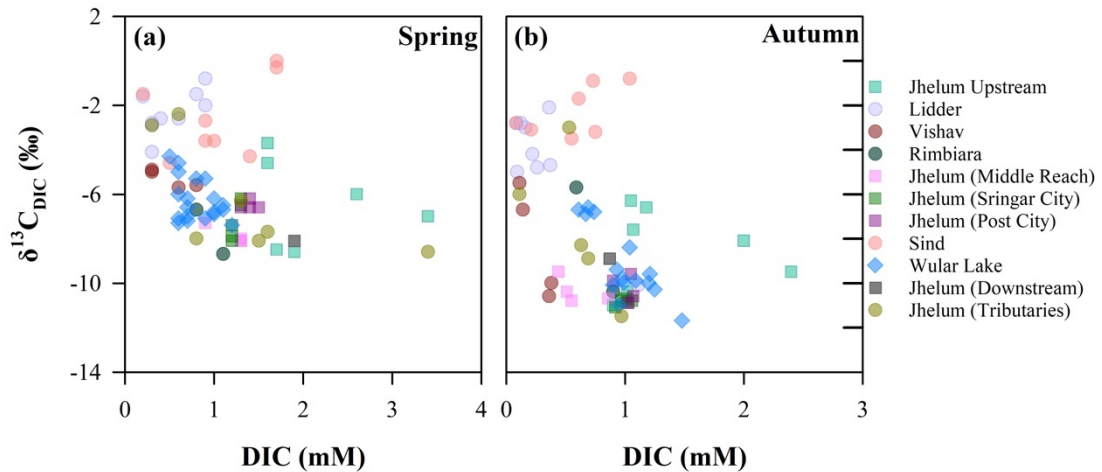


Fig. 4.28 Relationships between DIC and $\delta^{13}\text{C}_{\text{DIC}}$ in (a) spring and (b) autumn.

4.3.4.2 Particulate matter dynamics along the river – lake continuum

Low POC and PN in the Lidder and Sind is attributed to high water velocity and low water temperatures, which negatively affects primary productivity (Beusen et al., 2005). Furthermore, both Lidder and Sind receive meltwater contribution which are low in OM. Few sites in the Vishav and Rimbiara showed very high POC and PN concentrations, which was due to stormflow during rain events in the spring as discussed earlier. Stormflow mobilises soil organic matter and flushes surface litter, contributing to the riverine POM. Increase in biomass was observed as the river entered the city limits, probably due to increasing primary productivity in the higher order rivers, as hypothesised in the river continuum concept (Vannote et al., 1980). Also, inputs of DIN in urban settings could enhance the productivity of the river system. No clear shift in $\delta^{13}\text{C}_{\text{POC}}$ across seasons and sampling locations (except for the Wular lake) was seen. In the Wular Lake, the $\delta^{13}\text{C}_{\text{POC}}$ was relatively lower than the rivers during both spring and autumn, indicating contribution from *in situ* production. In the autumn, high C/N ratio in the Wular Lake and a significant +ve relationship ($p < 0.05$) between POC and C/N ratio indicated enhanced primary productivity (Fig 4.30), whereas in spring a significant +ve relationship ($p < 0.05$) between POC and $\delta^{13}\text{C}_{\text{POC}}$ (Fig 4.30 & 4.32) suggested increased contribution of allochthonous OM. No significant correlation was observed between PN and $\delta^{15}\text{N}_{\text{PN}}$ (Fig 4.29, 4.30 & 4.33) indicating a very dynamic processing of PN and a complex N biogeochemistry. A -ve correlation between C/N ratio and $\delta^{15}\text{N}_{\text{PN}}$ ($p < 0.05$; Fig 4.29) along with low $\delta^{15}\text{N}_{\text{PN}}$, particularly in tributaries implies potential N_2 fixation, however, this needs to be verified through qualification of N_2 fixation rates.

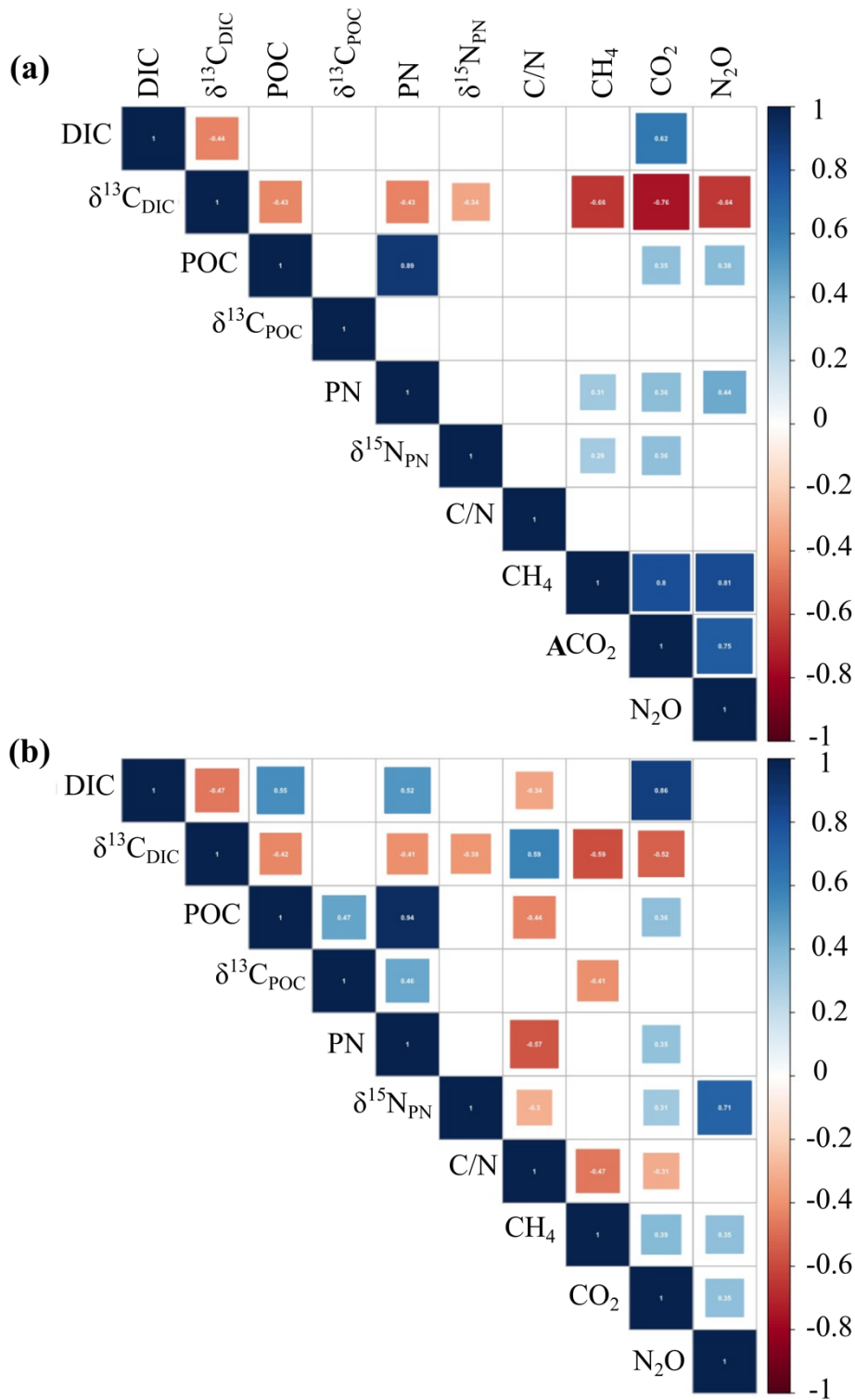


Fig. 4.29 Correlation plots (Spearman; $p < 0.05$) between measured parameters along the Jhelum mainstem and tributaries during (a) spring and (b) autumn.

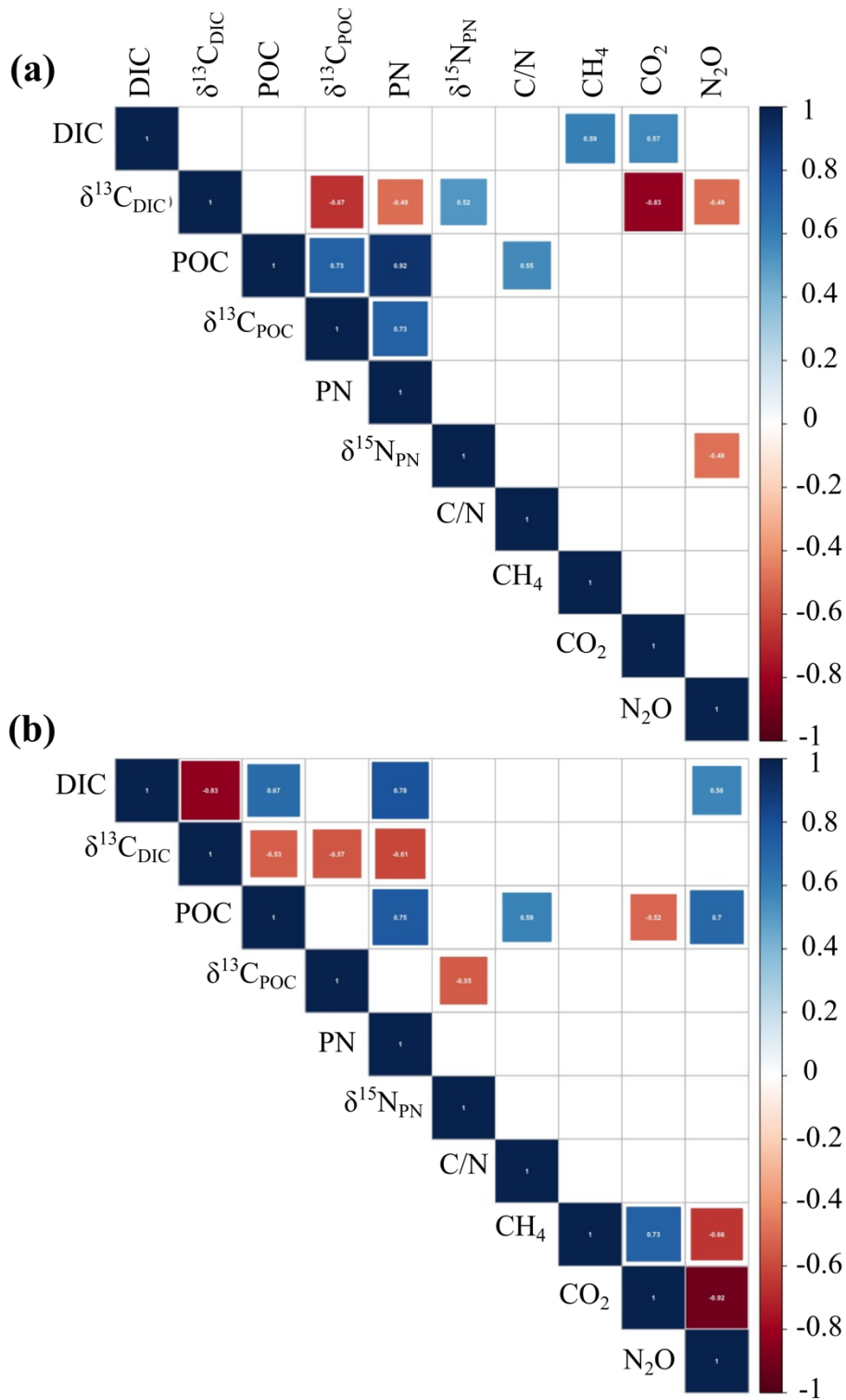


Fig. 4.30 Correlation plots (Spearman; $p < 0.05$) between measured parameters in the Wular lake during (a) spring and (b) autumn.

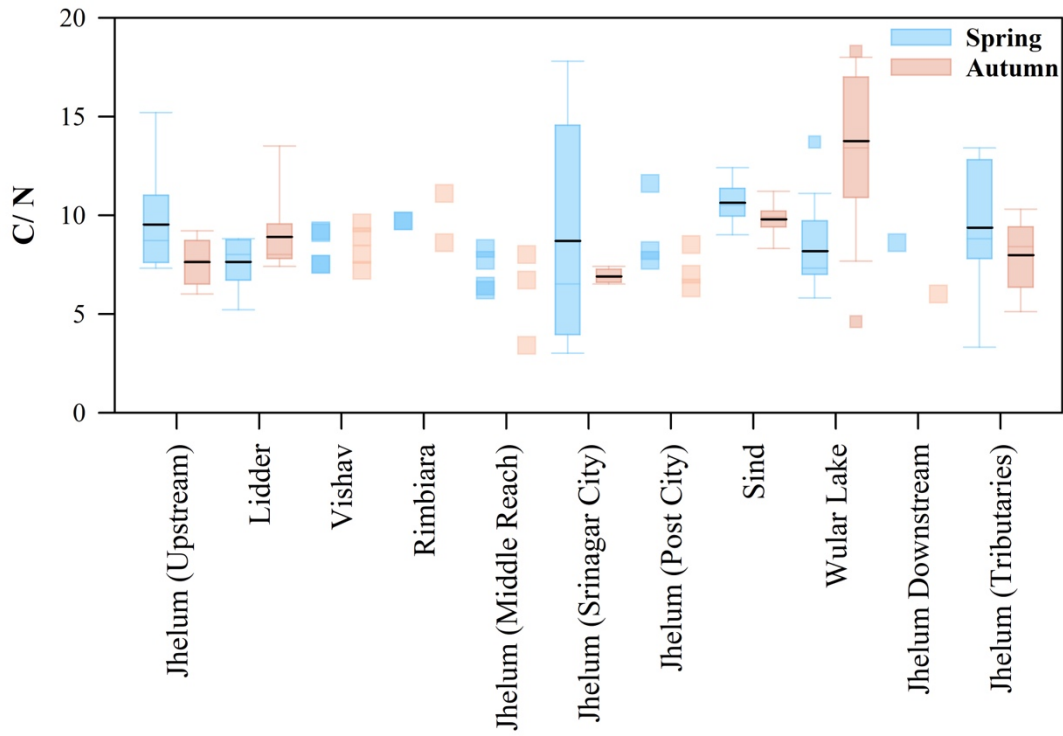


Fig. 4.31 C/N ratios of particulate matter in different sample classes.

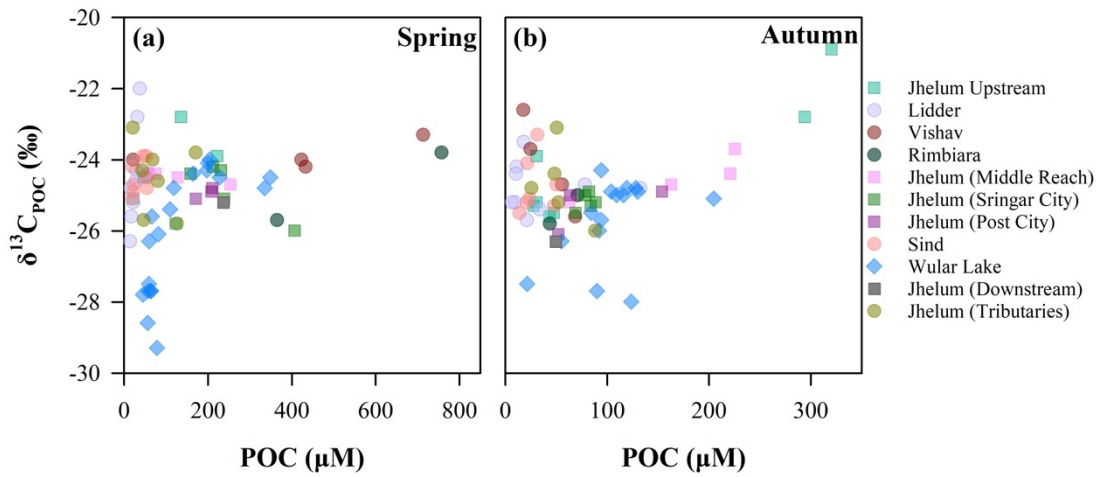


Fig. 4.32 Scatter plot showing relationship between particulate organic carbon and its isotopic composition during (a) spring and (b) autumn.

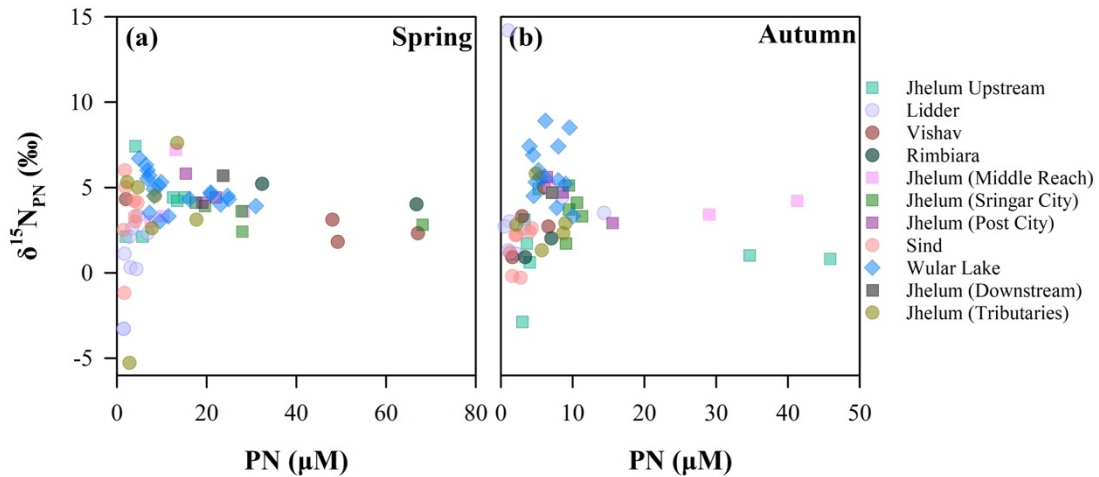


Fig. 4.33 Scatter plot showing relationship between particulate nitrogen and its isotopic composition during (a) spring and (b) autumn.

4.3.4.3 Dissolved CH_4 , CO_2 , and N_2O

Dissolved CH_4 dynamics in the Jhelum River was governed by the availability of OM as substrate for methanogenesis. Extremely low concentrations of CH_4 in the Lidder and Sind, which were also low in POC and PN (Fig 4.25a, 4.26a, and 4.27a) supports the above statement. Increasing CH_4 in the middle reaches of Jhelum and within city limits indicated the direct effect of anthropogenic inputs of wastewater and organic contaminants on the CH_4 cycling. Along with CH_4 , CO_2 also showed strong seasonality with higher concentration during spring and lower during autumn, indicating a shift from heterotrophy to autotrophy (Fig 4.27b). Relatively lower concentration of CO_2 in the Sind and Lidder during spring indicates dominance of meltwater inputs, which are relatively lower in DIC as well, and therefore CO_2 . Interestingly, in the Wular, CH_4 and CO_2 were positively correlated with each other during autumn but negatively correlated to N_2O (Fig 4.30b). It was earlier argued that primary productivity was enhanced during autumn which would lead to higher availability of OM for degradation as well as to act as substrate for methanogenesis leading to correlation of CH_4 and CO_2 . It has been observed that higher OM in stratified lakes can inhibit the process of nitrifier denitrification leading to low N_2O production (Webb et al., 2019), which could be the case with Wular as well. A significant positive relationship between CH_4 , CO_2 , and N_2O in the Jhelum and its tributaries (Fig 4.29) imply that the environmental conditions and availability of OM and nutrients controlled the processes like mineralisation, methanogenesis, nitrification and denitrification as expected. In terms of fluxes of GHGs from the Jhelum – Wular continuum, all sample locations except few pristine sites appeared to be potential source of GHGs as ambient dissolved concentrations were

higher than the equilibrium concentrations (Fig 4.27). However, exact quantification using well constrained gas transfer velocity needs to be performed.

4.3.5 Conclusion

The present study attempted to understand the flow of C and N along the high altitude Jhelum River and its tributaries; specifically, tracking the transformations at the interface of the Jhelum River and the Wular lake. It was observed that DIC was high in the upstream reach of the Jhelum River and DIC with high isotopic composition was observed in the major tributaries (Lidder and Sind) indicating weathering of carbonate rocks during spring (i.e. the melt season). Biomass was least in these two rivers (Lidder and Sind) as they were dominantly fed by melting snow and the river was turbulent in these reaches. It was observed that as the Jhelum river entered city limits or the Wular Lake, *in situ* production appeared to be enhanced, which was reflected on the isotopic composition of POM (i.e. low $\delta^{13}\text{C}_{\text{POC}}$). The availability of biomass as substrate along with environmental factors controlled the greenhouse gas dynamics in the Jhelum – Wular continuum. Higher CH_4 concentrations was observed in productive waters along with higher CO_2 , the latter decreasing during autumn due to transition of the system from heterotrophy to autotrophy.

Chapter 5

Particulate black carbon cycling in aquatic systems

Black carbon is derived from incomplete combustion of OM and forms a whole spectrum from labile char to highly recalcitrant soot with the increasing temperature of formation (Goldberg, 1985). In the environment, BC is produced mainly from biomass burning and fossil fuel combustion, the latter being an important contributor of soot which increases the residence time of the BC pool (Elmquist et al., 2006; Ascough et al., 2011; Bird et al., 2015). Globally, biomass burning and fossil fuel combustion contributes to 128 ± 84 and $5 - 13$ Tg year⁻¹ of PBC to the environment, respectively (Bond et al., 2013; Jones et al., 2020). A major chunk of the BC produced via biomass burning is deposited in close proximity and incorporated into the soil matrix which then acts as a potent sink for C. Alternatively, soil BC can get mobilised into aquatic systems via erosion and surface runoff (Forbes et al., 2006; Liang et al., 2008; Saiz et al., 2014). It is observed that majority of BC mobilised from fire affected soils are in the particulate form (Boot et al., 2014; Wagner et al., 2015) and $17 - 37$ Tg year⁻¹ of PBC is transported by the rivers to the ocean (Moody and Martin, 2001; Leori et al., 2014; Wagner et al., 2015; Santin et al., 2016; Pyle et al., 2017; Coppola et al., 2018). Additionally, aerosol BC deposition (wet and dry) to the global ocean is estimated at 12 Tg year⁻¹ (Jurado et al., 2008). PBC in rivers forms $\sim 12 \pm 5$ % of the POC and adds a refractory component to the otherwise labile organic pool (Coppola et al., 2018; Huang et al., 2021; Li et al., 2021; Meng et al., 2023).

The recalcitrant nature of BC enables it to sequester C in long timescales and therefore recognising it as a potential climate mitigator (Bird et al., 2015; Coppola and Druffel, 2016; Coppola et al., 2022). Research on BC in aquatic systems is limited across the globe with handful of studies focussing on its dissolved fraction (Wagner et al., 2015; Qi et al., 2020). The particulate fraction remains poorly explored, especially in the inland waters (Fig. 5.1a). With more studies exploring the degradation of BC in the environment (Bistarelli et al., 2021; Zimmerman et al., 2012), it becomes imperative to understand the cycling of BC in aquatic systems which are the active conduits of BC along the land-ocean continuum. Bowring et al. (2022) highlighted the challenges of constraining the impact of fire derived C offsets on the terrestrial C balance due to lack of understanding of the mineralisation of BC in aquatic systems and availability of robust numbers for mineralisation rates.

5.1 Transport and transformation of particulate black carbon in rivers

In riverine systems, the transport and transformation of BC is controlled by the residence time which is indirectly governed by the flow regime of the river system. With rapid urbanisation and engineered modifications of river channels, there is a drastic shift in the various in-stream biogeochemical processes (Begum et al., 2021). The effect of modulations of river channels on the BC cycling is still unknown. To address the research gaps in the field of BC cycling in aquatic systems, this part of the thesis aims to understand the movement and transformations (if any) of PBC along the river continuum. The hypothesis conceived for this purpose are (i) PBC in rivers ages along the continuum and this transformation is embedded in its stable isotopic composition and (ii) engineered modification of river channels would affect the PBC biogeochemistry. Due to scarcity of well constrained flux estimates from across the globe, an attempt to generate the first estimates of PBC export flux to the Arabian Sea has also been made.

5.1.1 Sampling

To address the above objectives, sampling was conducted across the continuum of six river basins and a lined canal in the western India. As discussed in Chapter 2, particulate matter samples collected from Sabarmati, Mahi, and Narmada Canal during October 2020 and February 2021 to capture the high flow and low flow conditions were also analyzed for PBC and its isotopic composition. These samples in the Sabarmati river fell in distinct classes based on the level of engineered modification (Pristine upstream, stagnant riverfront, polluted downstream, and tributaries; Fig 4.6 and 4.7). Additional sampling for particulate matter to investigate PBC in Banas, Berach, Ambika, and Girna rivers was also conducted during November 2021 and August 2022 (Post monsoon and monsoon seasons – both representing high flow) (Fig 5.1).

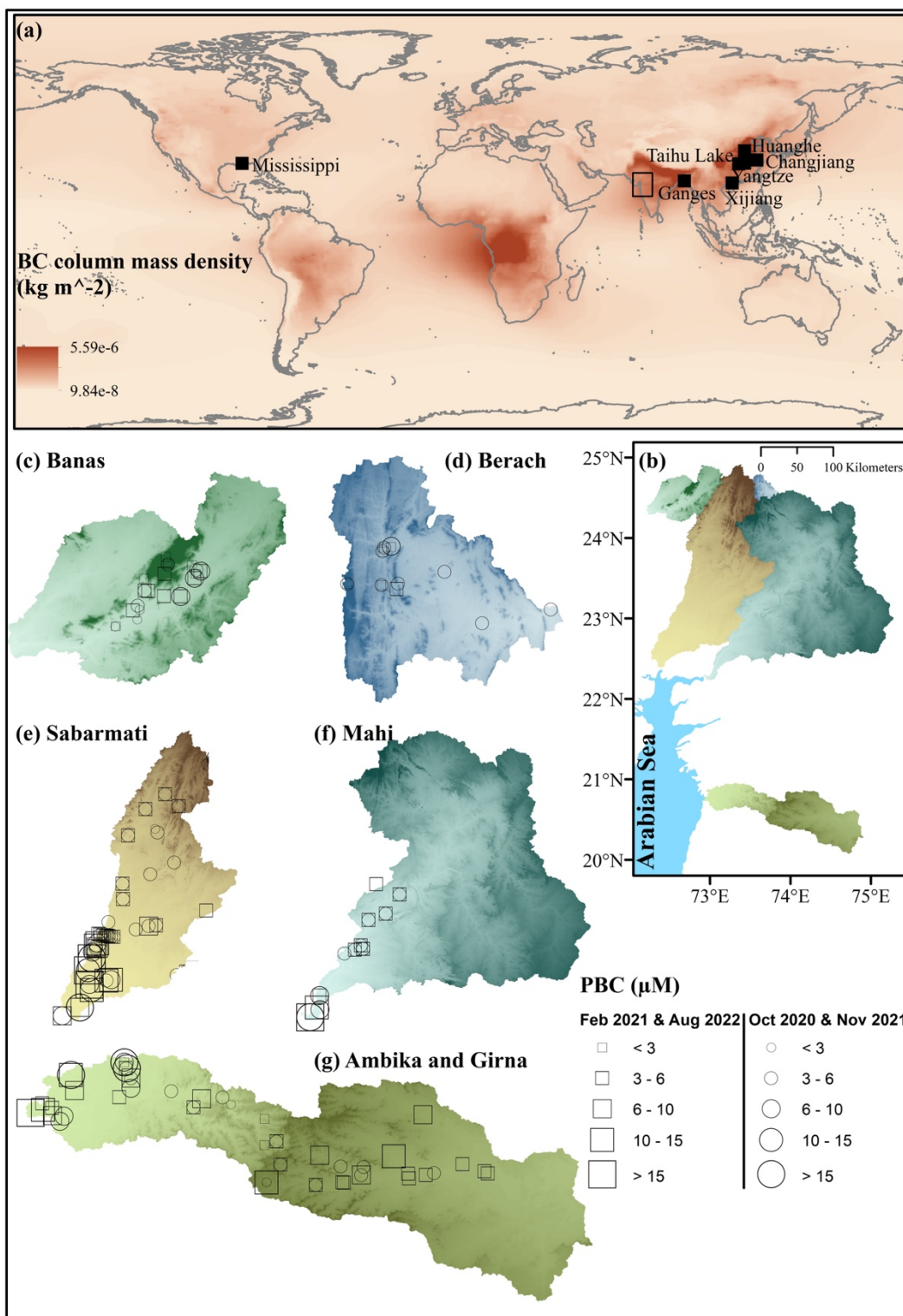


Fig. 5.1 (a) Existing studies on particulate black carbon in riverine particulate matter, (b) the present study area representing the river basins, (c – g) locations of samples analyzed for particulate black carbon in the six river basins.

5.1.2 Results and Discussion

Below we discuss the patterns of transport and evidence of modulations of PBC along the river continuum.

5.1.2.1 Distribution of particulate black carbon in the river basins

PBC concentration ranged between 0.70 to 56.90 μM with the highest concentrations observed at the downstream sites of river basins (Fig 5.1c – g). Among the studied systems, the downstream reach of Sabarmati exhibited the highest median PBC concentrations (ANOVA, $p < 0.001$) during both low flow ($31.57 \pm 20.41 \mu\text{M}$) and high flow periods ($12.19 \pm 1.23 \mu\text{M}$; Fig 5.2a – d). Almost 86 % of the samples across the six river basins showed PBC concentrations below 10 μM which is low compared to PBC in rivers elsewhere [143 μM in Xijiang River (Liu and Han, 2021); 0.65 – 49.30 in Yangtze River (Meng et al., 2023)].

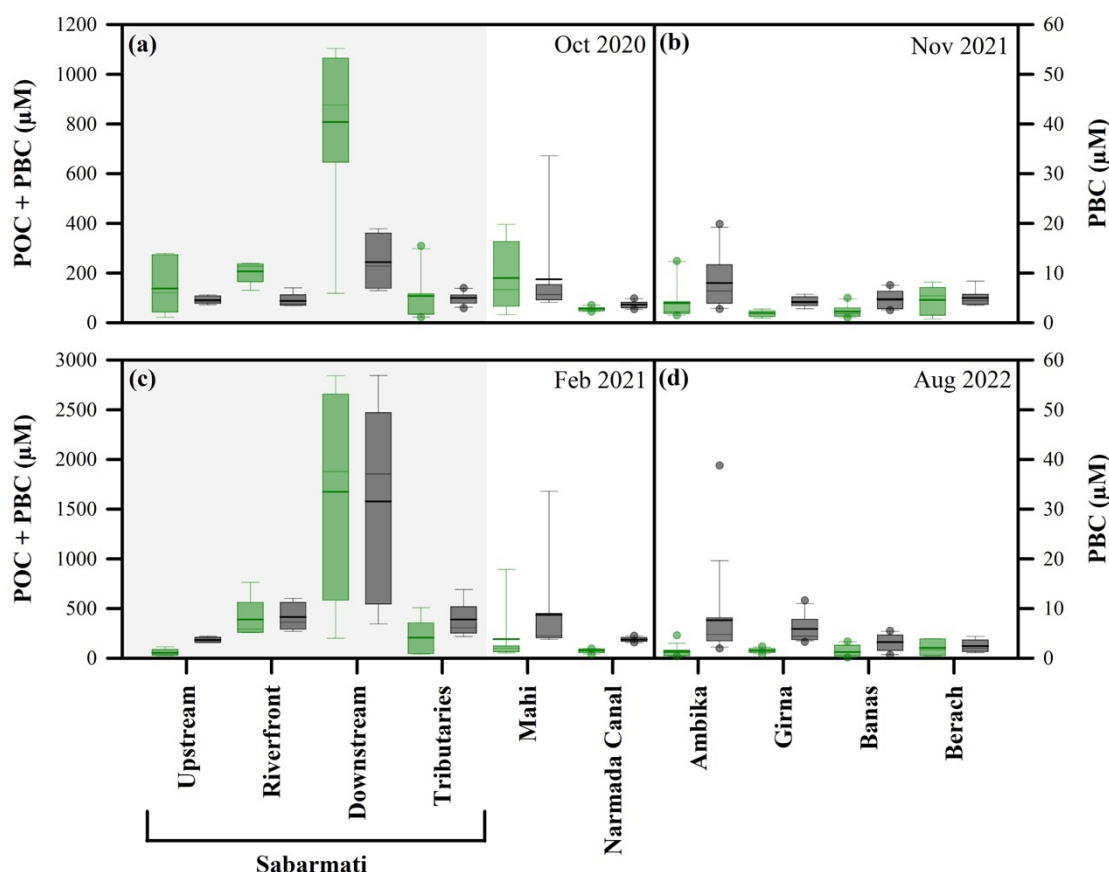


Fig. 5.2 Bulk particulate organic carbon (POC + PBC; Green boxes –left axis) and PBC (Black boxes – right axis) in Sabarmati, Mahi, and Narmada Canal during (a) Oct 2020 (high flow) and (c) Feb 2021 (low flow); Ambika, Girna, Banas and Berach during (b) Nov 2021 (post-monsoon) and (d) Aug 2022 (monsoon). Both sampling periods in Ambika, Girna, Banas and Berach represented high flow condition.

High PBC concentration in the polluted downstream reach of Sabarmati and downstream locations along Mahi and Ambika aligns with similar observations made in the Yangtze River of increasing PBC with gross domestic product index (Meng et al., 2023). The % PBC (fraction of PBC in POC+PBC) was higher in Banas (13.4 ± 8.7 % and 7.9 ± 6.6 %), Berach (8.9 ± 7.1 % and 3.1 ± 2.8 %), Ambika (11.8 ± 4.7 % and 11.9 ± 4.7 %) and Girna (11.8 ± 3.8 % and 8.3 ± 4.8 %) during post monsoon and monsoon, respectively, compared to Sabarmati (5.1 ± 4.1 % and 5.4 ± 5.0 %) and Mahi (5.5 ± 1.8 % and 6.0 ± 3.8 %) during high and low flow periods, respectively (Fig 5.3 a and b). The low % PBC in Sabarmati and Mahi can be attributed to the high POC concentrations (Fig 5.2a and c). The % PBC in world rivers is reported to be around 12 ± 5 % (Coppola et al., 2022) with the highest observed in Xijiang River (34.2 %; Liu and Han, 2021) and Huanghe River (9 – 45.2 %; Xu et al., 2016) in China.

The stable isotopic composition of PBC was statistically higher (ANOVA, $p < 0.05$) in Banas (-23.4 ± 2.6 ‰ and -22.0 ± 1.9 ‰) and Berach (-24.2 ± 1.3 ‰ and -21.6 ± 2.3 ‰) compared to Ambika (-26.4 ± 1.1 ‰ and -22.9 ± 1.6 ‰) and Girna (-26.5 ± 0.6 ‰ and -23.9 ± 1.5 ‰) during post monsoon and monsoon, respectively (Fig 5.3c – f). The median $\delta^{13}\text{C}_{\text{PBC}}$ in these small river basins were higher than Sabarmati (-25.5 ± 0.9 ‰ and -25.3 ± 1.6 ‰) and Mahi (-25.9 ± 1.8 ‰ and -23.9 ± 3.4 ‰) during low and high flow periods as well (Fig 5.3 c-f). These values are in range of those reported in Xijiang (-27.1 ‰; Liu and Han, 2021), Yangtze (-24.48 ± 0.67 ‰; Meng et al., 2023), and Santa Clara (-24.9 ± 0.3 ‰; Masiello and Druffel, 2001).

5.1.2.2 Transformation of particulate black carbon in rivers

Aging of PBC by convention is the changes in physio-chemical signatures via biotic and abiotic transformations. The idea of aging PBC is highly debatable considering the recalcitrant nature of soot. Aging of PBC can happen via leaching or photodegradation, the latter being a significant mechanism of modulating DBC dynamics in aquatic systems (Stubbins et al. 2012; Wagner et al. 2015). In this study, $\delta^{13}\text{C}_{\text{PBC}}$ showed variation along the river continuum indicating either input from variable sources and/or transformation of PBC during its journey. When different sample classes in Sabarmati were analyzed separately, significant increase ($p < 0.05$) in $\delta^{13}\text{C}_{\text{PBC}}$ was observed from upper to lower sampling points in Sabarmati downstream and tributaries during high flow, and Mahi during both high and low flow conditions (Fig 5.4a). During low flow,

$\delta^{13}\text{C}_{\text{PBC}}$ decreased from upper to lower sampling points in Sabarmati upstream (Fig 5.4a).

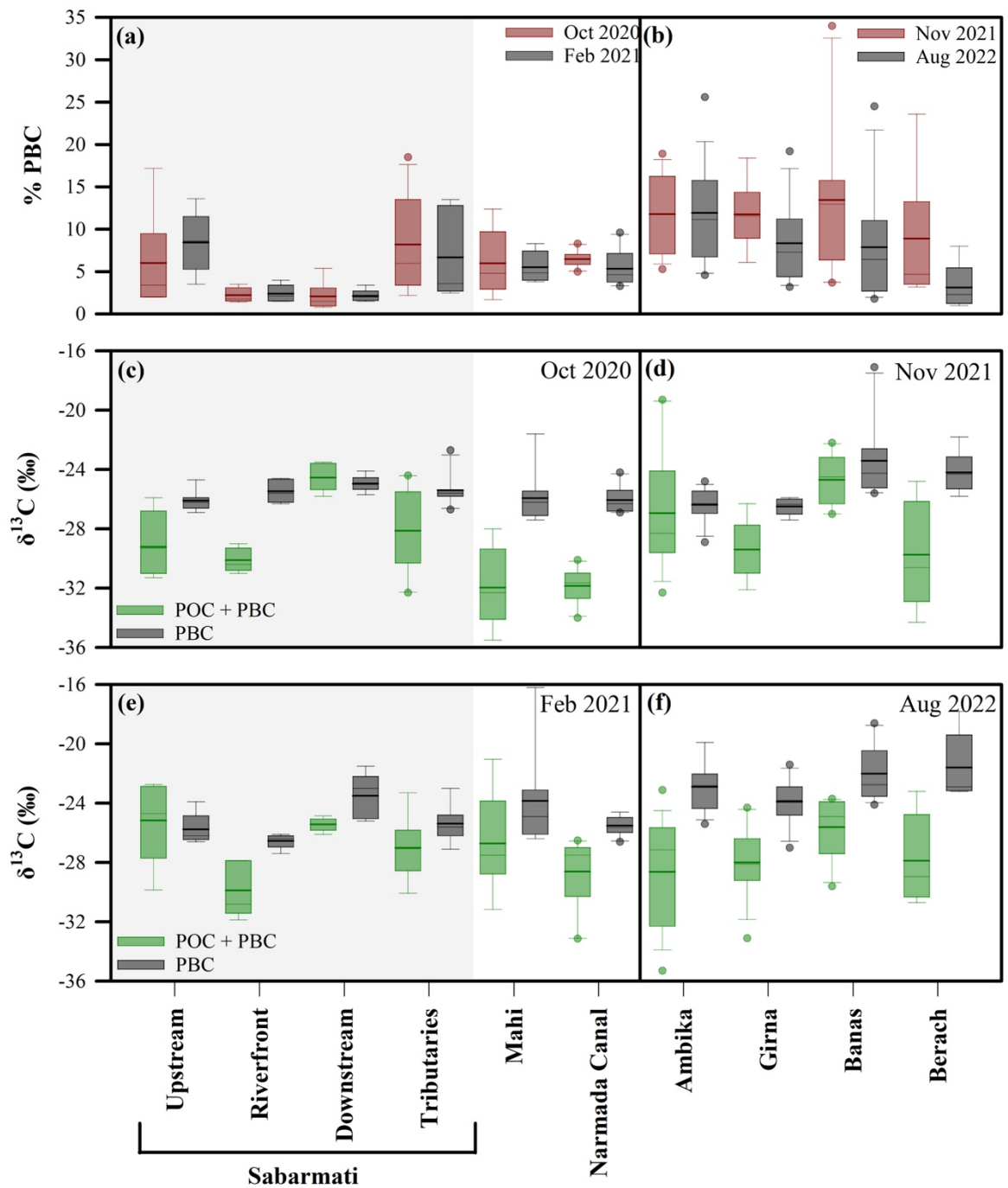


Fig. 5.3 % PBC in the (a) Sabarmati, Mahi and Narmada Canal during Oct 2020 (High flow) and Feb 2021 (Low flow), and (b) Ambika, Girna, Banas and Berach rivers during Nov 2021 (Post monsoon) and Aug 2020 (Monsoon). $\delta^{13}\text{C}$ of bulk particulate organic carbon (POC + PBC) and PBC in Sabarmati, Mahi and Narmada Canal during (c) Oct 2020 and (d) Feb 2021; Ambika, Girna, Banas and Berach during (e) Nov 2021 and (f) Aug 2022. Both sampling periods in Ambika, Girna, Banas and Berach represented high flow condition.

Using multiple correlations [distance vs PBC (Fig 5.4a) and $\delta^{13}\text{C}_{\text{PBC}}$ vs PBC (Fig 5.4b)], it was possible to decipher the processes that were responsible for the change in $\delta^{13}\text{C}_{\text{PBC}}$ observed in these river systems (Fig 5.4c). It was found that during high flow periods, the lower sampling points in each sampled class of the Sabarmati (upstream, downstream and tributaries) along with Mahi received PBC from the catchment that was isotopically enriched. This could indicate contribution from aged soil BC that got mobilised by surface runoff during the wet periods. It has been observed that aged BC stocks in soils can be a major source of BC in rivers (Dittmar et al., 2012; Ding et al., 2013). In contrast, during low flow condition, the Sabarmati upstream and downstream indicated loss of PBC from upper to lower sampling points with increase in isotopic composition, which is intriguing (Fig 5.4c). Source of PBC to Ambika was isotopically enriched during monsoon and relatively depleted during post monsoon. However, poor correlation among measured parameters makes it difficult to interpret transformation pathways in these smaller basins with confidence. Overall, due to lack of detailed investigation on the cycling of BC in aquatic systems (Coppola et al., 2022), the mechanisms affecting PBC leading to changes in its concentration and isotopic composition are largely unknown and warrants further research.

5.1.2.3 Transformation of PBC in engineered aquatic systems

Inland waters are experiencing severe impacts of anthropogenic interventions like damming, water diversions, salinization, and wastewater discharge. The rapid changes in stressors along the river continuum are directly reflected on the C cycle with shifting rates and directions of processes like mineralisation and uptake. In the earlier section, it was established that PBC pool is not as recalcitrant as classically believed and PBC evolved along the river continuum as indicated by its stable isotopic signatures. But it is challenging to decouple *in situ* transformation from allochthonous sources of variable isotopic compositions. The Narmada Canal and Sabarmati Riverfront which are lined systems and are cut off from the catchment provides us the opportunity to demystify this effect (catchment control vs *in situ* processes). In the Riverfront, which holds water in stagnancy right in the heart of the megacity Ahmedabad, inputs of depleted PBC during both high and low flow periods (Fig 5.4c) were observed. This could be attributed to atmospheric deposition as the primary source of PBC ($\delta^{13}\text{C}_{\text{BC}}$ of atmospheric PM over Ahmedabad = -27.8‰). Similarly, the Narmada Canal is a lined canal that flows for ~ 458 kms transporting water from Narmada River to different parts

of Gujarat, India. Here, PBC dynamics along a 100 km stretch starting from the city limits of Ahmedabad was explored. Interestingly, significant + and – relationships (Fig 5.4b) between PBC and $\delta^{13}\text{C}_{\text{PBC}}$ during high and low flow conditions, respectively, were observed, which pointed towards the signature of enriched river water during the wet periods. During the low flow conditions, signatures of transformation of PBC through degradation were observed in the Narmada Canal (Fig 5.4c).

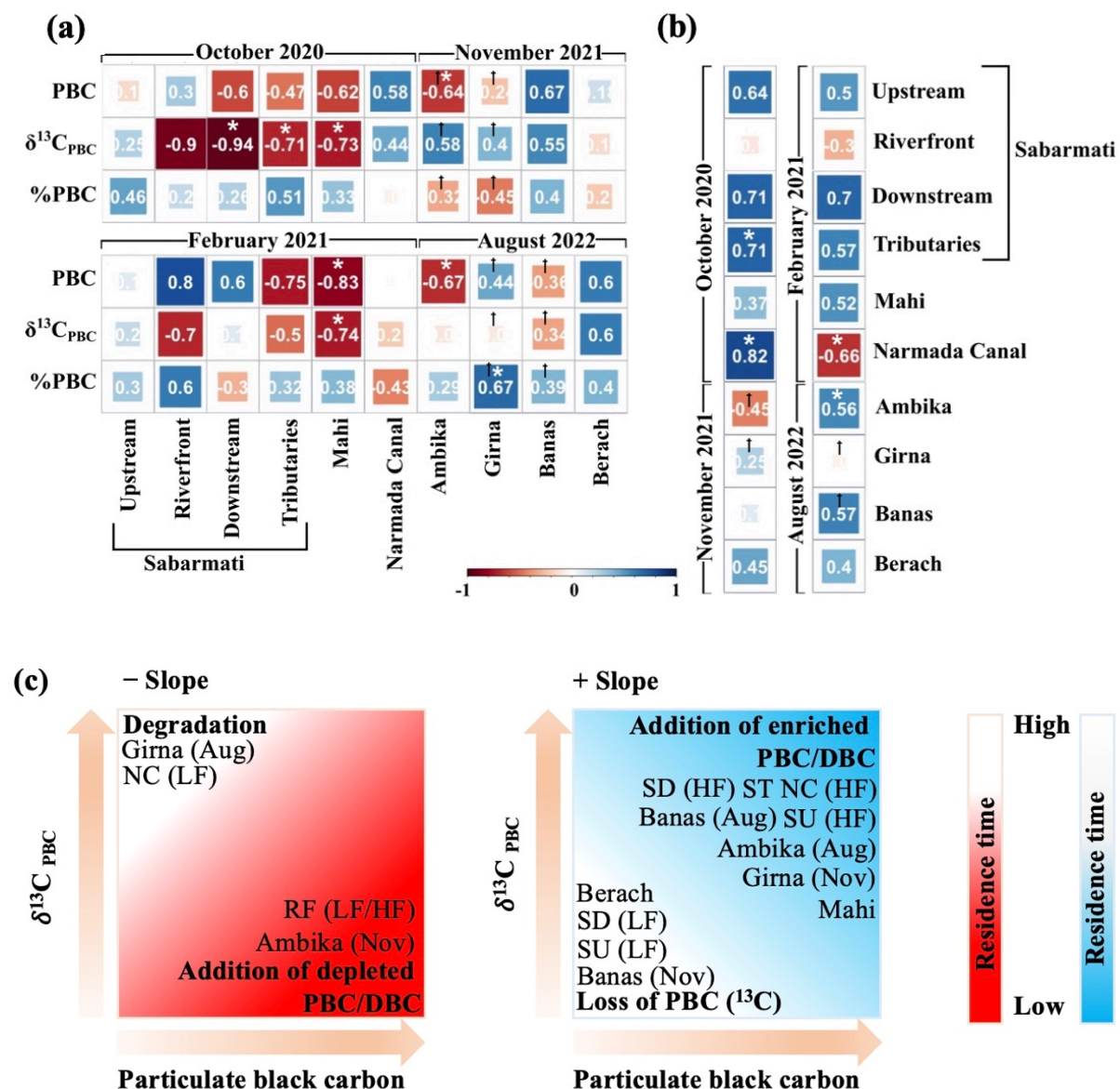


Fig. 5.4 Spearman and Pearson correlation (shown by †) between (a) distance from the river mouth and PBC, $\delta^{13}\text{C}_{\text{PBC}}$ and % PBC, and (b) PBC and $\delta^{13}\text{C}_{\text{PBC}}$ in different classes during sampling period. * shows correlations with $p < 0.05$. (c) Conceptual figure showing the process dynamics of PBC in each sample classes (SU = Sabarmati Upstream; SD = Sabarmati Downstream; RF = Riverfront; ST = Sabarmati Tributaries; NC = Narmada Canal; M = Mahi; LF = Low flow; HF = High flow).

5.1.2.4 Export fluxes and yields of particulate black carbon

The PBC export fluxes in world rivers have been estimated by Coppola et al., (2014) based on a suite of samples of river suspended matter, river bed sediments, flood plain deposits, and shelf sediments. Comprehensive export flux estimates of PBC based solely on the suspended matter samples are sparse (Fig 5.1a). Flux of PBC in this study was estimated for the Sabarmati, Mahi, and Ambika rivers using the PBC concentrations at downstream sites with discharge data from Krishna et al. (2019). This led to export fluxes of 0.589, 4.4, and 0.723 Gg yr⁻¹ of PBC from the Sabarmati, Mahi, and Ambika rivers, respectively. Furthermore, PBC export fluxes from 70 mountainous rivers draining the western Ghats in southern India were computed using POC export flux data from Reddy et al., (2021) and the % PBC of downstream sites of this study as representative of % PBC. The total (sum) PBC export flux from these 70 rivers was $\sim 64.78 \pm 45.03$ Gg yr⁻¹, which led to the net export estimate of 70.49 ± 45.03 Gg yr⁻¹ to the Arabian Sea. This estimate is quite low (0.21 – 0.44 %) compared to the global PBC export from land to ocean via rivers (Coppola et al., 2014), which could be due to non-inclusion of some of the major rivers draining into the Arabian Sea (Narmada, Tapi, Periyar) due to paucity of POC flux data.

5.1.3 Conclusions

Movement of PBC along the river continuum of six river basins and a lined canal was explored. Stable isotopic composition of PBC varied along the continuum and across river basins indicating different sources of PBC with varying isotopic signatures and/or modulation of riverine PBC via biotic and abiotic processes during its transport. During the high flow periods, allochthonous inputs of aged (isotopically enriched) PBC dominated the riverine PBC pool. Other processes that governed the PBC pool were degradation (leading to isotopic enrichment of residual pool) and atmospheric deposition of isotopically depleted PBC. Considering the significance of the recalcitrant nature of PBC in mitigating global climate, our evidence of modulations of riverine PBC advocates rethinking and re-evaluating the global impact of BC. Furthermore, export flux estimates of PBC need to take all major rivers into account.

5.2 Isotopic evidence for aging of particulate black carbon in the ocean

This section of the chapter explores the dynamics of particulate black carbon along the atmosphere – river – ocean continuum. Although well represented in the China Sea (Fang et al. 2015; 2018a; 2018b; 2019; 2021) and the Northwestern Pacific (Fang et al. 2016; Yamashita et al. 2021), corresponding global observations of DBC and PBC are currently extremely sparse. In particular, PBC has been estimated and explored in limited regions of the global ocean (Fig 5.5) and little is known about its transport and possible transformation along the atmosphere-river-ocean continuum. The hypotheses of this study are (i) the major sources of PBC to the oceans are riverine inputs and atmospheric deposition and (ii) PBC undergoes degradation during its transport along the continuum resulting in an increase in the $\delta^{13}\text{C}_{\text{PBC}}$.

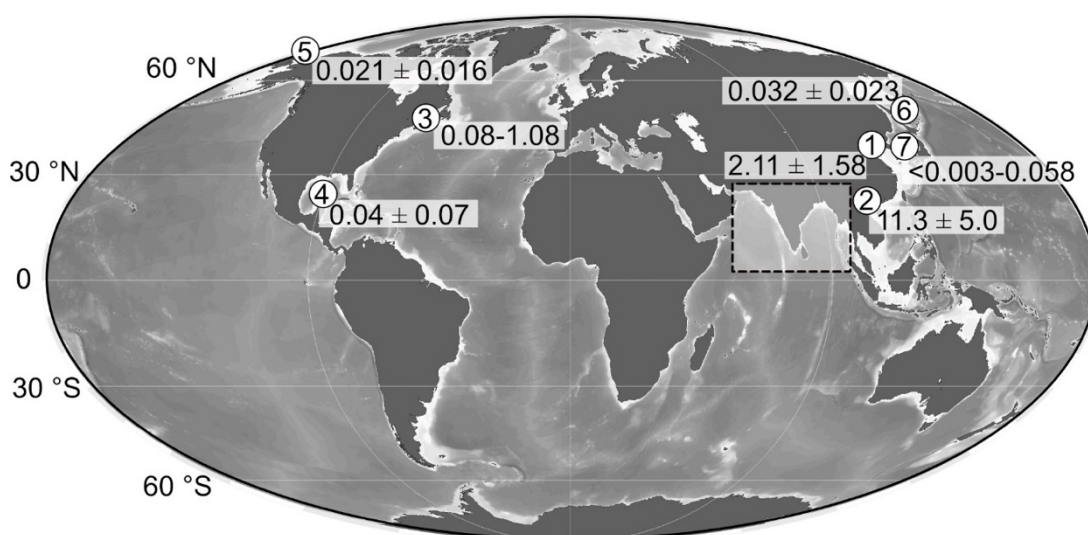


Fig. 5.5 Map of existing studies on oceanic particulate black carbon. Circles numbered 1 – 7 represent the locations with PBC concentrations in μM (1: Fang et al. 2021; 2: Mari et al. 2017; 3: Flores-Cervantes et al. 2009; 4: Yang and Guo 2014; 5,6,7: Fang et al. 2016). The shaded box represents the present study region.

5.2.1 Sampling

To address the above hypotheses, apart from the riverine samples discussed in previous section, sampling of surface particulate matter was conducted in the coastal regions (Mahanadi Estuary and Andaman Creeks) of India and the northern Indian Ocean [Arabian Sea (AS), Bay of Bengal (BoB), and Andaman Sea (AnS)] (Fig 5.6). Particulate matter was collected from the Mahanadi Estuary during October 2019 ($n = 72$) at 3 stations (a riverine, an estuarine, and a nearshore coastal location) at a time

interval of 6 hours for 9 consecutive days. Samples were also collected from the Andaman and Nicobar Islands during Nov–Dec 2020 ($n = 31$) from 9 creeks. In the open ocean, samples were collected (5–10 meters) from the AS during December 2019 onboard ORV *Sagar Kanya* (SK 364) at 11 stations along with subsurface sampling (50–75 meters) at three stations ($n = 15$). Samples were collected from the BoB ($n = 10$), AnS ($n = 5$), and southern AS ($n = 4$) during September–October 2021 onboard ORV *Sagar Kanya* (SK 373 and SK 374). Atmospheric PM was collected onto Quartz microfiber filters over megacities Ahmedabad and Hyderabad.

5.2.2 Results

The PBC in the coastal AS ranged from 0.87 to 2.72 μM (mean \pm stdev: 1.40 ± 0.71), whereas it ranged from 0.27 to 1.84 μM (0.84 ± 0.46) in the open ocean (Fig 5.6a). Similarly, in the BoB, PBC ranged from 0.62–1.21 μM (0.77 ± 0.25) at the coastal locations and 0.57–0.81 μM (0.71 ± 0.10) in the open BoB (Fig 5.6a). AnS had PBC in the range of 0.42–1.47 μM (0.89 ± 0.38) (Fig 5.6a). The three stations in the Mahanadi estuary did not show significant difference in PBC with overall concentrations ranging from 0.72 to 4.75 μM (2.03 ± 0.94) (Fig 5.6b). The Sabarmati downstream and the Andaman Creeks, however, showed significantly high PBC abundance with concentrations ranging from 6.49 – 56.90 μM and 2.07 – 18.56 μM , respectively, compared to that observed in seawater (Fig 5.6c).

The PBC pool showed distinct isotopic signatures across the studied systems. Although the coastal stations of the BoB and the AS showed similar $\delta^{13}\text{C}_{\text{PBC}}$ of $-18.8 \pm 1.0\text{‰}$ and $-18.4 \pm 1.0\text{‰}$, respectively, the $\delta^{13}\text{C}_{\text{PBC}}$ was significantly higher in the open AS ($-16.2 \pm 1.3\text{‰}$) compared to the open BoB ($-20.0 \pm 0.7\text{‰}$) (Fig 5.6a). The AnS showed similar $\delta^{13}\text{C}_{\text{PBC}}$ ($-20.4 \pm 1.0\text{‰}$) as that of open BoB. The $\delta^{13}\text{C}_{\text{PBC}}$ of the Mahanadi Estuary was around $-25.0 \pm 1.3\text{‰}$ with the three stations showing similar range (Fig 5.6b). The Andaman Creeks had similar $\delta^{13}\text{C}_{\text{PBC}}$ ($-24.5 \pm 1.1\text{‰}$) as the Mahanadi Estuary (Fig 5.6c). The $\delta^{13}\text{C}_{\text{BC}}$ of ambient aerosol over Ahmedabad and Hyderabad were -25.5‰ and -27.8‰ , respectively. Overall, $\delta^{13}\text{C}_{\text{PBC}}$ of the open saline waters (AS, BoB, and AnS; Fig 5.6) was significantly enriched in ^{13}C compared to the fresher waters and atmospheric PM.

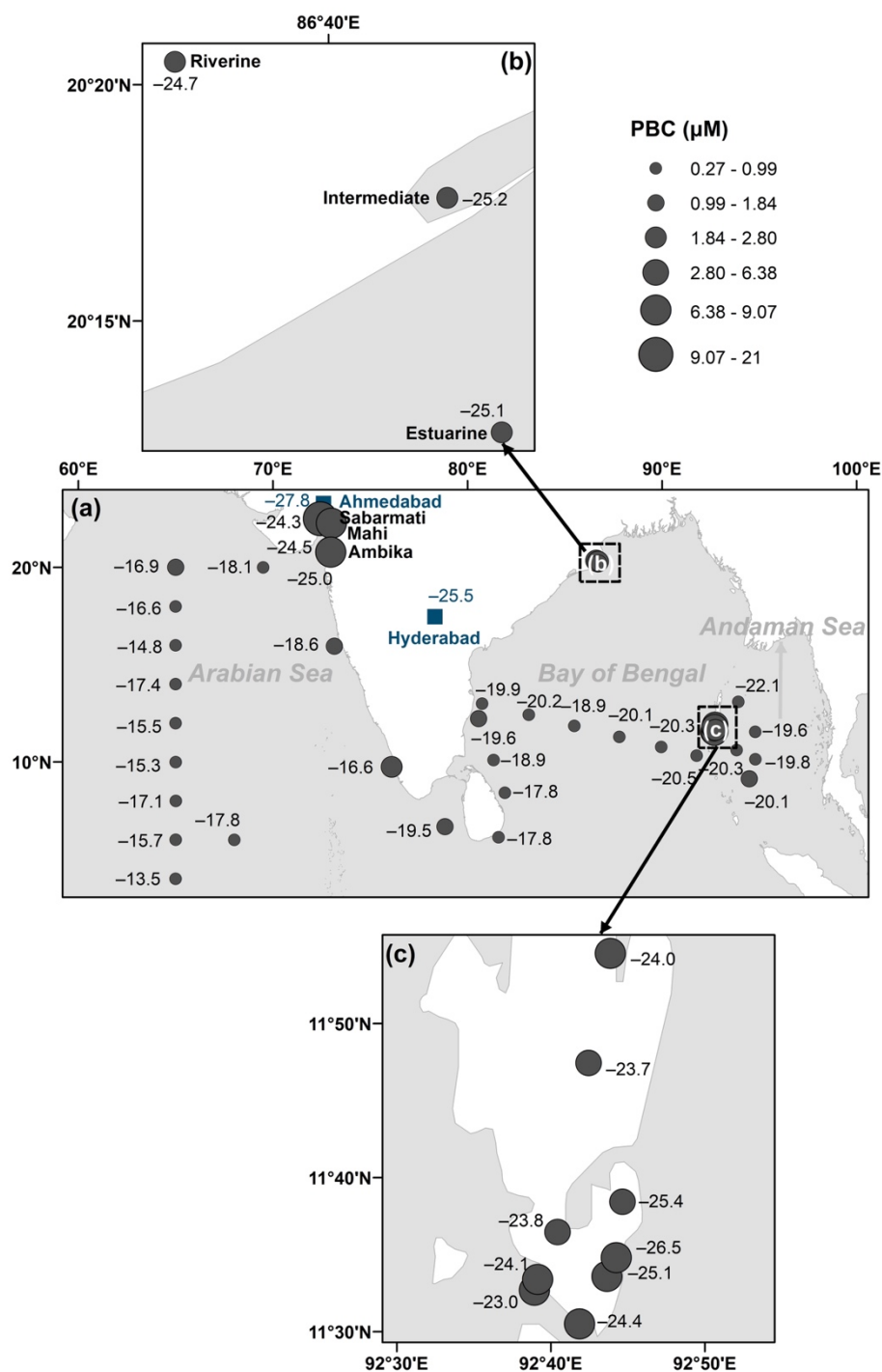


Fig. 5.6 Sampling locations showing the concentrations and isotopic compositions of particulate black carbon in the (a) northern Indian Ocean, (b) Mahanadi Estuary, and (c) Andaman Creeks. The average concentration and isotopic composition of PBC in the downstream reach of Sabarmati, along with Mahi and Ambika rivers are also shown by circles. The size of the circles denotes the concentration of PBC in μM and the labels denote the isotopic compositions in permil (‰). Sampling locations for atmospheric particulate matter are denoted by blue squares.

5.2.3 Discussion

5.2.3.1 Abundance and isotopic composition of PBC

Limited studies on PBC dynamics in the global ocean have made it challenging to understand the causal factors for its spatial variability and determine the dominant sources and sinks. Among the studies conducted so far, the abundance of PBC in the northern Indian Ocean was similar to the Gulf of Maine (0.08–1.08 μM ; Flores-Cervantes et al. 2009) and the Bohai Sea and Northern Yellow Sea during summer (0.97 ± 0.72 ; Fang et al. 2021) but extremely high compared to mid-latitude Pacific Ocean (<0.003 – 0.058 μM ; Fang et al. 2016). However, the highest PBC observed in the marine setting during this study is still significantly lower than that observed during winter in the Bohai Sea and Northern Yellow Sea (3.26 ± 3.07 μM ; Fang et al. 2021) as well as the Halong Bay, North Vietnam (11.30 ± 5.0 μM ; Mari et al. 2017) (Fig 5.5). A significant decrease in median PBC concentrations from coast to the open sea was observed in both the AS and BoB, which was in agreement with observations elsewhere (Flores-Cervantes et al. 2009; Yang and Guo 2014; Fang et al. 2016). Compared to PBC concentrations, $\delta^{13}\text{C}_{\text{PBC}}$ measurements in the global ocean are even rarer. To the best of our knowledge, only two studies related to $\delta^{13}\text{C}_{\text{PBC}}$ have been conducted in the marine environment, which includes -45% observed by Flores-Cervantes et al. (2009) in the Gulf of Maine and -32.8% observed by Yang and Guo (2014) in the Gulf of Mexico. Compared to these two studies, PBC in the Northern Indian Ocean was highly enriched in ^{13}C . Similar to our observation of ^{13}C enriched PBC pool in the open ocean, Wagner et al. (2019) also observed low concentration of DBC with highly enriched BPCA-specific $\delta^{13}\text{C}_{\text{DBC}}$ in the Pacific and Atlantic Ocean (DBC: 0.58 – 0.78 μM ; $\delta^{13}\text{C}_{\text{DBC}}$: $\sim -23.6\%$) as compared to that in rivers (Amazon, Congo, Northern Dvina, Kolyma and Mississippi; DBC: 19 – 115 μM ; $\delta^{13}\text{C}_{\text{DBC}}$: $\sim -30.0\%$).

5.2.3.2 Sources of PBC to the open ocean

The PBC in the surface waters of global ocean has two major sources: (i) atmospheric deposition and (ii) fluvial inputs. Near shore stations exhibiting high BC are understood to receive most of the BC flux from rivers and aeolian deposition (Jurado et al. 2008; Flores-Cervantes et al. 2009; Jaffe et al. 2013; Yang and Guo 2014). To estimate the source $\delta^{13}\text{C}_{\text{PBC}}$ for oceanic PBC during this study, Miller Tans plots were employed, which resulted in source $\delta^{13}\text{C}_{\text{PBC}}$ for the open BoB and AS to be $-20.9 \pm 0.8\%$ and $-17.7 \pm 0.6\%$, respectively (Fig 5.7a; Table 5.1). Also, the average $\delta^{13}\text{C}_{\text{BC}}$ over the AS

has been reported to be -25.0% (Dasari et al. 2020), which is similar to atmospheric $\delta^{13}\text{C}_{\text{BC}}$ over Ahmedabad and Hyderabad during this study.

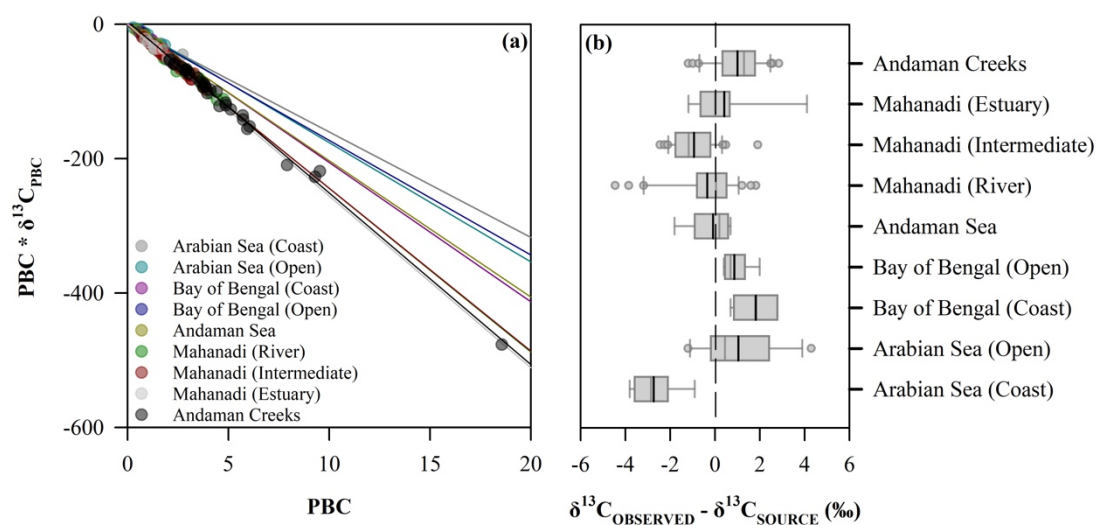


Fig. 5.7 (a) Miller Tans Plot for particulate black carbon (PBC). The slope of the regression represents the $\delta^{13}\text{C}_{\text{PBC}}$ of the source. The equations and statistics for each regression is shown in Table 5.1, (b) box – whisker plot showing the relative change is $\delta^{13}\text{C}_{\text{PBC}}$ between the calculated $\delta^{13}\text{C}_{\text{PBC}}$ of source (from Miller Tans Plot) and the observed values of $\delta^{13}\text{C}_{\text{PBC}}$.

Assuming rivers and atmosphere to be only sources of BC in the northern Indian Ocean, the high $\delta^{13}\text{C}_{\text{PBC}}$ observed during this study does not appear to be simply a result of two endmember mixing as both these sources are isotopically depleted. This rejects our first hypothesis and warrants a contribution from an isotopically enriched source of PBC to the open ocean or provide evidence for potential aging of PBC causing isotopic enrichment. The source- $\delta^{13}\text{C}_{\text{PBC}}$ for the open AS was close to the average $\delta^{13}\text{C}_{\text{PBC}}$ of coastal waters ($-18.4 \pm 1.0\%$). Therefore, the PBC in open ocean could have been transported from the coastal region. The high source- $\delta^{13}\text{C}_{\text{PBC}}$ ($-15.7 \pm 0.8\%$) in the coastal AS could be attributed to resuspended sediments and BC of high $\delta^{13}\text{C}$ due to coastal upwelling during southwest monsoon. Alternatively, the source could be laterally advected aged PBC from the BoB through the western Indian coastal current (Kumar et al. 2001; Gupta et al. 2016). Similar observations were made in the coastal Bohai Sea where the monsoon driven Shandong Coastal Current transports resuspended sediments and PBC to the Northern Yellow Sea through the Bohai Strait (Fang et al. 2021).

Table 5.1 Summary of the least-square linear regression model equations in the Miller-Tans plots for PBC presented in Fig 5.7a with the parameters of the linear equation along with standard error in brackets for the slope, R^2 , and number of observations (n). An approximation of the $\delta^{13}\text{C}$ source values can be deduced from the slope of the Miller-Tans equation.

Region	Equation	R^2	n
Arabian Sea (Coast)	$\delta^{13}\text{C}_{\text{PBC}} \times \text{PBC}$ $= -15.68 (\pm 0.81) \times \text{PBC} - 3.3656$	0.99	6
Arabian Sea (Open)	$\delta^{13}\text{C}_{\text{PBC}} \times \text{PBC}$ $= -17.73 (\pm 0.60) \times \text{PBC} + 1.1470$	0.99	12
Andaman Sea	$\delta^{13}\text{C}_{\text{PBC}} \times \text{PBC}$ $= -20.32 (\pm 1.32) \times \text{PBC} - 0.0867$	0.99	5
Bay of Bengal (Coast)	$\delta^{13}\text{C}_{\text{PBC}} \times \text{PBC}$ $= -20.66 (\pm 1.42) \times \text{PBC} + 1.3466$	0.99	5
Bay of Bengal (Open)	$\delta^{13}\text{C}_{\text{PBC}} \times \text{PBC}$ $= -20.85 (\pm 0.80) \times \text{PBC} + 0.3890$	1	4
Mahanadi (River)	$\delta^{13}\text{C}_{\text{PBC}} \times \text{PBC}$ $= -24.34 (\pm 0.54) \times \text{PBC} - 0.6829$	0.99	33
Mahanadi (Intermediate)	$\delta^{13}\text{C}_{\text{PBC}} \times \text{PBC}$ $= -24.24 (\pm 0.48) \times \text{PBC} - 1.6374$	0.99	31
Mahanadi (Estuary)	$\delta^{13}\text{C}_{\text{PBC}} \times \text{PBC}$ $= -25.55 (\pm 0.79) \times \text{PBC} - 0.1624$	1	7
Andaman Creeks	$\delta^{13}\text{C}_{\text{PBC}} \times \text{PBC}$ $= -25.53 (\pm 0.36) \times \text{PBC} + 4.2185$	0.99	31

5.2.3.3 Aging of PBC in ocean water

The present results of an isotopically enriched PBC pool in the ocean as compared to the riverine and atmospheric endmembers raise a very crucial question regarding the aging of PBC in ocean waters (Fig 5.8). Similarly, in the Andaman Creeks, aging of PBC of the creek waters resulted in an enriched source signature of PBC to the AnS (Fig 5.7b). These observations affirm the hypothesis of the aging of PBC in aquatic systems resulting in an increase in $\delta^{13}\text{C}_{\text{PBC}}$. Isotopic enrichment of the PBC pool is possible if there is a preferential loss of ^{12}C via photodegradation or microbial activity on the PBC. Zimmerman et al. (2012) observed abiotic release of CO_2 from pyrogenic

C, attributing the source to polycyclic aromatic compounds rather than labile C fractions. Long term release of CO₂ from PBC might be a significant loss process of C leading to isotopic enrichment of the residual PBC pool. Another study exploring the effect of pyrogenic C on stream biogeochemistry observed the release of dissolved OM from pyrogenic C (Bistarelli et al. 2021). The reactivity of PBC in aquatic systems provides fresh insights into its ability to actively participate in the global C cycle and the limited ability to sequester C as otherwise anticipated.

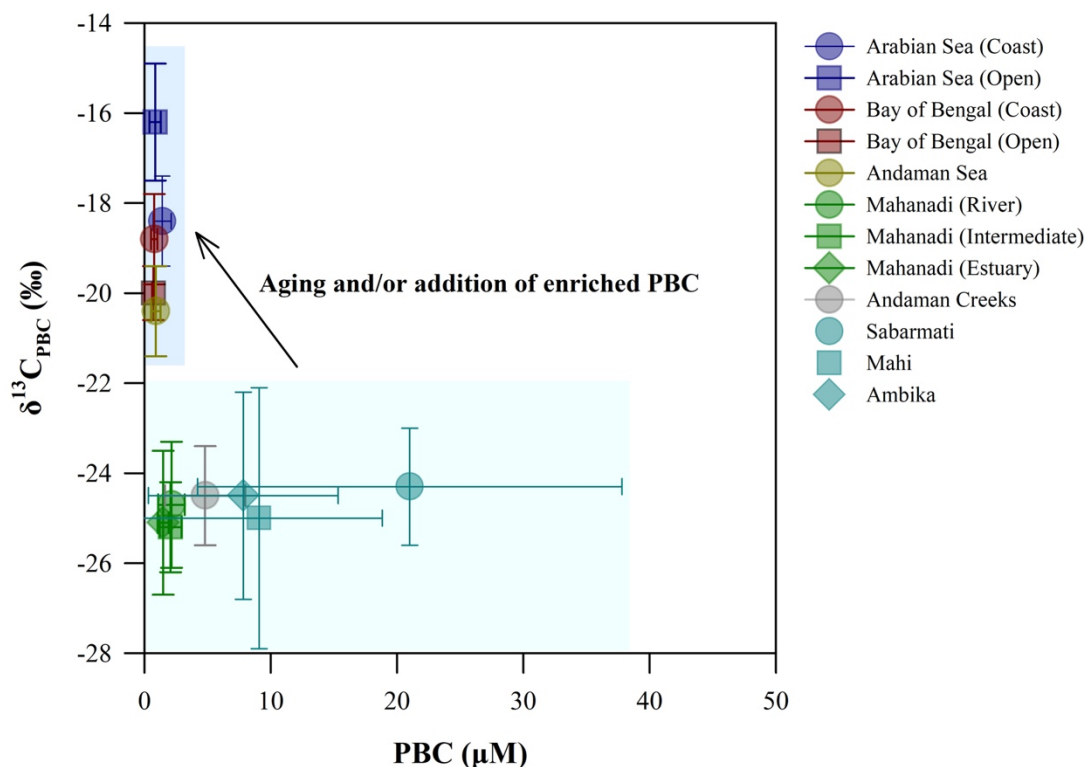


Fig. 5.8 Scatter plot of PBC and $\delta^{13}\text{C}_{\text{PBC}}$ showing shift in concentration and isotopic composition from riverine to marine environment. For Sabarmati being an engineered river, samples from the downstream reach are considered.

5.2.3.4 Significance of particulate black carbon in ocean C biogeochemistry

The PBC biogeochemistry in the global ocean remains poorly explored with most of the studies focusing on DBC due to its potential to photochemically degrade and transform (Coppola et al., 2022). However, our observation of a significant negative relationship between % PBC and $\delta^{13}\text{C}_{\text{PBC}+\text{POC}}$ in the AS indicates some influence of aged PBC in regulating the bulk POC isotopic composition (i.e., POC+PBC: which is normally measured and interpreted as organic carbon). To see the effect of PBC on the POC isotopic composition, we recalculated the POC concentration and its isotopic

composition after correcting for the PBC fraction using two components isotopic mixing model (Goni et al., 2003; Lohmann et al., 2009):

$$\delta^{13}\text{C}_{\text{POC}} = (\delta^{13}\text{C}_{\text{PBC+POC}} - \delta^{13}\text{C}_{\text{PBC}} \times f_{\text{PBC}}) / f_{\text{POC}} \quad \text{Eq (1)}$$

where, $\delta^{13}\text{C}_{\text{POC}}$ is the $\delta^{13}\text{C}$ of POC and f_{PBC} and f_{POC} are the fractions of PBC and POC in the bulk POC pool (POC+ PBC), respectively. This exercise was performed on the bulk POC data available with us from the AS and Andaman Creeks. We did not observe a significant difference between the $\delta^{13}\text{C}_{\text{PBC+POC}}$ and $\delta^{13}\text{C}_{\text{POC}}$ (recalculated) values (ANOVA; $p > 0.05$). However, PBC and POC concentrations are positively correlated in the AS and Andaman Creeks indicating coupling of the two C pools, similar to the one observed in the coastal China Sea (Fang et al. 2020). Regions with significant proportion of BC in the particulate C pool can experience inefficient mineralization of bulk POC to CO_2 during its settling (Flores-Cervantes et al., 2009). The average % PBC in the bulk POC pool (POC + PBC) was 14.8% in the AS and 11% in the Andaman Creeks. This fraction of PBC is high when compared to DBC which comprises 2–6% of the marine DOC pool (Dittmer and Paeng, 2009; Kleber, 2010; Coppola et al., 2022). Potential PBC interference in the biogenic POC flux estimations (where % PBC is higher) and ultimately an overestimation of the fluxes of organic carbon has also been highlighted by Yang and Guo (2014). Furthermore, with the isotopic evidence of aging of PBC presented in this study along with the known mechanisms of release of CO_2 from the PBC pool (Zimmerman et al., 2012), we advocate a significant role of PBC in regulating the C dynamics of aquatic systems.

5.2.4 Conclusion

This study explores the evolution of PBC along the atmosphere – river – ocean continuum supporting the challenge to the classical understanding of the refractory nature of BC in the environment. Significant enhancement in the stable isotopic composition of PBC in the open ocean as compared to the riverine and atmospheric end members was observed. This provides evidence for two possibilities: (i) existence of a third source of PBC to the ocean water with high $\delta^{13}\text{C}_{\text{BC}}$ and/or (ii) degradation and aging of PBC in aquatic systems through photodegradation/leaching or any other unknown mechanism. The processing of PBC in the aquatic continuum has huge scientific implications pertaining to interpretation of sediment core $\delta^{13}\text{C}_{\text{BC}}$ signatures. Furthermore, the processing of PBC in aquatic systems highlights the uncertainties in the global C budgets where BC is considered recalcitrant and a long-term sink for C.

Chapter 6

Summary and future scope

6.1 Summary

The thesis aimed at understanding the C and N biogeochemistry in aquatic systems. The major contributions of the thesis are as follows:

6.1.1 Lake biogeochemistry (freshwater and saline)

- i. Lakes in semi – arid and arid climate setting witness drastic seasonal variation in lake volume and salinity.
- ii. Nalsarovar lost ~ 47 % and Sambhar Lake lost ~ 89 % of the lake water from wet to dry periods, respectively.
- iii. Lake volume reduction is accompanied by steady increase in major ions, DIC, POC, and PN.
- iv. NH_4^+ in the lake water increased manifold as the lake volume reduced and salinity increased, whereas NO_3^- concentrations did not increase simultaneously indicating inhibition of nitrification at high salinity.
- v. Low $\delta^{15}\text{N}_{\text{PN}}$ corresponding to high lake biomass indicates potential for N_2 fixation, even in nutrient rich saline environment.
- vi. Significantly high $\delta^{13}\text{C}_{\text{SOM}}$ and $\delta^{15}\text{N}_{\text{TN}}$ of sediments compared to $\delta^{13}\text{C}_{\text{POC}}$ and $\delta^{15}\text{N}_{\text{PN}}$ indicates high mineralisation of POM in the water column and post deposition.
- vii. In the freshwater lake, CH_4 production was supported by increase in lake biomass (which acts as substrate for methanogenesis). CO_2 was low during productive months, and N_2O was surprisingly lowest during periods of high lake biomass indicating a negative effect of productivity on N_2O production (competition for DIN/complete denitrification).

6.1.2 River biogeochemistry

- i. Altitude has a strong control over the C/N ratio and $\delta^{13}\text{C}_{\text{POC}}$ of total suspended matter in the Ganges, Mekong, and Yellow.
- ii. High total suspended matter with high $\delta^{13}\text{C}_{\text{POC}}$ was observed during high flow periods compared to low flow, indicating allochthonous inputs (SOM and C4 vegetation).
- iii. Primary production dominated in all three river systems during the dry seasons (high C/N) with evidence of potential N_2 fixation (low $\delta^{15}\text{N}_{\text{POM}}$).
- iv. Export fluxes of POC and PN to the oceans reduced drastically over the decades.

- v. In the urban engineered river, high concentrations of DIC, POM, and dissolved CH₄, CO₂, and N₂O were observed in the polluted reaches of river channel.
- vi. Higher POM in the stagnant riverfront compared to lined canal indicated enhanced productivity in stagnant condition, followed by higher CH₄ production.
- vii. Increase in CH₄ compared to N₂O in polluted reach indicate dominance of methanogens in organic rich anoxic environments/ complete denitrification resulting in low N₂O.
- viii. The studied systems were net source of GHGs except for some lower order streams that acted as sink of N₂O during low flow condition.
- ix. In the high altitude rivers, higher DIC with high isotopic composition was observed during spring compared to autumn, indicating enhanced post thaw weathering.
- x. Dissolved GHGs increases as the river enters city limits and with increasing availability of substrate (POM).

6.1.3 Particulate black carbon in aquatic systems

- i. Along the river continuum (headwaters – estuary) the source isotopic signatures (allochthonous inputs) are reflected on the riverine PBC.
- ii. Particulate BC concentration decreases from riverine to marine environment.
- iii. The stable isotopic composition of marine PBC is significantly higher than that of riverine and atmospheric PBC pool.
- iv. Overall, there is evidence of aging of PBC in the atmosphere – river – ocean continuum.

6.2 Scope for future research

This thesis contributed to the understanding of C and N biogeochemistry in aquatic systems by addressing specific research questions. The study lays the groundwork for future research as discussed below:

- i. In saline lakes, the increasing biomass with desiccation could be derived from both living as well as detrital OM. To resolve this, primary productivity experiments should be conducted using isotope tracer techniques.
- ii. Indication of N₂ fixation was inferred from low $\delta^{15}\text{N}_{\text{POM}}$ even in nutrient rich environments. This warrants N₂ fixation experiments, which would provide direct evidence that can be used in N budgeting of the system.
- iii. The effect of salinisation and desiccation on C and N biogeochemistry was studied through field observations. Well constrained numbers could be generated if controlled lab experiments are performed by spiking salinity and regulating water volume to see the changes in rates of primary productivity, N₂ fixation, methanogenesis and other such processes.
- iv. In the Sabarmati River, a 70 km anoxic stretch was identified downstream of Ahmedabad city. It is expected that the biogeochemical processes in this stretch would be different from other reaches. High greenhouse gases in this region warrants experimental studies to calculate rates of production. Furthermore, the effect of anoxic river discharge with high DIC, particulate matter, and GHGs to the coastal waters should be investigated.
- v. In the high altitude river – lake continuum, this study was limited in terms of calculating emission fluxes of GHGs due to unavailability of flow velocity data. In future, seasonality could be captured with comprehensive environmental variables.
- vi. There is paucity of data on C uptake rates, N₂ fixation rates, and GHGs production rates in high altitude aquatic systems. This research gap could be addressed in the future.
- vii. Our speculations on the aging of BC in the marine environment relies on isotopic evidences. However, incubation experiments to track the products and rates of degradation would validate the above speculation.

References

- Aggarwal, S.C., 1951. The Sambhar lake salt source. Manager, Government of India Press.
- Alling, V., Porcelli, D., Mörth, C.M., Anderson, L.G., Sanchez-Garcia, L., Gustafsson, Ö., Andersson, P.S. and Humborg, C., 2012. Degradation of terrestrial organic carbon, primary production and out-gassing of CO₂ in the Laptev and East Siberian Seas as inferred from $\delta^{13}\text{C}$ values of DIC. *Geochimica et Cosmochimica Acta*, 95, pp.143-159.
- Alshboul, Z., Encinas-Fernandez, J., Hofmann, H. and Lorke, A., 2016. Export of dissolved methane and carbon dioxide with effluents from municipal wastewater treatment plants. *Environmental science & technology*, 50(11), pp.5555-5563.
- Amal, K., 1990. A stream trap hypothesis for the evolution of some saline lakes in the Indian desert. *Zeitschrift Für Geomorphologie* 34: 37–47.
- Andrei, A. E., L. M. Smith, D. A. Haukos, J. G. Surlis & W. P. Johnson, 2009. Foraging ecology of migrant shorebirds in saline lakes of the Southern Great Plains. *Waterbirds* 32: 138–148.
- Ascough, P.L., Bird, M.I., Francis, S.M., Thornton, B., Midwood, A.J., Scott, A.C. and Apperley, D., 2011. Variability in oxidative degradation of charcoal: influence of production conditions and environmental exposure. *Geochimica et Cosmochimica Acta*, 75(9), pp.2361-2378.
- Asselman, N.E., Middelkoop, H. and Van Dijk, P.M., 2003. The impact of changes in climate and land use on soil erosion, transport and deposition of suspended sediment in the River Rhine. *Hydrological Processes*, 17(16), pp.3225-3244.
- Aucour, A.M., France-Lanord, C., Pedoja, K., Pierson-Wickmann, A.C. and Sheppard, S.M., 2006. Fluxes and sources of particulate organic carbon in the Ganga-Brahmaputra river system. *Global Biogeochemical Cycles*, 20(2).
- Bade, D. L., S. R. Carpenter, J. J. Cole, P. C. Hanson & R. H. Hesslein, 2004. Controls of $\delta^{13}\text{C}$ -DIC in lakes: geochemistry, lake metabolism, and morphometry. *Limnology and Oceanography* 49: 1160–1172.
- Balakrishna, K., and Probst, J. L. (2005). Organic carbon transport and C/N ratio variations in a large tropical river: Godavari as a case study, India. *Biogeochemistry* 73 (3), 457–473.
- Bastviken, D., Cole, J., Pace, M. and Tranvik, L., 2004. Methane emissions from lakes: Dependence of lake characteristics, two regional assessments, and a global estimate. *Global biogeochemical cycles*, 18(4).
- Bastviken, D., Cole, J.J., Pace, M.L. and Van de Bogert, M.C., 2008. Fates of methane from different lake habitats: Connecting whole-lake budgets and CH₄ emissions. *Journal of Geophysical Research: Biogeosciences*, 113(G2).

- Bastviken, D., Tranvik, L. J., Downing, J. A., Crill, P. M., and Enrich-Prast, A. (2011). Freshwater methane emissions offset the continental carbon sink. *Science* 331 (6013), 50.
- Batanero, G. L., E. León-Palmero, L. Li, A. J. Green, M. Rendón-Martos, C. A. Suttle & I. Reche, 2017. Flamingos and drought as drivers of nutrients and microbial dynamics in a saline lake. *Scientific Reports* 7: 1–13.
- Begum, M.S., Bogard, M.J., Butman, D.E., Chea, E., Kumar, S., Lu, X., Nayna, O.K., Ran, L., Richey, J.E., Tareq, S.M. and Xuan, D.T., 2021. Localized pollution impacts on greenhouse gas dynamics in three anthropogenically modified Asian river systems. *Journal of Geophysical Research: Biogeosciences*, 126(5), p.e2020JG006124.
- Begum, M.S., Jang, I., Lee, J.M., Oh, H.B., Jin, H. and Park, J.H., 2019. Synergistic effects of urban tributary mixing on dissolved organic matter biodegradation in an impounded river system. *Science of the total environment*, 676, pp.105-119.
- Benchimol, M. and Peres, C.A., 2015. Widespread forest vertebrate extinctions induced by a mega hydroelectric dam in lowland Amazonia. *PloS one*, 10(7), p.e0129818.
- Beusen, A. H. W., Dekkers, A. L. M., Bouwman, A. F., Ludwig, W., and Harrison, J. (2005). Estimation of global river transport of sediments and associated particulate C, N, and P. *Glob. Biogeochem. Cycles* 19 (4).
- Bhavya, P.S., Kumar, S., Gupta, G.V.M., Sudharma, K.V. and Sudheesh, V., 2018. Spatio-temporal variation in $\delta^{13}\text{C}_{\text{DIC}}$ of a tropical eutrophic estuary (Cochin estuary, India) and adjacent Arabian Sea. *Continental Shelf Research*, 153, pp.75-85.
- Biddanda, B. A. (2017). Global significance of the changing freshwater carbon cycle. *Eos*, 98.
- Bistarelli, L.T., Poyntner, C., Santín, C., Doerr, S.H., Talluto, M.V., Singer, G. and Sigmund, G., 2021. Wildfire-derived pyrogenic carbon modulates riverine organic matter and biofilm enzyme activities in an in situ flume experiment. *ACS Es&t Water*, 1(7), p.1648.
- Blomqvist, S., A. Gunnars & R. Elmgren, 2004. Why the limiting nutrient differs between temperate coastal seas and freshwater lakes: a matter of salt. *Limnology and Oceanography* 49: 2236–2241.
- Bodelier, P. L. E., M. Stomp, L. Santamaria, M. Klaassen & H. J. Laanbroek, 2006. Animal–plant–microbe interactions: direct and indirect effects of swan foraging behaviour modulate methane cycling in temperate shallow wetlands. *Oecologia* 149: 233–244.
- Boix-Fayos, C., Nadeu, E., Quiñonero, J.M., Martínez-Mena, M., Almagro, M. and De Vente, J., 2015. Sediment flow paths and associated organic carbon dynamics across a Mediterranean catchment. *Hydrology and Earth System Sciences*, 19(3), pp.1209-1223.

- Bond, T.C., Doherty, S.J., Fahey, D.W., Forster, P.M., Berntsen, T., DeAngelo, B.J., Flanner, M.G., Ghan, S., Kärcher, B., Koch, D. and Kinne, S., 2013. Bounding the role of black carbon in the climate system: A scientific assessment. *Journal of geophysical research: Atmospheres*, 118(11), pp.5380-5552.
- Bordovskiy, O.K., 1965. Sources of organic matter in marine basins. *Marine Geology*, 3(1-2), pp.5-31.
- Boutton, T.W., 1996. Stable carbon isotope ratios of soil organic matter and their use as indicators of vegetation and climate change. *Mass spectrometry of soils.*, pp.47-82.
- Bouwman, A.F., Bierkens, M.F.P., Griffioen, J., Hefting, M.M., Middelburg, J.J., Middelkoop, H. and Slomp, C.P., 2013. Nutrient dynamics, transfer and retention along the aquatic continuum from land to ocean: towards integration of ecological and biogeochemical models. *Biogeosciences*, 10(1), pp.1-22.
- Bowring, S.P., Jones, M.W., Ciais, P., Guenet, B. and Abiven, S., 2022. Pyrogenic carbon decomposition critical to resolving fire's role in the Earth system. *Nature Geoscience*, 15(2), pp.135-142.
- Broadbent, F.E., Rauschkolb, R.S., Lewis, K.A. and Chang, G.Y., 1980. Spatial variability of nitrogen-15 and total nitrogen in some virgin and cultivated soils. *Soil Science Society of America Journal*, 44(3), pp.524-527.
- Bulletin of Chinese River Sediment (BCRS) (2000). Ministry of Water Resources Conservancy. Beijing, China. Available at: <http://www.mwr.gov.cn/xygb/hlnsgb/index.aspx>. (in Chinese).
- Camacho, A., A. Picazo, C. Roquera, A. C. Santamans, D. Morant, J. Miralles-Lorenzo & A. Castillo-Escrivà, 2017. Methane emissions in Spanish saline lakes: current rates, temperature and salinity responses, and evolution under different climate change scenarios. *Water* 9: 659.
- Campeau, A., Wallin, M.B., Giesler, R., Löfgren, S., Mörrth, C.M., Schiff, S., Venkiteswaran, J.J. and Bishop, K., 2017. Multiple sources and sinks of dissolved inorganic carbon across Swedish streams, refocusing the lens of stable C isotopes. *Scientific Reports*, 7(1), p.9158.
- Canadell, J.G., Monteiro, P.M., Costa, M.H., Da Cunha, L.C., Cox, P.M., Eliseev, A.V., Henson, S., Ishii, M., Jaccard, S., Koven, C. and Lohila, A., 2021. Global carbon and other biogeochemical cycles and feedbacks.
- Caniani, D., Caivano, M., Pascale, R., Bianco, G., Mancini, I.M., Masi, S., Mazzone, G., Firouzian, M. and Rosso, D., 2019. CO₂ and N₂O from water resource recovery facilities: Evaluation of emissions from biological treatment, settling, disinfection, and receiving water body. *Science of the Total Environment*, 648, pp.1130-1140.
- Carpenter, S.R. and Lodge, D.M., 1986. Effects of submersed macrophytes on ecosystem processes. *Aquatic botany*, 26, pp.341-370.

- Catalán, N., Marcé, R., Kothawala, D.N. and Tranvik, L.J., 2016. Organic carbon decomposition rates controlled by water retention time across inland waters. *Nature Geoscience*, 9(7), pp.501-504.
- Central Pollution Control Board (CPCB) (2013). Pollution assessment: River Ganga. CPCB. Available at: <https://cpcb.nic.in>.
- Chakrapani, G.J. and Veizer, J., 2005. Dissolved inorganic carbon isotopic compositions in the Upstream Ganga river in the Himalayas. *Current Science*, 89(3), pp.553-556.
- Chang, H., Makido, Y., and Foster, E. (2021). Effects of land use change, wetland fragmentation, and best management practices on total suspended solids concentrations in an urbanizing Oregon watershed, USA. *J. Environ. Manag.* 282, 111962.
- Chapman, A. D. & C. L. Schelske, 1997. Recent appearance of cylindrospemopsis (Cyanobacteiua) in five hypereutrophic Florida lakes 1. *Journal of Phycology* 33: 191–195.
- Chapra, S.C., Dove, A. and Rockwell, D.C., 2009. Great Lakes chloride trends: long-term mass balance and loading analysis. *Journal of Great Lakes Research*, 35(2), pp.272-284
- Chen, J., Wang, F., Meybeck, M., He, D., Xia, X., and Zhang, L. (2005). Spatial and temporal analysis of water chemistry records (1958–2000) in the Huanghe (Yellow River) basin. *Glob. Biogeochem. cycles* 19 (3).
- Ciais, P., Sabine, C., Bala, G., Bopp, L., Brovkin, V., Canadell, J., Chhabra, A., DeFries, R., Galloway, J., Heimann, M. and Jones, C., 2014. Carbon and other biogeochemical cycles. In *Climate change 2013: the physical science basis. Contribution of Working Group I to the Fifth Assessment Report of the Intergovernmental Panel on Climate Change* (pp. 465-570). Cambridge University Press.
- Cole, J.J., Prairie, Y.T., Caraco, N.F., McDowell, W.H., Tranvik, L.J., Striegl, R.G., Duarte, C.M., Kortelainen, P., Downing, J.A., Middelburg, J.J. and Melack, J., 2007. Plumbing the global carbon cycle: integrating inland waters into the terrestrial carbon budget. *Ecosystems*, 10, pp.172-185.
- Conway, W. C., L. M. Smith & J. D. Ray, 2005. Shorebird breeding biology in wetlands of the playa lakes, Texas, USA. *Waterbirds* 28: 129–138.
- Coppola, A.I. and Druffel, E.R., 2016. Cycling of black carbon in the ocean. *Geophysical Research Letters*, 43(9), pp.4477-4482.
- Coppola, A.I., Wagner, S., Lennartz, S.T., Seidel, M., Ward, N.D., Dittmar, T., Santín, C. and Jones, M.W., 2022. The black carbon cycle and its role in the Earth system. *Nature Reviews Earth & Environment*, pp.1-17.
- Coppola, A.I., Wiedemeier, D.B., Galy, V., Haghypour, N., Hanke, U.M., Nascimento, G.S., Usman, M., Blattmann, T.M., Reisser, M., Freymond, C.V. and Zhao, M.,

2018. Global-scale evidence for the refractory nature of riverine black carbon. *Nature Geoscience*, 11(8), pp.584-588.
- Coppola, A.I., Ziolkowski, L.A., Masiello, C.A. and Druffel, E.R., 2014. Aged black carbon in marine sediments and sinking particles. *Geophysical Research Letters*, 41(7), pp.2427-2433.
- Corsi, S.R., Graczyk, D.J., Geis, S.W., Booth, N.L. and Richards, K.D., 2010. A fresh look at road salt: aquatic toxicity and water-quality impacts on local, regional, and national scales. *Environmental science & technology*, 44(19), pp.7376-7382
- Cotovicz Jr, L.C., Knoppers, B.A., Brandini, N., Poirier, D., Costa Santos, S.J. and Abril, G., 2016. Spatio-temporal variability of methane (CH₄) concentrations and diffusive fluxes from a tropical coastal embayment surrounded by a large urban area (Guanabara Bay, Rio de Janeiro, Brazil). *Limnology and Oceanography*, 61(S1), pp.S238-S252.
- Daims, H., Lebedeva, E.V., Pjevac, P., Han, P., Herbold, C., Albertsen, M., Jehmlich, N., Palatinszky, M., Vierheilig, J., Bulaev, A. and Kirkegaard, R.H., 2015. Complete nitrification by *Nitrospira* bacteria. *Nature*, 528(7583), pp.504-509.
- Das, A., Krishnaswami, S. and Bhattacharya, S.K., 2005. Carbon isotope ratio of dissolved inorganic carbon (DIC) in rivers draining the Deccan Traps, India: sources of DIC and their magnitudes. *Earth and Planetary Science Letters*, 236(1-2), pp.419-429.
- Dasari, S., Andersson, A., Stohl, A., Evangeliou, N., Bikkina, S., Holmstrand, H., Budhavant, K., Salam, A. and Gustafsson, O., 2020. Source quantification of South Asian black carbon aerosols with isotopes and modeling. *Environmental science & technology*, 54(19), pp.11771-11779.
- Davidson, E.A., 2009. The contribution of manure and fertilizer nitrogen to atmospheric nitrous oxide since 1860. *Nature Geoscience*, 2(9), pp.659-662.
- de Tezanos Pinto, P. and O'Farrell, I., 2014. Regime shifts between free-floating plants and phytoplankton: a review. *Hydrobiologia*, 740, pp.13-24.
- Deemer, B.R., Harrison, J.A., Li, S., Beaulieu, J.J., DelSontro, T., Barros, N., Bezerra-Neto, J.F., Powers, S.M., Dos Santos, M.A. and Vonk, J.A., 2016. Greenhouse gas emissions from reservoir water surfaces: a new global synthesis. *BioScience*, 66(11), pp.949-964.
- Delwiche, C. C. & P. L. Steyn, 1970. Nitrogen isotope fractionation in soils and microbial reactions. *Environmental Science & Technology* 4: 929–935.
- Deocampo, D. M. & R. W. Renaut, 2016. Geochemistry of African soda lakes. In Schagerl, M. (ed), *Soda Lakes of East Africa* Springer, Cham: 77–93.
- Deshmukh, G. P., & V. Rai, 1991. Some observations on the origin of saline lakes/ranns of Rajasthan, India. *Proceedings of Quaternary Landscape of Indian Sub-Continent*, MS University, Baroda, Geology Department: 41–47.
- Dessborn, L., R. Hessel & J. Elmerg, 2016. Geese as vectors of nitrogen and phosphorus to freshwater systems. *Inland Waters* 6: 111–122.

- Dittmar, T., Hertkorn, N., Kattner, G. and Lara, R.J., 2006. Mangroves, a major source of dissolved organic carbon to the oceans. *Global biogeochemical cycles*, 20(1).
- Dlugokencky, E. and Tans, P., 2022. Trends in atmospheric carbon dioxide, National Oceanic and Atmospheric Administration, Global Monitoring Laboratory (NOAA/GML).
- Doering, P.H., Oviatt, C.A., Nowicki, B.L., Klos, E.G. and Reed, L.W., 1995. Phosphorus and nitrogen limitation of primary production in a simulated estuarine gradient. *Marine Ecology Progress Series*, 124, pp.271-287
- Duarte, C. M., Y. T. Prairie, C. Montes, J. J. Cole, R. Striegl, J. Melack & J. A. Downing, 2008. CO₂ emissions from saline lakes: a global estimate of a surprisingly large flux. *Journal of Geophysical Research: Biogeosciences*.
- Dugdale, R. and Wilkerson, F., 1992. Nutrient limitation of new production in the sea. In *Primary productivity and biogeochemical cycles in the sea* (pp. 107-122). Boston, MA: Springer US.
- Dunne, T., and Ongweny, G. S. O. (1976). A new estimate of sedimentation rates on the upper Tana River. *Kenyan Geogr.* 2 (2), 26–109.
- Ehleringer, J. R. (1978). Implications of quantum yield differences on the distributions of C₃ and C₄ grasses. *Oecologia* 31 (3), 255–267.
- Ehleringer, J., and Pearcy, R. W. (1983). Variation in quantum yield for CO₂ uptake among C₃ and C₄ plants. *Plant Physiol.* 73 (3), 555–559.
- Ellis, E. E., Keil, R. G., Ingalls, A. E., Richey, J. E., and Alin, S. R. (2012). Seasonal variability in the sources of particulate organic matter of the Mekong River as discerned by elemental and lignin analyses. *J. Geophys. Res. Biogeosciences* 117 (G1).
- Elmquist, M., Cornelissen, G., Kukulska, Z. and Gustafsson, Ö., 2006. Distinct oxidative stabilities of char versus soot black carbon: Implications for quantification and environmental recalcitrance. *Global biogeochemical cycles*, 20(2).
- Epstein, S. & T. Mayeda, 1953. Variation of O¹⁸ content of waters from natural sources. *Geochimica Et Cosmochimica Acta* 4: 213–224.
- Estep, M. L. F. & S. Vigg, 1985. Stable carbon and nitrogen isotope tracers of trophic dynamics in natural populations and fisheries of the Lahontan Lake system, Nevada. *Canadian Journal of Fisheries and Aquatic Sciences* 42: 1712–1719.
- Eugster, H. P. & L. A. Hardie, 1978. Saline lakes. In Lerman, A. (ed), *Lakes: Chemistry, Geology, and Physics*. Springer, New York.
- Evans, M. and Frick, C., 2001. The effects of road salts on aquatic ecosystems.
- Fang, Y., Chen, Y., Hu, L., Tian, C., Luo, Y., Li, J., Zhang, G., Zheng, M. and Lin, T., 2019. Large-river dominated black carbon flux and budget: a case study of the estuarine-inner shelf of East China Sea, China. *Science of the Total Environment*, 651, pp.2489-2496.

- Fang, Y., Chen, Y., Huang, G., Hu, L., Tian, C., Xie, J., Lin, J. and Lin, T., 2020. Particulate and dissolved black carbon in coastal China seas: Spatiotemporal variations, dynamics, and potential implications. *Environmental Science & Technology*, 55(1), pp.788-796.
- Fang, Y., Chen, Y., Lin, T., Hu, L., Tian, C., Luo, Y., Yang, X., Li, J. and Zhang, G., 2018. Spatiotemporal trends of elemental carbon and char/soot ratios in five sediment cores from Eastern China Marginal Seas: indicators of anthropogenic activities and transport patterns. *Environmental science & technology*, 52(17), pp.9704-9712.
- Fang, Y., Chen, Y., Tian, C., Lin, T., Hu, L., Huang, G., Tang, J., Li, J. and Zhang, G., 2015. Flux and budget of BC in the continental shelf seas adjacent to Chinese high BC emission source regions. *Global Biogeochemical Cycles*, 29(7), pp.957-972.
- Fang, Y., Chen, Y., Tian, C., Wang, X., Lin, T., Hu, L., Li, J., Zhang, G. and Luo, Y., 2018. Cycling and budgets of organic and black carbon in coastal Bohai Sea, China: impacts of natural and anthropogenic perturbations. *Global Biogeochemical Cycles*, 32(6), pp.971-986.
- Fang, Y., Huang, G., Chen, Y., Hu, L., Lin, J. and Lin, T., 2021. Particulate and Dissolved Black Carbon in Bohai and Laizhou Bays, China: Distributions, Sources, and Contrasts Under Two Distinct Fluvial Hydrological Regimes. *Frontiers in Earth Science*, p.729
- Fang, Z., Yang, W., Chen, M., Zheng, M. and Hu, W., 2016. Abundance and sinking of particulate black carbon in the western Arctic and Subarctic Oceans. *Scientific Reports*, 6(1), pp.1-11.
- Fellbaum, C.R., Gachomo, E.W., Beesetty, Y., Choudhari, S., Strahan, G.D., Pfeffer, P.E., Kiers, E.T. and Bücking, H., 2012. Carbon availability triggers fungal nitrogen uptake and transport in arbuscular mycorrhizal symbiosis. *Proceedings of the National Academy of Sciences*, 109(7), pp.2666-2671.
- Findlay, S.E. and Kelly, V.R., 2011. Emerging indirect and long-term road salt effects on ecosystems. *Annals of the New York Academy of Sciences*, 1223(1), pp.58-68.
- Flores-Cervantes, D.X., Plata, D.L., MacFarlane, J.K., Reddy, C.M. and Gschwend, P.M., 2009. Black carbon in marine particulate organic carbon: Inputs and cycling of highly recalcitrant organic carbon in the Gulf of Maine. *Marine Chemistry*, 113(3-4), pp.172-181.
- Forbes, M.S., Raison, R.J. and Skjemstad, J.O., 2006. Formation, transformation and transport of black carbon (charcoal) in terrestrial and aquatic ecosystems. *Science of the total environment*, 370(1), pp.190-206.
- Forster, P., Ramaswamy, V., Artaxo, P., Berntsen, T., Betts, R., Fahey, D.W., Haywood, J., Lean, J., Lowe, D.C., Myhre, G. and Nganga, J., 2007. Changes in atmospheric constituents and in radiative forcing. *Climate Change 2007: The Physical Science Basis. Contribution of Working Group I to the 4th Assessment Report of the Intergovernmental Panel on Climate Change*.

- Friedlingstein, P., O'sullivan, M., Jones, M.W., Andrew, R.M., Gregor, L., Hauck, J., Le Quéré, C., Luijkx, I.T., Olsen, A., Peters, G.P. and Peters, W., 2022. Global carbon budget 2022. *Earth System Science Data Discussions*, 2022, pp.1-159.
- Fry, B., 2006. *Stable isotope ecology* (Vol. 521, p. 318). New York: Springer.
- Galloway, J.N., 2005. The global nitrogen cycle: Past, present and future. *Science in China Series C: Life Sciences*, 48, pp.669-678.
- Gao, X., Shi, Y., Han, Z., Wang, M., Wu, J., Zhang, D., et al. (2017). Performance of RegCM4 over major river basins in China. *Adv. Atmos. Sci.* 34 (4), 441–455.
- Garnier, J., Vilain, G., Silvestre, M., Billen, G., Jehanno, S., Poirier, D., Martinez, A., Decuq, C., Cellier, P. and Abril, G., 2013. Budget of methane emissions from soils, livestock and the river network at the regional scale of the Seine basin (France). *Biogeochemistry*, 116, pp.199-214.
- Gat, J. R., & R. Gonfanti, 1981. Stable isotope hydrology: deuterium and oxygen-18 in the water cycle. Technical reports series No. 210. Retrieved from https://inis.iaea.org/search/search.aspx?orig_q=RN:13677657
- Giresse, P., and Maley, J. (1998). The dynamic of organic carbon in South Cameroon: Fluxes in a tropical River system and a lake system as a varying sink on a glacial interglacial time scale. *Glob. Planet. Change* 16, 53–74.
- Glassom, D. & G. M. Branch, 1997. Impact of predation by greater flamingos *Phoenicopterus ruber* on the macrofauna of two southern African lagoons. *Marine Ecology Progress Series* 149: 1–12.
- Glibert, P.M., Wilkerson, F.P., Dugdale, R.C., Raven, J.A., Dupont, C.L., Leavitt, P.R., Parker, A.E., Burkholder, J.M. and Kana, T.M., 2016. Pluses and minuses of ammonium and nitrate uptake and assimilation by phytoplankton and implications for productivity and community composition, with emphasis on nitrogen-enriched conditions. *Limnology and Oceanography*, 61(1), pp.165-197.
- Goldberg, E.D., 1985. *Black carbon in the environment: properties and distribution*.
- Gondwe, M. J., S. J. Guildford & R. E. Hecky, 2008. Planktonic nitrogen fixation in Lake Malawi/Nyasa. *Hydrobiologia* 596: 251–267.
- Goni, M.A., Aceves, H.L., Thunell, R.C., Tappa, E., Black, D., Astor, Y., Varela, R. and Muller-Karger, F., 2003. Biogenic fluxes in the Cariaco Basin: a combined study of sinking particulates and underlying sediments. *Deep Sea Research Part I: Oceanographic Research Papers*, 50(6), pp.781-807.
- Grasshoff, K., Ehrhardt, M., and Kremling, K.: *Methods of Seawater Analysis*, 2nd Edn., Weinheim, Verlag Chemie, 1983.
- Grey, J., R. I. Jones & D. Sleep, 2001. Seasonal changes in the importance of the source of organic matter to the diet of zooplankton in Loch Ness, as indicated by stable isotope analysis. *Limnology and Oceanography* 46: 505–513.
- Grill, G., Lehner, B., Thieme, M., Geenen, B., Tickner, D., Antonelli, F., Babu, S., Borrelli, P., Cheng, L., Crochetiere, H. and Ehalt Macedo, H., 2019. Mapping the world's free-flowing rivers. *Nature*, 569(7755), pp.215-221.

- Gross, M., 2017. The world's vanishing lakes. Elsevier.
- Gu, B. & V. Alexander, 1993. Estimation of N₂ fixation based on differences in the natural abundance of ¹⁵N among freshwater N₂-fixing and non- N₂-fixing algae. *Oecologia* 96: 43–48.
- Gu, B. & V. Alexander, 1996. Stable carbon isotope evidence for atmospheric CO₂ uptake by cyanobacterial surface scums in a Eutrophic lake. *Applied and Environmental Microbiology* 62: 1803–1804.
- Gu, B., 2009. Variations and controls of nitrogen stable isotopes in particulate organic matter of lakes. *Oecologia* 160:421–431.
- Gu, B., A. D. Chapman & C. L. Schelske, 2006. Factors controlling seasonal variations in stable isotope composition of particulate organic matter in a soft water eutrophic lake. *Limnology and Oceanography* 51: 2837–2848.
- Gu, B., C. L. Schelske & M. N. Waters, 2011. Patterns and controls of seasonal variability of carbon stable isotopes of particulate organic matter in lakes. *Oecologia* 165:1083–1094.
- Gulev, S.K., Thorne, P.W., Ahn, J., Dentener, F.J., Domingues, C.M., Gerland, S., Gong, D., Kaufman, D.S., Nnamchi, H.C., Quaas, J. and Rivera, J.A., 2021. Changing state of the climate system.
- Gupta, G.V.M., Sudheesh, V., Sudharma, K.V., Saravanane, N., Dhanya, V., Dhanya, K.R., Lakshmi, G., Sudhakar, M. and Naqvi, S.W.A., 2016. Evolution to decay of upwelling and associated biogeochemistry over the southeastern Arabian Sea shelf. *Journal of Geophysical Research: Biogeosciences*, 121(1), pp.159-175.
- Gustafsson, Ö., Bucheli, T.D., Kukulska, Z., Andersson, M., Largeau, C., Rouzaud, J.N., Reddy, C.M. and Eglinton, T.I., 2001. Evaluation of a protocol for the quantification of black carbon in sediments. *Global Biogeochemical Cycles*, 15(4), pp.881-890.
- Hahn, S., S. Bauer & M. Klaassen, 2008. Quantification of allochthonous nutrient input into freshwater bodies by herbivorous waterbirds. *Freshwater Biology* 53: 181–193.
- Hahn, Stefen, S. Bauer & M. Klaassen, 2007. Estimating the contribution of carnivorous waterbirds to nutrient loading in freshwater habitats. *Freshwater Biology* 52: 2421–2433.
- Hammer, U. T., 1981. Primary production in saline lakes. In Williams, W. D. (ed), *Salt Lakes* Springer, Dordrecht:47–57.
- Harrison, J.A., Maranger, R.J., Alexander, R.B., Giblin, A.E., Jacinthe, P.A., Mayorga, E., Seitzinger, S.P., Sobota, D.J. and Wollheim, W.M., 2009. The regional and global significance of nitrogen removal in lakes and reservoirs. *Biogeochemistry*, 93, pp.143-157.
- Havens, K. E., E. J. Philips, M. F. Cichra & B. Li, 1998. Light availability as a possible regulator of cyanobacteria species composition in a shallow subtropical lake. *Freshwater Biology* 39: 547–556.

- He, Y., Wang, X., Chen, H., Yuan, X., Wu, N., Zhang, Y., Yue, J., Zhang, Q., Diao, Y. and Zhou, L., 2017. Effect of watershed urbanization on N₂O emissions from the Chongqing metropolitan river network, China. *Atmospheric Environment*, 171, pp.70-81.
- Herbert, E.R., Boon, P., Burgin, A.J., Neubauer, S.C., Franklin, R.B., Ardón, M., Hopfensperger, K.N., Lamers, L.P. and Gell, P., 2015. A global perspective on wetland salinization: ecological consequences of a growing threat to freshwater wetlands. *Ecosphere*, 6(10), pp.1-43.
- Hillebrand, G., Hardenbicker, P., Fischer, H., Otto, W. and Vollmer, S., 2018. Dynamics of total suspended matter and phytoplankton loads in the river Elbe. *Journal of Soils and Sediments*, 18, pp.3104-3113.
- Hilt, S., Brothers, S., Jeppesen, E., Veraart, A.J. and Kosten, S., 2017. Translating regime shifts in shallow lakes into changes in ecosystem functions and services. *BioScience*, 67(10), pp.928-936.
- Hoering, T. C. & H. T. Ford, 1960. The isotope effect in the fixation of nitrogen by azotobacter. *Journal of the American Chemical Society* 82: 376–378.
- Hope, D., Billett, M. F., and Cresser, M. S. (1994). A review of the export of carbon in river water: Fluxes and processes. *Environ. Pollut.* 84 (3), 301–324.
- Hopkinson, C. S., Buffam, I., Hobbie, J., Vallino, J., Perdue, M., Eversmeyer, B., et al. (1998). Terrestrial inputs of organic matter to coastal ecosystems: An intercomparison of chemical characteristics and bioavailability. *Biogeochemistry* 43 (3), 211–234.
- Horsfield, B., Curry, D.J., Bohacs, K., Littke, R., Rullkötter, J., Schenk, H.J., Radke, M., Schaefer, R.G., Carroll, A.R., Isaksen, G. and Witte, E.G., 1994. Organic geochemistry of freshwater and alkaline lacustrine sediments in the Green River Formation of the Washakie Basin, Wyoming, USA. *Organic Geochemistry* 22: 415–440.
- Hu, B., Wang, D., Zhou, J., Meng, W., Li, C., Sun, Z., Guo, X. and Wang, Z., 2018. Greenhouse gases emission from the sewage draining rivers. *Science of the Total Environment*, 612, pp.1454-1462.
- Huang, C., Lu, L., Li, Y., He, Y., Shang, N., Bai, Y., Yu, H., Huang, T., Zhu, A.X., Yang, H. and Zhao, K., 2021. Anthropogenic-driven alterations in black carbon sequestration and the structure in a deep plateau lake. *Environmental science & technology*, 55(9), pp.6467-6475.
- Huang, G. & M. Isobe, 2012. Carrying capacity of wetlands for massive migratory waterfowl. *Hydrobiologia* 697: 5–14.
- Hulthe, G., S. Hulth & P. O. J. Hall, 1998. Effect of oxygen on degradation rate of refractory and labile organic matter in continental margin sediments. *Geochimica Et Cosmochimica Acta* 62: 1319–1328.
- Humborg, C., MÖRTH, C.M., Sundbom, M., Borg, H., Blenckner, T., Giesler, R. and Ittekkot, V., 2010. CO₂ supersaturation along the aquatic conduit in Swedish watersheds as constrained by terrestrial respiration, aquatic respiration and weathering. *Global Change Biology*, 16(7), pp.1966-1978.

- Hunter, H. M., and Walton, R. S. (2008). Land-use effects on fluxes of suspended sediment, nitrogen and phosphorus from a river catchment of the Great Barrier Reef, Australia. *J. hydrology* 356 (1-2), 131–146.
- Iglesias, M.C.A., 2020. A review of recent advances and future challenges in freshwater salinization. *Limnetica*, 39(1), pp.185-211.
- Isaji, Y., H. Kawahata, N. O. Ogawa, J. Kuroda, T. Yoshimura & F. J. Jiménez-Espejo, 2019a. Efficient recycling of nutrients in modern and past hypersaline environments. *Scientific Reports* 9: 1–12.
- Isaji, Y., H. Kawahata, Y. Takano, N. O. Ogawa, J. Kuroda, T. Yoshimura, S. Lugli, V. Manzi, M. Roveri & N. Ohkouchi, 2019c. Diazotrophy drives primary production in the organic-rich shales deposited under a stratified environment during the Messinian salinity crisis (Vena Del Gesso, Italy). *Frontiers in Earth Science* 7: 85.
- Isaji, Y., T. Yoshimura, D. Araoka, J. Kuroda, N. O. Ogawa, H. Kawahata & N. Ohkouchi, 2019b. Magnesium isotope fractionation during synthesis of chlorophyll a and bacteriochlorophyll a of benthic phototrophs in hypersaline environments. *ACS Earth and Space Chemistry* 3:1073–1079.
- Ittekkot, V. (1988). Global trends in the nature of organic matter in river suspensions. *Nature* 332 (6163), 436–438.
- Ittekkot, V. and Zhang, S., 1989. Pattern of particulate nitrogen transport in world rivers. *Global Biogeochemical Cycles*, 3(4), pp.383-391.
- Jaffé, R., Ding, Y., Niggemann, J., Vähätalo, A.V., Stubbins, A., Spencer, R.G., Campbell, J. and Dittmar, T., 2013. Global charcoal mobilization from soils via dissolution and riverine transport to the oceans. *Science*, 340(6130), pp.345-347
- Janssen, A.B., Hilt, S., Kosten, S., de Klein, J.J., Paerl, H.W. and Van de Waal, D.B., 2021. Shifting states, shifting services: Linking regime shifts to changes in ecosystem services of shallow lakes. *Freshwater Biology*, 66(1), pp.1-12.
- Jellison, R., R. F. Anderson, J. M. Melack & D. Heil, 1996. Organic matter accumulation in sediments of hypersaline Mono Lake during a period of changing salinity. *Limnology and Oceanography* 41: 1539–1544.
- Jellison, R., W. D. Williams, B. Timms, J. Alcocer & N. V. Aladin, 2008. Salt lakes: values, threats and future. In Polunin, N. V. C. (ed), *Aquatic Ecosystems: Trends and Global Prospects* Cambridge University Press, Cambridge: 94–110.
- Jeppesen, E., Meerhoff, M., Davidson, T., Trolle, D., Sondergaard, M., Lauridsen, T., Beklioglu, M., Brucet, S., Volta, P., González-Bergonzoni, I. and Nielsen, A., 2014. Climate change impacts on lakes: an integrated ecological perspective based on a multi-faceted approach, with special focus on shallow lakes. *Journal of Limnology*, 73.
- Jin, H., Yoon, T.K., Begum, M.S., Lee, E.J., Oh, N.H., Kang, N. and Park, J.H., 2018. Longitudinal discontinuities in riverine greenhouse gas dynamics generated by dams and urban wastewater. *Biogeosciences*, 15(20), pp.6349-6369.

- Johnson, K.M., Sieburth, J.M., leB Williams, P.J. and Brändström, L., 1987. Coulometric total carbon dioxide analysis for marine studies: automation and calibration. *Marine Chemistry*, 21(2), pp.117-133.
- Jones, B.F. and Deocampo, D.M., 2003. Geochemistry of saline lakes. *Treatise on geochemistry*, 5, p.605.
- Jones, M.W., Coppola, A.I., Santín, C., Dittmar, T., Jaffé, R., Doerr, S.H. and Quine, T.A., 2020. Fires prime terrestrial organic carbon for riverine export to the global oceans. *Nature communications*, 11(1), pp.1-8.
- Jones, N.E., 2010. Incorporating lakes within the river discontinuum: longitudinal changes in ecological characteristics in stream–lake networks. *Canadian Journal of Fisheries and Aquatic Sciences*, 67(8), pp.1350-1362.
- Jones, R.I., King, L., Dent, M.M., Maberly, S.C. and Gibson, C.E., 2004. Nitrogen stable isotope ratios in surface sediments, epilithon and macrophytes from upland lakes with differing nutrient status. *Freshwater Biology* 49: 382–391.
- Jurado, E., Dachs, J., Duarte, C.M. and Simo, R., 2008. Atmospheric deposition of organic and black carbon to the global oceans. *Atmospheric Environment*, 42(34), pp.7931-7939.
- Kamp, A., Høgslund, S., Risgaard-Petersen, N. and Stief, P., 2015. Nitrate storage and dissimilatory nitrate reduction by eukaryotic microbes. *Frontiers in microbiology*, 6, p.1492.
- Karthik, V., Bhaskar, B.V., Ramachandran, S. and Kumar, P., 2023. Black carbon flux in terrestrial and aquatic environments of Kodaikanal in the Western Ghats, South India: Estimation, source identification, and implication. *Science of the Total Environment*, 854, p.158647.
- Kaushal, S.S., Likens, G.E., Pace, M.L., Reimer, J.E., Maas, C.M., Galella, J.G., Utz, R.M., Duan, S., Kryger, J.R., Yaculak, A.M. and Boger, W.L., 2021. Freshwater salinization syndrome: From emerging global problem to managing risks. *Biogeochemistry*, 154, pp.255-292.
- Keil, R.G. and Mayer, L.M., 2014. Mineral matrices and organic matter. *Treatise on geochemistry*, pp.337-359.
- Keller, P.S., Catalan, N., von Schiller, D., Grossart, H.P., Koschorreck, M., Obrador, B., Frassl, M.A., Karakaya, N., Barros, N., Howitt, J.A. and Mendoza-Lera, C., 2020. Global CO₂ emissions from dry inland waters share common drivers across ecosystems. *Nature communications*, 11(1), p.2126.
- Kendall, C., Silva, S.R. and Kelly, V.J., 2001. Carbon and nitrogen isotopic compositions of particulate organic matter in four large river systems across the United States. *Hydrological processes*, 15(7), pp.1301-1346.
- Kim, D., Begum, M.S., Choi, J., Jin, H., Chea, E. and Park, J.H., 2019. Comparing effects of untreated and treated wastewater on riverine greenhouse gas emissions. *APN Science Bulletin*.

- King, D. and Nedwell, D.B., 1985. The influence of nitrate concentration upon the end-products of nitrate dissimilation by bacteria in anaerobic salt marsh sediment. *FEMS Microbiology Ecology*, 1(1), pp.23-28.
- Kitchell, J. F., D. E. Schindler, B. R. Herwig, D. M. Post, M. H. Olson & M. Oldham, 1999. Nutrient cycling at the landscape scale: the role of diel foraging migrations by geese at the Bosque del Apache National Wildlife Refuge, New Mexico. *Limnology and Oceanography* 44: 828–836.
- Kitheka, J.U., Obiero, M. and Nthenge, P., 2005. River discharge, sediment transport and exchange in the Tana Estuary, Kenya. *Estuarine, Coastal and Shelf Science*, 63(3), pp.455-468.
- Kiyashko, SI, Richard, P., Chandler, T., Kozlova, TA and Williams, DF, 1998. Stable carbon isotope ratios differentiate autotrophs supporting animal diversity in Lake Baikal. *Comptes Rendus de l'Académie des Sciences-Series III-Life Sciences* , 321 (6), pp.509-516.
- Kleber, M., 2010. What is recalcitrant soil organic matter?. *Environmental Chemistry*, 7(4), pp.320-332.
- Kopprio, G. A., G. Kattner, R. H. Freije, S. J. de Paggi & R. J. Lara, 2014. Seasonal baseline of nutrients and stable isotopes in a saline lake of Argentina: biogeochemical processes and river runoff effects. *Environmental Monitoring and Assessment* 186: 3139–3148.
- Kortelainen, P., Larmola, T., Rantakari, M., Juutinen, S., Alm, J. and Martikainen, P.J., 2020. Lakes as nitrous oxide sources in the boreal landscape. *Global Change Biology*, 26(3), pp.1432-1445.
- Krishna, M.S., Viswanadham, R., Prasad, M.H., Kumari, V.R. and Sarma, V.V., 2019. Export fluxes of dissolved inorganic carbon to the northern Indian Ocean from the Indian monsoonal rivers. *Biogeosciences*, 16(2), pp.505-519.
- Kristensen, E., S. I. Ahmed & A. H. Devol, 1995. Aerobic and anaerobic decomposition of organic matter in marine sediment: which is fastest? *Limnology and Oceanography* 40: 1430–1437.
- Kumar, S., P. S. Bhavya, R. Ramesh, G. V. M. Gupta, F. Chiriboga, A. Singh, I. Karunasagar, A. Rai, A. S. RehnstamHolm, L. Edler & A. Godhe, 2018. Nitrogen uptake potential under different temperature-salinity conditions: implications for nitrogen cycling under climate change scenarios. *Marine Environmental Research* 141: 196–204.
- Kumar, S.P., Ramaiah, N., Gauns, M., Sarma, V.V.S.S., Muraleedharan, P.M., Raghukumar, S., Kumar, M.D. and Madhupratap, M., 2001. Physical forcing of biological productivity in the Northern Arabian Sea during the Northeast Monsoon. *Deep Sea Research Part II: Topical Studies in Oceanography*, 48(6-7), pp.1115-1126.
- Kuypers, M.M., Marchant, H.K. and Kartal, B., 2018. The microbial nitrogen-cycling network. *Nature Reviews Microbiology*, 16(5), pp.263-276.

- Langenegger, T., Vachon, D., Donis, D. and McGinnis, D.F., 2022. Methane oxidation dynamics in a stratified lake: Insights revealed from a mass balance and carbon stable isotopes. *Limnology and Oceanography*, 67(10), pp.2157-2173.
- Last, W. M., 1993. Rates of sediment deposition in a hypersaline lake in the northern Great Plains, western Canada. *International Journal of Salt Lake Research* 2: 47.
- Lees, A.C., Peres, C.A., Fearnside, P.M., Schneider, M. and Zuanon, J.A., 2016. Hydropower and the future of Amazonian biodiversity. *Biodiversity and conservation*, 25, pp.451-466.
- Lehmann, M. F., S. M. Bernasconi, J. A. McKenzie, A. Barbieri, M. Simona & M. Veronesi, 2004. Seasonal variation of the $\delta^{13}\text{C}$ and $\delta^{15}\text{N}$ of particulate and dissolved carbon and nitrogen in Lake Lugano: constraints on biogeochemical cycling in a eutrophic lake. *Limnology and Oceanography* 49(2): 415–429.
- Leigh, J.A. and Dodsworth, J.A., 2007. Nitrogen regulation in bacteria and archaea. *Annu. Rev. Microbiol.*, 61, pp.349-377.
- Leithold, E.L., Blair, N.E. and Perkey, D.W., 2006. Geomorphologic controls on the age of particulate organic carbon from small mountainous and upland rivers. *Global Biogeochemical Cycles*, 20(3).
- Leng, M.J., LAMB, A.L., HEATON, T.H., MARSHALL, J.D., WOLFE, B.B., JONES, M.D., HOLMES, J.A. and ARROWSMITH, C., 2006. Isotopes in lake sediments (pp. 147-184). Springer Netherlands.
- Li, S., Gu, S., Liu, W., Han, H., and Zhang, Q. (2008). Water quality in relation to land use and land cover in the upper Han River Basin, China. *Catena* 75 (2), 216–222.
- Li, X., Yao, H., Yu, Y., Cao, Y. and Tang, C., 2020. Greenhouse gases in an urban river: Trend, isotopic evidence for underlying processes, and the impact of in-river structures. *Journal of Hydrology*, 591, p.125290.
- Li, Y., Fu, C., Zeng, L., Zhou, Q., Zhang, H., Tu, C., Li, L. and Luo, Y., 2021. Black carbon contributes substantially to allochthonous carbon storage in deltaic vegetated coastal habitats. *Environmental science & technology*, 55(9), pp.6495-6504.
- Liang, B., Lehmann, J., Solomon, D., Sohi, S., Thies, J.E., Skjemstad, J.O., Luizao, F.J., Engelhard, M.H., Neves, E.G. and Wirrick, S., 2008. Stability of biomass-derived black carbon in soils. *Geochimica et Cosmochimica Acta*, 72(24), pp.6069-6078.
- Liang, X., Wang, B., Gao, D., Han, P., Zheng, Y., Yin, G., Dong, H., Tang, Y. and Hou, L., 2022. Nitrification regulates the spatiotemporal variability of N₂O emissions in a eutrophic lake. *Environmental Science & Technology*, 56(23), pp.17430-17442.
- Liu, J. and Han, G., 2021. Tracing Riverine particulate black carbon sources in Xijiang river Basin: insight from stable isotopic composition and Bayesian mixing model. *Water Research*, 194, p.116932.

- Lohmann, R., Bollinger, K., Cantwell, M., Feichter, J., Fischer-Bruns, I. and Zabel, M., 2009. Fluxes of soot black carbon to South Atlantic sediments. *Global biogeochemical cycles*, 23(1).
- Louchouart, P., Lucotte, M. and Farella, N., 1999. Historical and geographical variations of sources and transport of terrigenous organic matter within a large-scale coastal environment. *Organic Geochemistry*, 30(7), pp.675-699.
- Louchouart, P., Lucotte, M., Canuel, R., Gagne, J.P. and Richard, L.F., 1997. Sources and early diagenesis of lignin and bulk organic matter in the sediments of the Lower St. Lawrence Estuary and the Saguenay Fjord. *Marine Chemistry*, 58(1-2), pp.3-26.
- Lu, X.X., Zhang, S. and Xu, J., 2010. Climate change and sediment flux from the Roof of the World. *Earth Surface Processes and Landforms: The Journal of the British Geomorphological Research Group*, 35(6), pp.732-735.
- Ludwig, W., Probst, J.L. and Kempe, S., 1996. Predicting the oceanic input of organic carbon by continental erosion. *Global Biogeochemical Cycles*, 10(1), pp.23-41.
- Maavara, T., Lauerwald, R., Laruelle, G.G., Akbarzadeh, Z., Bouskill, N.J., Van Cappellen, P. and Regnier, P., 2019. Nitrous oxide emissions from inland waters: Are IPCC estimates too high?. *Global change biology*, 25(2), pp.473-488.
- Mackenzie, F.T., Ver, L.M. and Lerman, A., 2002. Century-scale nitrogen and phosphorus controls of the carbon cycle. *Chemical Geology*, 190(1-4), pp.13-32..
- Maeck, A., DelSontro, T., McGinnis, D.F., Fischer, H., Flury, S., Schmidt, M., Fietzek, P. and Lorke, A., 2013. Sediment trapping by dams creates methane emission hot spots. *Environmental science & technology*, 47(15), pp.8130-8137.
- Manny, B. A., W. C. Johnson & R. G. Wetzel, 1994. Nutrient additions by waterfowl to lakes and reservoirs: predicting their effects on productivity and water quality. In Kerekes, J. J. (ed), *Aquatic Birds in the Trophic Web of Lakes* Springer, Dordrecht: 121–132.
- Marcé, R., B. Obrador, L. Gómez-Gener, N. Catalán, M. Koschorreck, M. I. Arce, G. Singer & D. von Schiller, 2019. Emissions from dry inland waters are a blind spot in the global carbon cycle. *Earth-Science Reviews* 188: 240–248.
- Mari, X., Chu Van, T., Guinot, B., Brune, J., Lefebvre, J.P., Raimbault, P., Dittmar, T. and Niggemann, J., 2017. Seasonal dynamics of atmospheric and river inputs of black carbon, and impacts on biogeochemical cycles in Halong Bay, Vietnam. *Elementa: Science of the Anthropocene*, 5.
- Masiello, C.A. and Druffel, E.R., 2001. Carbon isotope geochemistry of the Santa Clara River. *Global Biogeochemical Cycles*, 15(2), pp.407-416.
- Masson-Delmotte, V.P., Zhai, P., Pirani, S.L., Connors, C., Péan, S., Berger, N., Caud, Y., Chen, L., Goldfarb, M.I. and Scheel Monteiro, P.M., 2021. *Ipcc, 2021: Summary for policymakers. in: Climate change 2021: The physical science basis. contribution of working group i to the sixth assessment report of the intergovernmental panel on climate change.*

- McKee, B., 2003. The transport, transformation, and fate of carbon in riverdominated ocean margins. In *Community Workshop Report*, <http://www.tulane.edu/~riomar>.
- Mehmood, M.A., Shafiq-ur-Rehman, A.R. and Ganie, S.A., 2017. Spatio-temporal changes in water quality of Jhelum River, Kashmir Himalaya. *Int J Environ Bioener*, 12(1), pp.1-29.
- Mekong River Commission (2005). Overview of the hydrology of the Mekong Basin. Vientiane: Mekong River Commission, 82.
- Melack, J. M., 1981. Photosynthetic activity of phytoplankton in tropical African soda lakes. In *Salt lakes*: 71–85. Springer.
- Mendonça, R., Müller, R.A., Clow, D., Verpoorter, C., Raymond, P., Tranvik, L.J. and Sobek, S., 2017. Organic carbon burial in global lakes and reservoirs. *Nature communications*, 8(1), p.1694.
- Meng, L., Hao, W., Zhao, C., Li, S., Xue, J., Li, J., Tu, L., Huang, T., Yang, H., Yu, Z. and Yuan, L., 2023. Anthropogenic Activities Generate High-Refractory Black Carbon along the Yangtze River Continuum. *Environmental Science & Technology*.
- Messenger, M. L., B. Lehner, G. Grill, I. Nedeva & O. Schmitt, 2016. Estimating the volume and age of water stored in global lakes using a geo-statistical approach. *Nature Communications* 7: 1–11.
- Meybeck, M., 1982. Carbon, nitrogen, and phosphorus transport by world rivers. *American journal of Science*, 282(4), pp.401-450.
- Meybeck, M., 1983. Atmospheric inputs and river transport of dissolved substances. *Dissolved loads of rivers and surface water quantity/quality relationships*, (141), pp.173-192.
- Meybeck, M. and Ragu, A., 1997. River discharges to the oceans: an assessment of suspended solids, major ions and nutrients (Vol. 245). Nairobi, Kenya: UNEP.
- Meyers, P.A., 1997. Organic geochemical proxies of paleoceanographic, paleolimnologic, and paleoclimatic processes. *Organic geochemistry*, 27(5-6), pp.213-250.
- Meyers, P. A., 1994. Preservation of source identification of sedimentary organic matter during and after deposition. *Chemical Geology* 144: 289–302.
- Meyers, Philip A., 2003. Applications of organic geochemistry to paleolimnological reconstructions: a summary of examples from the Laurentian Great Lakes. *Organic Geochemistry* 34: 261–289.
- Miao, C., Ni, J., Borthwick, A.G. and Yang, L., 2011. A preliminary estimate of human and natural contributions to the changes in water discharge and sediment load in the Yellow River. *Global and Planetary Change*, 76(3-4), pp.196-205.
- Miller, J.B. and Tans, P.P., 2003. Calculating isotopic fractionation from atmospheric measurements at various scales. *Tellus B: Chemical and Physical Meteorology*, 55(2), pp.207-214.

- Milliman, J. D., and Farnsworth, K. L. (2011). River discharge to the coastal ocean: A global synthesis. Cambridge University Press.
- Milliman, J.D. and Meade, R.H., 1983. World-wide delivery of river sediment to the oceans. *The Journal of Geology*, 91(1), pp.1-21.
- Milliman, J.D. and Syvitski, J.P., 1992. Geomorphic/tectonic control of sediment discharge to the ocean: the importance of small mountainous rivers. *The journal of Geology*, 100(5), pp.525-544.
- Milliman, J.D., Qinchun, X. and Zuosheng, Y., 1984. Transfer of particulate organic carbon and nitrogen from the Yangtze River to the ocean. *American Journal of Science*, 284(7), pp.824-834.
- Milucka, J., Kirf, M., Lu, L., Krupke, A., Lam, P., Littmann, S., Kuypers, M.M. and Schubert, C.J., 2015. Methane oxidation coupled to oxygenic photosynthesis in anoxic waters. *The ISME journal*, 9(9), pp.1991-2002.
- Mir, R.A. and Jeelani, G.H., 2015. Textural characteristics of sediments and weathering in the Jhelum River basin located in Kashmir Valley, western Himalaya. *Journal of the Geological Society of India*, 86, p
- Mir, R.A., Jeelani, G. and Dar, F.A., 2016. Spatio-temporal patterns and factors controlling the hydrogeochemistry of the river Jhelum basin, Kashmir Himalaya. *Environmental monitoring and assessment*, 188, pp.1-24.
- Mirzoyeva, N., L. Gulina, S. Gulin, O. Plotitsina, A. Stetsuk & S. Arkhipova, 2015. Radionuclides and mercury in the salt lakes of the Crimea. *Chinese Journal of Oceanology and Limnology* 33: 1413–1425.
- Mitra, S., Bianchi, T.S., McKee, B.A. and Sutula, M., 2002. Black carbon from the Mississippi River: Quantities, sources, and potential implications for the global carbon cycle. *Environmental science & technology*, 36(11), pp.2296-2302.
- Mohanty, B., Das, A., Mandal, R., Banerji, U. and Acharyya, S., 2021. Heavy Metals in Soils and Vegetation from Wastewater Irrigated Croplands Near Ahmedabad, Gujarat: Risk to Human Health. *Nature Environment & Pollution Technology*, 20(1).
- Mook, W. G., J. C. Bommerson & W. H. Staverman, 1974. Carbon isotope fractionation between dissolved bicarbonate and gaseous carbon dioxide. *Earth and Planetary Science Letters* 22: 169–176.
- MRC: Mekong River Commission (2019). State of the basin report 2018. Vientiane, Lao PDR.
- Müller, P. J. (1977). Ratios in Pacific deep-sea sediments: Effect of inorganic ammonium and organic nitrogen compounds sorbed by clays. *Geochimica Cosmochimica Acta* 41 (6), 765–776.
- Mwanake, R.M., Gettel, G.M., Aho, K.S., Namwaya, D.W., Masese, F.O., Butterbach-Bahl, K. and Raymond, P.A., 2019. Land use, not stream order, controls N₂O concentration and flux in the upper Mara River basin, Kenya. *Journal of Geophysical Research: Biogeosciences*, 124(11), pp.3491-3506.

- Naftz, D., C. Angeroth, T. Kenney, B. Waddell, N. Darnall & S. Silva, 2008. Anthropogenic influences on the input and biogeochemical cycling of nutrients and mercury in Great Salt Lake, Utah, USA. *Applied Geochemistry* 23:1731–1744.
- Naftz, D.L., W.P. Johnson, M. Freeman, K. Beisner, and X. Diez, 2008b. Estimation of selenium loads entering the south arm of Great Salt Lake, Utah. US Geological Survey scientific investigations report 5069. Retrieved from <https://pubs.usgs.gov/sir/2008/5069/>
- Nilsson, C. and Berggren, K., 2000. Alterations of riparian ecosystems caused by river regulation: Dam operations have caused global-scale ecological changes in riparian ecosystems. How to protect river environments and human needs of rivers remains one of the most important questions of our time. *BioScience*, 50(9), pp.783-792.
- Nissenbaum, A., 1993. *The Dead Sea—An Economic Resource for 10000 Years*, Springer, Dordrecht:
- O'Dwyer, M., Butman, D. E., Striegl, R. G., Dornblaser, M. M., Wickland, K. P., Kuhn, Oertel, C., Matschullat, J., Zurba, K., Zimmermann, F. and Erasmi, S., 2016. Greenhouse gas emissions from soils—A review. *Geochemistry*, 76(3), pp.327-352.
- Olden, J.D., 2016. Challenges and opportunities for fish conservation in dam-impacted waters. *Conservation of freshwater fishes*, pp.107-148.
- Oren, A., 1999. Bioenergetic aspects of halophilism. *Microbiology and Molecular Biology Reviews* 63: 334–348.
- Paerl, H. W. & M. L. Fogel, 1994. Isotopic characterization of atmospheric nitrogen inputs as sources of enhanced primary production in coastal Atlantic Ocean waters. *Marine Biology* 119: 635–645.
- Panneer Selvam, B., Natchimuthu, S., Arunachalam, L. and Bastviken, D., 2014. Methane and carbon dioxide emissions from inland waters in India—implications for large scale greenhouse gas balances. *Global change biology*, 20(11), pp.3397-3407.
- Paranaíba, J. R., R. Aben, N. Barros, G. Quadra, A. Linkhorst, A. M. Amado, S. Brothers, N. Catalán, J. Condon, C. M. Finlayson & H. P. Grossart, 2022. Cross-continental importance of CH₄ emissions from dry inland-waters. *Science of the Total Environment* 814: 151925.
- Park, J. H., Nayna, O. K., Begum, M. S., Chea, E., Hartmann, J., Keil, R. G., et al. (2018). Reviews and syntheses: Anthropogenic perturbations to carbon fluxes in Asian river systems—concepts, emerging trends, and research challenges. *Biogeosciences* 15 (9),3049–3069.
- Parua, P. K. (2010). *The Ganga: Water use in the Indian subcontinent*(vol 64). Springer Science & Business Media.
- Patel, L., Singh, R. and Thottathil, S.D., 2023. Land use drivers of riverine methane dynamics in a tropical river basin, India. *Water Research*, 228, p.119380.

- Peng, J., Chen, S., and Dong, P. (2010). Temporal variation of sediment load in the Yellow River basin, China, and its impacts on the lower reaches and the river delta. *Catena* 83 (2-3), 135–147.
- Pickard, A., White, S., Bhattacharyya, S., Carvalho, L., Dobel, A., Drewer, J., Jamwal, P. and Helfter, C., 2021. Greenhouse gas budgets of severely polluted urban lakes in India. *Science of the Total Environment*, 798, p.149019.
- Pocklington, R., and Tan, F. C. (1987). Seasonal and annual variations in the organic matter contributed by the St Lawrence River to the Gulf of St. Lawrence. *Geochimica Cosmochimica Acta* 51 (9), 2579–2586.
- Post, D. M., J. P. Taylor, J. F. Kitchell, M. H. Olson, D. E. Schindler & B. R. Herwig, 1998. The role of migratory waterfowl as nutrient vectors in a managed wetland. *Conservation Biology* 12: 910–920.
- Prasad, S., Kusumgar, S. and Gupta, S.K., 1997. A mid to late Holocene record of palaeoclimatic changes from Nal Sarovar: a palaeodesert margin lake in western India. *Journal of Quaternary Science: Published for the Quaternary Research Association*, 12(2), pp.153-159.
- Premke, K., Dharanivasan, G., Steger, K., Nitzsche, K.N., Jayavignesh, V., Nambi, I.M. and Seshadri, S., 2020. Anthropogenic Impact on Tropical Perennial River in South India: Snapshot of Carbon Dynamics and Bacterial Community Composition. *Water*, 12(5), p.1354.
- Pyle, L.A., Magee, K.L., Gallagher, M.E., Hockaday, W.C. and Masiello, C.A., 2017. Short-term changes in physical and chemical properties of soil charcoal support enhanced landscape mobility. *Journal of Geophysical Research: Biogeosciences*, 122(11), pp.30
- Qi, Y., Fu, W., Tian, J., Luo, C., Shan, S., Sun, S., Ren, P., Zhang, H., Liu, J., Zhang, X. and Wang, X., 2020. Dissolved black carbon is not likely a significant refractory organic carbon pool in rivers and oceans. *Nature Communications*, 11(1), p.5051.
- Qian, N., and Dai, D. Z. (1980). “The problems of river sedimentation and the present status of its research in China,” in *Proceedings of the International Symposium on River Sedimentation*. Guanghua Press 24 (29), 19–39.
- Qu, B., Aho, K.S., Li, C., Kang, S., Sillanpää, M., Yan, F. and Raymond, P.A., 2017. Greenhouse gases emissions in rivers of the Tibetan Plateau. *Scientific Reports*, 7(1), p.16573.
- Qu, Y., Jin, Z., Wang, J., Wang, Y., Xiao, J., Gou, L. F., et al. (2020). The sources and seasonal fluxes of particulate organic carbon in the Yellow River. *Earth Surf. Process. Landforms* 45 (9), 2004–2019.
- Quick, A.M., Reeder, W.J., Farrell, T.B., Tonina, D., Feris, K.P. and Benner, S.G., 2019. Nitrous oxide from streams and rivers: A review of primary biogeochemical pathways and environmental variables. *Earth-Science Reviews*, 191, pp.224-262.

- Ran, L., Lu, X.X., Sun, H., Han, J., Li, R. and Zhang, J., 2013. Spatial and seasonal variability of organic carbon transport in the Yellow River, China. *Journal of Hydrology*, 498, pp.76-88.
- Rather, M.I., Rashid, I., Shahi, N., Murtaza, K.O., Hassan, K., Yousuf, A.R., Romshoo, S.A. and Shah, I.Y., 2016. Massive land system changes impact water quality of the Jhelum River in Kashmir Himalaya. *Environmental Monitoring and Assessment*, 188, pp.1-20.
- Raymond, P.A., Saiers, J.E. and Sobczak, W.V., 2016. Hydrological and biogeochemical controls on watershed dissolved organic matter transport: Pulse-shunt concept. *Ecology*, 97(1), pp.5-16.
- Reay, D.S., Davidson, E.A., Smith, K.A., Smith, P., Melillo, J.M., Dentener, F. and Crutzen, P.J., 2012. Global agriculture and nitrous oxide emissions. *Nature climate change*, 2(6), pp.410-416.
- Reddy, S.K.K., Gupta, H. and Reddy, D.V., 2019. Dissolved inorganic carbon export by mountainous tropical rivers of the Western Ghats, India. *Chemical Geology*, 530, p.119316.
- Reddy, S.K.K., Gupta, H., Badimela, U., Reddy, D.V., Kurakalva, R.M. and Kumar, D., 2021. Export of particulate organic carbon by the mountainous tropical rivers of Western Ghats, India: Variations and controls. *Science of The Total Environment*, 751, p.142115.
- Reid, A.J., Carlson, A.K., Creed, I.F., Eliason, E.J., Gell, P.A., Johnson, P.T., Kidd, K.A., MacCormack, T.J., Olden, J.D., Ormerod, S.J. and Smol, J.P., 2019. Emerging threats and persistent conservation challenges for freshwater biodiversity. *Biological Reviews*, 94(3), pp.849-873.
- Richardson, D.C., Holgerson, M.A., Farragher, M.J., Hoffman, K.K., King, K.B., Alfonso, M.B., Andersen, M.R., Cheruveil, K.S., Coleman, K.A., Farruggia, M.J. and Fernandez, R.L., 2022. A functional definition to distinguish ponds from lakes and wetlands. *Scientific reports*, 12(1), p.10472.
- Richey, J.E., Melack, J.M., Aufdenkampe, A.K., Ballester, V.M. and Hess, L.L., 2002. Outgassing from Amazonian rivers and wetlands as a large tropical source of atmospheric CO₂. *Nature*, 416(6881), pp.617-620.
- Robinson, D., 2001. $\delta^{15}\text{N}$ as an integrator of the nitrogen cycle. *Trends in Ecology & Evolution* 16: 153–162.
- Rodríguez-Pérez, H. & A. J. Green, 2006. Waterbird impacts on widgeongrass *Ruppia maritima* in a Mediterranean wetland: comparing bird groups and seasonal effects. *Oikos* 112: 525–534.
- Rounsevell, M., Fischer, M., Rando, A.T.M., Mader, A., Caplat, P., Ekroos, J. and Smith, H.G., 2018. The IPBES regional assessment report on biodiversity and ecosystem services for Europe and Central Asia. Intergovernmental Science-Policy Platform on Biodiversity and Ecosystem Services (IPBES).
- Roy, A. B., 1999. Evolution of saline lakes in Rajasthan. *Current Science* 76: 290–295.

- Saiz, G., Wynn, J.G., Wurster, C.M., Goodrick, I., Nelson, P.N. and Bird, M.I., 2015. Pyrogenic carbon from tropical savanna burning: production and stable isotope composition. *Biogeosciences*, 12(6), pp.1849-1863.
- Sangha, H. S., 2008. The birds of Sambhar Lake and its environs. *Indian Birds* 4: 82-97. Retrieved from <https://www.indianbirds.in/portfolio/may-jun-2008/>
- Santín, C., Doerr, S.H., Kane, E.S., Masiello, C.A., Ohlson, M., de la Rosa, J.M., Preston, C.M. and Dittmar, T., 2016. Towards a global assessment of pyrogenic carbon from vegetation fires. *Global Change Biology*, 22(1), pp.76-91.
- Sarkar, S., Khan, M.A., Sharma, N., Rahman, A., Bhushan, R., Sudheer, A.K. and Kumar, S., 2023. Lake desiccation drives carbon and nitrogen biogeochemistry of a sub-tropical hypersaline lake. *Hydrobiologia*, pp.1-18.
- Sarkar, S., Verma, S., Begum, M.S., Park, J.H. and Kumar, S., 2023. Sources, supply, and seasonality of total suspended matter and associated organic carbon and total nitrogen in three large Asian rivers—Ganges, Mekong, and Yellow. *Frontiers in Earth Science*, 11, p.1067744.
- Saunoy, M., Stavert, A.R., Poulter, B., Bousquet, P., Canadell, J.G., Jackson, R.B., Raymond, P.A., Dlugokencky, E.J., Houweling, S., Patra, P.K. and Ciais, P., 2020. The global methane budget 2000–2017. *Earth system science data*, 12(3), pp.1561-1623.
- Schade, J.D., Bailio, J. and McDowell, W.H., 2016. Greenhouse gas flux from headwater streams in New Hampshire, USA: patterns and drivers. *Limnology and Oceanography*, 61(S1), pp.S165-S174.
- Scheffer, M. and Carpenter, S.R., 2003. Catastrophic regime shifts in ecosystems: linking theory to observation. *Trends in ecology & evolution*, 18(12), pp.648-656.
- Scheffer, M. and van Nes, E.H., 2007. Shallow lakes theory revisited: various alternative regimes driven by climate, nutrients, depth and lake size. In *Shallow Lakes in a Changing World: Proceedings of the 5th International Symposium on Shallow Lakes, held at Dalfsen, The Netherlands, 5–9 June 2005* (pp. 455-466). Springer Netherlands.
- Scheffer, M., 1998. *Ecology of shallow lakes* (Vol. 1). London: Chapman & Hall.
- Schindler, D.W., 2009. Lakes as sentinels and integrators for the effects of climate change on watersheds, airsheds, and landscapes. *Limnology and oceanography*, 54(6part2), pp.2349-2358.
- Schlesinger, W.H. and Bernhardt, E.S., 2013. The global cycles of nitrogen and phosphorus. *Biogeochemistry*, pp.445-467.
- Shadrin, N., Zheng, M. and Oren, A., 2015. Past, present and future of saline lakes: research for global sustainable development. *Chinese Journal of Oceanology and Limnology*, 33, pp.1349-1353.
- Silver, S. and Donini, A., 2021. Physiological responses of freshwater insects to salinity: molecular-, cellular-and organ-level studies. *Journal of Experimental Biology*, 224(20), p.jeb222190.

- Singh, I. B. (2007). "The Ganga river," in *Large rivers: Geomorphology and management* (Chichester: Wiley), 347–371.
- Sinha, R. & B. C. Raymahashay, 2004. Evaporite mineralogy and geochemical evolution of the Sambhar Salt Lake, Rajasthan, India. *Sedimentary Geology* 166: 59–71.
- Sobek, S., E. Durisch-Kaiser, R. Zurbrügg, N. Wongfun, M. Wessels, N. Pasche & B. Wehrli, 2009. Organic carbon burial efficiency in lake sediments controlled by oxygen exposure time and sediment source. *Limnology and Oceanography* 54(6): 2243–2254.
- Sobek, S., Zurbrügg, R. and Ostrovsky, I., 2011. The burial efficiency of organic carbon in the sediments of Lake Kinneret. *Aquatic Sciences*, 73, pp.355-364.
- Sobek, S., Tranvik, L.J. and Cole, J.J., 2005. Temperature independence of carbon dioxide supersaturation in global lakes. *Global Biogeochemical Cycles*, 19(2).
- Solomon, S. ed., 2007. *Climate change 2007-the physical science basis: Working group I contribution to the fourth assessment report of the IPCC (Vol. 4)*. Cambridge university press.
- Song, K. S., S. Y. Zang, Y. Zhao, L. Li, J. Du, N. N. Zhang, X. D. Wang, T. T. Shao, Y. Guan & L. Liu, 2013. Spatiotemporal characterization of dissolved carbon for inland waters in semi-humid/semi-arid region, China. *Hydrology and Earth System Sciences* 17: 4269–4281.
- Song, K., Senbati, Y., Li, L., Zhao, X., Xue, Y. and Deng, M., 2022. Distinctive microbial processes and controlling factors related to indirect N₂O emission from agricultural and urban rivers in Taihu watershed. *Environmental Science & Technology*, 56(7), pp.4642-4654.
- Stanley, E.H., Casson, N.J., Christel, S.T., Crawford, J.T., Loken, L.C. and Oliver, S.K., 2016. The ecology of methane in streams and rivers: patterns, controls, and global significance. *Ecological Monographs*, 86(2), pp.146-171.
- Stein, L.Y., 2019. Insights into the physiology of ammonia-oxidizing microorganisms. *Current opinion in chemical biology*, 49, pp.9-15.
- Sterner, R. W. & J. J. Elser, 2002. *Ecological Stoichiometry: The Biology of Elements from Molecules to the Biosphere*, Princeton University Press, Princeton:
- Stocker, T. ed., 2014. *Climate change 2013: the physical science basis: Working Group I contribution to the Fifth assessment report of the Intergovernmental Panel on Climate Change*. Cambridge university press.
- Stubbins, A., Niggemann, J. and Dittmar, T., 2012. Photo-lability of deep ocean dissolved black carbon. *Biogeosciences*, 9(5), pp.1661-1670.
- Amiotte Suchet, P., Probst, J.L. and Ludwig, W., 2003. Worldwide distribution of continental rock lithology: Implications for the atmospheric/soil CO₂ uptake by continental weathering and alkalinity river transport to the oceans. *Global Biogeochemical Cycles*, 17(2).

- SyvÄRanta, J., H. Haemaelaeninen & R. I. Jones, 2006. Within-lake variability in carbon and nitrogen stable isotope signatures. *Freshwater Biology* 51: 1090–1102.
- Tamoooh, F., Van den Meersche, K., Meysman, F., Marwick, T. R., Borges, A. V., Merckx, R., et al. (2012). Distribution and origin of suspended matter and organic carbon pools in the Tana River Basin, Kenya. *Biogeosciences* 9 (8), 2905–2920.
- Timms, B. V., 2007. The biology of the saline lakes of central and eastern inland of Australia: a review with special reference to their biogeographical affinities. *Hydrobiologia* 576: 27–37.
- Tranvik, L.J., Downing, J.A., Cotner, J.B., Loiselle, S.A., Striegl, R.G., Ballatore, T.J., Dillon, P., Finlay, K., Fortino, K., Knoll, L.B. and Kortelainen, P.L., 2009. Lakes and reservoirs as regulators of carbon cycling and climate. *Limnology and oceanography*, 54(6part2), pp.2298-2314.
- Van Kessel, M.A., Speth, D.R., Albertsen, M., Nielsen, P.H., Op den Camp, H.J., Kartal, B., Jetten, M.S. and Lückner, S., 2015. Complete nitrification by a single microorganism. *Nature*, 528(7583), pp.555-559.
- Van Meter, R.J. and Swan, C.M., 2014. Road salts as environmental constraints in urban pond food webs. *PloS one*, 9(2), p.e90168.
- Vannote, R.L., Minshall, G.W., Cummins, K.W., Sedell, J.R. and Cushing, C.E., 1980. The river continuum concept. *Canadian journal of fisheries and aquatic sciences*, 37(1), pp.130-137.
- Veraart, A.J., De Klein, J.J. and Scheffer, M., 2011. Warming can boost denitrification disproportionately due to altered oxygen dynamics. *PLoS One*, 6(3), p.e18508.
- Vörösmarty, C.J., McIntyre, P.B., Gessner, M.O., Dudgeon, D., Prusevich, A., Green, P., Glidden, S., Bunn, S.E., Sullivan, C.A., Liermann, C.R. and Davies, P.M., 2010. Global threats to human water security and river biodiversity. *nature*, 467(7315), pp.555-561.
- Vuorio, K., M. Meili & J. Sarvala, 2006. Taxon-specific variation in the stable isotopic signatures ($\delta^{13}\text{C}$ and $\delta^{15}\text{N}$) of lake phytoplankton. *Freshwater Biology* 51: 807–822.
- Wagner, S. and Jaffé, R., 2015. Effect of photodegradation on molecular size distribution and quality of dissolved black carbon. *Organic Geochemistry*, 86, pp.1-4.
- Wagner, S., Brandes, J., Spencer, R.G., Ma, K., Rosengard, S.Z., Moura, J.M.S. and Stubbins, A., 2019. Isotopic composition of oceanic dissolved black carbon reveals non-riverine source. *Nature communications*, 10(1), pp.1-8.
- Wagner, S., Cawley, K.M., Rosario-Ortiz, F.L. and Jaffé, R., 2015. In-stream sources and links between particulate and dissolved black carbon following a wildfire. *Biogeochemistry*, 124, pp.145-161.
- Walling, D. E., and Fang, D. (2003). Recent trends in the suspended sediment loads of the world's rivers. *Glob. Planet. change* 39 (1-2), 111–126.
- Walter, M. R., R. Buick & J. S. R. Dunlop, 1980. Stromatolites 3400–3500 Myr old from the North pole area, Western Australia. *Nature* 284: 443–445.

- Wang, C., Lv, Y. and Li, Y., 2018. Riverine input of organic carbon and nitrogen in water-sediment system from the Yellow River estuary reach to the coastal zone of Bohai Sea, China. *Continental Shelf Research*, 157, pp.1-9.
- Wang, H., Bi, N., Saito, Y., Wang, Y., Sun, X., Zhang, J. and Yang, Z., 2010. Recent changes in sediment delivery by the Huanghe (Yellow River) to the sea: causes and environmental implications in its estuary. *Journal of Hydrology*, 391(3-4), pp.302-313.
- Wang, J.J., Lu, X.X. and Kummu, M., 2011. Sediment load estimates and variations in the Lower Mekong River. *River Research and Applications*, 27(1), pp.33-46.
- Wang, J., Zhang, J., Xie, H., Qi, P., Ren, Y. and Hu, Z., 2011. Methane emissions from a full-scale A/A/O wastewater treatment plant. *Bioresource technology*, 102(9), pp.5479-5485.
- Wang, J.N., Chen, N.W., Yan, W.J., Wang, B. and Yang, L.B. (2015) Effect of dissolved oxygen and nitrogen on emission of N₂O from rivers in China. *Atmospheric Environment* 103, 347-356.
- Wang, L. and Macko, S.A., 2011. Constrained preferences in nitrogen uptake across plant species and environments. *Plant, Cell & Environment*, 34(3), pp.525-534.
- Wang, S., Fu, B., Piao, S., Lü, Y., Ciais, P., Feng, X. and Wang, Y., 2016. Reduced sediment transport in the Yellow River due to anthropogenic changes. *Nature Geoscience*, 9(1), pp.38-41.
- Wang, X., He, Y., Chen, H., Yuan, X., Peng, C., Yue, J., Zhang, Q. and Zhou, L., 2018. CH₄ concentrations and fluxes in a subtropical metropolitan river network: Watershed urbanization impacts and environmental controls. *Science of the Total Environment*, 622, pp.1079-1089.
- Wang, X., He, Y., Yuan, X., Chen, H., Peng, C., Yue, J., Zhang, Q., Diao, Y. and Liu, S., 2017. Greenhouse gases concentrations and fluxes from subtropical small reservoirs in relation with watershed urbanization. *Atmospheric Environment*, 154, pp.225-235.
- Wang, X., Ma, H., Li, R., Song, Z. and Wu, J., 2012. Seasonal fluxes and source variation of organic carbon transported by two major Chinese Rivers: The Yellow River and Changjiang (Yangtze) River. *Global Biogeochemical Cycles*, 26(2).
- Wang, X., Xu, C., Druffel, E.M., Xue, Y. and Qi, Y., 2016. Two black carbon pools transported by the Changjiang and Huanghe Rivers in China. *Global Biogeochemical Cycles*, 30(12), pp.1778-1790.
- Ward, N.D., Bianchi, T.S., Medeiros, P.M., Seidel, M., Richey, J.E., Keil, R.G. and Sawakuchi, H.O., 2017. Where carbon goes when water flows: carbon cycling across the aquatic continuum. *Frontiers in Marine Science*, 4, p.7.
- Webb, J.R., Hayes, N.M., Simpson, G.L., Leavitt, P.R., Baulch, H.M. and Finlay, K., 2019. Widespread nitrous oxide undersaturation in farm waterbodies creates an unexpected greenhouse gas sink. *Proceedings of the National Academy of Sciences*, 116(20), pp.9814-9819.

- Weiguo, L., Zisheng, A.N., Weijian, Z., Head, M.J. and Delin, C., 2003. Carbon isotope and C/N ratios of suspended matter in rivers: an indicator of seasonal change in C4/C3 vegetation. *Applied Geochemistry*, 18(8), pp.1241-1249.
- Wenk, C.B., Frame, C.H., Koba, K., Casciotti, K.L., Veronesi, M., Niemann, H., Schubert, C.J., Yoshida, N., Toyoda, S., Makabe, A. and Zopfi, J., 2016. Differential N₂O dynamics in two oxygen-deficient lake basins revealed by stable isotope and isotopomer distributions. *Limnology and Oceanography*, 61(5), pp.1735-1749.
- Williams, W. D., 1993. Conservation of salt lakes. *Hydrobiologia* 267: 291–306.
- Williams, W. D., 1996. What future for saline lakes. *Environment: Science and Policy for Sustainable Development* 38: 12–39.
- Williams, W. D., 2002. Environmental threats to salt lakes and the likely status of inland saline ecosystems in 2025. *Environmental Conservation* 29: 154–167.
- Williamson, C.E., Saros, J.E., Vincent, W.F. and Smol, J.P., 2009. Lakes and reservoirs as sentinels, integrators, and regulators of climate change. *Limnology and Oceanography*, 54(6part2), pp.2273-2282.
- Wu, L., Huh, Y., Qin, J., Du, G., and van Der Lee, S. (2005). Chemical weathering in the upper Huang He (Yellow River) draining the eastern Qinghai Tibet plateau. *Geochimica Cosmochimica Acta* 69 (22), 5279–5294.
- Wurtsbaugh, W. A., C. Miller, S. E. Null, R. J. DeRose, P. Wilcock, M. Hahnenberger, et al., 2017. Decline of the world’s saline lakes. *Nature Geoscience* 10: 816–821.
- Xu, C., Xue, Y., Qi, Y. and Wang, X., 2016. Quantities and fluxes of dissolved and particulate black carbon in the Changjiang and Huanghe Rivers, China. *Estuaries and Coasts*, 39(6), pp.1617-1625.
- Xu, G., Fan, X. and Miller, A.J., 2012. Plant nitrogen assimilation and use efficiency. *Annual review of plant biology*, 63, pp.153-182.
- Xu, H., Ren, Y.A., Zhang, W., Meng, W., Yun, X., Yu, X., Li, J., Zhang, Y., Shen, G., Ma, J. and Li, B., 2021. Updated global black carbon emissions from 1960 to 2017: improvements, trends, and drivers. *Environmental Science & Technology*, 55(12), pp.7869-7879.
- Xu, J. and Ma, Y., 2009. Response of the hydrological regime of the Yellow River to the changing monsoon intensity and human activity. *Hydrological Sciences Journal*, 54(1), pp.90-100.
- Xu, L., Cheng, S., Fang, H., Xin, X., Xu, X. and Tang, H., 2019. Soil inorganic nitrogen composition and plant functional type determine forage crops nitrogen uptake preference in the temperate cultivated grassland, Inner Mongolia. *Soil science and plant nutrition*, 65(5), pp.501-510.
- Xu, R., Tian, H., Lu, C., Pan, S., Chen, J., Yang, J. and Zhang, B., 2017. Preindustrial nitrous oxide emissions from the land biosphere estimated by using a global biogeochemistry model. *Climate of the Past*, 13(7), pp.977-990.

- Xu, Z. and Xu, Y.J., 2018. Dissolved carbon transport in a river-lake continuum: A case study in a subtropical watershed, USA. *Science of the total environment*, 643, pp.640-650.
- Yadav, D. N., M. M. Sarin & S. Krishnaswami, 2007. Hydrogeochemistry of Sambhar Salt Lake, Rajasthan: implication to recycling of salt and annual salt budget. *Journal of Geological Society of India* 69: 139.
- Yadav, D.N., 1997. Oxygen isotope study of evaporating brines in Sambhar Lake, Rajasthan (India). *Chemical Geology*, 138(1-2), pp.109-118.
- Yadav, D.N., Sarin, M.M. and Krishnaswami, S., 2007. Hydrogeochemistry of Sambhar Salt Lake, Rajasthan: implication to recycling of salt and annual salt budget. *Geological Society of India*, 69(1), pp.139-152.
- Yamashita, Y., Kojima, D., Yoshida, N. and Shibata, H., 2021. Relationships between dissolved black carbon and dissolved organic matter in streams. *Chemosphere*, 271, p.129824.
- Yamashita, Y., Nakane, M., Mori, Y., Nishioka, J. and Ogawa, H., 2022. Fate of dissolved black carbon in the deep Pacific Ocean. *Nature Communications*, 13(1), pp.1-7.
- Yan, F., Sillanpää, M., Kang, S., Aho, K.S., Qu, B., Wei, D., Li, X., Li, C. and Raymond, P.A., 2018. Lakes on the Tibetan Plateau as conduits of greenhouse gases to the atmosphere. *Journal of Geophysical Research: Biogeosciences*, 123(7), pp.2091-2103.
- Yang, J., H. Jiang, G. Wu, W. Hou, Y. Sun, Z. Lai & H. Dong, 2012. Co-occurrence of nitrite-dependent anaerobic methane oxidizing and anaerobic ammonia oxidizing bacteria in two Qinghai-Tibetan saline lakes. *Frontiers of Earth Science* 6: 383–391.
- Yang, W. and Guo, L., 2014. Abundance, distribution, and isotopic composition of particulate black carbon in the northern Gulf of Mexico. *Geophysical Research Letters*, 41(21), pp.7619-7625.
- Yang, X., Xue, L., Li, Y., Han, P., Liu, X., Zhang, L. and Cai, W.J., 2018. Treated wastewater changes the export of dissolved inorganic carbon and its isotopic composition and leads to acidification in coastal oceans. *Environmental science & technology*, 52(10), pp.5590-5599.
- Yao, F., Livneh, B., Rajagopalan, B., Wang, J., Crétaux, J.F., Wada, Y. and Berge-Nguyen, M., 2023. Satellites reveal widespread decline in global lake water storage. *Science*, 380(6646), pp.743-749.
- Yoon, T.K., Jin, H., Begum, M.S., Kang, N. and Park, J.H., 2017. CO₂ outgassing from an urbanized river system fueled by wastewater treatment plant effluents. *Environmental Science & Technology*, 51(18), pp.10459-10467.
- Yu, M., Eglinton, T.I., Haghypour, N., Montlucon, D.B., Wacker, L., Hou, P., Zhang, H. and Zhao, M., 2019. Impacts of natural and human-induced hydrological variability on particulate organic carbon dynamics in the Yellow River. *Environmental science & technology*, 53(3), pp.1119-1129.

- Yu, Y., Wang, H., Shi, X., Ran, X., Cui, T., Qiao, S. and Liu, Y., 2013. New discharge regime of the Huanghe (Yellow River): Causes and implications. *Continental Shelf Research*, 69, pp.62-72.
- Zhang, J., Huang, W.W. and Shi, M.C., 1990. Huanghe (Yellow River) and its estuary: sediment origin, transport and deposition. *Journal of Hydrology*, 120(1-4), pp.203-223.
- Zhang, J., Huang, W.W., Letolle, R. and Jusserand, C., 1995. Major element chemistry of the Huanghe (Yellow River), China-weathering processes and chemical fluxes. *Journal of Hydrology*, 168(1-4), pp.173-203.
- Zhang, S., Gan, W.B. and Ittekkot, V., 1992. Organic matter in large turbid rivers: the Huanghe and its estuary. *Marine Chemistry*, 38(1-2), pp.53-68.
- Zhang, W., Li, H., Xiao, Q. and Li, X., 2021. Urban rivers are hotspots of riverine greenhouse gas (N₂O, CH₄, CO₂) emissions in the mixed-landscape chaohu lake basin. *Water Research*, 189, p.116624.
- Zhang, X., Ward, B.B. and Sigman, D.M., 2020. Global nitrogen cycle: critical enzymes, organisms, and processes for nitrogen budgets and dynamics. *Chemical reviews*, 120(12), pp.5308-5351.
- Zhang, X., Wu, Y. and Gu, B., 2015. Urban rivers as hotspots of regional nitrogen pollution. *Environmental Pollution*, 205, pp.139-144.
- Zhao, M.M., Wang, S.M., Chen, Y.P., Wu, J.H., Xue, L.G. and Fan, T.T., 2020. Pollution status of the Yellow River tributaries in middle and lower reaches. *Science of The Total Environment*, 722, p.137861.
- Zhao, Q., Zhang, Y., Guo, F., Leigh, C. and Jia, X., 2021. Increasing anthropogenic salinisation leads to declines in community diversity, functional diversity and trophic links in mountain streams. *Chemosphere*, 263, p.127994.
- Zheng, M., 2001. On salinology. *Hydrobiologia* 466: 339–347.
- Zheng, Y., Wu, S., Xiao, S., Yu, K., Fang, X., Xia, L., Wang, J., Liu, S., Freeman, C. and Zou, J., 2022. Global methane and nitrous oxide emissions from inland waters and estuaries. *Global Change Biology*, 28(15), pp.4713-4725.
- Zhu, D., Wu, Y., Wu, N., Chen, H., He, Y., Zhang, Y. and Peng, C., 2015. Nitrous oxide emission from infralittoral zone and pelagic zone in a shallow lake: Implications for whole lake flux estimation and lake restoration. *Ecological Engineering*, 82, pp.368-375.
- Zhu, L., Shi, W., Van Dam, B., Kong, L., Yu, J. and Qin, B., 2020. Algal accumulation decreases sediment nitrogen removal by uncoupling nitrification-denitrification in shallow eutrophic lakes. *Environmental science & technology*, 54(10), pp.6194-6201.
- Zimmerman, A.R., 2010. Abiotic and microbial oxidation of laboratory-produced black carbon (biochar). *Environmental science & technology*, 44(4), pp.1295-1301.

- Zimmermann, M., Bird, M.I., Wurster, C., Saiz, G., Goodrick, I., Barta, J., Capek, P., Santruckova, H. and Smernik, R., 2012. Rapid degradation of pyrogenic carbon. *Global Change Biology*, 18(11), pp.3306-3316.
- Zohary, T., J. Erez, M. Gophen, I. Berman-Frank & M. Stiller, 1994. Seasonality of stable carbon isotopes within the pelagic food web of Lake Kinneret. *Limnology and Oceanography* 39: 1030–1043.

List of Publications

Associated with thesis work

- 1 **Sarkar, S.**, Rahman, A., Khan, MA., Rathi, A., Ragavan, P., Singh, A. and Kumar, S., Isotopic evidence for aging of particulate black carbon in the ocean. *Geophysical Research Letters*. **(Accepted)**.
- 2 **Sarkar, S.**, Rathi, A., Khan, MA. and Kumar, S., Demystifying the particulate black carbon conundrum in aquatic systems. *Environmental Research Communications*. **(Under Review)**.
- 3 **Sarkar, S.** and Kumar, S., Water stagnancy and wastewater input enhance primary productivity in an engineered river system. *River*. **(Under Review)**.
- 4 **Sarkar, S.**, Verma, S., Begum, M.S., Park, J.H. and Kumar, S., 2023. Sources, supply, and seasonality of total suspended matter and associated organic carbon and total nitrogen in three large Asian rivers—Ganges, Mekong, and Yellow. *Frontiers in Earth Science*, 11, p.1067744. <https://doi.org/10.3389/feart.2023.1067744>
- 5 **Sarkar, S.**, Khan, M.A., Sharma, N., Rahman, A., Sudheer A.K., Bhushan R. and Kumar, S. (2023). Lake desiccation drives carbon and nitrogen biogeochemistry of a sub-tropical hypersaline lake. *Hydrobiologia*. <https://doi.org/10.1007/s10750-023-05193-8>

Publications through collaborative projects

- 6 Ragavan, P., Rahman, A., **Sarkar, S.**, Verma, S., Jeeva, C., Mohan, PM. and Kumar, S., 2023. Variability in soil organic carbon stock and isotopic signature in a tropical island mangrove forests of India. *Regional Environmental Change*. <https://doi.org/10.1007/s10113-023-02130-2>
- 7 Shaw, C., **Sarkar, S.**, Kumar, S. and Rastogi, N., 2023. High Release of Isotopically Depleted CO₂ and CH₄ from the Photo-Degradation of Plastic: A Pilot Laboratory Study. *Physics and Chemistry of the Earth*. <https://doi.org/10.1016/j.pce.2023.103474>
- 8 Reinl, K.L., Harris, T.D., North, R.L., Almela, P., Berger, S.A., Bizic, M., Burnet, S.H., Grossart, H.-P., Ibelings, B.W., Jakobsson, E., Knoll, L.B., Lafrancois, B.M., McElarney, Y., Morales-Williams, A.M., Obertegger, U., Ogashawara, I., Paule-Mercado, M.C., Peierls, B.L., Rusak, J.A., **Sarkar, S.**, Sharma, S., Trout-Haney, J.V., Urrutia-Cordero, P., Venkiteswaran, J.J., Wain, D.J., Warner, K., Weyhenmeyer, G.A. and Yokota, K. (2023), Blooms also like it cold. *Limnol. Oceanogr. Lett.* <https://doi.org/10.1002/lol2.10316>
- 9 Attri, P., **Sarkar, S.** and Mani, D., 2022. Classification and transformation of aerosols over selected Indian cities during reduced emissions under Covid-19 lockdown. *Journal of Earth System Science*, 131(3), p.190. <https://doi.org/10.1007/s12040-022-01916-y>

- 10 Rahman, A., **Sarkar, S.** and Kumar, S., 2020. Paleoenvironment of the Central Himalaya during late MIS 3 using stable isotopic compositions of lacustrine organic matter occluded in diatoms and sediments. *Quaternary International*, 558, pp.1-9 <https://doi.org/10.1016/j.quaint.2020.08.024>

Presentations at Conferences and Meetings

- 1 **Sarkar, S.**, Rahman, A., Rathi, A., Khan, A., Ragavan, P., Singh, A., and Kumar, S., 2023, June. Isotopic evidence of aging of particulate black carbon in the open ocean. *ASLO Aquatic Sciences Meeting*.
- 2 **Sarkar, S.**, Sebastian, J.G., Badnal, M., Warriar, A.K., Mohan, R., & Kumar, S., 2023, May. Spatial and diel variations in CH₄, CO₂, and N₂O in the lakes of the Schirmacher Oasis, East Antarctica. In *National Polar Science Conference*, NCPOR, India.
- 3 **Sarkar, S.**, Shah, R.A. and Kumar, S., 2022, May. Sources and transformation of dissolved inorganic carbon in a Himalayan river system. In *EGU General Assembly Conference Abstracts* (pp. EGU22-12674).
- 4 **Sarkar, S.**, Kumar, S., 2021, June. Dissolved inorganic carbon dynamics in an engineered tropical river continuum. *ASLO Aquatic Sciences Meeting*.
- 5 **Sarkar, S.**, Rathi, A and Kumar. S., 2021, April. Greenhouse gas dynamics in an anthropogenically modified tropical river continuum. In *EGU General Assembly Conference Abstracts* (pp. EGU21 – 9361).
- 6 **Sarkar, S.**, Khan, M.A., Sharma, N., Rahman, A. and Kumar, S., 2020, December. Hydro-and biogeo-chemistry of the largest hypersaline lake of India. In *AGU Fall Meeting Abstracts* (Vol. 2020, pp. H114-0003).